Titre: Title:	Development of a Critically Evaluated Thermodynamic Databse for the Systems Containing Alkaline-Earth Oxides
Auteur: Author:	Adarsh Shukla
Date:	2012
Type:	Mémoire ou thèse / Dissertation or Thesis
Référence: Citation:	Shukla, A. (2012). Development of a Critically Evaluated Thermodynamic Databse for the Systems Containing Alkaline-Earth Oxides [Thèse de doctorat, École Polytechnique de Montréal]. PolyPublie. https://publications.polymtl.ca/885/

UNIVERSITÉ DE MONTRÉAL

DEVELOPMENT OF A CRITICALLY EVALUATED THERMODYNAMIC DATABASE FOR THE SYSTEMS CONTAINING ALKALINE-EARTH OXIDES

ADARSH SHUKLA

DÉPARTEMENT DE GÉNIE CHIMIQUE

ÉCOLE POLYTECHNIQUE DE MONTRÉAL

THÈSE PRÉSENTÉE EN VUE DE L'OBTENTION

DU DIPLÔME DE PHILOSOPHIAE DOCTOR

(GÉNIE MÉTALLURGIQUE)

JUILLET 2012

UNIVERSITÉ DE MONTRÉAL

ÉCOLE POLYTECHNIQUE DE MONTRÉAL

Cette thèse intitulée

DEVELOPMENT OF A CRITICALLY EVALUATED THERMODYNAMIC DATABASE FOR THE SYSTEMS CONTAINING ALKALINE-EARTH OXIDES

présentée par : SHUKLA Adarsh

en vue de l'obtention du diplôme de : Philosophiae Doctor

a été dûment acceptée par le jury d'examen constitué de :

M. CHARTRAND Patrice, Ph.D., président

M. PELTON Arthur, Ph.D., membre et directeur de recherche

M. DECTEROV Serguei, Ph.D., membre et codirecteur de recherche

M. JUNG In-Ho, Ph.D., membre et codirecteur de recherche

M. BALE Christopher W., Ph.D., membre

M. KOEPSEL Detlef, Ph.D., membre

DEDICATION

I want to dedicate this thesis to my family in India.

ACKNOWLEDGMENTS

I would like to express my gratitude towards my mentor Dr. Arthur D. Pelton, without whom this work was not at all possible. His guidance and support provided the impetus for successful completion of this work.

I am also grateful to my co-directors, Drs. Sergei Decterov and In-Ho Jung, for their continual helpful advice and collaboration in this study. I enjoyed all discussions with them during my study. I also thank Dr. Pierre Hudon for his guidance and assistance in performing the experiments.

I also thank Drs. D. Koespel, P. Chartrand, C.W. Bale and S. Schiefelbein for their critical review and constructive comments on this thesis.

I am indebted to Eugenia for her assistance in the literature survey. I am grateful to James for proofreading this thesis. I sincerely thank Aimen and Christian for the French translation. I thank Katherine for all her assistance. I am also thankful to Eve, Jacques, Liling and all the other members of the CRCT for their help and friendship during my study in Canada.

I also express my gratitude towards Dr. S. Srikanth whose encouragement during my studies in India helped me to develop an interest for the higher education.

RÉSUMÉ

Dans un système thermodynamique multicomposant, les relations de phases entre les constituants sont généralement très complexes. En particulier, les systèmes à base d'oxydes sont souvent très difficiles à étudier en raison des températures très élevées et de l'action corrosive des laitiers. A cause de ces difficultés, de grandes incohérences et dispersions sont souvent observées parmi les données expérimentales disponibles dans la littérature. Afin d'étudier et de comprendre de manière efficace les relations de phases complexes, il est très utile de développer des banques de données thermodynamiques contenant les paramètres optimisés d'un modèle d'énergie libre de Gibbs, permettant de dériver les propriétés thermodynamiques de toutes les phases en fonction de la température et de la composition. Dans une optimisation thermodynamique, les paramètres ajustables du modèle d'énergie libre de Gibbs sont calculés en utilisant simultanément toutes les données thermodynamiques et d'équilibres de phases disponibles afin d'obtenir un ensemble d'équations en fonction de la température et de la composition. Les données thermodynamiques, telles que les activités, peuvent aider à évaluer les diagrammes de phases, et les informations sur les équilibres de phases peuvent être utilisées pour déduire les propriétés thermodynamiques. Ainsi, il est souvent possible de résoudre les divergences observées entre les données expérimentales disponibles. A partir des équations du modèle, toutes les propriétés thermodynamiques et les diagrammes de phases peuvent être calculés rétrospectivement. Il est également possible d'effectuer des interpolations et extrapolations de manière cohérente d'un point de vue thermodynamique. Les données sont ainsi rendues auto-cohérentes et, conformément aux principes thermodynamiques, les données expérimentales disponibles sont reproduites par un petit jeu de paramètres du modèle; ce qui est idéal pour le stockage informatique.

Dans le cadre d'un vaste projet de recherche au Centre de Recherche en Calcul Thermochimique (CRCT) au sein de l'Ecole Polytechnique de Montréal, nous avons développé une banque de données thermodynamiques pour les systèmes d'oxydes multicomposants. Cette thèse consiste en l'ajout des composants SrO et BaO à la banque de données multicomposante existant déjà pour le système SiO_2-B_2O_3-Al_2O_3-CaO-MgO. Au fil des années, en collaboration avec de nombreuses compagnies industrielles, une banque de données thermodynamiques a été développée pour le système SiO_2-B_2O_3-Al_2O_3-CaO-MgO de manière tout à fait satisfaisante. L'objectif du présent travail est d'améliorer l'applicabilité de cette banque de données en y ajoutant les nouveaux composants SrO et BaO. Les banques de données élaborées dans ce travail seront d'une importance particulière pour les industries des verres et de l'acier.

Dans le système SiO_2-B_2O_3-Al_2O_3-CaO-MgO-BaO-SrO, il y a 11 sous-systèmes binaires et 25 sous-systèmes ternaires contenant soit BaO, soit SrO ou bien les deux à la fois. Pour la plupart de ces systèmes binaires, et pour aucun de ces systèmes ternaires, des « optimisations » thermodynamiques sont déjà disponibles dans la littérature. Dans cette thèse, nous présentons l'évaluation et l'optimisation thermodynamique de 11 sous-systèmes binaires, 17 sous-systèmes ternaires et 5 sous-systèmes quaternaires contenant BaO et/ou SrO issus du système SiO_2-B_2O_3-Al_2O_3-CaO-MgO-BaO-SrO. Toutes ces optimisations thermodynamiques ont été effectuées en se basant sur les données expérimentales disponibles dans la littérature, à l'exception du système SrO-B_2O_3-SiO_2 qui a été optimisé à partir de données expérimentales obtenues dans le présent travail en conjonction avec les données issues de la littérature.

Dans cette thèse, tous les calculs ont été réalisés à l'aide du logiciel FactSage^{TM} de calcul d'équilibres thermodynamiques. Le Modèle Quasichimique Modifié (MQM) prenant en compte l'ordre à courte distance a été utilisé pour la phase liquide. Tous les systèmes binaires ont été évalués de manière critique et optimisés à partir des données thermodynamiques et d'équilibre de phases disponibles dans la littérature. Les paramètres du modèle obtenus ont été utilisés pour représenter les énergies de Gibbs de toutes les phases en fonction de la température et de la composition. Les paramètres binaires du modèle ont été utilisés pour estimer les propriétés thermodynamiques des phases dans les systèmes ternaires. Des modèles « géométriques » appropriés ont été utilisés pour ces estimations. Les diagrammes de phases ternaires ont été calculés et comparés avec les données expérimentales disponibles. Des paramètres d'interaction ternaires ont également été ajoutés lorsque cela était nécessaire.

La première partie de cette thèse est consacrée à une revue exhaustive de la littérature sur le thème de la modélisation thermodynamique et des techniques expérimentales de détermination de diagrammes de phases. Les chapitres suivants comprennent la revue de la littérature ainsi que les optimisations thermodynamiques des différents systèmes. La dernière partie de cette thèse est consacrée à la présentation du travail expérimental (trempe et EPMA) effectué pour le système SrO-B_2O_3-SiO_2.

ABSTRACT

In a thermodynamic system which contains several elements, the phase relationships among the components are usually very complex. Especially, systems containing oxides are generally very difficult to investigate owing to the very high experimental temperatures and corrosive action of slags. Due to such difficulties, large inconsistencies are often observed among the available experimental data. In order to investigate and understand the complex phase relationships effectively, it is very useful to develop thermodynamic databases containing optimized model parameters giving the thermodynamic properties of all phases as functions of temperature and composition. In a thermodynamic optimization, adjustable model parameters are calculated using, simultaneously, all available thermodynamic and phase-equilibrium data in order to obtain one set of model equations as functions of temperature and composition. Thermodynamic data, such as activities, can aid in the evaluation of the phase diagrams, and information on phase equilibria can be used to deduce thermodynamic properties. Thus, it is frequently possible to resolve discrepancies in the available data. From the model equations, all the thermodynamic properties and phase diagrams can be back-calculated, and interpolations and extrapolations can be made in a thermodynamically correct manner. The data are thereby rendered self-consistent and consistent with thermodynamic principles, and the available data are distilled into a small set of model parameters, ideal for computer storage.

As part of a broader research project at the *Centre de Recherche en Calcul Thermochimique* (CRCT), Ecole Polytechnique to develop a thermodynamic database for multicomponent oxide systems, this thesis deals with the addition of components SrO and BaO to the existing

multicomponent database of the SiO_2-B_2O_3-Al_2O_3-CaO-MgO system. Over the years, in collaboration with many industrial companies, a thermodynamic database for the SiO_2-B_2O_3-Al_2O_3-CaO-MgO system has been built quite satisfactorily. The aim of the present work was to improve the applicability of this five component database by adding SrO and BaO to it. The databases prepared in this work will be of special importance to the glass and steel industries.

In the SiO_2-B_2O_3-Al_2O_3-CaO-MgO-BaO-SrO system there are 11 binary systems and 25 ternary systems which contain either BaO or SrO or both. For most of these binary systems, and for none of these ternary systems, is there a previous thermodynamic optimization available in the literature. In this thesis, thermodynamic evaluation and optimization for the 11 binary, 17 ternary and 5 quaternary BaO- and SrO- containing systems in the SiO_2-B_2O_3-Al_2O_3-CaO-MgO-BaO-SrO system is presented. All these thermodynamic optimizations were performed based on the experimental data available in the literature, except for the SrO-B_2O_3-SiO_2 system. This latter system was optimized on the basis of a few experimental data points generated in the present work together with the data from the literature.

In the present work, all the calculations were performed using the FactSage^{TM} thermochemical software. The Modified Quasichemical Model (MQM), which is capable of taking short-range ordering into account, was used for the liquid phase. All the binary systems were critically evaluated and optimized using available phase equilibrium and thermodynamic data. The model parameters obtained as a result of this simultaneous optimization were used to represent the Gibbs energies of all phases as functions of temperature and composition. Optimized binary

model parameters were used to estimate the thermodynamic properties of phases in the ternary systems. Proper "geometric" models were used for these estimations. Ternary phase diagram were calculated and compared with available experimental data. Wherever required, ternary interaction parameters were also added.

The first part of this thesis comprises a general literature review on the subject of thermodynamic modeling and experimental techniques for phase diagram determination. The next chapters include the literature review and the thermodynamic optimizations of the various systems. The last part of the thesis is the presentation of experiments performed in the present work, by quenching and EPMA, in the SrO-B_2O_3-SiO_2 system. The experiments were designed to generate the maximum amount of information with the minimum number of experiments using the thermodynamic optimization, based only on the data available in the literature, as a guide. These newly-obtained data improved the (preceding) thermodynamic optimization, based on the experimental data in the literature, of this ternary system.

TABLE OF CONTENTS

LIST OF TABLES

LIST OF FIGURES

LIST OF SYMBOLS

C_p	Molar heat capacity (J/mol·K)
G^0_i	Standard Gibbs energy of *i* (J/mol)
G^m	Gibbs energy of solution (J)
G^E	Excess Gibbs energy in solution (J)
g^E	Molar excess Gibbs energy in solution (J/mol)
g^0_i	Molar Gibbs energy of *i* (J/mol)
Δg_{ij}	Gibbs energy change for the formation of two moles of *i-j* pairs (J)
H^0_i	Standard enthalpy of *i* relative to a standard elemental reference (J/mol)
ΔH	Molar enthalpy of mixing (J/mol)
ΔH_T	Enthalpy of formation of the compound from elements (J/mol)
n_{ij}	Number of moles of *i-j* bonds
q^{ij}_{AB}	Excess interaction parameter between A and B (J/mol)
S^0_i	Standard entropy of component *i* (J/mol·K)
ΔS_T	Entropy of formation of the compound from elements (J/mol·K)
ΔS^{conf}	Molar configurational entropy of solution (J/mol·K)
$S^{non\text{-}conf}$	Molar non-configurational entropy of solution (J/mol·K)
n_i	Number of moles of component *i*
T	Absolute temperature (K)
wt. %	Weight percent
y_i	Site fraction of component *i*
Y_i	Coordination-equivalent fractions
X_i	Mole fraction of component *i* in solution
X_{ij}	Pair fraction of *i-j* pairs
Z_i	Coordination number of *i*
Z^i_{ii}	The values of Z_i when all the nearest neighbors of an *i* are *i*'s
Z^i_{ij}	The values of Z_i when all the nearest neighbors of an *i* are *j*'s

INTRODUCTION

In a thermodynamic system which contains several elements, the phase relationships among the components are very complex. Especially, the systems containing oxides are extremely difficult to investigate owing to the very high experimental temperatures and corrosive action of slags. Due to such difficulties in oxide systems, large inconsistencies are often observed among the available experimental data. In order to investigate and understand the complex phase relationships effectively, it is very useful to develop thermodynamic databases containing model parameters giving the thermodynamic properties of all phases as functions of temperature and composition.

Such thermodynamic databases are prepared by critical evaluation, modeling, and optimization. In a thermodynamic optimization, adjustable model parameters are calculated using, simultaneously, all available thermodynamic and phase-equilibrium data in order to obtain one set of model equations as functions of temperature and composition. Thermodynamic data, such as activities, can aid in the evaluation of the phase diagrams, and information on phase equilibria can be used to deduce thermodynamic properties. Thus, it is frequently possible to resolve discrepancies in the available data. From the model equations, all of the thermodynamic properties and phase diagrams can be back-calculated, and interpolations and extrapolations can be made in a thermodynamically correct manner. The data are thereby rendered self-consistent and consistent with thermodynamic principles, and the available data are distilled into a small set of model parameters, ideal for computer storage.

In addition to the development of new models to represent the Gibbs energies of phases and the development of thermodynamic databases to describe the behavior of solutions, the *Centre de Recherche en Calcul Thermochimique* (CRCT) at Ecole Polytechnique, Montreal has developed the software FactSage^{TM} (FactSage 2008). FactSage^{TM} is the fusion of the FACT-Win/F*A*C*T and ChemSage/SOLGASMIX (Eriksson and Hack, 1990) thermochemcial packages that were founded 25 years ago. The FactSage package runs on a PC operating under Microsoft Windows and consists of a series of information, database, calculation and manipulation modules that enable one to access and manipulate databases for pure substances and solutions. Using FactSage^{TM} one will be able to access the databases to calculate the amounts and compositions of all phases at equilibrium at any temperature and composition in multicomponent systems, to follow the course of equilibrium or non-equilibrium cooling, to calculate corresponding heat effects, *etc*. The phase diagrams and thermodynamic data generated by these databases will also be helpful in systematic planning of future experiments. This will greatly reduce the number of experiments required, and in turn resources and time will be saved.

As part of a broader research project at the *Centre de Recherche en Calcul Thermochimique* (CRCT), Ecole Polytechnique to develop a thermodynamic database for multicomponent oxide systems, the present work deals with the addition of the components SrO and BaO to the existing multicomponent database of the SiO_2-B_2O_3-Al_2O_3-CaO-MgO system. Over the years, in collaboration with many industrial companies, a thermodynamic database for the SiO_2-B_2O_3-Al_2O_3-CaO-MgO system has been built quite satisfactorily. SiO_2, B_2O_3, and Al_2O_3 are commercially important oxides used extensively in various industrial applications. CaO and MgO

oxides are used as network-modifiers in glasses. BaO and SrO are also very important oxides in many industrial applications. BaO is one of the major components in some of the optical glasses. BaO and SrO are used to block X-rays in cathode ray and TV tubes. BaO-SrO-Al_2O_3-SiO_2 is a key system to understand the degradation of uranium oxide and reaction with cement walls in nuclear power plants. SrO and BaO are vying with other oxides for many potential applications in the steel industry. BaO and SrO are now looked upon as future fluxing materials for refining of molten steel and ferro-alloys: removal of sulfur, phosphorous, carbon, and other impurities. The databases prepared in this project will be of special importance to these industries. In fact, this work is partially funded by three glass companies: Corning (USA), Schott (Germany), St-Gobain (Paris); and by a steel company, POSCO (South Korea). Moreover, for most of the SrO and BaO containing binary and higher-order oxide systems there is no thermodynamic assessment available in the literature. Hence, there are immense opportunities to critically evaluate these systems.

In the SiO_2-B_2O_3-Al_2O_3-CaO-MgO-BaO-SrO system there are 11 binary systems which contain either BaO or SrO (or both):

1. SrO-BaO
2. SrO-CaO
3. BaO-MgO
4. SrO-MgO
5. BaO-CaO
6. SrO-SiO_2

7. $BaO\text{-}SiO_2$
8. $SrO\text{-}Al_2O_3$
9. $BaO\text{-}Al_2O_3$
10. $BaO\text{-}B_2O_3$
11. $SrO\text{-}B_2O_3$

In the present work, all of these 11 binary systems were critically evaluated and optimized.

And, in the $SiO_2\text{-}B_2O_3\text{-}Al_2O_3$-CaO-MgO-BaO-SrO system there are 25 ternary systems which contain either BaO or SrO (or both):

1. $BaO\text{-}SrO\text{-}SiO_2$
2. $CaO\text{-}SrO\text{-}SiO_2$
3. $BaO\text{-}CaO\text{-}SiO_2$
4. $SrO\text{-}MgO\text{-}SiO_2$
5. $BaO\text{-}MgO\text{-}SiO_2$
6. $CaO\text{-}SrO\text{-}Al_2O_3$
7. $BaO\text{-}CaO\text{-}Al_2O_3$
8. $SrO\text{-}BaO\text{-}Al_2O_3$
9. $BaO\text{-}MgO\text{-}Al_2O_3$
10. $BaO\text{-}Al_2O_3\text{-}SiO_2$
11. $SrO\text{-}Al_2O_3\text{-}SiO_2$
12. $BaO\text{-}B_2O_3\text{-}SiO_2$
13. $SrO\text{-}B_2O_3\text{-}SiO_2$

14. $BaO-B_2O_3-Al_2O_3$
15. $SrO-B_2O_3-Al_2O_3$
16. $SrO-BaO-B_2O_3$
17. $BaO-CaO-B_2O_3$
18. SrO-BaO-CaO
19. SrO-BaO-MgO
20. $SrO-CaO-B_2O_3$
21. SrO-CaO-MgO
22. $SrO-MgO-B_2O_3$
23. $SrO-MgO-Al_2O_3$
24. BaO-CaO-MgO
25. $BaO-MgO-B_2O_3$

In the literature, whenever experimental data were available for these systems they were critically evaluated and optimized. A few experimental data for the higher-order (quaternary) system were also available. They were also evaluated and optimized.

In the present work, a few experimental data in the $SrO-B_2O_3-SiO_2$ system, by quenching and EPMA, were also generated. The experiments were designed to generate the maximum amount of information with the minimum number of experiments using the thermodynamic optimization, based only on the data available in the literature, as a guide. These newly obtained data improved the (preceding) thermodynamic optimization of this system.

The Modified Quasichemical Model (MQM) developed at the *Centre de Recherche en Calcul Thermochimique* at Ecole Polytechnique, Montreal was used to model the liquid phase. This model is capable of taking into account ordering or clustering in the liquid phase. The liquid phase is technologically one of the most important phases appearing in every system. The adequate representation of its Gibbs energy plays a decisive role in database preparation for multicomponent systems. This model has been satisfactorily used by its developers and others to model not only liquid oxides but also alloys, mattes and salts.

In the present work, first the binary systems containing BaO and SrO were critically evaluated. (All other binary sub-systems have been critically evaluated and optimized previously.) All available thermodynamic and phase diagram data for these systems were collected and critically assessed for their reliability. The Gibbs energies of all phases were represented by appropriate model equations. The parameters of these models were obtained by an optimization procedure using the FactSage^{TM} (FactSage 2008) software. These binary parameters were then used along with the models to predict the thermodynamic properties and phase diagrams of the ternary systems. All available data on the ternary systems (containing BaO and SrO) were collected. The predictions for the ternary systems were compared with the available ternary data, and the models were refined through the inclusion of ternary parameters, where required, for those systems where sufficient data were available.

1. LITERATURE REVIEW

In this chapter a general review of the literature on the topic of evaluation and optimization of phase diagrams is given. A brief review of experimental techniques for phase diagram measurement is also presented. In this literature survey, the doctoral thesis by Jung (Jung, 2003) and masters thesis by Shukla (Shukla, 2008) on a similar work on database preparation for oxides and alloys were of immense help. The literature on specific systems optimized in the present work is not reviewed in this chapter as they are presented in the following chapters.

1.1. CALPHAD

Calphad is an acronym for the CALculation of PHAse Diagrams [Spencer (2008)]. It is better described as "The Computer Coupling of Phase Diagrams and Thermochemistry".

Kattner (Kattner, 1997) described phase diagrams as "visual representations of the equilibrium state of a material as a function of temperature, pressure and concentrations of the constituent components." They are, therefore, frequently hailed as basic blueprints or roadmaps for alloy design, development, processing and basic understanding. Pelton and Schmalzried (Pelton and Schmalzried, 1973) defined a phase diagram as "the geometrical representation of the loci of the thermodynamic parameters when equilibrium among phases under a specified set of conditions is established". Phase diagrams provide vital inputs required for addressing many technological problems involving multi-component, multi-phase equilibria.

The correlation between thermodynamics and phase equilibria was established more than a century ago by J.W. Gibbs. Later, J. J. van Laar (Van Laar, 1908) published his mathematical synthesis of hypothetical binary systems. With the advance of computing technology, construction of multicomponent thermodynamic databases began in the late 1960's. Kattner (Kattner, 1997) has summarized some early examples, between 1908 and 1970, of mathematical calculations of phase diagrams. In 1970 Kaufman and Bernstein (Kaufman and Bernstein, 1970) summarized the general features of the calculation of phase diagrams and also presented listings of computer programs. In 1973 Larry Kaufman organized the first project meeting of the international CALPHAD group.

Under the CALPHAD technique, all types of thermodynamic information such as phase diagrams, enthalpy of mixing in a phase, activities *etc*. are critically evaluated and optimized simultaneously, using proper thermodynamic models, in order to construct multicomponent databases. The thermodynamic models required to represent the thermochemistry of phases have also been developed. A model capable of closely reflecting the thermochemical properties of a phase with a minimum number of adjustable parameters should be chosen. Also, these models should be based on a good physical microscopic picture of a solution to obtain better predictions in multicomponent systems using these models from lower-order optimized parameters.

Normally a software package capable of performing multivariable optimizations is used in the optimization process. All the input data are back-calculated from the single set of model parameters obtained from the optimization. The databases containing model parameters for

lower-order (binary and ternary) systems are used to predict the thermodynamic properties in multicomponent systems. There are various techniques (Section 1.2.3) to extrapolate the Gibbs energy from binary systems into higher-order systems. In case these predictions are not able to reproduce the available data in the higher-order system within the experimental error limits, then higher-order interaction parameters is included to reproduce the available data.

Recently, new approaches to thermodynamic modeling have been conducted with the advent of computing technologies. First-principles calculations can be cited in this area. A first-principles calculation starts from quantum mechanics to examine the fundamental properties of materials such as which structure is stable at a certain temperature and pressure. First-principles calculations are extensively used in conjunction with the "Cluster Variation Method" (CVM) which was introduced in the 1950's by Kikuchi (Kikuchi, 1951) who introduced this method to treat order-disorder phenomena in solid phases. Although these calculations are computationally very intensive, enormous progress in recent years in the area of computing techniques have made them easier.

Nevertheless, these techniques are still in their nascent stages and cannot be satisfactorily applied to complex systems. The phase diagrams predicted by these techniques are generally approximately correct but currently still lack sufficient accuracy for practical applications. In conclusion, the development of thermodynamic databases for applications in complex industrial processes can be done by the CALPHAD technique, although first-principles calculations can

often provide reasonable estimations of certain properties, particularly enthalpies of stoichiometric solids, when experimental data are lacking.

1.2 Thermodynamic modeling

Thermodynamic models are required to adequately represent the thermodynamic properties of materials. Complex solutions require sophisticated and refined models for the proper representation of their thermochemical properties. A good model should be able to represent the thermodynamic properties with just a small numbers of adjustable parameters. For this, the model should be based on the structure of the solution to adequately represent the configurational entropy of the solution. Also these models have high predictive capability in higher-order systems. Hence, models should be developed which can describe the configurational entropy of the solutions without the addition of large arbitrary model parameters.

The standard Gibbs energy of a pure component ***i*** is written as:

$$G^0_i = H^0_i - TS^0_i \qquad (1.2.1)$$

where G^0_i, H^0_i, and S^0_i are respectively the standard Gibbs energy, enthalpy (relative to standard elemental reference (SER) state) and entropy of ***i***, and T is the absolute temperature.

When two components A and B are mixed then the energy of the solution depends upon the interaction between the A and B atoms or molecules. The Gibbs energy of a solution in which

there is no change in its energy because of mixing i.e. the value of the A-B bond energy is the average of that of the A-A and B-B bonds is an ideal solution for which:

$$G^m = g^0_A n_A + g^0_B n_B - T\Delta S^{conf} \quad (1.2.2)$$

where G^m is the Gibbs energy of the solution, g^0_i is the molar Gibbs energy of component i, and ΔS^{conf} is configurational entropy obtained by randomly mixing n_A moles of A and n_B mole of B on the same sublattice:

$$\Delta S^{conf} = -R\,(n_A \ln X_A + n_B \ln X_B) \quad (1.2.3)$$

Practically however, all solutions do have interactions among the atoms mixing to form a solution. Such interactions can be called g^E, the molar excess Gibbs energy of the solution. In this case the energy of the solution is given by:

$$G^m = g^0_A n_A + g^0_B n_B - T\Delta S^{conf} + (n_A+n_B)\, g^E \quad (1.2.4)$$

g^E is often expanded as a polynomial in the mole fractions as:

$$g^E = \Sigma\, q^{ij}_{AB}\, X^i_A X^j_B \quad (1.2.5)$$

where the excess interaction parameters q^{ij}_{AB} (= a +bT +cT^2 + …..) may be temperature dependent.

In many cases, the thermodynamic properties of a binary solution can be described by using the expression in Eq. 1.2.5. Although it is satisfactory in binary systems which are not showing large deviations from ideality, problems arise when such an expression is used to predict the

thermodynamic properties of the higher-order systems from the model parameters of the lower-order sub-systems. In this case, large arbitrary parameters are often needed in these higher-order systems to reproduce the available data. Even sometimes in a binary system also a large number of interaction parameters are needed in this simple polynomial based model in order to adequately represent all the thermodynamic properties of the system.

To adequately represent the thermodynamic properties of the liquid phase, Pelton and co-workers (Pelton, Degterov, Eriksson, Robelin and Dessureault, 2000) and Pelton and Chartrand (Pelton and Chartrand 2001) developed the Modified Quasichemical Model (MQM). They modified the classical quasichemical model by improving the configurational entropy term of the model. Other modifications were also made to make it more flexible and practical for real and complicated systems.

The MQM developed by Pelton *et al.* (Pelton, Degterov, Eriksson, Robelin and Dessureault, 2000) has been applied not only to simple metallic alloys but to liquid slags, sulphides, and salts. In fact, the utility of the MQM over a simple polynomial or random- mixing model can be better realized with those solutions which show more ordering than metallic solutions, and where the configurational entropy terms become more important. Simple models cannot take this ordering into account.

1.2.1 Modified Quasichemical Model (MQM)

In the present work the MQM was used to model the liquid phase in the binary and ternary systems. The model has been described in detail by Pelton and co-workers [Pelton, Decterov, Eriksson, Robelin, and Dessureault (2000); Pelton and Chartrand (2001); Chartrand and Pelton (2001); Pelton, Chartrand, and Eriksson (2001)]. A brief summary of this model is presented here.

In the MQM in the pair approximation, the following pair exchange reaction between atoms *A* and *B* on neighboring lattice sites is considered

$$(A-A)+(B-B)=2(A-B); \qquad \Delta g_{AB} \tag{1.2.6}$$

where $(i-j)$ represents a first-nearest-neighbor pair. The non-configurational Gibbs energy change for the formation of two moles of $(A-B)$ pairs is Δg_{AB}.

In a binary silicate melt such as MO-SiO_2, one might identify the "A" and "B" particles with M and Si which mix on a cationic quasi-lattice. The tendency to ordering through the preferential formation of A-B pairs could then be identified with the formation of orthosilicate ions and the resultant creation of second-nearest neighbour A-B pairs. At the orthosilicate composition, M_2SiO_4, a completely ordered solution could be considered to consist of only M^{2+} cations and SiO_4^{4-} anions. This is equivalent to saying that there are only M-Si and no Si-Si or M-M second-nearest neighbour pairs. A B-B pair would be identified as a Si-Si second-nearest neighbour pair joined by an "oxygen bridge", and a A-A pair is an M^{2+}-M^{2+} second-nearest neighbour pair separated by an O^{2-} ion.

However, it must be stressed that the modified quasichemical theory as presented by Pelton and co-workers is not intended as a complete theory of silicate or slag (or any other liquid oxide phase) structure but as a mathematical formalism capable of reflecting structural changes in a solution. The model must has advantages of simplicity and generality and the characteristics required for relatively reliable interpolations and extrapolations.

Let n_A and n_B be the number of moles of A and B, n_{ij} be the number of moles of $(i-j)$ pairs, and Z_A and Z_B be the coordination numbers of A and B. The pair fractions, mole fractions, and "coordination-equivalent" fractions are defined respectively as:

$$X_{ij} = n_{ij}/(n_{AA}+n_{BB}+n_{AB}) \tag{1.2.7}$$

$$X_A = n_A/(n_A+n_B) = 1-X_B \tag{1.2.8}$$

$$Y_A = Z_A n_A/(Z_A n_A + Z_B n_B) = Z_A X_A/(Z_A X_A + Z_B X_B) = 1-Y_B \tag{1.2.9}$$

The following equations may be written:

$$Z_A X_A = 2n_{AA} + n_{AB} \tag{1.2.10}$$

$$Z_B X_B = 2n_{BB} + n_{AB} \tag{1.2.11}$$

The Gibbs energy of the solution is given by:

$$G^m = \left(n_A g_A^\circ + n_B g_B^\circ\right) - T\Delta S^{\text{config}} + \left(n_{AB}/2\right)\Delta g_{AB} \tag{1.2.12}$$

$$= \left(n_A g_A^\circ + n_B g_B^\circ \right) - T\Delta S^{\text{config}} + g^E$$

(1.2.13)

where g_A° and g_B° are the molar Gibbs energies of the pure components and ΔS^{config} is the configurational entropy of mixing given by randomly distributing the $(A-A)$, $(B-B)$ and $(A-B)$ pairs in the one-dimensional Ising approximation:

$$\begin{aligned} \Delta S^{\text{config}} &= -\text{R}\left(n_A \ln X_A + n_B \ln X_B \right) \\ &\quad -\text{R}\left[n_{AA} \ln\left(X_{AA}/Y_A^2 \right) + n_{BB} \ln\left(X_{BB}/Y_B^2 \right) + n_{AB} \ln\left(X_{AB}/2Y_A Y_B \right) \right] \end{aligned} \tag{1.2.14}$$

Δg_{AB} is expanded in terms of the pair fractions:

$$\Delta g_{AB} = \Delta g_{AB}^\circ + \sum_{i\geq 1} g_{AB}^{i0} X_{AA}^{i} + \sum_{j\geq 1} g_{AB}^{0j} X_{BB}^{j} \tag{1.2.15}$$

where Δg_{AB}°, g_{AB}^{i0} and g_{AB}^{0j} are the parameters of the model which may be functions of temperature.

The equilibrium pair distribution is calculated by setting

$$\left(\partial G/\partial n_{AB} \right)_{n_A, n_B} = 0 \tag{1.2.16}$$

(It should be noted that in the FactSage software pair fractions are calculated by Equilib module using the Gibbs energy minimization algorithm widely known as SOLGASMIX [Eriksson (1975)].

This gives the "equilibrium constant" for the "quasichemical reaction" of (Eq. 1):

$$\frac{X_{AB}^2}{X_{AA} X_{BB}} = 4 \exp\left(-\frac{\Delta g_{AB}}{\text{R}T} \right) \tag{1.2.17}$$

As Δg_{AB} becomes progressively more negative, the reaction (Eq. 1) is shifted progressively to the right, and the calculated enthalpy and configurational entropy of mixing assume, respectively, the negative "V" and "m" shapes characteristic of SRO.

The composition of maximum SRO is determined by the ratio of the coordination numbers Z_B/Z_A, as given by the following equations:

$$\frac{1}{Z_A} = \frac{1}{Z_{AA}^A}\left(\frac{2n_{AA}}{2n_{AA}+n_{AB}}\right) + \frac{1}{Z_{AB}^A}\left(\frac{n_{AB}}{2n_{AA}+n_{AB}}\right) \qquad (1.2.18)$$

$$\frac{1}{Z_B} = \frac{1}{Z_{BB}^B}\left(\frac{2n_{BB}}{2n_{BB}+n_{AB}}\right) + \frac{1}{Z_{BA}^B}\left(\frac{n_{AB}}{2n_{BB}+n_{AB}}\right) \qquad (1.2.19)$$

where Z_{AA}^A and Z_{AB}^A are the values of Z_A respectively when all the nearest neighbors of an A are A's, and when all nearest neighbors of an A are B's, and where Z_{BB}^B and Z_{BA}^B are defined similarly.

In the systems where composition of SRO is known experimentally the ratio Z_B/Z_A is fixed by that value. For example, in the binary CaO-SiO_2 system, ordering is observed about X_{SiO2} (mole fraction) = 1/3. This ordering is generally attributed to the formation of othrosilicate ions. This fixes the Z_{Ca}/Z_{Si} to 1/2. Although the model is sensitive to the ratio of the coordination numbers, it is less sensitive to their absolute values. It must be noted that the use of the one-dimensional

Ising model in Eq. 1.2.14 introduces a mathematical approximation into the model. The $\Delta S^{\text{config}} = 0$, only when $\Delta g_{AB} = -\infty$ and $Z_A=Z_B=2$. Therefore, for highly ordered solutions like liquid silicates (where $\Delta g_{AB} << 0$), better results are expected if coordination numbers equal to 2 are used. However, $Z_A=Z_B=2$ will reproduce SRO at 50 mole% composition. To reproduce SRO at the desired composition, absolute values of Z_A and Z_B are chosen with the additional condition, along with the one that they should be closest to 2, that ΔS^{config} approaches zero when Δg_{AB} approaches $-\infty$. Pelton and Blander (1984) presented a detailed description on the choice of these coordination numbers. In the CaO-SiO_2 system, with this additional condition, the absolute value of Z_{Ca} is 1.37744375 and of Z_{Si} is 2.75488750. These values will reproduce SRO close to X_{SiO2} (mole fraction) = 1/3.

Recently, Saulov (Saulov, 2007) pointed out some issues which may provide a useful note of caution in the use of the MQM. Pelton and Chartrand (Pelton and Chartrand, 2007) replied on these issues that they rarely cause any problem in real systems. Saulov's issue on the stability calculations of the Gibbs energy of a solution phase by the MQM is due to the use of improbable and physically unlikely values of the quasichemical parameter Δg_{AB}. Saulov's suggestions on the use of coordination number as a function of mole fraction and the use of splines for the Gibbs energy of the quasichemical reaction are not of any particular advantages and their usage result in mathematically cumbersome expansions. Use of splines may be useful for binary systems, but then a simple general equation for multicomponent systems could not be written.

1.2.2 Charge compensation effect

Chartrand and Pelton (1999) reported that the assumptions of the MQM were inadequate in the case of Na_2O-Al_2O_3-SiO_2 solutions. They listed two features based on which model needed to be improved. The first feature was the liquidus of mullite in Fig. 1.2.1. This liquidus descends very steeply from the SiO_2-Al_2O_3 binary system to the SiO_2-$NaAlO_2$ join. This shows that liquid SiO_2-Al_2O_3 solutions are very strongly stabilized by the addition of Na_2O up to a molar Na:Al ratio of 1:l. The second feature was the liquidus along the SiO_2-$NaAlO_2$ join (Fig. 1.2.2, between the SiO_2 and $NaAlSi_3O_8$ phases). In the limit as X_{SiO2} approaches 1, the limiting slope of the SiO_2-liquidus is given by Raoult's law as:

$$\lim_{X_{SiO_2}\to 1} \frac{dX_{SiO_2}}{dT} = \frac{\Delta h^0_{f(SiO_2)}}{\nu R T^2_{fus(SiO_2)}}$$

where $\Delta h^0_{f(SiO_2)}$ and $T_{fus(SiO_2)}$ are the enthalpy and temperature of fusion of SiO_2 and ν is the number of moles of independent atoms or ions introduced per mole of $NaAlO_2$ (or of $NaAlSi_3O_8$). The experimental points in Fig. 1.2.2 show that the limiting liquidus slope corresponds closely to ν = 1. That is, Na^{+1} and Al^{+3} enter into solution as $(NaAl)^{+4}$ associates. The simple quasichemical model, however, predicts ν = 2 in the limit as X_{SiO2} approaches 1.

Chartrand and Pelton (1999) reported that the above observations arise from a "charge compensation effect". They explained it as the replacement of Si^{+4} in the silica network by $(NaAl)^{+4}$ associates. The dissolution of alumina in silica by the replacement of Si^{+4} in the tetrahedral network by Al^{+3} is energetically unfavourable because it results in a negative charge centre. However, upon addition of Na_2O this negative charge can be compensated by a Na^+ ion

placed next to the aluminum as illustrated in Fig. 1.2.3. Hence, the addition of Na_2O, up to a Na:Al ratio of 1:1, decreases the Gibbs energy of the solution markedly. To model this effect, Chartrand and Pelton (1999) considered the $(NaAl)^{+4}$ associates to be a separate species. The ternary solution is then formally treated as a quaternary solution with components $NaO_{1/2}$, $AlO_{3/2}$, SiO_2 and $(NaAl)O_2$ where the mole fraction X_{NaAlO2} gives the concentration of the $(NaAl)^{+4}$ associates, while $X_{NaO1/2}$ and $X_{AlO3/2}$ are the concentrations of "free" Na and Al. The formation of the $(NaAl)^{+4}$ associates is formally treated through the Gibbs energy change of the following reaction among the components:

$NaO_{1/2} + AlO_{3/2} = (NaAl)O_2$;

$$g^0_{(NaAlO2)} = g^0_{(NaO1/2)} + g^0_{(Al2O3)} + \Delta g^0_{(NaAlO2)}$$

where, $g^0_{(NaAlO2)}$ is the standard Gibbs energy of the hypothetical pure component $(NaAl)O_2$. During optimization, the $\Delta g^0_{(NaAlO2)}$ was fixed by assuming a reasonable value which make the $(NaAl)^{+4}$ associates practically unstable in the binary Na_2O-Al_2O_3 system.

The Gibbs energies of formation of the following second-nearest-neighbors pairs were also introduced so that $(NaAl)^{+4}$ associates can be stabilized in the SiO_2-rich region of the liquid solution (where the silica network is present).

(Si + Si) + (NaAl-NaAl) = 2(NaAl-Si); $\Delta g^0_{(NaAl)Si}$

(Al-Al) + (NaAl-NaAl) = 2(NaAl-Al); $\Delta g^0_{(NaAl)Al}$

(Na-Na) + (NaAl-NaAl) = 2(NaAl-Na); $\Delta g^0_{(NaAl)Na}$

These Gibbs energies of formation were model parameters obtained by simultaneous optimization of all the available data.

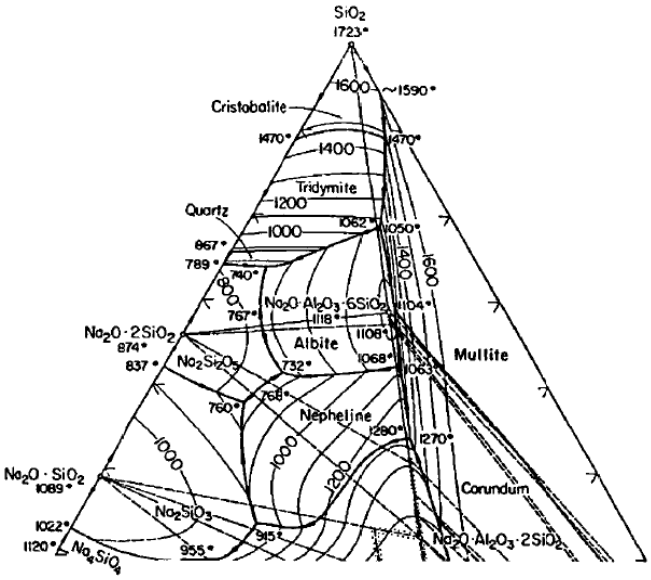

Fig. 1.2.1 Experimentally determined liquidus surface of the Na_2O-Al_2O_3-SiO_2 system in the SiO_2-rich region (reproduced from (Chartrand and Pelton, 1999)).

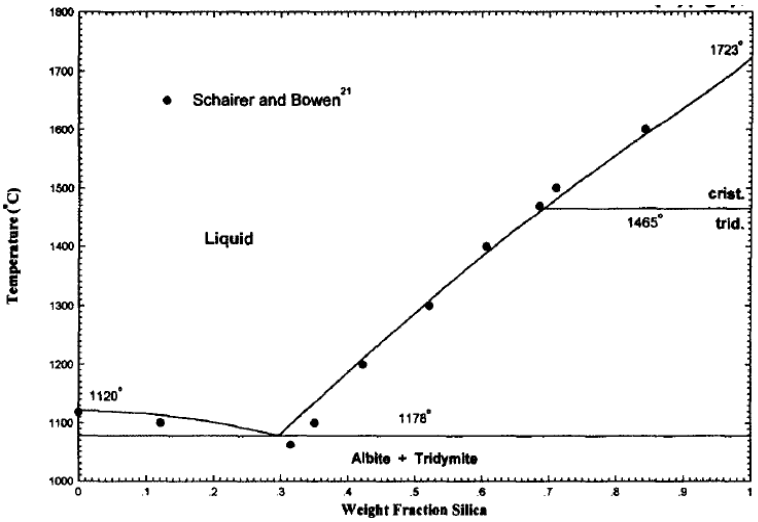

Fig. 1.2.2 Calculated liquidus surface along the $NaAlSi_3O_8$-SiO_2 join compared with experimental data (reproduced from (Chartrand and Pelton, 1999)).

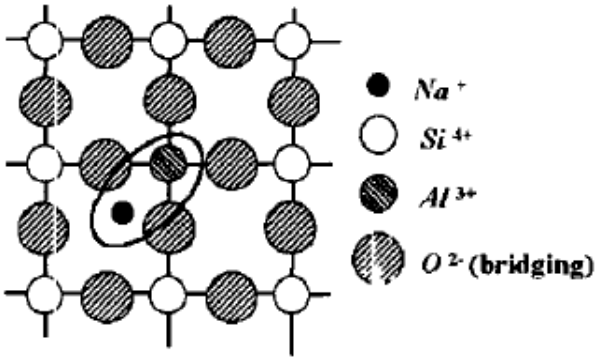

Fig. 1.2.3 A simplified two-dimensional representation of the charge compensation effect in the SiO_2-rich melts (reproduced from (Chartrand and Pelton, 1999)).

1.2.3 Thermodynamic modeling of solids

Solid phases appear in phase diagrams as stoichiometric compounds, terminal solid solutions or stoichiometric compounds with ranges of homogeneity. Sometimes some compounds have such a large homogeneity range that they are called solutions with specific names.

The Gibbs energy function for any stoichiometric phase A_xB_y per mole of atoms is represented as:

$$g^{A_xB_y}(T) = \frac{x}{x+y}\ g_A^0 + \frac{y}{x+y}\ g_B^0 + \Delta H_T - T\Delta S_T \qquad (1.2.20)$$

where ΔH_T and ΔS_T are the enthalpy and entropy of formation of the compound from the states *i* and *j* of elements A and B respectively.

The terminal solid solutions appearing in a binary system are usually treated with a random-mixing single-sublattice model. As the name suggests, this model assumes the random mixing of the atoms, one randomly replacing the other by substitution on lattice sites. The Gibbs energy of such a solution in which atoms A and B replace each other on lattice sites is given as:

$$G^m = (x\ g_A^0 + x_B\ g_B^0) + RT[x_A \ln x_A + x_B \ln x_B] + g^E \qquad (1.2.21)$$

Where, $G^E = \sum q_{AB}^{ij} (X_A)^i (X_B)^j$ and q_{AB}^{ij} are the model parameters.

The phases with two or more sublattices exhibiting ranges of homogeneity are modeled using sublattice models. The sublattice model with random-mixing on each sublattice in its most general form is called as Compound Energy Formalism (CEF). This formalism was advanced by Hillert who has given a detailed description (Hillert, 2000). In the CEF, the Gibbs energy per mole of solution in the compound $(A, B)_P\ (D,E)_Q$ is given by;

$$\begin{aligned} G = {} & y_A y_D G_{A:D} + y_A y_E G_{A:E} + y_B y_D G_{B:D} + y_B^a y_E^b G_{B:E} + PRT\left(y_A \ln y_A + y_B \ln y_B\right) + \\ & QRT\left(y_D \ln y_D + y_E \ln y_E\right) + \left(\sum_{k=D,E} y_A y_B y_k L_{AB:k} + \sum_{k=A,B} y_k y_D y_E L_{k:DE}\right) \end{aligned} \qquad (1.2.22)$$

where, P and Q are the number of sites in each sublattice.

In the CEF the atoms are assumed to mix randomly on each sublattice. The interactions between the atoms on different sublattices are taken into account by the Gibbs energy of end members $G_{i:j}$, and interactions among the atoms on the same sublattice is taken into account by excess terms (the last term in the above equation). The Gibbs energy of end members $G_{i:j}$ and excess parameters $L_{ij:k}$ are the model parameters.

1.2.4 Extension to a ternary system from binary systems

To estimate the excess Gibbs energy of a ternary solution from optimized binary model parameters, several "geometric" models have been proposed. Pelton (Pelton, 2001) presented a detailed description of these models. Some of these models are illustrated in Fig. 1.2.1 (reproduced from (Pelton, 2001)). In all of these models the excess Gibbs energy (g^E in Eq.1. 2.13) at any composition *p* can be estimated from the binary interaction parameters or the excess Gibbs energies of the binary sub-systems at points *a*, *b* and *c*. This excess Gibbs energy when the solution is modeled using the MQM is estimated as:

$$g^E = X_{12}\Delta g_{12}/2 + X_{13}\Delta g_{13}/2 + X_{23}\Delta g_{23}/2 + (ternary\ terms) \quad (1.2.23)$$

where Δg_{ij} is the Gibbs energy change for the reaction:

$$i\text{-}i + j\text{-}j = 2(i\text{-}j) \quad (1.2.24)$$

If ternary data are available, they can be used to estimate the ternary interactions. However, these terms should not be large, otherwise doubt is cast upon the predictive ability of the model. These ternary terms are identically zero in the three binary sub- systems.

The Kohler and Muggianu models in Fig. 1.2.1 are "symmetric" models, whereas the Kohler/Toop and Muggianu/Toop models in Fig. 1.2.1 are "asymmetric" models inasmuch as one component is singled out. An asymmetric model is more physically reasonable than a symmetric model if component 2 and 3 are chemically similar while component 1 is chemically different. When g^E is large and Δg_{ij} depends strongly upon composition, a symmetric model and an

asymmetric model will give very different results. Pelton (Pelton, 2001) showed that improper use of these models can lead to thermodynamically inconsistent and unjustifiable results.

Pelton and Chartrand (Pelton and Chartrand, 2001) presented a detailed description of the estimation of the excess Gibbs energies in a ternary solution from binary model parameters when the MQM is used to model the liquid phase. If the data for the three binary subsystems of a ternary system have been optimized and the parameters are in the form of Eq. 1.2.15, when a symmetric Kohler-type approximation is chosen for the 1-2 subsystem, then Δg_{12} can be written:

$$\Delta g_{12} = \Delta g_{12}^{0} + \sum_{1\le(i+j)} g_{12}^{ij} \left(\frac{X_{11}}{X_{11}+X_{12}+X_{22}} \right)^{i} \left(\frac{X_{22}}{X_{11}+X_{12}+X_{22}} \right)^{j} \qquad (1.2.25)$$

If a Toop-type approximation is chosen, then Δg_{12} can be written:

$$\Delta g_{12} = \Delta g_{12}^{0} + \sum_{1\le(i+j)} g_{12}^{ij} X_{11}^{i} \left(X_{22} + X_{23} + X_{33} \right)^{j} \qquad (1.2.26)$$

The form of these expressions was chosen because in the limit of a very small degree of short-range ordering they reduce to the well-known Kohler and Kohler-Toop approximations with the Bragg-Williams random-mixing model.

The FactSage^{TM} thermodynamic software (FactSage, 2008) allows users to use any of these "geometric models" to increase the flexibility and the ability to estimate the Gibbs energy of ternary or multicomponent solutions from the optimized lower-order parameters.

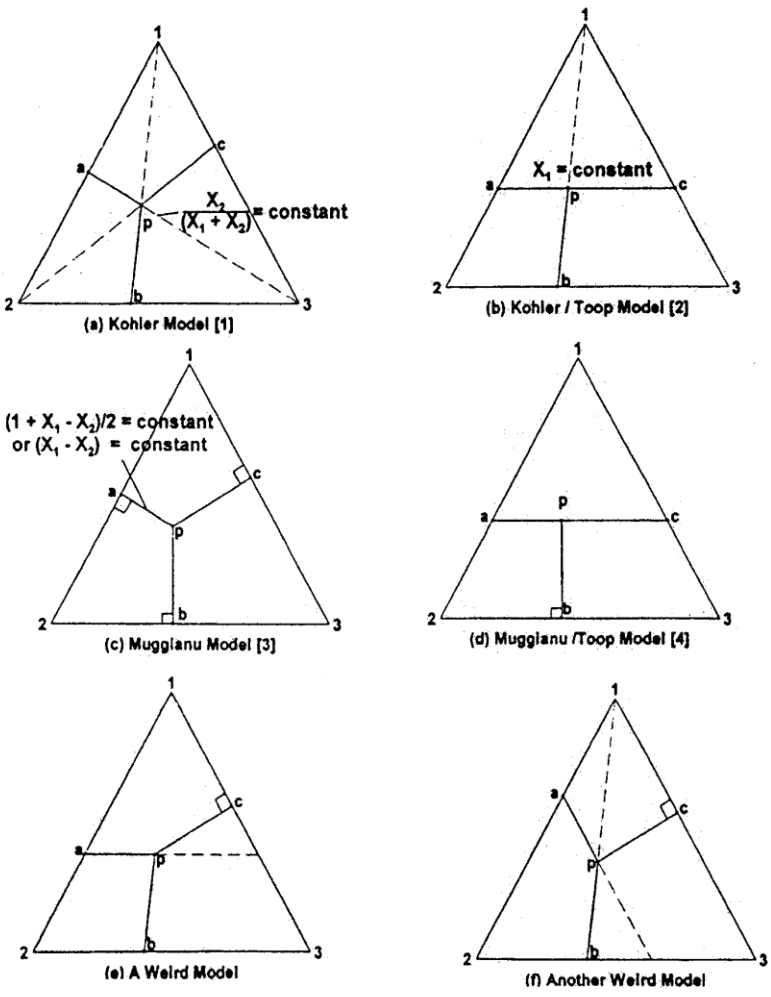

Fig. 1.2.4 Some geometric models for estimating ternary thermodynamic properties from the optimized binary data (reproduced from Pelton, 2001).

1.2.5 Predictions using only binary parameters

The choice of a model must be based not only on how well it reproduces data in binary systems, but also on how well it predicts and represents properties of ternary solutions. Pelton and Kang (Pelton and Kang, 2007) showed how the MQM generally predicts better the property of ternary solutions from the optimized model parameters than does the random-mixing model.

In a ternary system A-B-C in which the binary solution A-B exhibits a strong tendency to short-range ordering, while the B-C and C-A binary solutions are closer to ideality, positive deviations from ideal mixing behavior will be observed, centered along the A_xB_y-C join where A_xB_y is the binary composition of maximum short-range ordering . If the ordering in the A-B system is sufficiently large, then a miscibility gap is observed along the A_xB_y-C join. Such positive deviations are expected because the addition of C atoms breaks the energetically favored A-B pairs, and consequently the solution tends to maximize the number of A-B pairs by separating into A_xB_y-rich and C-rich solutions.

A Bragg-Williams model overestimates the positive deviations observed in such ternary systems. In fact, it may predict a miscibility gap when there is none experimentally observed. An associate model [(Luck, Gerling and Predel (1989); (Pelton and Kang, 2007)] in which the short-range ordering in the A-B binary solution is modeled as being due to A_xB_y molecules or associates, will not at all predict such deviations. The associate model simply predicts that, along the A_xB_y-C

join, the solution is an ideal mixture of A_xB_y associates and C atoms. The MQM, with proper choice of coordination numbers, predicts better such positive deviations along the A_xB_y-C join.

Pelton and Kang (Pelton and Kang, 2007) also showed that usually the MQM better predicts extensions of binary miscibility gaps into a ternary system. A miscibility gap in a binary liquid phase modeled using the MQM is much flatter with a comparatively lower consolute temperature than is obtained by a random-mixing model. As a result, the MQM predicts a smaller extension of a binary miscibility gap into a ternary system.

1.3 Experimental techniques for phase diagram determination

The different methods used in phase diagram determination involve procedures for examining the phase reactions and identifying the phases present. The experimental techniques used in phase equilibria studies can be divided into two main groups: dynamic and static methods. The dynamic method is based on the measurement of property change that occurs as the system is undergoing a phase transformation. Changes in several properties of a sample can be observed at the critical point of phase transformation. The most widely used dynamic techniques are thermal analysis (TA), differential thermal analysis (DTA), differential scanning calorimetry (DSC) and thermogravimetric analysis (TGA). These techniques are more accurate in those systems where equilibrium is readily obtained. The static methods are based on the *in situ* measurement of a property of a sample at the equilibrium state. In these techniques, all potentials of the systems are fixed until equilibrium is achieved, after which the sample is examined by chemical analysis, X-

ray diffraction (XRD) or metallography. These methods are more appropriate where reactions are slow.

Most phase diagrams are constructed by using of phase equilibria and property change data obtained by a variety of experimental methods. Invariably, there are differences between the data obtained from various investigations. There are no fixed rules that can be used to decide which data are to be preferred. However, there are several factors that are generally important in the experimental determination of phase equilibrium relations, such as:

1) Starting materials should be of high purity. Impurities can greatly influence phase equilibria.
2) The area of contact among the constituents in starting materials should be maximized. Thorough mixing of fine-particle starting materials aids in the rapid attainment of equilibrium.
3) Sufficient time must be allowed at a given temperature to attain equilibrium.
4) The presence of a liquid phase promotes attainment of equilibrium. For this purpose, a lower liquid viscosity is more effective than a higher.

Thus, apart from these general factors, there are many specific conditions relevant in the evaluation of the reliability of a particular experimental technique used for phase diagram determination. In the following pages, the main experimental techniques used in oxide phase diagram determination, their advantages and disadvantages, and the evaluation criteria are discussed.

1.3.1 Annealing and quenching techniques

These techniques are widely applied wherever reactions and phase transformations are quite slow and long times are required to reach equilibrium. This technique is applied to especially silicate and other ceramic melts as they are highly viscous and crystallize very slowly. In this technique, the compositions to be studied are equilibrated at a particular temperature, after which samples are quenched. Microscopic examination, XRD or chemical analyses of these samples then identify the phases present and their composition.

The first step in this technique is the preparation of the sample and its homogenization. Extreme care should be taken in the selection of starting materials if accurate composition is to be obtained. For example, the use of alkali oxides and La_2O_3 should be avoided because they form carbonates or hydrolyze in contact with the atmosphere. Similarly, it should be ascertained whether cations present in the starting materials can exist in different oxidation states. For example, wustite (ferrous oxide) does not have the composition FeO, CrO_2 loses oxygen on standing, and the composition of praseodymium, cerium, and terbium oxides depend upon their previous heat treatment and vary between $REO_{1.5}$ and REO_2 (RE=Rare Earth). If the pure component has a high vapor pressure, like PbO, then a significant amount of mass can be lost during equilibration.

After the starting materials are selected, attainment of equilibrium is favoured by treatment in several pre-processing steps such as precalcination, mixing, grinding, master slag formation etc.

Important here is the homogenization of the starting materials, in order to ensure uniform microstructures. They are homogenized by firing at high temperatures and then grinding. To obtain good homogenization, firings and grindings are repeated several times. Here it should be noted that firing is performed below the subsolidus temperature. If a liquid phase forms, then crystals will separate from the liquid and result in inhomogeneity. This may persist even after grinding to a powder. Sometimes high melting oxides like silica make attainment of equilibrium difficult to achieve. In such cases high melting oxide mixtures are pre-treated by melting them at lower temperatures and then rapidly cooled. These intermediate glassy master slags can then be used to prepare final mixtures for high-temperature equilibration.

After homogenization, samples are equilibrated for phase equilibria studies. The selection of crucibles used in this step is quite important. At these high temperatures sample reaction with the crucible material should be avoided; otherwise, the data obtained may be erroneous. Usually, platinum and iridium crucibles are used up to 2000 ºC. However, if samples contain transition-metal ions, these ions can diffuse into the crucible material. Therefore, for samples containing transition-metal ions or for higher temperatures, crucibles made of refractory oxides like Al_2O_3 or ZrO_2, or refractory metals like tungsten, molybdenum, or tantalum are used. The refractory ceramic materials are not used when corrosive slags are under study. Platinum is suitable for oxidizing conditions; molybdenum and iron can be used in reducing or neutral gas atmospheres. However, despite these precautions, a final check should be performed for interaction between the sample and crucible. The material and thickness of the crucible also greatly affects the cooling rate, as it is the crucible material that first contacts the quenching medium.

Along with the material used in the crucible, its design is important in the annealing and quenching techniques because it is the crucible which comes in first contact with the quenching medium. Some of these designs are shown in Fig. 1.3.1. In crucibles the sample mass used is typically in the range of 1-50 g enabling convenient wet chemical analysis to be undertaken. In contrast, the slag mass used with envelopes and open support systems (Fig. 1.3.1) is of the order of 0.1 g or less. Open support systems use surface tension to hold the slag on the outside of the metal or compound substrate. On quenching, the slag comes into direct contact with the quenching medium resulting in rapid cooling. Normally the support is made of inert material or a primary phase material. This enables isothermal single-phase and multi-phase saturation experiments to be undertaken in those systems in which a suitable crucible material is not available. Thus, open support systems are advisable both where very high quenching rates are required and where some of the components are highly reactive and a suitable crucible material cannot be found. When reaction with crucibles is unavoidable, an electromagnetic levitation of metal drops can be used. In this case, slag is attached to the metal through surface tension forces. The principal difficulty in this technique is to obtain the levitation power, temperature ranges and stable temperature control. The temperature of the slag phase in this arrangement is determined indirectly through the metal droplet.

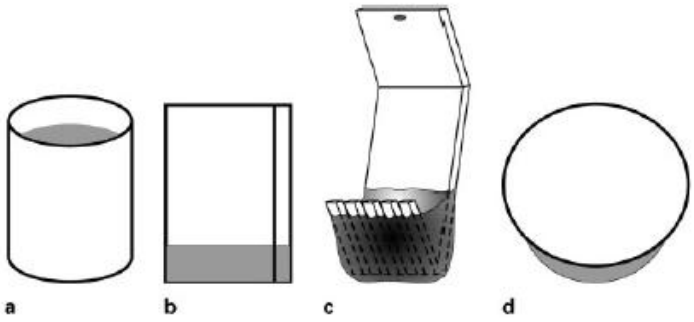

a crucible, metal, ceramic; *b* envelope, metal, ceramic; *c* open support, metal, primary phase; *d* levitated metal drop, metal

Fig. 1.3.1 Design of crucibles to support samples for slag phase equilibria determination [Jak and Hayes, 2004].

The very important step in quenching and annealing techniques is to decide the heating regime for the sample for equilibration. The time and thermal treatment required to achieve equilibrium depends upon the particular reaction system and conditions. For example, a peritectic reaction is quite slow because of diffusion from the primary phase for precipitation of the secondary phase. To avoid this slow diffusion, premelting can be done at high temperature where there is only liquid and then quenched to glass. This glass can then be equilibrated at the temperature of interest and the equilibrium phase can be obtained from metastable liquid. Otherwise, for melts having high viscosities and very low rates of crystallization a premelting temperature below the liquidus can be chosen. This will precipitate some primary phase which acts as seeds for further crystallization and reduces the time to achieve equilibrium.

If sufficient experiments have been performed on the system then the final results can be judged on the basis of consistency. There are also many other specific criteria. Results can be monitored

as a function of time allotted to reach equilibrium. A metastable equilibrium which persists long enough can lead to erroneous conclusions. In this case, the sample should be equilibrated a second time. If the result does not change with second and subsequent equilibrations, it can be assumed that equilibrium has been achieved. The sample microstructure where equilibrium has been achieved shows uniformity in the distribution of phases and an absence of corroded crystals. In attaining equilibrium, it is good practice to approach equilibrium from both sides of the chosen composition. For example, a liquid of a given composition could be quenched from above the liquidus temperature and, also a sample of the same composition could be fired at sub-solidus temperatures. These two samples then could be equilibrated at the temperature of interest; if they show same results then it can be concluded with greater confidence that equilibrium has been achieved. Of course, this technique requires at least an approximate knowledge of liquidus and solidus temperatures.

After equilibration, the sample is then quenched for further examination. Quenching should be as rapid as possible to “freeze-in” the phases present at the equilibration temperature and to avoid diffusion. In the case of slags, water or brine is used as quenching medium. Liquid nitrogen can also be used in this case; however this results in the formation of a protective nitrogen gas atmosphere which affects the heat transfer and cooling rate. Nevertheless, liquid nitrogen is used as quenching medium where it is necessary to protect the outer layer of the sample from oxidation. There are other techniques for rapid solidification such as spinning wheels and piston and anvil devices. Moving surface devices such as the spinning wheel are suitable for low viscosity melts like metals and not for high viscosity ceramic melts.

After quenching, samples are characterized with techniques like XRD, optical microscopy or chemical analysis like EPMA. Sometimes even simple visual inspection provides useful information about phases in the quenched samples. If grains of different phases are sufficiently large and the phases are of different colors then the sample appears spotted. A small amount of colored phase which cannot be detected by XRD can be visually inspected. At temperatures below the liquidus and above the solidus, the sample may exhibit a slight rounding of sharp edges or sticking to the sample container. The presence of significant cracking and crumbling signifies the existence of an "unquenchable" phase transition. Optical microscopy is widely used to identify small amounts of a second phase. Samples quenched above the liquidus will not show the presence of crystalline phases but the samples below the liquidus will do so. The presence of rounded, corroded, or poorly distributed crystals indicates that equilibrium might have not been reached. XRD is often the most satisfactory method to identify the phases in the quenched samples.

One of the disadvantages of using this technique is that it is very difficult to find the exact temperature of phase transformation. Normally, this technique allows investigator to bracket the values instead of giving the exact temperature of transformation. It is a common assumption that during quenching all the phases present at equilibrium are "frozen-in", i.e., there is no change in phase assemblage. However, cases have been found, especially in metals, where the high-temperature phases cannot be retained while quenching and undergo decomposition or transformation. In such cases use of this technique alone will lead to erroneous results. This

problem can be avoided by using hot stage microscopy or high-temperature XRD where samples are examined at high temperatures without quenching.

1.3.2 Segregation method for liquidus determination

This is a static method in which liquid of a given composition is held at a particular temperature T_x in Fig. 1.3.2, for a sufficient time for equilibrium to be established. Once the equilibrium has been established, the solid and liquid phases separate due to density differences. Here it must be ensured that equilibrium has been achieved by annealing the samples for different times at a given temperature. If the solid sinks, then a liquid sample may be drawn off using a ceramic suction tube; if it floats, then appropriate devices and methods are available to draw the liquid from beneath the surface. If there is only a very small density difference between solid and liquid, centrifuging can separate them. After separation of the phases, they are analyzed for their chemical compositions.

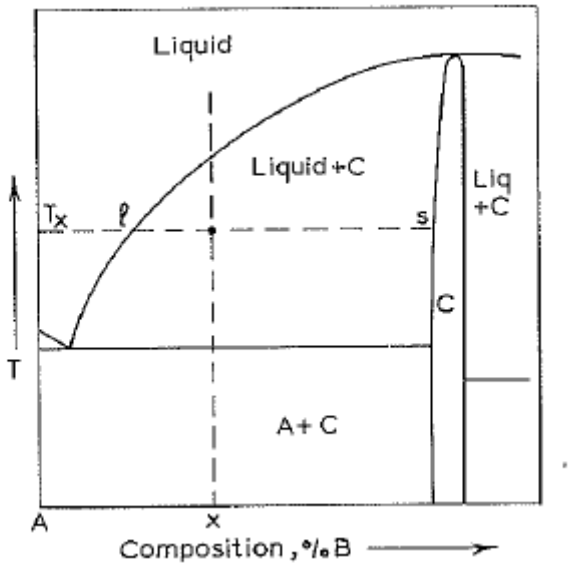

Fig. 1.3.2 The principle of the segregation method for investigating liquidus curves [Raynor, 1976].

This method is especially useful in determining steep liquidus where thermal analysis gives faulty results. An additional advantage of this method is that chemical analysis of the sample is done after the achievement of equilibrium; thus changes in bulk composition at high temperature do not affect the final results. However, feasibility of this method depends upon the accuracy of a clean separation of the liquid sample. The most common source of error here is the removal of small particles of solid along with the liquid, and this error becomes more probable as the density difference between solid and liquid becomes smaller.

1.3.3 Isothermal equilibration/quenching/microanalysis technique

This static technique is similar to quenching/annealing, but equilibration is done deliberately at subliquidus temperature as in the segregation method. Therefore this technique can be said to be a combination of quenching/annealing and segregation. Thus a bulk composition x is first isothermally equilibrated and then quenched. Analysis of the sample is performed by accurate electron probe X-ray microanalysis (EPMA). This method has been recently extensively used by Jak and Hayes [Jak and Hayes, 2004] for many oxide phase equilibria determinations. They have pointed out that many of the earlier techniques for oxide phase determination where isocompositional, which required the difficult task of controlling bulk sample composition at high temperature. Earlier studies were mainly based principally on annealing/quenching techniques which provided results that can only be bracketed to obtain solidus and liquidus. In the later method, unique values of solidus and liquidus data are obtained by EPMA analysis of the quenched sample. This method is especially useful in establishing the solidus where there is extensive solid solubility. Also, this method can be used to determine correctly phase equilibria accompanied by high vapor pressures, provided equilibrium between condensed phases have been reached. This method can be safely extended to double or multi-phase saturation without loss of accuracy. Thus, this approach greatly enhances the ability to provide accurate direct measurement of phase equilibria in complex multi-phase systems, and provides a wealth of important information on coexisting phases.

This technique differs in many respects from the conventional annealing/quenching techniques in phase characterization. After quenching, samples can be studied by XRD, optical microscopy and

other analytical methods. The application of modern EPMA techniques not only substantially increases analytical efficiency and accuracy but also provides important additional information.

EPMA analysis of a sample at a particular temperature provides liquidus and solidus data at that temperature. The same starting mixture can then be used at different temperatures to obtain the solidus and liquidus data at other temperatures. Moreover, the accuracy of EPMA is not dependent upon the minimum traceable amount present in the sample as it is in the case of XRD and DTA. In EPMA, any change in the bulk composition does not affect the final outcome, given that the sample remains in the same phase field. EPMA enables the glass composition to be measured as a function of position within the sample; therefore any inhomogeneity in the glass due to incomplete dissolution of one component or due to precipitation during quenching can be detected. Moreover coring can be detected in phases exhibiting solid solutions due to insufficient equilibration time.

In some cases, it is not possible to use EPMA alone to obtain an unequivocal identification of phases. For example, a compound may be present in more than one polymorphic form. In such cases, it is advisable to use other techniques like XRD or optical micrography to obtain a definite result.

1.3.4 Effect of oxygen partial pressure in oxide phase equilibria

Slag-gas equilibria play a very important role in phase diagram determination of oxides. In systems where each of the metal species exists in a single oxidation state the phase relations do not change with oxygen partial pressure of the system. However, transition metals, such as Fe, Mn, Ti and V can be present in more than one oxidation state. In slag systems containing these elements, the oxygen partial pressure of the system can have a significant effect on the liquidus temperatures and phase equilibria. One such example is presented by Kang and Lee [Kang and Lee, 2005] in the study of the MnO-SiO_2-TiO_2-Ti_2O_3 system. Mn and Ti are both transition metals and they have several valences in oxides; Mn^{+2}, Mn^{+3}, Mn^{+4}, Ti^{+2}, Ti^{+3} and Ti^{+4} depending on temperature, oxygen partial-pressure and phase in which they reside. Kang and Lee [Kang and Lee, 2005] studied the phase equilibria in the system by carefully controlling the oxygen partial pressure using a flowing CO/CO_2 gas mixture and CO with graphite holder. The results obtained by them at 1500 ºC and different oxygen partial pressures are shown in Fig. 1.3.3.

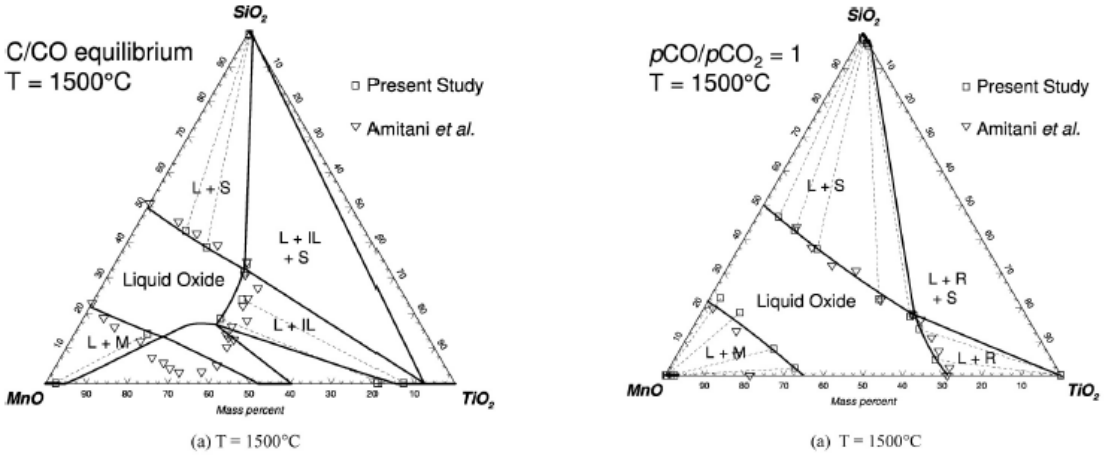

Fig. 1.3.3 Phase equilibrium data in the MnO-SiO_2-TiO_2 system at 1500 ºC under different oxygen partial pressure. [Kang and Lee, 2005].

Similarly, [Jak and Hayes, 2004] have shown the effect of oxygen partial pressure by FactSage calculations (Fig. 1.3.4) on the liquidus of the complex lead slag PbO-ZnO-FeO-Fe_2O_3-CaO-SiO_2. In this case the liquidus is displaced as much as 250 K in low lead slags for a change in oxygen partial pressure of six orders of magnitude. Jak and Hayes [Jak and Hayes, 2004] also reported that the difficulties in controlling the slag/gas phase equilibria are principal causes for inaccurate determination of many early experimental works on iron-containing slag systems. These difficulties include thermal segregation of gas mixtures, extensive equilibration times and problems in the control of gas ratios in dilute gas mixtures. For these reasons metal saturation techniques are normally preferred over gas equilibration.

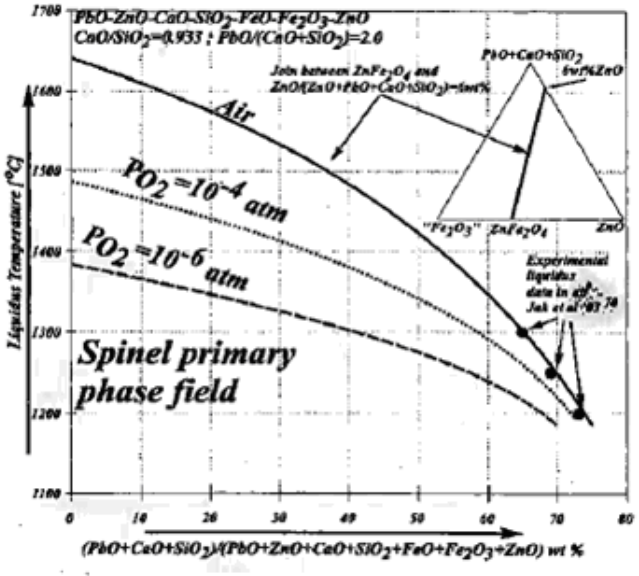

Fig. 1.3.4 The effect of oxygen partial pressure in oxide phase equilibria.

1.3.5 Equilibration/quenching/refractive index

This is a static technique mainly used by Hageman et al. [Hageman et al., 1986] for determination of liquid immiscibility in ceramic melts. This technique involves equilibration of the liquid sample at the temperature where demixing is to be measured and then quenching of the sample followed by refractive index measurement of the two separated glasses. Composition of the glasses is obtained from a standard refractive index curve drawn from the measurements, See Fig. 1.3.5 of the single phase liquid.

Hageman et al. [Hageman et al., 1986] have pointed out that thermal history of a sample often plays an important role in achieving the equilibrium. At temperatures close to the monotectic temperature, demixing is relatively fast and takes only a few minutes to reach equilibrium. In the vicinity of critical temperature, however if a low rate of heating is followed by short period of equilibration, the sample will not reach the equilibrium. For example, in the $CaO\text{-}SiO_2$ melt, in the lower region of demixing an equilibration time of 25-40 minutes is sufficient, whereas in the upper region of demixing an equilibration time of 60 minutes is required.

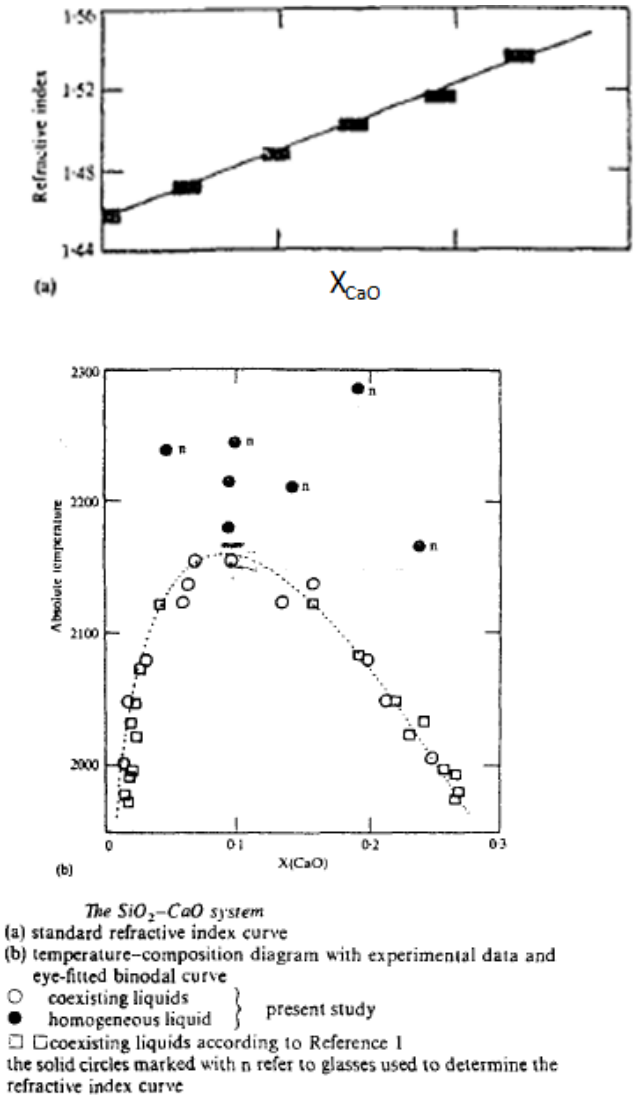

The SiO_2–CaO system
(a) standard refractive index curve
(b) temperature–composition diagram with experimental data and eye-fitted binodal curve
○ coexisting liquids } present study
● homogeneous liquid }
□ □coexisting liquids according to Reference 1
the solid circles marked with n refer to glasses used to determine the refractive index curve

Fig. 1.3.5 The miscibility gap in the CaO-SiO_2 system [Hageman et al., 1986].

1.3.6 X-ray diffraction techniques (XRD)

XRD techniques are based on the observation of the scattered intensity of an X-ray beam incident to a sample as a function of incident and scattered angle, polarization, and wavelength (energy). These techniques are used mainly qualitatively to identify the phases. The diffraction analysis will help in determining the number of phases present and the crystal structure of phases. In this

analysis, to identify a phase, it is necessary that an appreciable quantity is present so that its diffraction pattern can be obtained. XRD coupled with micrography are very powerful techniques to identify phases.

Apart from its qualitative use, XRD can be used quantitatively to determine the phase boundaries, e.g., solid solubility of one component into another or extent of immiscibility in a solid phase. These techniques include measurement of the lattice spacings, by XRD, of a number of alloys equilibrated at a particular temperature and then quenched. Of course, the assumption is made that no decomposition occurs during quenching. As the samples are analyzed after quenching, this technique can be classified as a static technique. In a single phase region lattice spacing varies continuously with the composition. In two-phase regions, the composition of two phases being constant, lattice spacing is also constant with composition. A typical lattice spacing *vs.* composition curve is shown in Fig. 1.3.6. The ***ab*** part of the curve is the lattice spacing in a single phase region. This is considered to be constant within the temperature range of the experiment. After this, the constant lattice spacings in two phase regions at different temperatures, parts ***bc*** and ***de***, are obtained. The intersection of the two parts of the curve gives the solubility limit. It is evident from Fig. 1.3.6 that points b (at T_H) and point d (at T_1) represent solid solubility limits. The accuracy of this method depends upon the accuracy with which the lattice-spacing *vs.* composition curve is measured and several precautions are necessary.

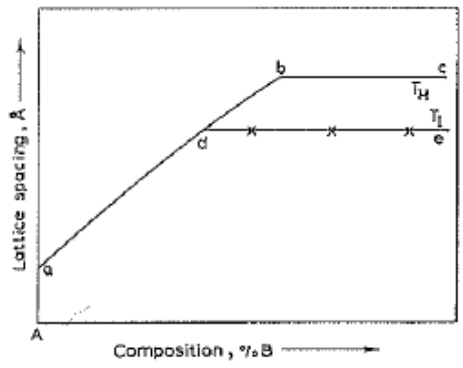

Fig. 1.3.6 Lattice spacing *vs.* composition curve for a binary system [Raynor, 1976].

The preparation of filings for final chemical analysis from the initial annealed and quenched ingots should be performed with utmost care. If filings are susceptible to contamination or oxidation, preparation should be done in an inert atmosphere. The adulteration of filings with carbonaceous material should be avoided by all means, otherwise, on subsequent annealing carbonaceous material is converted into carbon which interferes with chemical analysis. After preparation, filings must be annealed at the maximum possible temperature to relieve the stress introduced by the filing operation. From this stress-relieving temperature the filings are quenched and this, in certain cases, may cause quenching stress in the filings which may give slightly erroneous lattice spacings. The chemical analysis of the filings should be done at this stage because this analysis corresponds to filings which are actually exposed to X-rays.

The main advantage of this technique over micrographic and annealing/quenching techniques is that a single unique value is obtained for the solubility at a given temperature, whereas the other techniques give bracketed values.

During quantitative and qualitative application of XRD, the equilibrated samples are quenched and then exposed to X-rays. However, it is possible that the high-temperature phases cannot be retained during quenching. In such cases, samples maintained at high temperature are exposed to X-ray radiations and suitably protected from oxidation or contamination. This technique is usually called high-temperature XRD. The main difficulty when a diffractometer is used for high-temperature XRD is that of maintaining a uniform sample temperature (the sample is spread over a rather large area). This is avoided effectively by use of a spherical furnace which reduces thermal gradients and minimizes line broadening.

1.3.7 Thermal analysis

Thermal analysis is a non-isothermal dynamic technique whereby a sample is heated or cooled in a furnace, usually not exceeding 1 ºC per minute, through a transformation. Some property of the sample changes as a consequence of the transformation. Fig. 1.3.7 depicts the basic principle behind a thermoanalytical instrument. The temperature of the sample is measured by a calibrated recording thermocouple. This recorded temperature, when correlated with a change in property, leads to the determination of phase boundaries. For example, when a liquid sample is cooled, say, to the liquidus temperature, latent heat is evolved as crystallization starts. This produces a

thermal arrest which continues giving a constant temperature or a different slope to time-temperature plot until crystallization is complete. This time-temperature plots are shown in Fig. 1.3.8 where cooling curves at five compositions on a hypothetical binary system are shown. It can be seen that a slope change in temperature-time graph is an indication of a phase transformation. The first slope change in graphs 2 and 4 shows starting of solidification as the temperature of sample changes due to evolution of heat. The same constant temperature in graphs 2, 3 and 4 shows solidification has ceased and eutectic precipitation has started.

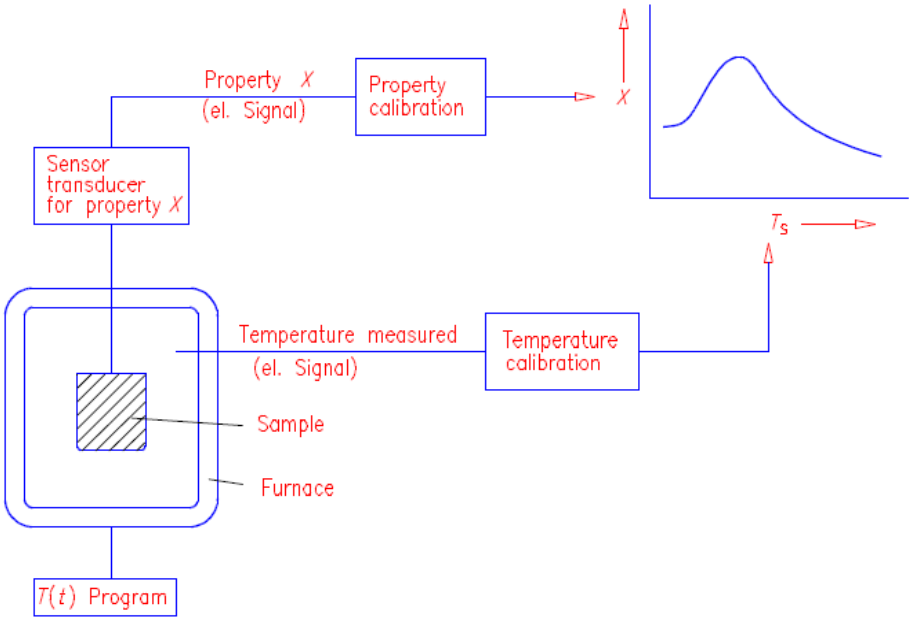

Fig. 1.3.7 Basic principle behind a thermoanalytical instrument [Hemminger and Sarge, 1999].

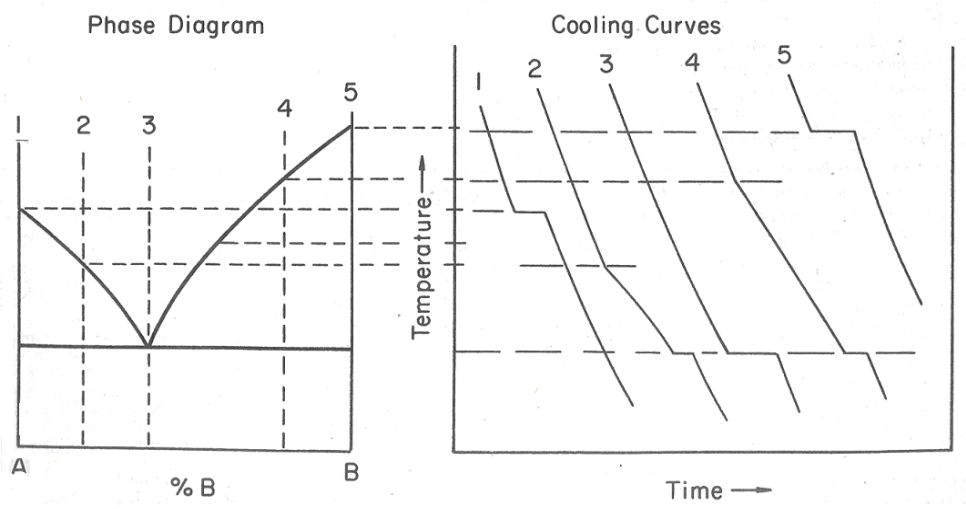

Fig. 1.3.8 Application of the cooling curve techniques for studying binary phase equilibria [Bergeron and Risbud, 1984].

A typical apparatus for such type of experiment consists of a dc amplifier to amplify the thermocouple signal and drive an XY recorder. Thermocouples are chosen to give the highest developed EMF consistent with their stability. Normally, large samples like 10 cm^3 in volume are used in this experiment. If it is necessary to protect the sample from oxidation by air then an inert or reducing atmosphere or sealed container is used.

It must be noted that the above temperature-time graphs are for hypothetical case to illustrate the concept. Here onset of a phase transformation is very clearly defined. The cooling curve obtained for a real experiment is compared with its ideal counterpart in Fig. 1.3.9. In a real experiment a degree of supercooling is invariably observed. The temperature of the sample, being cooled below the phase transformation during supercooling, rises again. However, at the liquidus, the

temperature never rises all the way back up to the liquidus. Therefore some kind of extrapolation technique must be used to estimate the liquidus temperature. At the eutectic it is possible to regain the eutectic temperature, given that a large quantity of sample is solidifying to yield a sufficient amount of heat. Supercooling may be minimized by stirring or by administration of mechanical shock of the sample to induce nucleation.

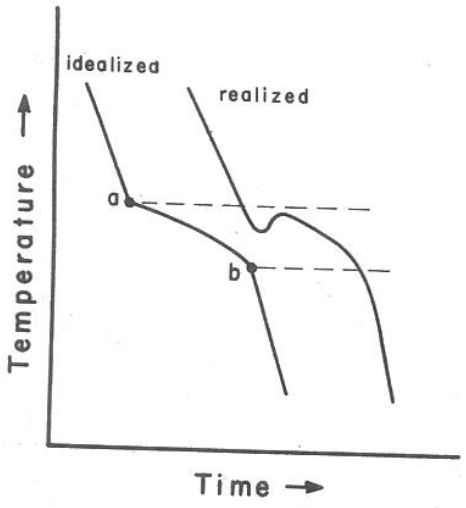

Fig. 1.3.9 Real temperature-time curve obtained in experiments with its ideal counterpart. [Pelton, 2001].

Another important factor in thermal analysis is that the sample should be kept at uniform temperature. Temperature gradients in the sample will cause a part of the sample to solidify before the rest and consequently a rounded slope will be detected. This uniformity of temperature can be ensured by constantly stirring the sample or by the use of a furnace with a good constant temperature zone or by bubbling a gas through the sample. Also, care should be taken for

volatilization or oxidation of the sample during repeated heating or cooling. If there is some sample loss or oxidation, the final composition of the sample cannot be taken as “weighed-out”.

Usually, for a steep liquidus, the cooling curve method returns lower liquidus temperature than the true behaviour. The amount of solid precipitated at a steep liquidus (by applying the lever rule) can be said to be comparatively small and hence a small amount of heat is evolved. Therefore, unless sufficient amount of solid precipitates at temperature lower than the liquidus temperature, phase change cannot be detected. Hence, thermal analysis is less precise for steep liquidus determination.

Solidus temperatures are less precisely determined by cooling curves especially if precipitated solid is a solution. If a solid solution is precipitated then the solid will contain composition gradients and solidification will not stop at the solidus temperature. Also, precipitated solid will insulate the thermocouple from the sample and, by the time solidus temperature is reached, the sample temperature will have lagged well behind the furnace temperature. Thus, cooling curves are not an appropriate technique to determine the solidus temperature. Solidus temperatures are often measured by annealing the solid solutions obtained from cooling curve experiments at maximum possible temperature and then using heating curves. Peritectic reactions are also not precisely measured by thermal arrest as they are kinetically hindered and require enough time for completion.

Normally, oxide phase equilibria are not usually precisely measured by thermal analysis. The viscosity of the liquid is very high and crystallization from such high-viscosity liquid proceeds with great difficulty, and accordingly, the attainment of equilibrium under such conditions requires excessively long periods of time.

A variation of thermal analysis technique is Differential Thermal Analysis (DTA). The principle behind DTA is measurement of the temperature difference between the sample of interest and a reference sample which is inert during a heating or cooling cycle and whose thermal behavior is accurately known. The sample and reference material are placed in separate chambers within a furnace and a thermocouple is then placed in both chambers directly in contact with the sample and connected in series. The differential obtained from the temperature difference at both the thermocouple is amplified by a suitable dc amplifier to attain a greatly increased sensitivity. Thus it is very useful in determining the temperatures for phase changes. One of the disadvantages of using DTA is that, because of large surface to volume ratio of the small samples used, sample temperatures often do not increase sufficiently after supercooling. Also, it is more difficult to avoid supercooling in DTA as the samples cannot be stirred. Fig. 1.3.10 shows a schematic representation of DTA measurement.

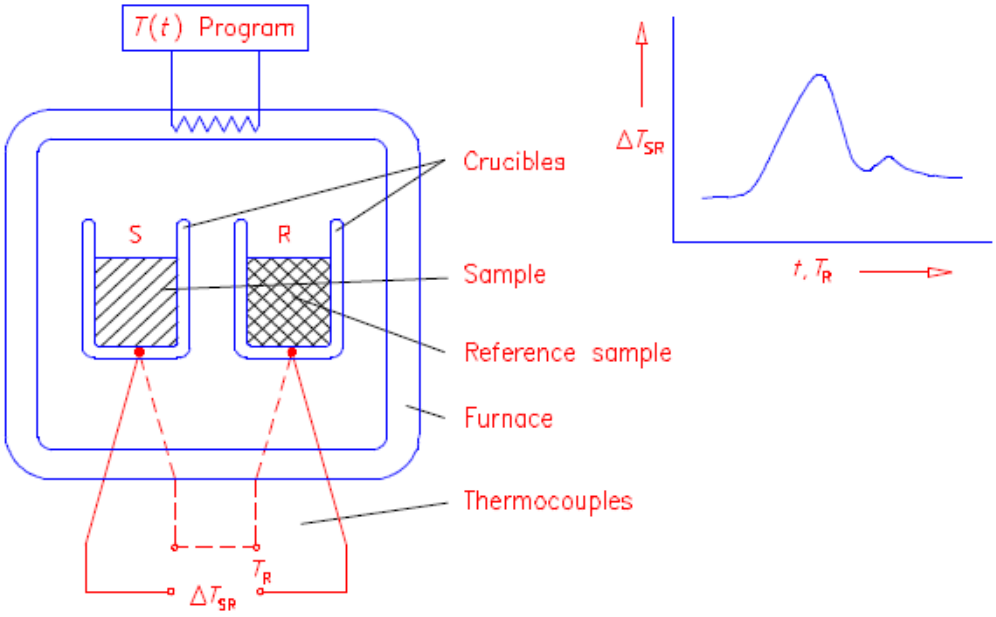

Fig. 1.3.10 Schematic representation of DTA measurement [Hemminger and Sarge, 1999].

1.4 Modus operandi for thermodynamic optimization

All the calculations and optimizations in the present work were performed with the FactSage™ thermochemical software. The various steps followed in the present work which collectively come under the CALPHAD approach were:

The binary systems to be optimized during the present work were identified.

Collection of data in the literature for the system:

All the data in the literature on the thermodynamic properties of the chosen systems were collected. These data were phase diagram data, thermodynamic properties like enthalpy of

mixing in a solution phase or enthalpy of formation for compounds, activity of constituents in a solution, *etc*. Sometimes data other than thermodynamic properties, such as magnetism or electrical conductivity, which can be helpful in evaluation of a system, were also collected. When enough data were not available in a lower-order binary system, data from a ternary system were used to deduce some necessary conclusions.

Selection of the appropriate thermodynamic model:

As stated previously, an adequate model representing the Gibbs energy functions for a phase is required. This is very important since a good physical model based on the structure of the phase increases the accuracy of predictions of solution properties in multicomponent systems. In the present work, the Modified Quasichemical Model (MQM) capable of taking into account ordering or clustering in the liquid phase was chosen. In the present work, the Gibbs energies of solid phases were written using formalisms presented by Eqs. 1.2.20-1.2.22. For this purpose, the crystal structures of the various solid phases were reviewed for proper distribution of components in different sublattices.

Critical evaluation of collected experimental data:

The experimental data by different authors were often found to differ from each other by more than the stated experimental error limits. Sometimes data were not thermodynamically consistent with each other. Therefore, all the available experimental data were evaluated on the basis of experimental techniques and thermodynamic consistency. When the accuracy of the experimental data was difficult to evaluate from the description of the experimental technique, their consistency or inconsistency was discernible during the simultaneous optimization of the data. Also, during evaluation of data it is very important to use original (raw) experimental data, not

the derived quantities. Mostly, the derived quantities have more error limits than the original data.

 # Optimization of model parameters for the system:

After evaluation of the experimental data, optimization was performed on the basis of selected reliable data to obtain the values of the model parameters. In this stage, optimization software, the OptiSage module in FactSage^{TM}, was quite useful.

OptiSage is an optimizer module which works on the principles of the Bayesian least squares technique. This module generates a consistent set of model parameters from a given set of experimental data which in turn are used to represent the Gibbs energies of phases. In simple words, OptiSage gives model parameters which can reproduce the input data. While using OptiSage to get the best fit, the researcher has to use his own judgment on the selection of parameters, such as which should be fixed or altered and if additional parameters have to be introduced. The convergence of the results in OptiSage depends upon the starting values given to the model parameters and the error limits set for the input data. Sometimes several steps are required to obtain the model parameters which can satisfactorily reproduce the input data. Also in some cases, it is easier and faster to obtain starting values from OptiSage, which can roughly reproduce the data, and then refine the fitting by the trial and error method. In the present work, the optimized parameters were obtained with the help of OptiSage or sometimes with both OptiSage and the trial and error method.

 # Back-calculation of all thermodynamic data and phase diagrams: Once satisfactory model parameters were obtained, all the thermodynamic data and experimental data were back-calculated for comparison with the optimized values.

 # Evaluation of ternary systems:

The presently obtained model parameters for the binary systems were combined with previously optimized binary parameters of the other binary sub-systems to estimate the Gibbs energies of solutions in the ternary systems using the techniques given in section 1.2.3. With the help of these Gibbs energies, evaluations and predictions were made for the ternary systems. Wherever required, ternary interaction parameters were also added.

2. THE UNARY AND BINARY SYSTEMS

In the present work, all the thermodynamic data for the CaO, MgO, Al_2O_3, B_2O_3 and SiO_2 phases were taken from the FToxide database. Over the years many assessments and thermodynamic optimizations have been performed using these data in the CRCT, Ecole Polytechnique. The thermodynamic data for these phases are quite well established in the FToxide database. As the present work involves incorporation of BaO and SrO into this big database, literature surveys and assessments were performed for the thermodynamic data of pure BaO and SrO phases. In the SiO_2-B_2O_3-Al_2O_3-CaO-MgO-BaO-SrO system there are 11 binary systems which contain either BaO or SrO (or both):

1. SrO-BaO
2. SrO-CaO
3. BaO-MgO
4. SrO-MgO
5. BaO-CaO
6. SrO-SiO_2
7. BaO-SiO_2
8. SrO-Al_2O_3
9. BaO-Al_2O_3
10. BaO-B_2O_3
11. SrO-B_2O_3

This chapter includes thermodynamic assessments and optimizations for the pure BaO and SrO phases and for these 11 binary systems.

2.1 Thermodynamic data for pure SrO

Risold, Hallstedt, and Gauckler (1996) reported an assessment of the Strontium-Oxygen system in which they reviewed the thermodynamic properties of SrO. The standard enthalpy of formation (ΔH^0_{298}), the standard entropy (S^0_{298}) and heat capacity (C_p) for SrO were taken from this publication. For the melting point of SrO, the lower melting point of 2430 ºC reported by Schumacher (1926), using his hand-made apparatus, was preferred over the higher melting point of 2597 ºC as accepted by Risold, et al. (1996). Our preferred value is also consistent with the measurement on pure SrO by Hanic, Chemekova, and Udalov (1979). The present accepted value agrees with the fact that the melting point of SrO is expected to be lower than the melting point of CaO, 2572 ºC (following the trend that melting points of alkaline-earth oxides decreases while descending the periodic table), accepted by us in our previous work [Eriksson, Wu, Blander, and Pelton (1994)]. The enthalpy of melting for SrO and heat capacity for liquid SrO were taken from the only available values in the literature reported by Irgashov, Tarasov, and Chekhovskii (1985) using DSC. Thus, thermodynamic data for liquid SrO, based upon the above values, and the thermodynamic data of solid SrO taken from Risold, et al. (1996) are given in Table 2.1.

Table 2.1 Thermodynamic data for the unary phase SrO.

SrO (solid)	ΔH^0_{298}= – 592.142 (kJ/mole) [Risold et al. ‘96]	S^0_{298}=53.580 (J/mol/K) [Risold et al. ‘96]	Cp = 47.56 + 0.00614 T – 380000 T^{-2} (298.15 < T < 6000 K) [Risold et al. ‘96] (J/mol/K)
SrO (liquid)	ΔH^0_{fusion}=80.950 (kJ/mole) [Irgashov et al. ‘85] T_{fusion} = 2430 °C [Schumacher ‘26]	ΔS^0_{fusion}=29.948 (J/mol/K)	C_p (liquid, SrO) = C_p (solid, SrO) (298.15<T< 2703 K) (J/mol/K) 73.1 (2703 < T < 3000 K) (J/mol/K) [Irgashov et al. ‘85]

2.2 Thermodynamic data for pure BaO

Zimmermann, Hack, and Neuschutz (1995) and Zhou, Arroyave, Randall, and Liu (2005) performed a thermodynamic assessment and optimization of the Barium-Oxygen system. The JANAF [Stull and Prophet (1985)] thermochemical tables also contain data for the BaO solid and liquid phases. The final assessed values of the standard enthalpy of formation (ΔH^0_{298}), standard entropy (S^0_{298}) and temperature of melting for the BaO solid phase used by Zimmermann, et al. (1995) and Zhou, et al. (2005) in their optimizations are close to the values reported in the JANAF tables. No experimental measurements for the heat capacity of the liquid BaO phase and enthalpy of melting for the solid BaO phase could be found in the literature. These values were estimated in the JANAF tables. In the present work, all the thermodynamic data of the BaO solid and liquid phases were taken from JANAF [Stull and Prophet (1985)], which are also presented in Table 2.2.

Table 2.2 Thermodynamic data for the unary phase BaO [Stull and Prophet (1985)].

BaO (solid)	ΔH^0_{298}= – 548.104 (kJ/mole)	S^0_{298}=72.069 (J/mol/K)	Cp = 59.418 + 0.00818 T – 156351 T^{-2} –3762 T^{-1} –0.216 $T^{0.5}$ (298.15 < T < 6000 K) (J/mol/K)
BaO (liquid)	ΔH^0_{fusion}=59.000 (kJ/mole)	ΔS^0_{fusion}=25.809 (J/mol/K)	C_p (liquid, BaO) = C_p (solid, BaO) (298.15< T < 1600 K) (J/mol/K)
	T_{fusion} = 2013 °C		66.944 (1600 < T < 3000 K) (J/mol/K)

2.3 The BaO-SrO, SrO-CaO, BaO-CaO, SrO-MgO and BaO-MgO systems

The optimized phase diagram for the BaO-SrO system is shown in Fig. 2.3.1 and optimized parameters are presented in Table 2.3. K. T. Jacob and Varghese (1995) measured the miscibility gap in the monoxide solid solution by lattice parameter measurements using XRD. These data are well reproduced in Fig. 2.3.1. The solid solution in Fig. 2.3.1 was modeled using a single-sublattice simple substitutional model (i.e., (Sr,Ba)O). Flidlider, Kovtunenko, Kiseleva, and Bundel (1966) measured the enthalpy of mixing in the monoxide phase by dissolving the samples prepared at 1150 °C in HCl. These data are compared with the present calculations in Fig. 2.3.2. Moreover, the experimental data in Figs. 2.3.1 and 2.3.2 are incompatible and cannot be simultaneously exactly fitted unless the entropy of mixing in the solid solution is assigned an unreasonable value. The small sub-regular term presented in Table 2.3.1 was required as the critical point composition is slightly shifted from the 50 mol% SrO composition. No phase diagram and thermodynamic data for the liquid phase in this system could be found in the literature. The liquid phase was assumed to be ideal in the present calculations.

The optimized phase diagram for the SrO-CaO system is shown in Fig. 2.3.3 and optimized parameters are presented in Table 2.3.1. K. Thomas Jacob and Waseda (1998) measured the miscibility gap in the monoxide solid solution by lattice parameters measurements using XRD. Roth (1990) also measured the extent of miscibility by unit cell measurements but the shape of the (im)miscibility curve determined by him was unusual. The solid solution in Fig. 2.3.3 was modeled using single-sublattice simple substitutional model (i.e., (Sr,Ca)O). Flidlider, et al. (1966), as in the BaO-SrO system, measured the enthalpy of mixing in the monoxide phase which is compared with the present calculations in Fig. 2.3.4. The small sub-regular term presented in Table was required as the critical point composition is slightly shifted from the 50 mol% SrO composition. No phase diagram and thermodynamic data for the liquid phase in this system could be found in the literature. The liquid phase was assumed to be ideal in the present calculations.

No phase diagram measurement in the literature could be found for the BaO-CaO system. Flidlider, et al. (1966), from the interpretation of their own calorimetric measurements, mentioned a very low mutual solubility among these solids. Van-der Kemp et al. (1994) calculated the phase diagram of this system by estimating the excess thermodynamic functions from the previously measured oxides and halides mixtures. Seo, Zhou, and Tsukihashi (2005) by molecular dynamics simulations estimated a liquidus similar to Van-der Kemp et al. (1994. As the BaO and CaO phases belong to the same structure, some amount of solid solubility among them can be expected. In the absence of any experimental data, the mutual solubility among the solid phases was estimated with the help of the following equation presented by Forland [Blander

(1962)] to calculate the columbic energy change by mixing two ionic liquid salt systems with a common anion (a case similar to the present situation where Ba and Ca cations are mixing with oxide anion, but in a solid solution):

$$\Delta_{\varepsilon c} = -e^2\left(\frac{1}{d_1}+\frac{1}{d_2}\right)\left(\frac{d_1-d_2}{d_1+d_2}\right)^2$$

where, $\Delta_{\varepsilon c}$ = columbic energy change, e = electronic charge, d_i = sum of radii of the anion and the mixing cation *i.*

For the systems BaO-SrO, SrO-CaO and CaO-MgO where critical temperatures of the miscibility gaps are known, the value $-\frac{\Delta_{\varepsilon c}}{e^2}$ was plotted against the critical temperature (the required ionic radii were taken from reference, (www.webelements.com (2012); O = 124pm, Ca = 114pm, Ba = 149pm). The straight line fit of these three points was extrapolated as shown in Fig. 2.3.5 to calculate the metastable critical temperature for the system BaO-CaO as 3033 °C. A regular solution parameter presented in Table 2.3.1 was used to reproduce this critical temperature. The solid solution was modeled using a single-sublattice simple substitutional model (i.e., (Ba,Ca)O). In the present calculations, the liquid phase in the BaO-CaO system was assumed ideal. The calculated phase diagram of the system is shown in Fig. 2.3.6.

Wartenberg and Prophet (1932) by equilibrium/quenching analysis measured the liquidus in the SrO-MgO system. No thermodynamic data or phase diagram data on mutual solubility of the two oxides could be found in the literature. As the two oxides belong to the same structure some

amount solid solubility can be expected. In the absence of any experimental data, the mutual solubility among the solid phases was estimated in the same way as in the BaO-CaO system (the required ionic radii were taken from reference, (www.webelements.com (2012); Sr = 132pm, Mg = 86 pm). The calculated extrapolated critical temperature (metastable) of immiscibility in this system is about 6800 °C (Fig. 2.3.5). A regular solution term presented in Table 2.3.1 was used to reproduce such a critical temperature. This gives negligible mutual solid solubility among the SrO and MgO phases. In the present calculations, the liquid phase was assumed as ideal. No effort was made to fit the experimental points of Wartenberg and Prophet because these points are not consistent with the melting points, which are comparatively better established in the literature, of the pure oxides (SrO and MgO). The present calculated phase diagram of the SrO-MgO system is shown in Fig. 2.3.7. Van-der Kemp, et al. (1994) calculated the phase diagram of this system by estimating the excess thermodynamic functions from the previously measured oxides and halides mixtures. Their calculated phase diagram also showed negligible solubility of SrO in MgO and a very small solubility of MgO in SrO.

Wartenberg and Prophet (1932) by equilibrium/quenching analysis measured the liquidus in the BaO-MgO system. No thermodynamic data or phase diagram data on mutual solubility of the two oxides could be found in the literature. As the two oxides belong to the same structure some amount of solid solubility can be expected. In the absence of any experimental data, the mutual solubility among the solid phases was estimated in the same way as in the BaO-CaO system. The calculated extrapolated critical temperature (metastable) of immiscibility in this system is above 9000 °C (Fig. 2.3.5). A regular solution term presented in Table 2.3.1 was used to reproduce such

a critical temperature. This gives negligible mutual solid solubility among the BaO and MgO phases. The calculated diagram of Van-der Kemp, et al. (1994) showed negligible solid solubility at either end of the phase diagram. In the present calculations, the liquid phase in the BaO-MgO system was assumed ideal and the calculated phase diagram is shown in Fig. 2.3.8. No effort was made to fit the experimental points of Wartenberg and Prophet because these points are not consistent with the melting points, which are comparatively better established in the literature, of the pure oxides (BaO and MgO).

Table 2.3.1 Optimized thermodynamic parameters (in Joules/mol) for the monoxide phase (Model parameters of Eq. 1.2.21).

Monoxide
$q^{11}_{CaSr} = 27748 - 6.359\,T$; $q^{12}_{CaSr} = -1674$
$q^{11}_{BaSr} = 35698 - 8.870T$; $q^{21}_{BaSr} = -3138$
$q^{11}_{BaCa} = 58600$
$q^{11}_{SrMg} = 117000$
$q^{11}_{BaMg} = 134000$

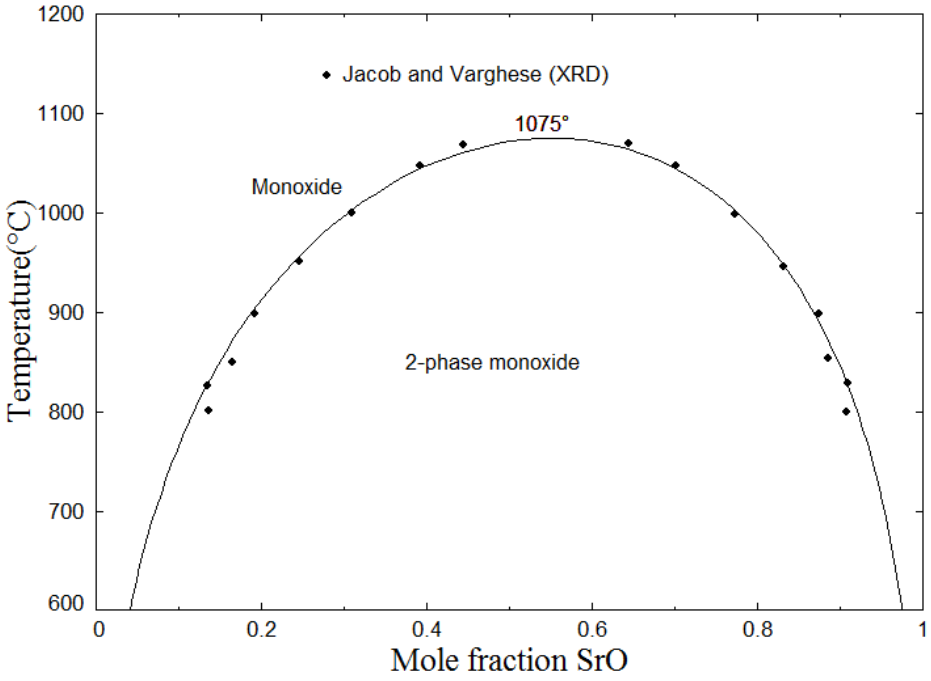

Fig. 2.3.1 Optimized phase diagram of the BaO-SrO system

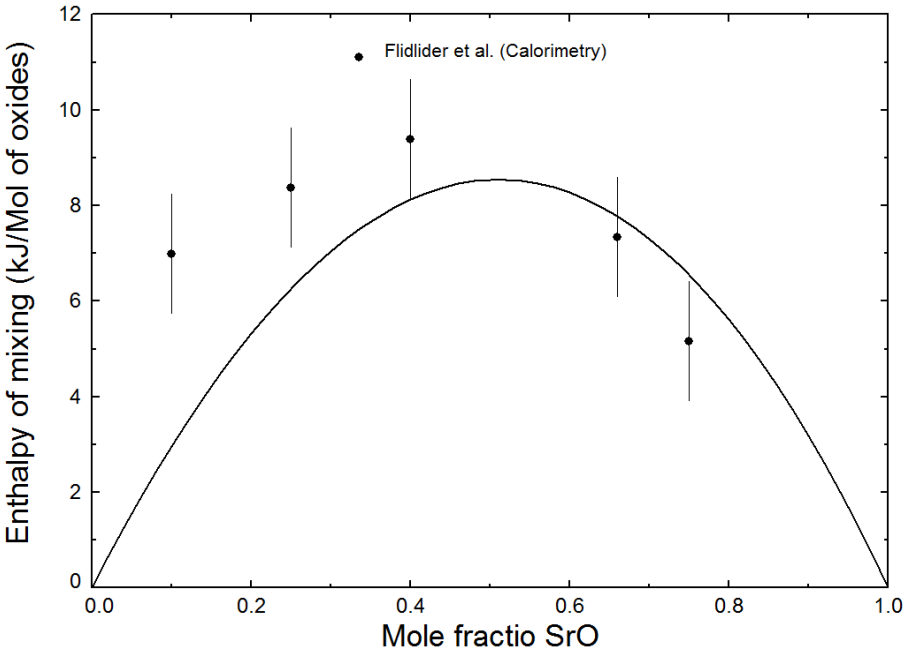

Fig. 2.3.2 Enthalpy of mixing in the BaO-SrO monoxide phase at 1150 °C.

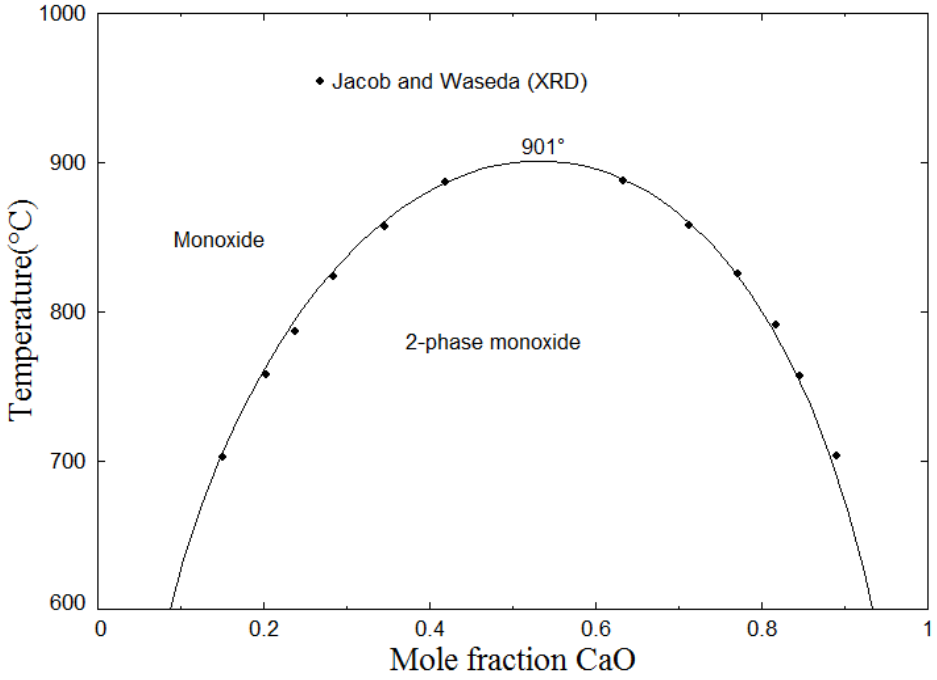

Fig. 2.3.3 Optimized phase diagram of the SrO-CaO system.

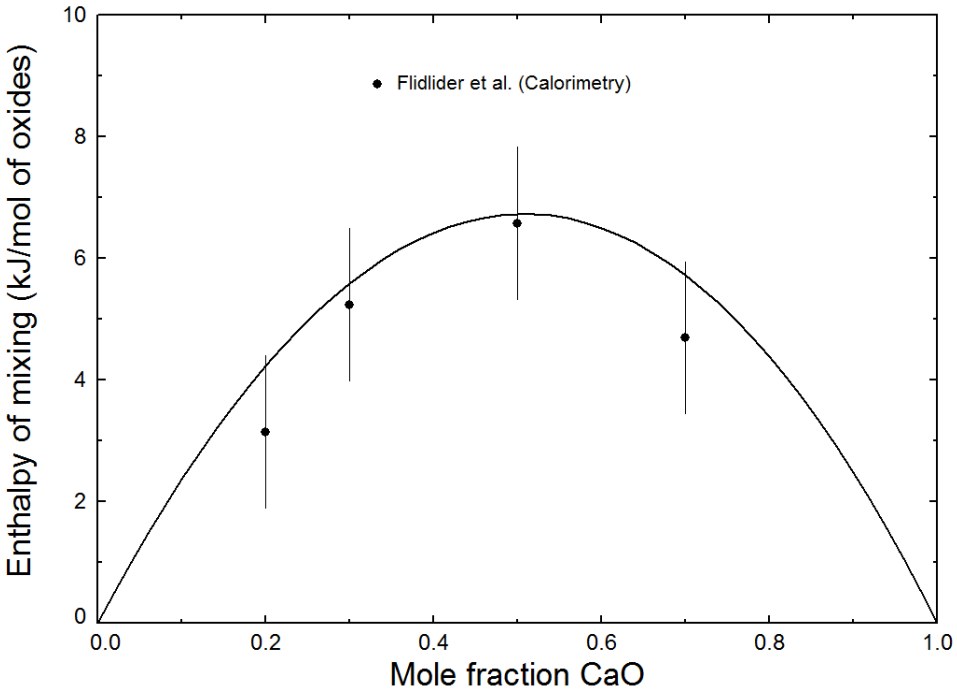

Fig. 2.3.4 Enthalpy of mixing in the SrO-CaO monoxide phase at 1150 °C.

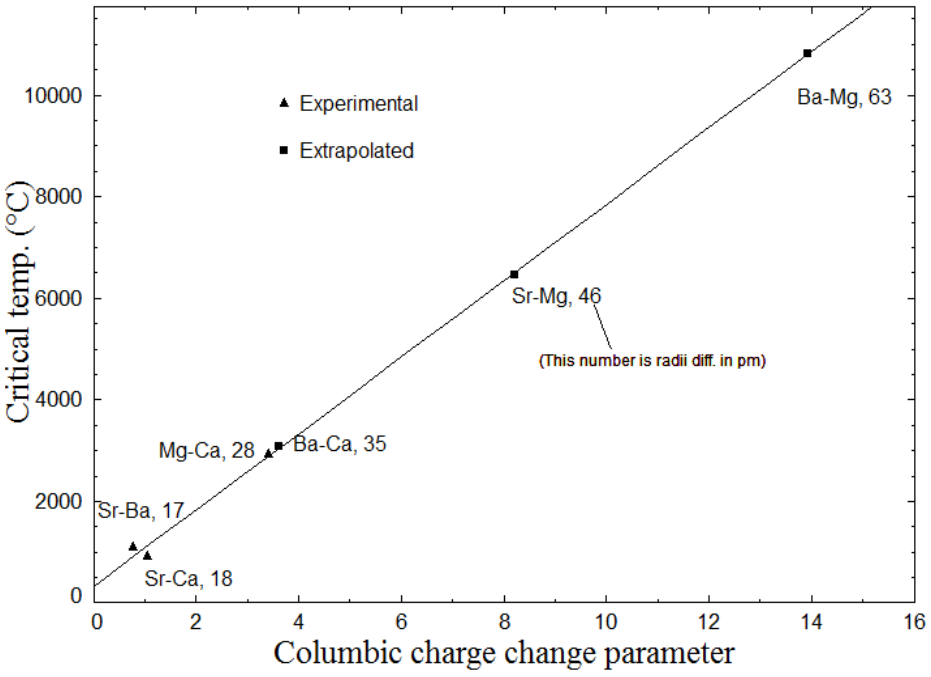

Fig. 2.3.5 Calculation of metastable critical temperature in alkaline-earth oxide systems.

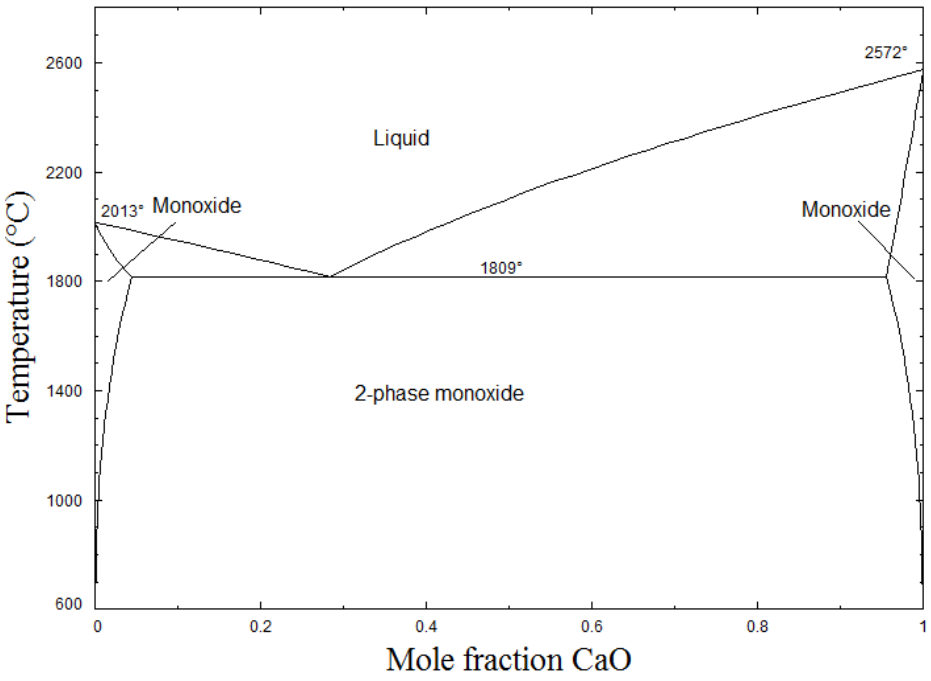

Fig. 2.3.6 Calculated phase diagram of the BaO-CaO system.

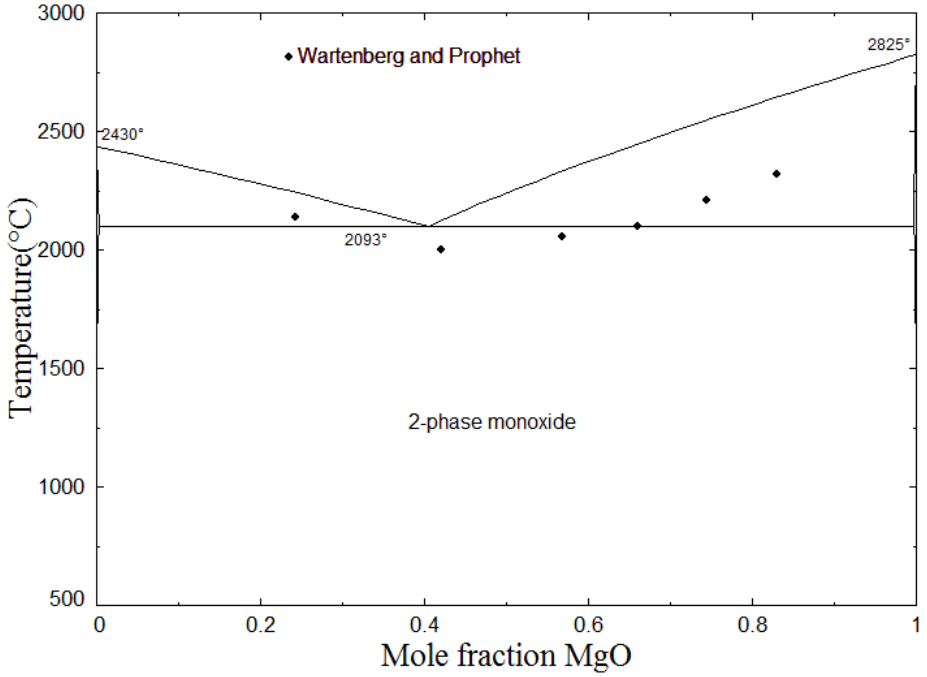

Fig. 2.3.7 Calculated phase diagram of the SrO-MgO system.

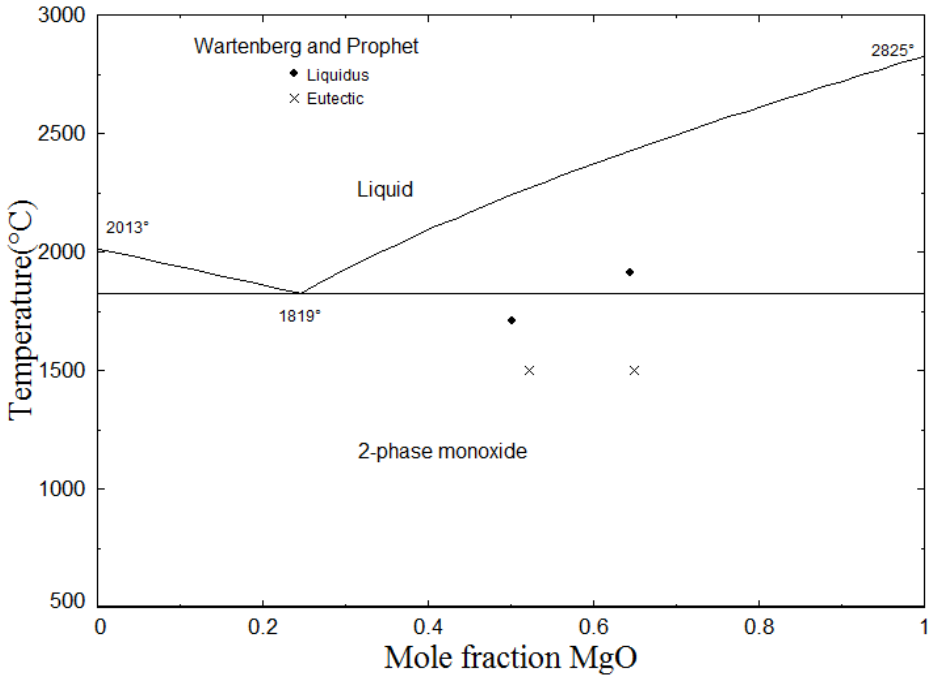

Fig. 2.3.8 Calculated phase diagram of the BaO-MgO system.

2.4 The SrO-SiO_2 system

The optimized phase diagram of the system is shown in Fig. 2.4.1 and optimized thermodynamic properties are presented in Table 2.4.1. The optimized MQM parameters (and the coordination numbers) for the liquid phase are presented in Table 2.4.1. For these parameters, the same notations were used as used by Pelton and coworkers [Pelton, et al. (2000)]. No thermodynamic optimization for this system was found in the literature.

Eskola (1922) first studied the system by annealing and quenching techniques followed by optical microscopy. He reported Sr_2SiO_4 (Sr_2S) and $SrSiO_3$ (SrS) as the equilibrium solid phases. Later, Nurse (1952) by X-ray diffraction (XRD) reported the Sr_3SiO_5 (Sr_3S) as equilibrium phase. Fields, Dear, and Brown (1972) measured the solidus and liquidus in the SrO-rich side of the system by visual inspection using an oxygen-acetylene torch. They reported all the three silicates shown in Fig. 2.4.1 as equilibrium phases by XRD. Huntelaar, Cordfunke, and Scheele (1993) by DTA measured the liquidus and solidus from 48 to 75 mol% SiO_2. Ghanbari-Ahari and Brett (1988), while studying SrO-MgO-SiO_2 system by annealing and quenching techniques, reported some data on the silica-rich side of the binary system. Greig (1927) measured the monotectic temperature and liquidus by equilibration and quenching techniques. V. B. Hageman and Oonk (1986) measured the miscibility gap in the system by equilibration and refractive index measurement of the quenched samples. Ol'shansky (1951) by quenching techniques studied the miscibility gaps in the alkaline-earth oxide-silica melts and reported the critical temperature for the miscibility gap in the SrO-SiO_2 system. All these data are compared with the optimized phase

diagram in Fig. 2.4.1. The low-temperature decomposition of Sr_3S was calculated as 1200 °C. There is no experimental evidence to prove that this phase is stable below this temperature. But, the instability of the Sr_3S phase at lower temperatures (as shown in Fig. 2.4.1) helped in fitting phase diagram data at 1350 °C in the ternary SrO-Al_2O_3-SiO_2 system. Fields, et al., reported the Sr_3S as stable in their binary phase diagram till 1200 °C. Hence, in the absence of any experimental data, the low-temperature decomposition was chosen as 1200 °C. A similar phase Ca_3SiO_5 (C_3S) also decomposes at 1300 °C. But, it should be noted that more experimental work is required to corroborate the low-temperature decomposition of the Sr_3S phase as shown in Fig. 2.4.1.

Polymorphism in the Sr_2S phase has been extensively studied [Catti, Gazzoni, Ivaldi, and Zanini (1983);Catti and Gazzoni (1983);Catti, Gazzoni, and Ivaldi (1983);J. Liu, Duan, Mei, Smith, and Hardy (2002);Hahn and Eysel (1970);Pieper, Eysel, and Hahn (1972);Catti, Gazzoni, and Ivaldi (1984)]. All these authors agree that room-temperature form is isostructural with larnite, β-Ca_2SiO_4 (space group, $P2_1/n$). It undergoes polymorphic transformation at around 85 ºC into the orthorhombic modification, similar to α'-Ca_2SiO_4 (space group, Pmcn). Pieper, et al. (1972) by DSC reported the enthalpy of this transformation as 213 J/mole. Hahn and Eysel (1970) predicted a further polymorphic transformation into high-K_2SO_4 structure, isotypic with α-Ca_2SiO_4 (space group, $P\bar{3}2/m$) at higher temperature while studying the structure of similar silicates and germanates. In a different work from the same laboratory, Pieper, et al. (1972), by DTA reported that this transformation occurs above 1550 ºC. Fields, et al. (1972) while studying the Ba_2SiO_4-Sr_2SiO_4 (B_2S-Sr_2S) system by optical and X-ray diffraction, noted two polymorphic forms of the

Sr_2S above 2100 ºC and showed this conversion at about 1700 °C in the phase diagram. They also suggested that the high-temperature form is non-quenchable. In the present work, following the suggestion of Hahn and Eysel (1970) the high-temperature form is considered as isotypic with α-Ca_2SiO_4. The temperature of transformation is assumed to be 1700 °C and the enthalpy of transformation is calculated the same as for the α'- to α-Ca_2SiO_4 conversion (4.2 kJ), from the FTOXID database. As explained below, the heat capacities of all these polymorphs of Sr_2S were assumed identical. No stable polymorphic transformation at atmospheric pressure could be found in the literature for strontium metasilicate. It has the pseudowollastonite structure [Eskola (1922);Buckner and Roy (1960)], (space group, C2/c [Yang and Prewitt (1999)]).

The standard enthalpies of formation (ΔH^0_{298}) for the Sr_2S and SrS phases were measured by authors [Huntelaar, Cordfunke, and Ouweltjes (1992b);Barany, King, and Todd (1957);Nacken (1930)] using solution calorimetry at room temperature. These values are compared with the present calculations in Fig. 2.4.2. This figure also compares the present calculations with the calculations performed using the FTOXID database for similar alkaline-earth systems. Nacken (1930) also measured ΔH^0_{298} for barium silicates (see BaO-SiO_2 system). He reported much less negative values for ΔH^0_{298} for barium silicates than strontium silicates. However, the reverse is expected. In the BaO-SiO_2 system also his data are not consistent with the other available data. The S^0_{298} for strontium ortho- and meta-silicates were reported by Huntelaar, Cordfunke, and Westrum (1992) and Weller and Kelley (1964) from low-temperature heat capacities measurements by adiabatic calorimetry. The present optimized S^0_{298} are compared with these data in Table 2.4.1. It is worth mentioning here that in all these references, for the measurement of

ΔH^0_{298} and S^0_{298}, ortho-silicate crystals were prepared by reacting starting materials in temperature ranges where the α'- modification is stable. No indication was given that crystals were quenched or slowly cooled from those temperatures to room temperature. However, the enthalpy of β (room-temperature modification) to α' transformation is quite low [Pieper, et al. (1972)]. Therefore, in the present calculations it was reasonably assumed that experiments were performed on the room-temperature modification. Huntelaar, et al. (1993) reported the enthalpy of fusion by calculating the area under the melting peak in DTA for SrS as 56 ± 6 kJ/mol. The present calculated value is 54.72 kJ/mol.

Huntelaar, Cordfunke, and Westrum (1992) also measured the enthalpy increments ($H^o_{(T)} - H^o_{(25)}$) in the range 227 ºC to 627 ºC using isothermal calorimetry for the Sr_2S and SrS phases. These enthalpy increments were used to optimize the heat-capacity (C_p) equations, presented in Table 2.4.1, for these compounds. The enthalpy increments are compared with the present calculations in Figs. 2.4.3 and 2.4.4 respectively. In these temperature ranges the α'- modification of Sr_2S is stable, hence the optimized heat capacity belongs to this modification. However, in the absence of any other experimental data on the heat capacities of other polymorphs of Sr_2S they were assumed to be equal to the heat capacity of the α'- modification. The optimized heat capacities were extrapolated to higher temperatures as shown in Figs. 2.4.5 and 2.4.6 where they are also compared with the heat capacities obtained from the sum of the heat capacities of the constituent oxides. The optimized standard entropy (S^0_{298}) and entropy of formation, with oxides as reference standards (ΔS^0_{298}), are presented in Table 2.4.1.

Róg, Langanke, Borchardt, and Schmalzried (1974) by EMF measured the Gibbs energy change of reactions which are compared with the present calculations in Figs. 2.4.7-2.4.9. The Gibbs energy of these solid phases were fixed, from the enthalpies and entropies of formation data (Table 2.4.1), and the present calculations differ from the data of Róg, et al. (1974). It is worth mentioning here that, by fitting Nacken's enthalpy of formation (keeping the entropies constant as previous values) for the Sr_2S and SrS phases, the calculated Gibbs energy change for the reaction (in which Sr_3S is not involved) in Fig. 2.4.9 deviates further from the present calculations. Hence, it can be said that Rog's data are inconsistent with the other available data.

Lopatin, Shugurov, Stolyarova, and Tyurnina (2006) measured the activities of SrO and SiO_2 in the system in the temperature range 1567-1697 ºC by high-temperature mass spectrometry. The calculated activities at 1647 ºC (as solid standard states) in the present work are compared with these data in Fig. 2.4.10 (the different experimental points at the same composition in Fig. 2.4.10 correspond to different temperatures; in the scale of this figure there is practically no difference in the calculated activities in this temperature range, therefore the present calculations were performed at 1647 °C). These data were not given much weight as they were found to be inconsistent with the phase diagram of the system. For example, at 1647 ºC, they reported unit activity of SrO in two phase regions ($0.3 \leq X_{SiO2} \leq 0.4$) where SrO is not present. Also, it is evident that SrO activity measured by them at the SiO_2-rich region is unreasonably high. Moreover, the Gibbs energy of formation at 1647 °C of the Sr_2S phase calculated with the help of these activities is -138 kJ whereas the present optimized value is -228 kJ. The present work fits the standard enthalpy of formation, entropy and heat capacity of this phase quite well. The

difference between the optimized Gibbs energy of formation at 1647 °C of the Sr_2S phase and the value obtained from the help of experimental activities suggest that these activities are not consistent with the other available thermodynamic data.

Richet and Bottinga (1985) by dropping melted samples into an ice-calorimeter (to a final glassy state) measured the enthalpy increments ($H_{(T)} - H_{(273)}$) in the liquid and glass (non-equilibrium liquid) phase for the composition SrS_2 (not for Sr_2S).Their data are compared with the present calculations in Fig. 2.4.11. It must be noted that for the exact comparison of these data, $H_{(273)}$ of the glassy phase is required, which is not available. The present calculations were performed by extrapolating the thermodynamic properties of the liquid phase to 0°C. However, it is evident in this figure that the optimized heat capacity agrees well with the experimental heat capacity (as the slope of the calculated curve is reasonably close to the experimental slope).

No data on the mutual solubility among the SrO and SiO_2 phases could be found in the literature. Moreover, their different crystal structures and the very large difference in the ionic radii of Sr and Si (Sr=132pm and Si=40pm [www.webelements.com (2012)]) also mitigate against any appreciable mutual solubility among them. Also, no data on the solid solubility in the solid phases appearing in the SrO-SiO_2 system were found. They were modeled as stoichiometric phases.

The enthalpy of mixing and entropy of mixing at 3000 ºC in the liquid phase in the SrO-SiO_2 is compared with the other alkaline-earth oxide-alumina systems in the next section (Figs. 2.5.6 and 2.5.7 respectively). The enthalpy of mixing follows the trend that it is expected to be more negative in the series CaO to BaO.

Table 2.4.1 Optimized thermodynamic parameters for the SrO-SiO_2 system.

Liquid phase (Quasichemical model parameters)			
Z^{Si}_{SiSi} = 2.75488750; Z^{Sr}_{SrSr} = 1.37744375 $\Delta g_{Sr\text{-}Si}$ = (–221752 + 17.614 *T*) – 20920 $X_{Sr\text{-}Sr}$ – 46024 $X_{Si\text{-}Si}$ + 74475 $X_{Si\text{-}Si}^3$ + (267125 – 123.428 *T*) $X_{Si\text{-}Si}^{11}$ J/mol			
Solid phases			
ΔH^0_{298} (kJ/mole)			
Compound	Calculated, elements as reference	Calculated, oxides (stable at room-temperature) as reference	Experimental values, oxides (stable at room-temperature) as reference
β-Sr_2SiO_4	–2304.000	–209.000	–209.370 ± 1.000 [Barany et al., '57] –137.890 [Nacken, '30] –210.716 [Huntelaar et al., '92b][(a)]
α'-Sr_2SiO_4	$\Delta H^{0\ (b)}_{tr}$ = 0.213 [Hahn and Eysel, '70] (at 85 ºC)		
α-Sr_2SiO_4	$\Delta H^{0\ (b)}_{tr}$ = 4.277 [estimated] (at 1700 ºC)		
$SrSiO_3$	–1632.000	–129.200	–130.710 ± 0.670 [Barany et al., '57] –103.180 [Nacken, '30] –132.458 [Huntelaar et al., '92b][(a)]
Sr_3SiO_5	– 2868.020	–180.900	
S^0_{298}, ΔS^0_{298} & $\Delta S^{0\ (c)}_{tr}$ (J/mol/K)			
Compound	Calculated value	Experimental values	ΔS^0_{298}, (calculated) oxides (stable at room-temperature) as reference

β-Sr_2SiO_4	155.600	153.134 ± 1.255 [Weller and Kelly, '64] 155.440 ± 0.250 [Huntelaar et al., '92]	6.980
$SrSiO_3$	95.600	96.650 ± 0.837 [Weller and Kelly, '64] 95.650 ± 0.210 [Huntelaar et al., '92]	0.560
Sr_3SiO_5	228.220		26.02

C_p (J/mol/K)

Compound	Optimized C_p
β, α',α -Sr_2SiO_4	156 + 0.0235 T –2718797 T^{-2} + 1.4E–5 T^2 –5.4E–9 T^3 (25 < T < 2127 °C) 217.92 (2127< T <2400 °C)
$SrSiO_3$	104 + 0.026 T –2113450 T^{-2} –1E–9 T^3 (25 < T < 2000 °C)
Sr_3SiO_5	C_p (Sr_2SiO_4) + C_p (SrO)

[(a)] In this ref. values of heat of formation from elements were given, so here they have been recalculated in terms of oxide by subtracting the heat of formation of oxides.
[(b)] Enthalpy of transformation from Room-Temperature (RT) to Low-Temperature form (LT) (kJ/Mole).
[(c)] Entropy of transformation from Room-Temperature (RT) to Low-Temperature form (LT) (J/mol/K).

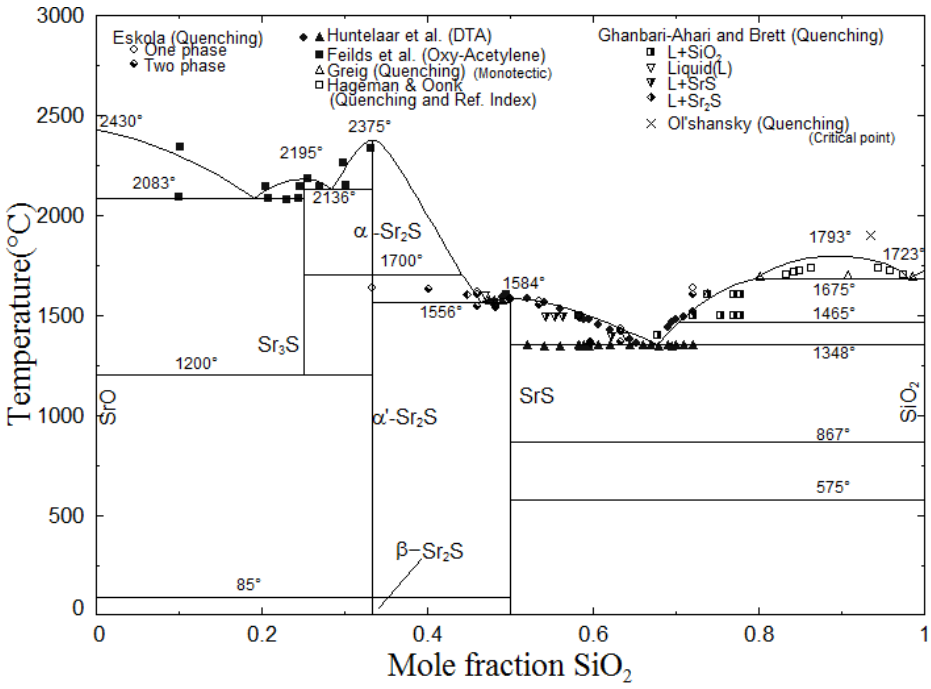

Fig. 2.4.1 Optimized phase diagram of the SrO-SiO_2 system.

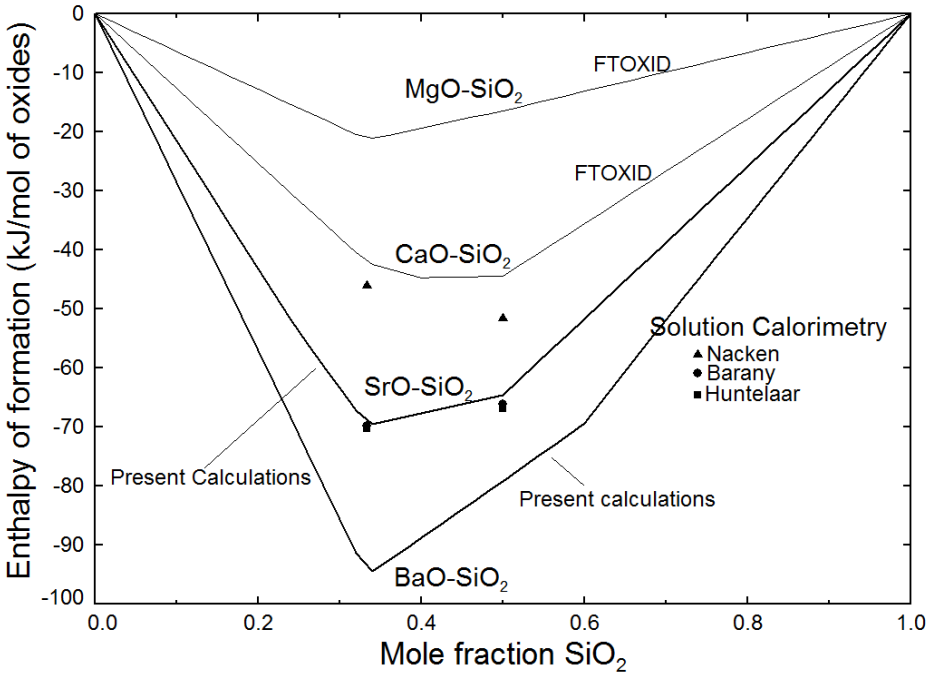

Fig. 2.4.2 Optimized standard enthalpy of formation in the alkaline-earth oxide-silica systems (All experimental points are for the $SrO\text{-}SiO_2$ system).

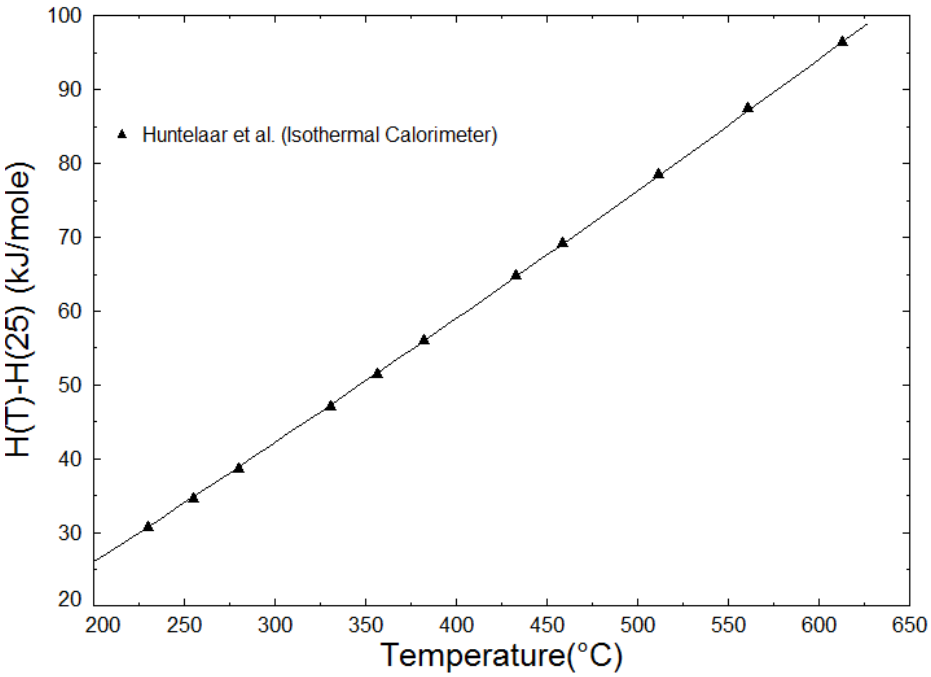

Fig. 2.4.3 Enthalpy increments ($H_{(T)} - H_{(298)}$) per mole of the Sr_2SiO_4 phase.

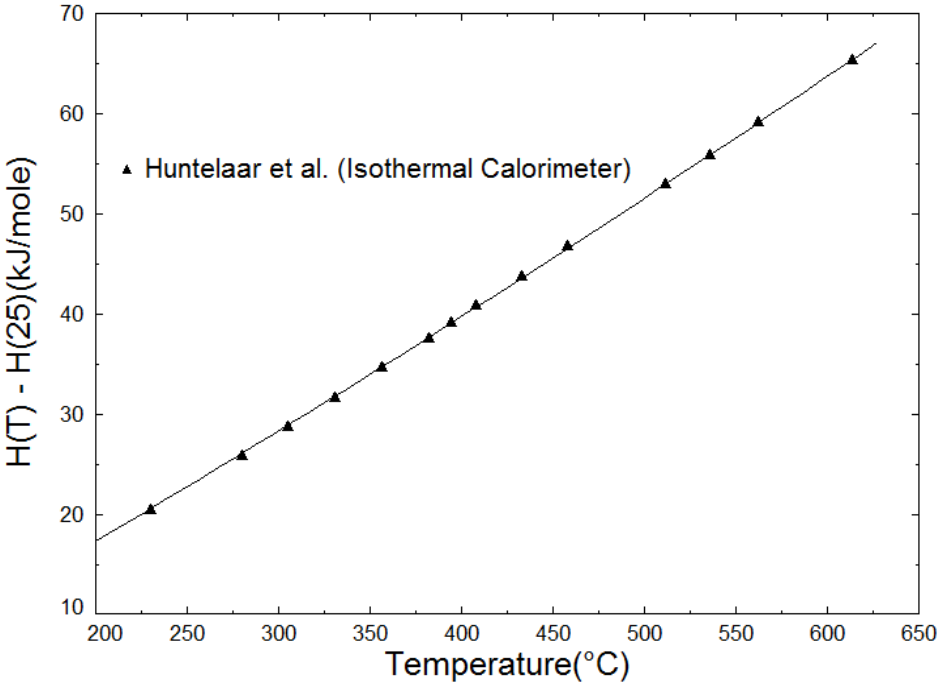

Fig. 2.4.4 Enthalpy increments ($H_{(T)} - H_{(298)}$) per mole of the $SrSiO_3$ phase.

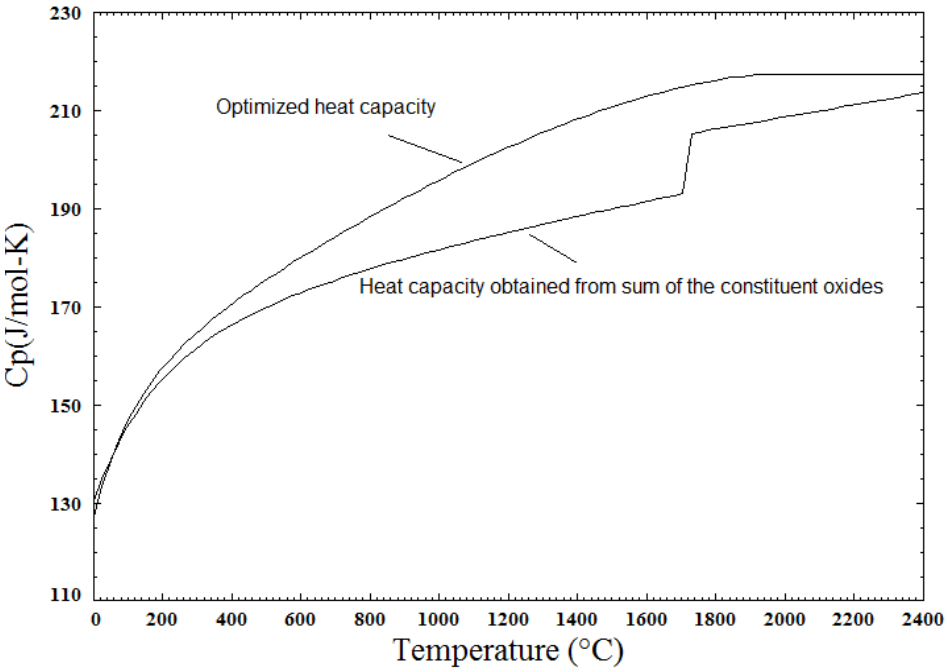

Fig. 2.4.5 Optimized heat capacity of the Sr_2SiO_4 phase compared with the heat capacity obtained from sum of the constituent oxides.

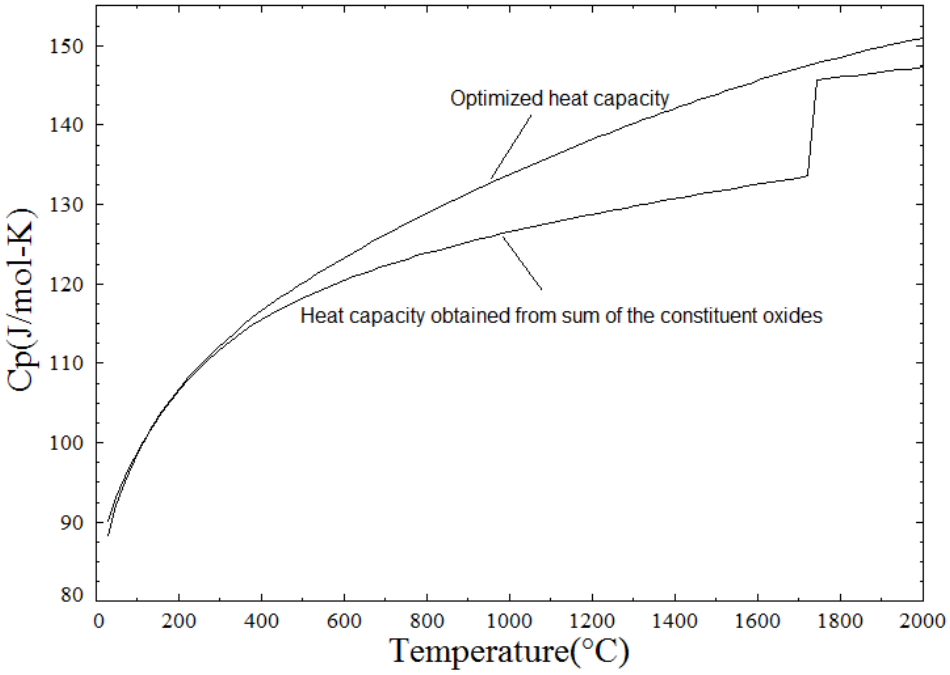

Fig. 2.4.6 Optimized heat capacity of the $SrSiO_3$ phase compared with the heat capacity obtained from sum of the constituent oxides.

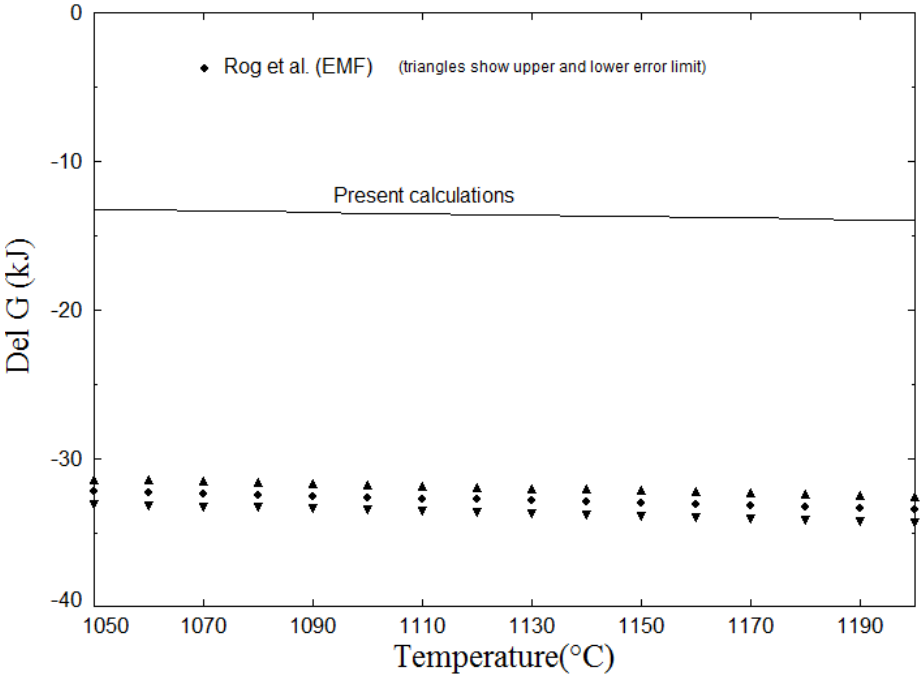

Fig. 2.4.7 Optimized Gibbs energy change in the reaction $SrO+Sr_2SiO_4=Sr_3SiO_5$.

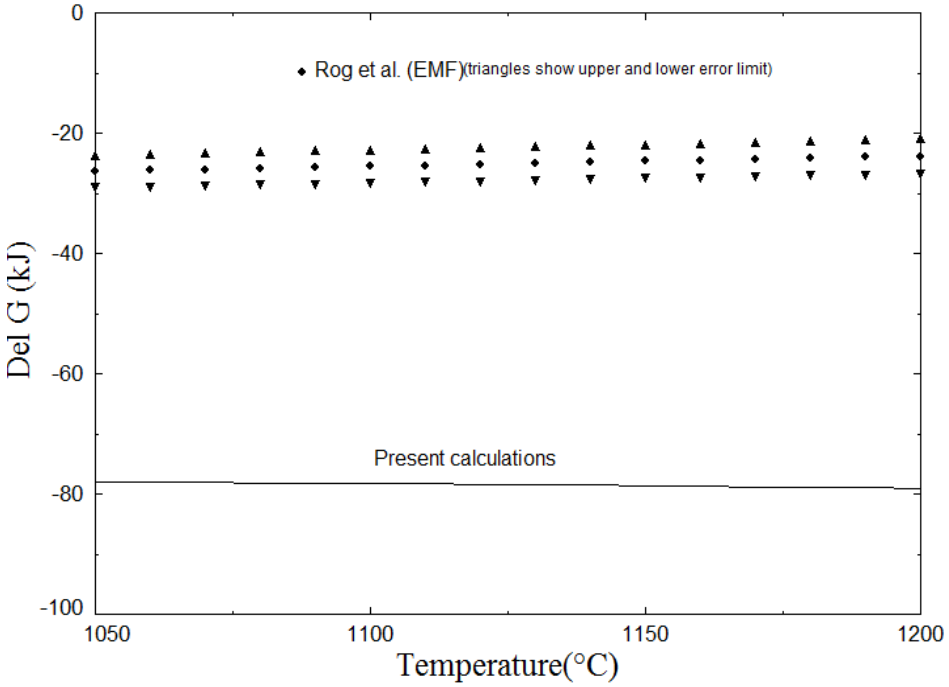

Fig. 2.4.8 Optimized Gibbs energy change in the reaction $Sr_3SiO_5+SrSiO_3=Sr_2SiO_4$.

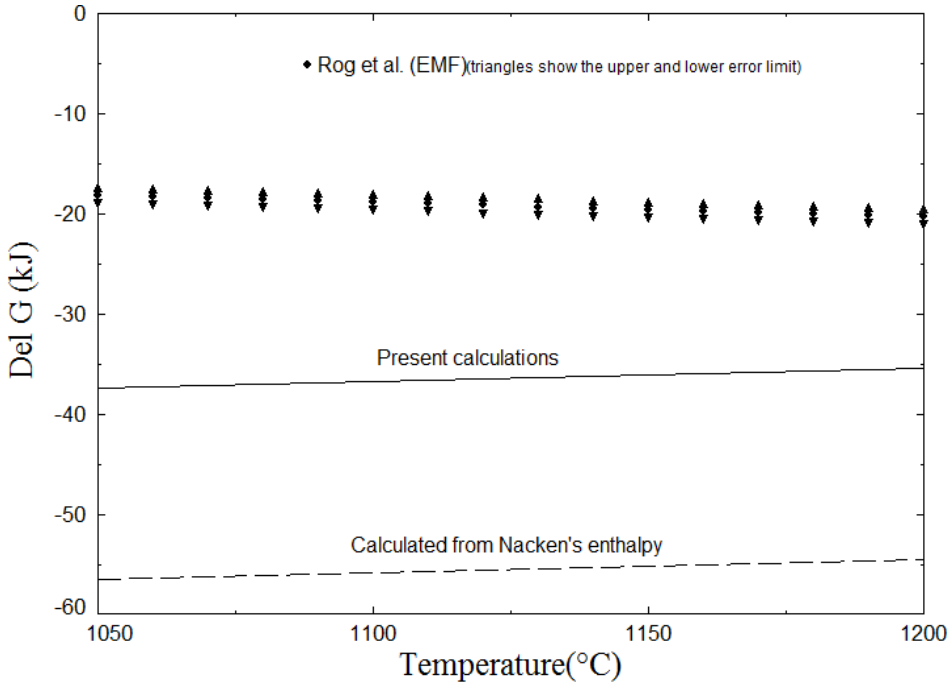

Fig. 2.4.9 Optimized Gibbs energy change in the reaction $Sr_2SiO_4+SiO_2=2SrSiO_3$.

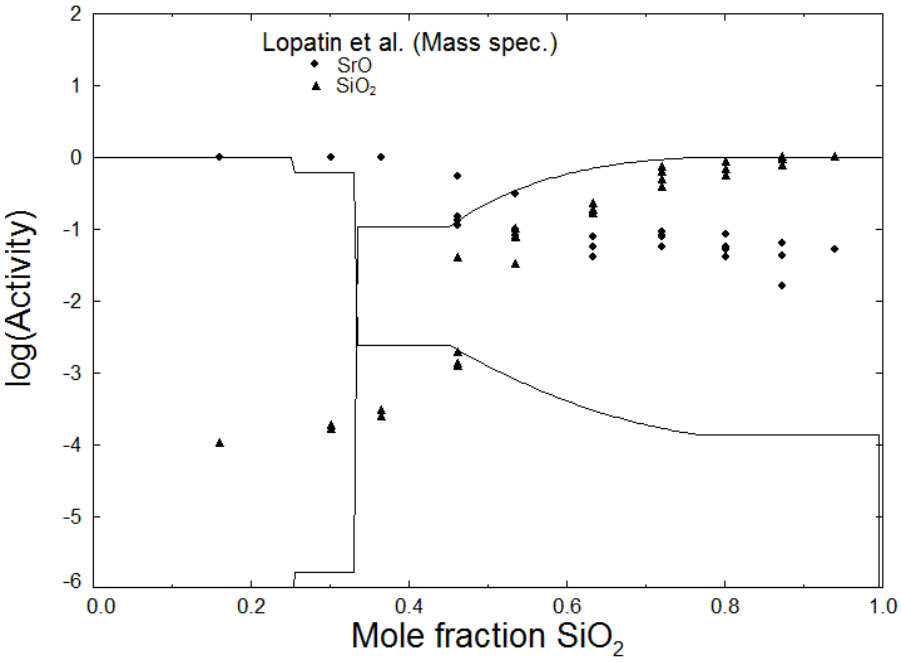

Fig. 2.4.10 Optimized activity at 1647 ºC (standard states are the respective solid phases) in the SrO-SiO_2 system.

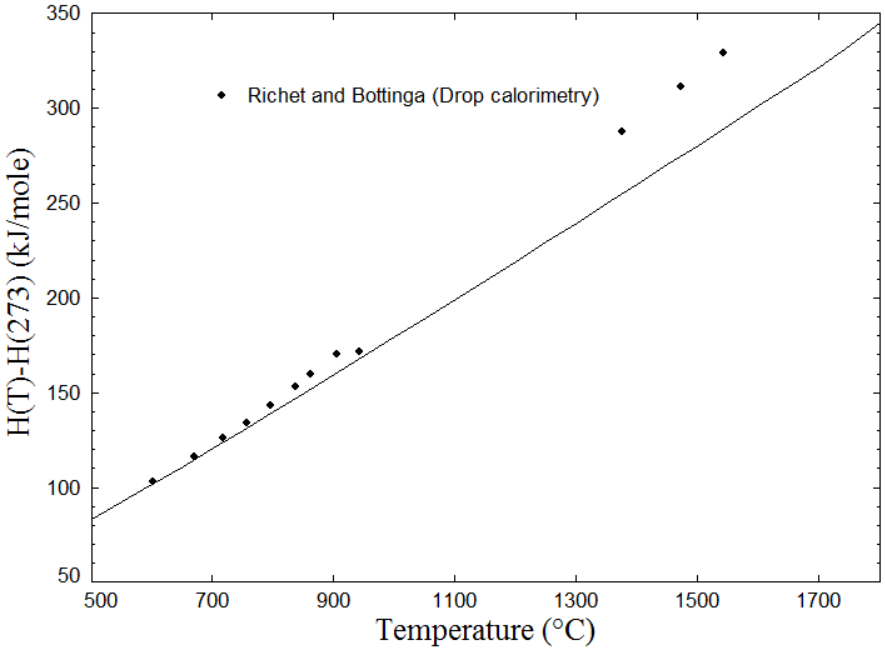

Fig. 2.4.11 Enthalpy increments ($H_{(T)}$-$H_{(273)}$) at the $SrSi_2O_4$ composition in the liquid and glass phase.

2.5 The BaO-SiO_2 system

The optimized phase diagram of the system is shown in Fig. 2.5.1 and optimized thermodynamic properties are presented in Table 2.5.1. The optimized MQM parameters (and the coordination numbers) for the liquid phase are presented in Table 2.5.1. For these parameters, the same notations were used as used by Pelton and coworkers [Pelton, et al. (2000)]. The BaO-SiO_2 system was optimized by Jung (2008). This optimization by Jung (2008) is presented here. Jung neglected the presence of two compounds (B_3S_5 and B_5S_8 in Fig. 2.5.1) in his optimization. These compounds were then later added during the present work. Cenerino, Chevalier, and Fischer (1992) presented an optimized phase diagram of the system. However, in this reference neither the data used for optimization nor optimized parameters were presented.

Eskola (1922) by quenching and optical microscopy first studied the system in the range 40-75 wt.% BaO. He reported congruent melting of $BaSiO_3$ (BS) and possible solid solution extending between the $Ba_2Si_3O_8$ (B_2S_3) and $BaSi_2O_5$ (BS_2) phases. Jaeger and Van Klooster (1916) by thermal analysis reported the melting point of BS as 1604 °C. Fields, et al. (1972) also reported this melting point very close to 1600 °C in their measured $BaSiO_3$-$SrSiO_3$ phase diagram. Roth and Levin (1959) by quenching followed by XRD and optical microscopy reinvestigated the phase diagram between the B_2S_3 and BS_2 phases. They found two additional compounds, $Ba_5Si_8O_{21}$ (B_5S_8) and $Ba_3Si_5O_{13}$ (B_3S_5) instead of the solid solution reported by Eskola (1922). The results of Roth and Levin (1959) were confirmed by Von Oehlschlegel (1971). Von Oehlschlegel also reported the decomposition of the B_3S_5 phase into B_5S_8 and BS_2 phases at 1300

°C. Von Oehlschlegel and Ohnmacht (1975) by quenching, optical microscopy and DTA studied the partial phase equilibria of the BaS_2-SiO_2 system. These data are compared with the present calculations in Fig. 2.5.1. There are XRD data [Glushkova and Keler (1957);Eysel (1970)] for the presence of the Ba_3SiO_5 (B_3S) phase. Pietro Appendino and Appendino Montorsi (1969), while studying the BaO-SrO-SiO_2 system, and Brisi and Appendino (1967), while studying the BaO-CaO-SiO_2 system, by quenching and XRD reported this phase as stable at 1100 °C. As the similar Sr_3S and C_3S phases decompose eutectoidly at lower temperature (see the SrO-SiO_2 section), the low-temperature decomposition for the B_3S phase was tentatively calculated as 1050 °C. No other phase diagram data for this compound could be found in the literature. In the present calculations, this compound was calculated to melt congruently similarly to Sr_3S (see SrO-SiO_2 section). The calculated melting temperature is tentative and further experimental work is required to confirm this.

There are different data on the melting temperature of the Ba_2SiO_4 (B_2S) phase. Toropov and Fedorov (1964) determined the melting point of B_2S as part of the phase diagram study for the Ca_2SiO_4-Ba_2SiO_4 (C_2S-B_2S) system. The method of the temperature determination was not specified. They claimed that the melting temperatures of B_2S measured in the previous studies [1820 ^oC by Braniski (1961); 1740 ^oC by Toropov, Galakhov, and Bondar (1954)] are lower than their measurement at 1960 ^oC due to partial contamination by $BaCO_3$ in the B_2S sample. Fields, et al. (1972) determined the melting point of B_2S as 2150 °C by visual observation with an optical pyrometer as part of the phase diagram study of the Ba_2SiO_4-Sr_2SiO_4 (B_2S-Sr_2S) section. During optimization, the melting point reported by Fields, et al. (1972) was found to fit much

better with the other available phase diagram and thermodynamic data. Unlike C_2S and Sr_2S, only one crystalline phase for B_2S is known (α'-structure which is isostructural with α'-C_2S; unmodulated β-K_2SO_4 type).

Greig (1927) first investigated the possibility of a liquid miscibility gap in the BaO-SiO_2 system. He observed a very flat SiO_2 liquidus at about 1680 ^oC between 85 to 97 mole % SiO_2, and no stable liquid immiscibility was observed in his quenched samples. Ol'shansky (1951) claimed that no liquid phase separation occurs in the BaO-SiO_2 system between 1800 and 2570 ^oC. Argyle and Hummel (1963) by electron microscopic observation reported stable liquid immiscibility above 1655 ^oC in the range 5-25 mole % BaO. Later, Seward, Uhlmann, and Turnbull (1968) by optical microscopy reported a metastable miscibility gap with upper consolute point at about 10 mole % BaO and 1460 ^oC. However, they also reported that liquid immiscibility was even observed for the 10 mole% BaO sample quenched from 1725 ^oC under the TEM micrograph image. In the present calculations, it was found very difficult to suppress the liquid miscibility gap in high SiO_2 region with the reproduction of the flat liquidus of SiO_2 as reported by Greig (1927). The present calculations favor a stable liquid miscibility gap as also reported by Argyle and Hummel (1963). The previous optimized phase diagram by Cenerino, et al. (1992) also predicted the stable liquid miscibility gap.

The standard enthalpy of formation (ΔH^0_{298}) for various barium silicates were measured by authors [Nacken (1930); Barany, et al. (1957); Huntelaar, Cordfunke, and Ouweltjes (1992a)] using solution calorimetry at room temperature. These data are well reproduced in Fig. 2.5.2. As

in the SrO-SiO_2 system, the data by Nacken (1930) differ considerably from the other available data. Also, Nacken (1930) reported ΔH^0_{298} of barium silicates much less negative than the strontium silicates. However, the reverse is expected. The standard entropies (S^0_{298}) for barium silicates were reported by Weller and Kelley (1964) using low-temperature heat capacity measurements by adiabatic calorimetry. These data are compared with the present optimized values in Table. 2.5.1. The heat capacities of B_2S and BS were taken from Barin (1995). These heat capacities are greater than the values obtained by adding the heat capacities of constituent oxides, which is in accordance with the case of the Sr_2S and SrS. For these strontium silicates, heat contents were measured up to 627 °C (see the SrO-SiO_2 section) and the optimized heat capacity is greater than that obtained by adding the heat capacities of constituent oxides. No high-temperature heat capacity or heat content measurements for the other barium silicates could be found in the literature. The heat capacities of other barium silicates are calculated from the sum of the constituent oxides, as shown in Table 2.5.1.

Rog (1980) by EMF measured the Gibbs energy of formation for barium silicates which are compared with the present calculations in Fig. 2.5.3. Unlike in similar work by the same author in the SrO-SiO_2 system (see the SrO-SiO_2 section), where the Gibbs energy change in the various EMF cells were presented in the form of fitted equations, here the Gibbs energies of formation for various silicates were presented in tabular form only for the three temperatures, 927, 1027 and 1127 °C. In this temperature range, on the scale of Fig. 2.5.3, there is practically no change in the values of the calculated Gibbs energies of formation for these compounds. The Gibbs energies of these compounds are fixed from the ΔH^0_{298} and S^0_{298} values (Table 2.5.1), Rog's data can be said

to be inconsistent with these data. In the SrO-SiO_2 system also, Rog's data are not consistent with the other available data.

Tyurnina, Lopatin, Shugurov, and Stolyarova (2006) by Knudsen effusion mass spectrometry determined the activities of SiO_2 and BaO in the BaO-SiO_2 system in the range 1567-1697 °C. These activities are compared with the present calculations at 1637 °C in Fig. 2.5.4 (the different experimental points at the same composition in Fig. 2.5.4 correspond to different temperature; in the scale of this figure there is practically no difference in the calculated activities in this temperature range, therefore the present calculations were done at 1637 °C). It is also evident that the measured SiO_2 activity in the BaO-rich compositions is too high but activities in the SiO_2-rich compositions are comparatively better reproduced. Moreover, the Gibbs energy of formation at 1637 °C of the orthosilicate phase calculated with the help of these activities is -182 kJ whereas the present optimized value is -271 kJ. The present work fits the standard enthalpy of formation and entropy quite well, and the heat capacity of this phase is reasonably well known. The difference between the optimized Gibbs energy of formation at 1637 °C of the orthosilicate phase and the value obtained from the help of experimental activities suggest that these activities are not consistent with the other available thermodynamic data.

Richet and Bottinga (1985) by dropping melted samples into an ice-calorimeter (to final glassy state) measured the enthalpy increments ($H_{(T)} - H_{(273)}$) in the liquid and glass (non-equilibrium liquid) phase for the composition $BaSi_3O_7$. Their data are compared with the present calculations in Fig. 2.5.5. It must be noted that for the exact comparison of these data, $H_{(273)}$ of the glassy

phase is required, which is not available. The present calculations were performed by extrapolating the thermodynamic properties of the liquid phase to 0°C. However, it is evident in this figure that the optimized heat capacity agrees well with the experimental heat capacity (as the slope of the calculated curve is reasonably close to the experimental slope).

The enthalpy of mixing and entropy of mixing in the liquid phase at 3000 ºC (temperature at which the liquid phase exists over the whole region in all the systems) in alkaline-earth oxide-silica systems are compared in Fig. 2.5.6 and 2.5.7 respectively. The enthalpy of mixing is expected to be more negative, i.e., more ordering is expected in the liquid phase in the series MgO to BaO. This trend can be observed in Fig. 2.5.6.

No data on the mutual solubility among the BaO and SiO_2 phases could be found in the literature. Moreover, their different crystal structures and the very large difference in the ionic radii of Ba and Si (Ba = 149 pm and Si = 40 pm, [www.webelements.com (2012)]) also mitigate against any appreciable mutual solubility among them. Also, no data on the solid solubility in the solid phases appearing in the BaO-SiO_2 system were found. They were modeled as stoichiometric phases.

Table 2.5.1 Optimized thermodynamic parameters (in Joules/mol) for the BaO-SiO_2 system.

Liquid phase (Quasichemical model parameters)			
Z^{Si}_{SiSi} = 2.75488750; Z^{Ba}_{BaBa} = 1.37744375			
$\Delta g_{Ba\text{-}Si}$ = (–238969 + 19.455T) + (–87695 + 25.104) $X_{Si\text{-}Si}$ + (–33679 + 38.087 T) $X_{Si\text{-}Si}^4$ (243694 – 107.702 T) $X_{Si\text{-}Si}^7$			
Solid phases			
ΔH^0_{298} (kJ/mole)			
Compound	Calculated, elements as reference	Calculated, oxides (stable at room-temperature) as reference	Experimental values, oxides (stable at room-temperature) as reference
Ba_3SiO_5	–2800.000	–245.000	
Ba_2SiO_4	–2292.422	–285.500	–285.292 ± 4.200 [Huntelaar et al., '92a] [(a)] –269.784 ± 1.171 [Barany et al., 57] –105.395 [Nacken, '30]
$BaSiO_3$	–1617.258	–158.454	–147.596 ± 2.600 [Huntelaar et al., '92a] [(a)] –159.117 ± 0.711[Barany et al., 57] –84.554 [Nacken, '30]
$Ba_2Si_3O_8$	–4173.220	–344.912	–344.845 ± 1.464 [Barany et al., 57]
$Ba_5Si_8O_{21}$	–10895.534	–869.414	
$Ba_3Si_5O_{13}$	–6715.246	–517.434	
$BaSi_2O_5$	–2543.200	–173.696	–172.715 ± 1.046 [Barany et al., 57]
S^0_{298} ,ΔS^0_{298} & ΔS^0_{tr} [(c)] (J/mol/K)			
Compound	Calculated value	Experimental values	ΔS^0_{298}, (calculated) oxides (stable at room-temperature) as reference
Ba_3SiO_5	284.400		26.733
Ba_2SiO_4	176.146	176.146 ± 1.674 [Weller and Kelly, '64]	–9.452
$BaSiO_3$	108.784	109.620 ± 1.255 [Weller and Kelly, '64]	–4.745

$Ba_2Si_3O_8$	260.450	258.153 ± 2.510 [Weller and Kelly, '64]	–8.068
$Ba_5Si_8O_{21}$	672.200		–19.825
$Ba_3Si_5O_{13}$	415.400		–8.107
$BaSi_2O_5$	153.400	153.134 ± 1.674 [Weller and Kelly, '64]	–1.589

Compound	Optimized C_p
Ba_3SiO_5	3 C_p(BaO) + C_p(SiO_2, Quartz(h))
Ba_2SiO_4	153.553 + 0.0430 T –2790728 T^{-2} [Barin (1995)] (25 < T < 1700 °C)
$BaSiO_3$	100.249+ 0.0387 T –1959786 T^{-2} [Barin (1995)] (25 < T < 2200 °C)
$Ba_2Si_3O_8$	2 C_p(BaO) + 3 C_p(SiO_2, Quartz(h))
$Ba_5Si_8O_{21}$	5 C_p(BaO) + 8 C_p(SiO_2, Quartz(h))
$Ba_3Si_5O_{13}$	3 C_p(BaO) + 5 C_p(SiO_2, Quartz(h))
$BaSi_2O_5$	C_p(BaO) + 2 C_p(SiO_2, Quartz(h))

(a) In this refs. values of heat of formation from elements were given, so they have been recalculated in terms of oxide by subtracting the heat of formation of oxides.

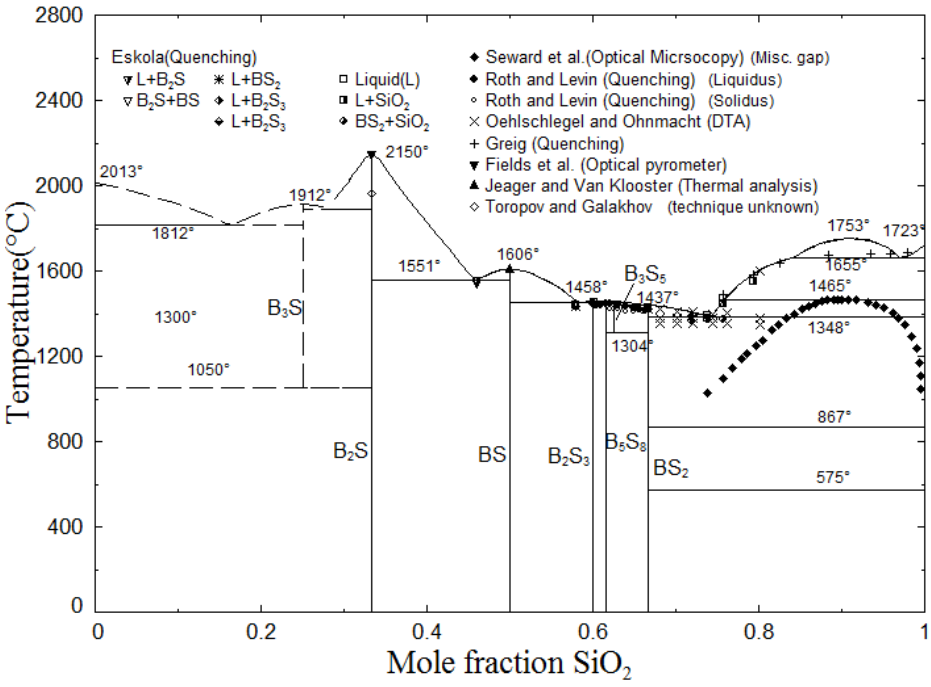

Fig. 2.5.1 Optimized phase diagram of the BaO-SiO_2 system.

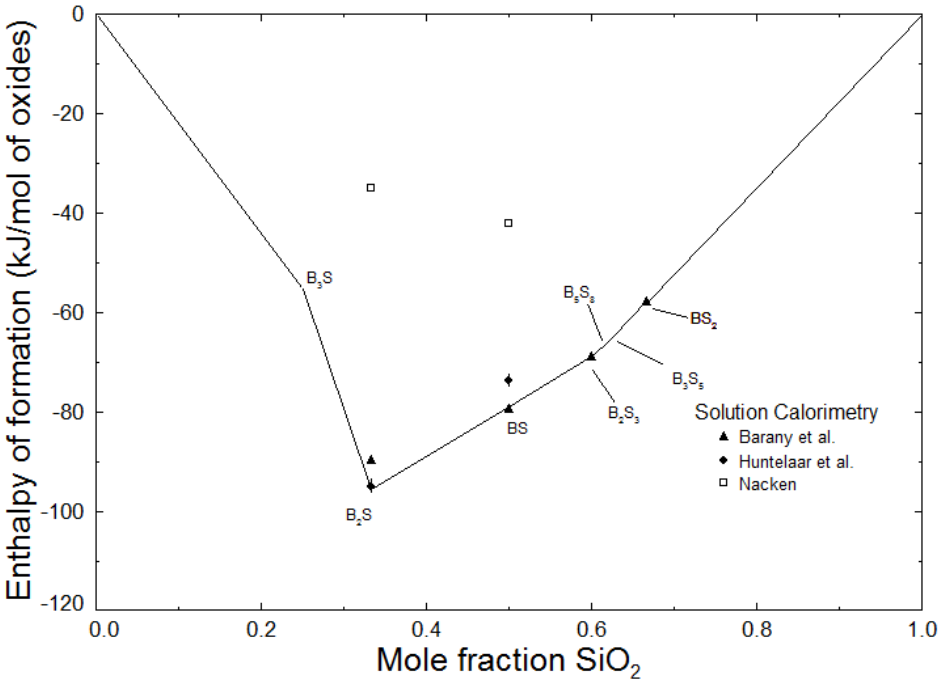

Fig. 2.5.2 Optimized enthalpies of formation (ΔH^0_{298}) in the barium silicates.

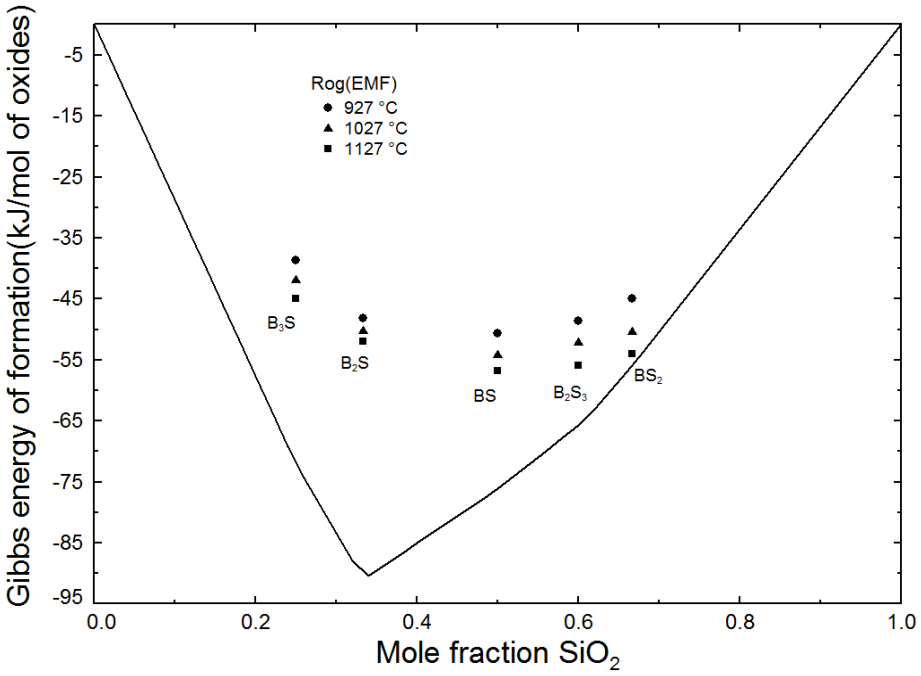

Fig. 2.5.3 Optimized Gibbs energy of formation at 1027 °C in barium silicates.

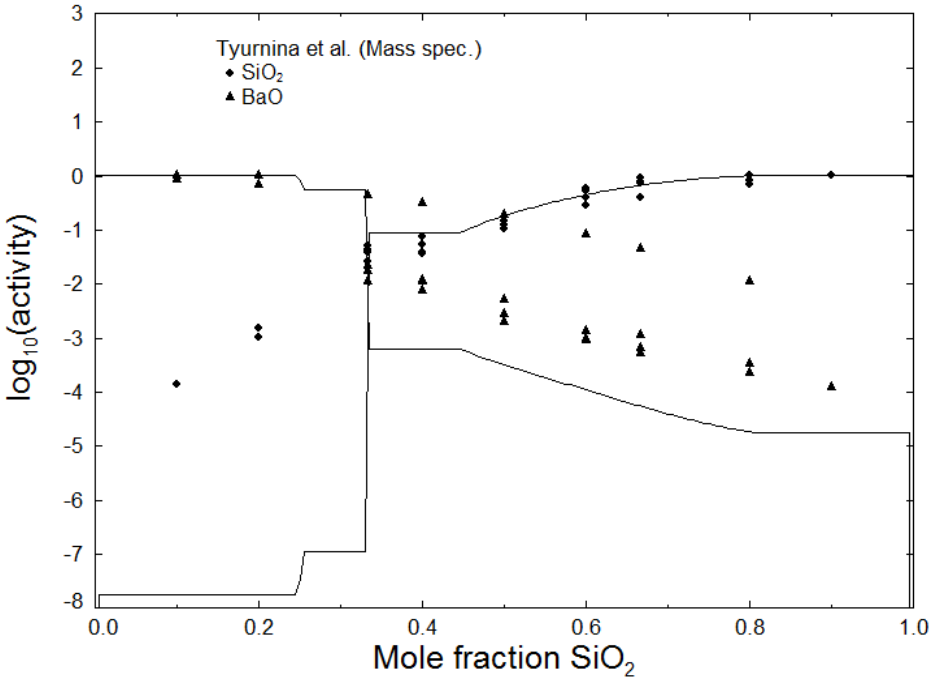

Fig. 2.5.4 Optimized activity of BaO and SiO_2 at 1637 °C (standard states are respective solid phases) in the BaO-SiO_2 system.

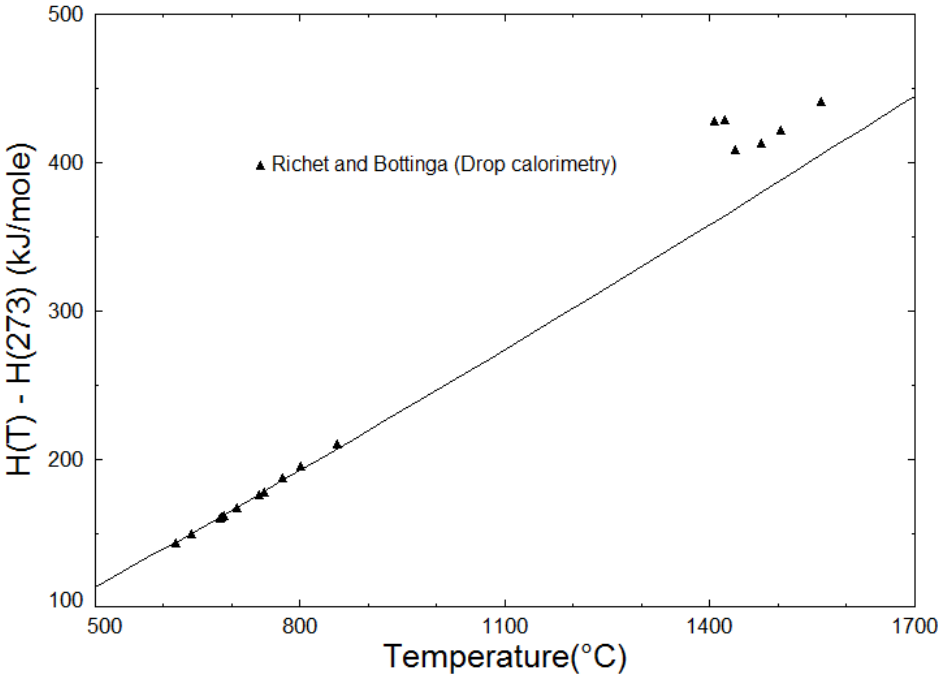

Fig. 2.5.5 Enthalpy increments ($H_{(T)}$-$H_{(273)}$) at the $BaSi_3O_7$ composition in the liquid and glass phase.

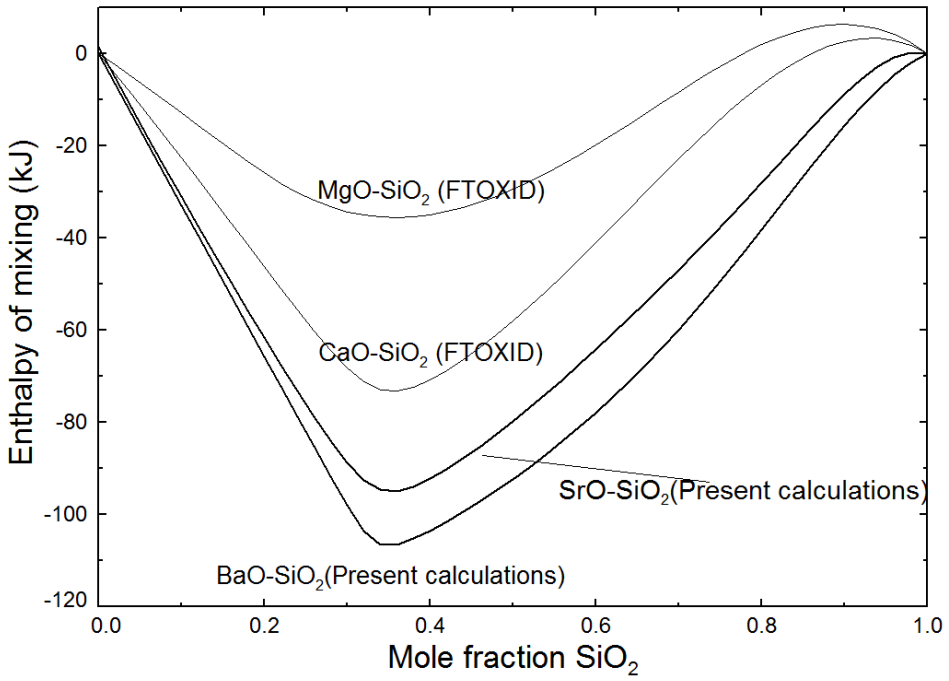

Fig. 2.5.6 Enthalpies of mixing in the liquid phase at 3000 ºC in the alkaline-earth oxide -silica systems.

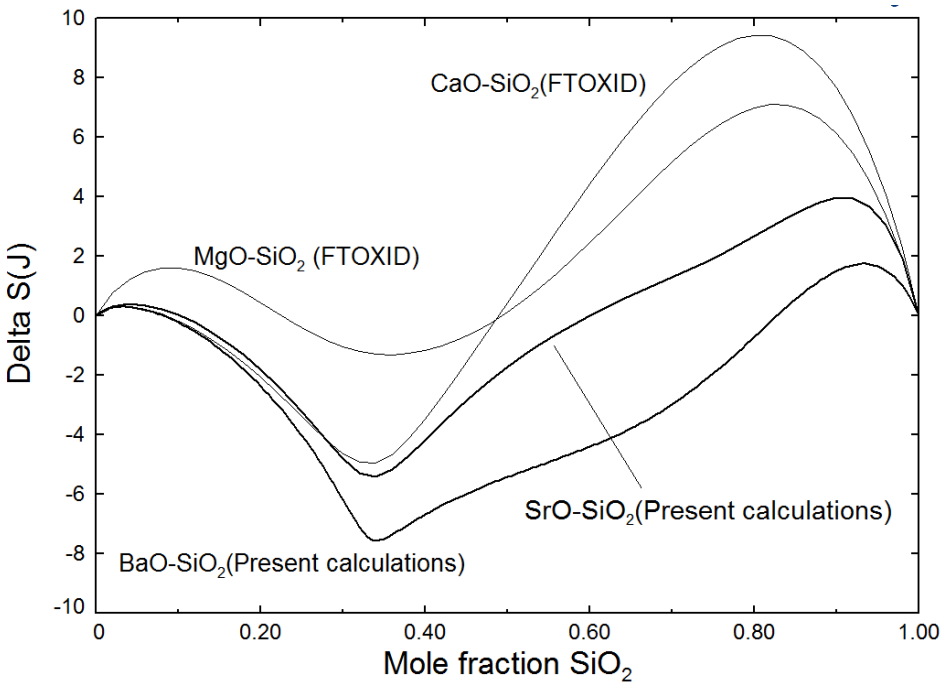

Fig. 2.5.7 Entropies of mixing in the liquid phase at 3000 ºC in the alkaline-earth oxide-silica system.

2.6 The SrO-Al_2O_3 system

The optimized phase diagram of the system is shown in Fig. 2.6.1 and optimized thermodynamic parameters are presented in Table 2.6.1. The optimized MQM parameters (and the coordination numbers) for the liquid phase are presented in Table 2.6.1. For these parameters, the same notations were used as used by Pelton and coworkers [Pelton, et al. (2000)]. Ye, Zhuang, Wang, Yuan, and Qiao (2007) optimized this system, treating the liquid phase by two-sublattice model for ionic solutions. In this work, however, the thermodynamic data of Bokeriya, Tsagareishvili, and Gvelesiani (1970b) and Levitskii, Skolis, Chentsov, and Golovanova (1972) were not taken into account.

In the SrO-Al_2O_3-SiO_2 system, to obtain the optimal fit of the available data, an additional component in the form of $SrAl_2$ associate was added to the liquid phase, i.e. $SrAl_2O_4$ was considered a separate component in the binary SrO-Al_2O_3 system (along with SrO and Al_2O_3). The optimized Gibbs energy of this component ($SrAl_2$ associate) and its coordination number in the liquid phase is presented in Table 2.6.1. Practically, these $SrAl_2$ associates are not stable in the binary SrO-Al_2O_3 system. They are stable in the ternary SrO-Al_2O_3-SiO_2 system, especially in the SiO_2-rich corner. In the SrO-Al_2O_3 system, at 2050 °C and at $X_{Al2O3} = 0.5$, the mole fraction of these associates is only 4.4×10^{-4}.

Hanic, et al. (1979) by DTA and high-temperature XRD, and Massazza (1959) by quenching and optical micrography techniques, reported $SrO.2Al_2O_3$ (SA_2), $SrO.Al_2O_3$ (SA) and $3SrO.Al_2O_3$ (S_3A) as congruently melting compounds and $4SrO.Al_2O_3$ (S_4A) and $SrO.6Al_2O_3$ (SA_6) as

incongruently melting compounds. Both Hanic, et al. (1979) and Massazza (1959), reported a polymorphic transformation of S_4A, the lower form dissolving 2-3% of Al_2O_3 and undergoing low-temperature decomposition. Hanic, et al. (1979) reported the temperature of the transformation as 1450 ºC and Massazza (1959) as 1320 ºC. The low-temperature decomposition of S_4A was measured at 1130 ºC and 1125 ºC by Hanic, et al. (1979) and Massazza (1959) respectively. Starczewski (1964) by cooling curves and XRD reported S_3A and SA as congruently melting and S_4A, SA_2 and SA_6 as incongruently melting compounds. Kadyrova (1999) measured the melting point of the SA_6 compound while studying the CaO-SrO-Al_2O_3 system. His data were consistent with the liquidus data measured by Starczewski (1964). Starczewski (1964) did not report any structural variation of S_4A. In the present work, the temperature for this polymorphic transformation was calculated as 1450 °C and the enthalpy of transformation was estimated from the standard enthalpy of formation [Brisi and Abbattista (1960)] determined by room-temperature solution calorimetry on the two polymorphs obtained by quenching. Bokeriya, et al. (1970b) by DTA reported a phase transformation for SA at 659 ºC. Ito, Banno, Suzuki, and Inagaki (1977) by XRD reported this transformation to occur at 650 ºC. Recently, Rodehorst, Carpenter, Marion, and Henderson (2003) summarized reported data on this transformation and studied the transformation by infrared powder absorption spectroscopy. They reported this transformation at about 677 °C.

P. Appendino (1972) observed that long annealing (of more than 200 hours at 1400 ºC) resulted in partial decomposition of SA_2 synthesized from the melt. He concluded that this compound forms from the melt and is stable only close to its melting point and then decomposes. Teoreanu

and Ciocea (1978), while studying the $SrAl_2O_4$-$BaAl_2O_4$-Al_2O_3 system, did not find this compound in their annealing the raw materials for 20 hours at 1700 °C. Capron and Douy (2002) by amorphous precursors and XRD reported SA_2 to be stable only at temperatures close to its melting point and below 1100 ºC; at intermediate temperatures it cannot crystallize. They also reported, by the same techniques, a new compound, $4SrO.7Al_2O_3$ (S_4A_7), stable between 1100 ºC to 1500 ºC. Hanic, et al. (1979) reported that SA_2 is stable below its melting point. Ye, et al. (2007) also calculated this phase as stable down to lower temperatures. In the present work, SA_2 was considered stable from its melting point to room temperature and the stability of S_4A_7 was calculated according to the data of Capron and Douy (2002).

Dear (1957) by XRD reported the presence of $5SrO.Al_2O_3$ (S_5A) with congruently melting behavior. Later, Jiang, Zhang, Huang, Jia, and Guo (2007) synthesized S_5A by the precursor method and studied its optical properties. In the present work, this compound is included as a stable phase with incongruent melting in order to be consistent with the SrO-rich liquidus reported by Hanic, et al. (1979) and Massazza (1959).

Bokeriya, et al. (1970b) performed calorimetric measurements to report the enthalpy increments ($H_{(T)}$–$H_{(298)}$) for SA which were fitted to obtain the heat capacity (C_p) equations presented in Table 2.6.1. These enthalpy increments are compared with the present calculations, in two different scales, in Fig. 2.6.2 and Fig. 2.6.3. The optimized heat capacity for SA was found to be close to the heat capacity obtained from adding the heat capacities of constituent oxides (C_p (SA) = C_p (SrO, solid) + C_p (Al_2O_3, corundum). Therefore, our estimations for the heat capacity of

compounds other than SA in Table 2.6.1 are reasonable. The enthalpy of transformation of SA from the low-temperature to the high-temperature form was calculated to be 2 kJ/mole by fitting the data in Fig. 2.6.3. The optimized standard entropy (S^0_{298}) and entropy of formation with oxides as reference standards (ΔS^0_{298}) are presented in Table 2.6.1. The ΔS^0_{298} values are always less than 10 J/(atom of metal) which is reasonable.

Brisi and Abbattista (1960), Massazza (1961) and Massazza and Cannas (1961) by solution calorimetry at room temperature reported enthalpies of formation of some intermediate compounds (ΔH^0_{298}). These data are well reproduced as shown in Fig. 2.6.4. Levitskii, et al. (1972) by EMF using the cell (+)Pt,O_2|$Sr_3Al_2O_6$, $SrAl_2O_4$, SrF_2|CaF_2|SrO, SrF_2| Pt,O_2(-) reported the Gibbs energy change for the reaction, 2SrO + SA = S_3A. These data are reasonably well reproduced as shown in Fig. 2.6.5.

No data on the mutual solubility among the SrO and Al_2O_3 phases could be found in the literature. Moreover, their different crystal structures and the very large difference in the ionic radii of Sr and Al (Sr = 132m and Al = 67.5 pm, [www.webelements.com (2012)]) also mitigate against any appreciable mutual solubility among them. Also, no data on the solid solubility in the solid phases (except for the low-temperature S_4A phase) appearing in the SrO-Al_2O_3 system were found. They were modeled as stoichiometric phases. Hanic, et al. (1979) reported small solubility of Al_2O_3 (1-2 mol%) in the "low-temperature" S_4A which was neglected in the present calculations.

The enthalpy of mixing and entropy of mixing at 3000 ºC in the liquid phase in the SrO-Al_2O_3 is compared with the other alkaline-earth oxide-alumina systems in the next section (Figs. 2.7.7 and 2.7.8 respectively). The enthalpy of mixing follows the trend that it is expected to be more negative in the series CaO to BaO.

Table 2.6.1 Optimized thermodynamic parameters for the SrO-Al_2O_3 system.

Liquid phase (Quasichemical model parameters)			
Z^{Al}_{AlAl} = 2.06616563; Z^{Sr}_{SrSr} = 1.37744375; $Z^{SrAl_2}_{SrAl_2SrAl_2}$ = 5.50977500; Z^{Sr}_{SrAl} = 2.75488750; Z^{Al}_{AlSr} = 1.37744375			
$\Delta g_{Sr\text{-}Al}$ = (–138072 + 16.736 T) – 117989 X_{SrSr} – 16736 X_{AlAl} J/mol			
g^0_{SrAl2} = g^0(SrO,Liq) + g^0(Al_2O_3,Liq) –112968 + 2.092 T J/mol			
Solid Phases			
ΔH^0_{298} (kJ/mole)			
Compound	Calculated, elements as reference	Calculated, oxides (stable at room-temperature) as reference	Experimental, oxides (stable at room-temperature) as reference
$Sr_5Al_2O_8$	–4730.769	–94.319	
LT-$Sr_4Al_2O_7$	–4135.526	–91.226	–92.717 ± 5.439 [Brisi and Abbattista, ‘60] –46.861 ± 5.021 [Massazza, ‘61]
HT-$Sr_4Al_2O_7$	$\Delta H_{trans}{}^*$ = 8.000 (at 1450 ºC)		$\Delta H_{trans}{}^*$ (exp) = 11.255 [Brisi and Abbattista, ‘60] $\Delta H_{trans}{}^*$ (exp) = 4.184 [Massazza, ‘61]
$Sr_3Al_2O_6$	–3545.865	–93.715	–97.738 ± 4.184 [Brisi and Abbattista, ‘60] –87.905 [Massazza and Cannas, ‘61]
LT-$SrAl_2O_4$	–2349.245	–81.395	–79.203 ± 2.929 [Brisi and Abbattista, ‘60]
HT-$SrAl_2O_4$	$\Delta H_{trans}{}^*$ = 2.000 (at 659 ºC)		
$SrAl_4O_7$	–4035.000	–91.450	
$Sr_4Al_{14}O_{25}$	–14446.205	–347.705	
$SrAl_{12}O_{19}$	–10755.475	–109.125	
S^0_{298}, ΔS^0_{298} and C_p (J/mol/K)			
Compound	S^0_{298}	ΔS^0_{298}, (calculated) oxides (stable at room-temperature) as reference	C_p
$Sr_5Al_2O_8$	363.000	44.280	C_p = 4 C_p (SrO) + C_p (HT-$SrAl_2O_4$)
LT-$Sr_4Al_2O_7$	308.000	42.860	C_p = 3 C_p (SrO) + C_p (HT-$SrAl_2O_4$)

HT-$Sr_4Al_2O_7$		ΔS_{trans}^{**} = 4.643 (at 1450 ºC)	$C_p = 3\ C_p\ (SrO) + C_p\ (HT\text{-}SrAl_2O_4)$
$Sr_3Al_2O_6$	249.000	37.440	$C_p = 2\ C_p\ (SrO) + C_p\ (HT\text{-}SrAl_2O_4)$
LT-$SrAl_2O_4$	124.000	19.600	$158 + 0.031\ T - 3813450\ T^{-2} - 8E{-}9\ T^3$; ($298 < T < 2400$)
HT-$SrAl_2O_4$		ΔS_{trans}^{**} = 2.146 (at 659 ºC)	$157 + 0.026\ T - 3613450\ T^{-2} - 2E{-}9\ T^3$; ($298 < T < 3000$)
$SrAl_4O_7$	181.000	25.780	$C_p = C_p\ (HT\text{-}SrAl_2O_4) + C_p\ (Al_2O_3\ (Corundum))$
$Sr_4Al_{14}O_{25}$	676.000	105.940	$C_p = 4\ C_p\ (SrO) + 7\ C_p\ (Al_2O_3)$
$SrAl_{12}O_{19}$	388.000	29.500	$C_p = C_p\ (HT\text{-}SrAl_2O_4) + 5\ C_p\ (Al_2O_3\ (Corundum))$

* Enthalpy of transformation from the low-temperature to the high-temperature $SrAl_2O_4$ (kJ/Mole).
** Entropy of transformation from the low-temperature to the high-temperature $SrAl_2O_4$ (J/mol/K).

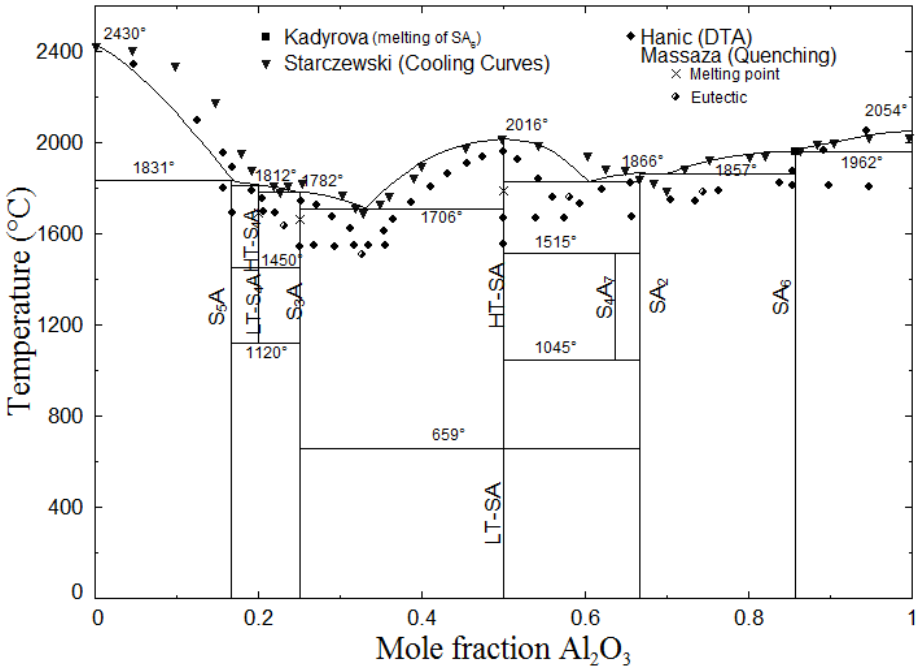

Fig. 2.6.1 Optimized phase diagram of the SrO-Al_2O_3 system.

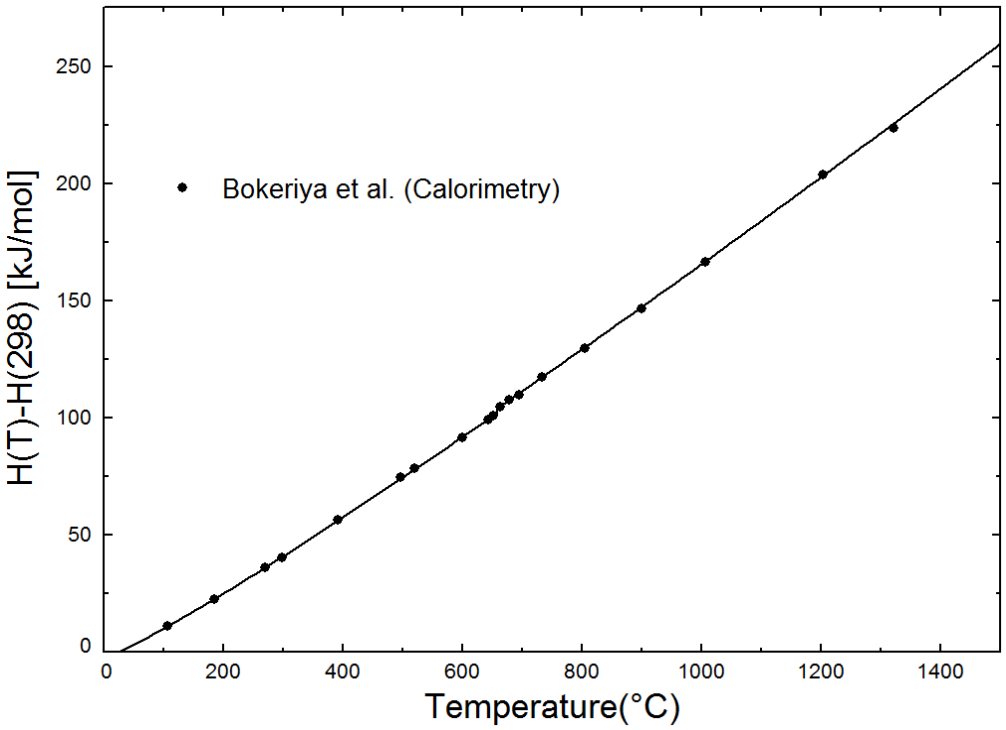

Fig. 2.6.2 Heat increments ($H_{(T)} - H_{(298)}$) per mole of the $SrAl_2O_4$ phase.

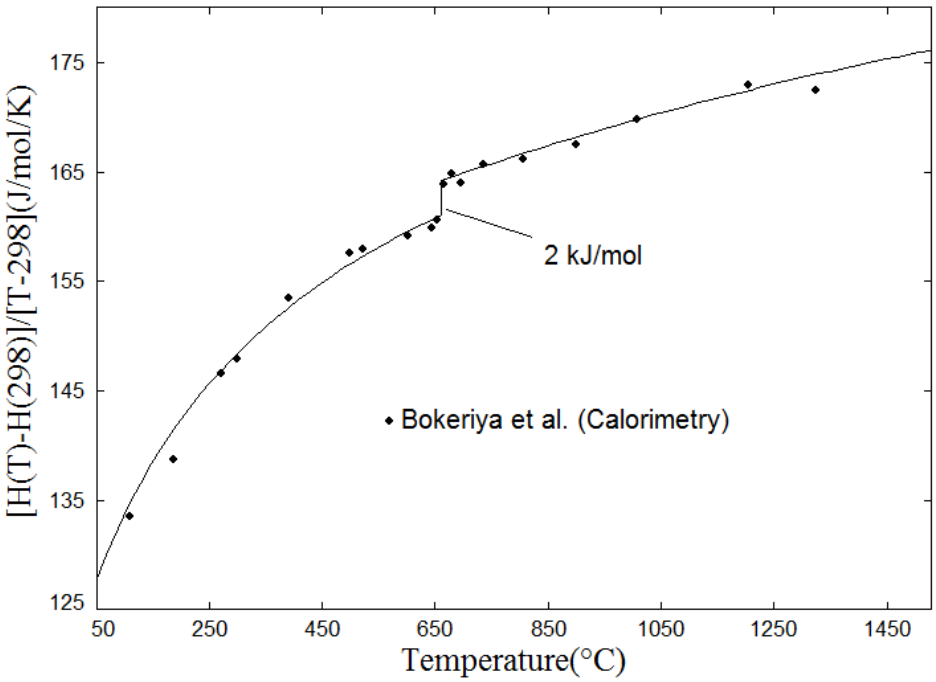

Fig. 2.6.3 Average heat capacity [$(H_{(T)} - H_{(298)})/(T - 298)$] per mole of the $SrAl_2O_4$ phase.

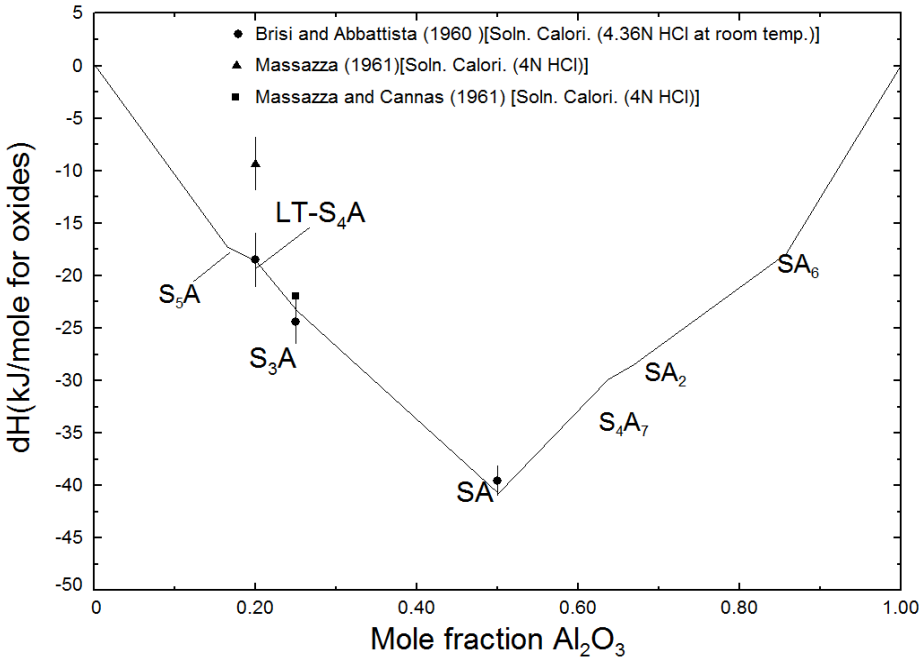

Fig. 2.6.4 Optimized standard enthalpy of formation (ΔH^0_{298}) in the SrO-Al_2O_3 system.

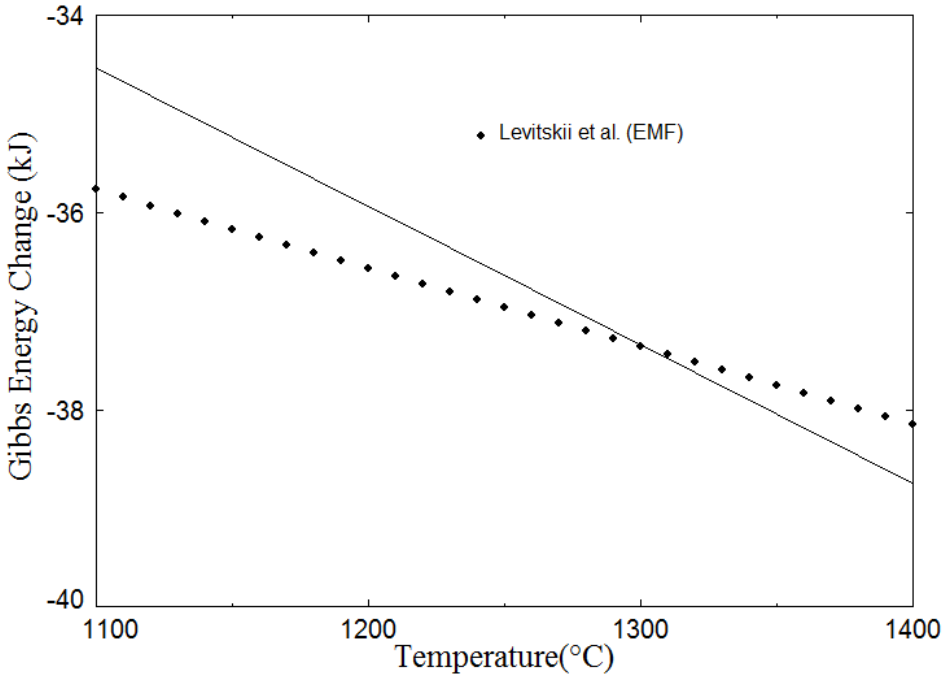

Fig. 2.6.5 Optimized Gibbs energy change in the reaction $2SrO + SrAl_2O_4 = Sr_3Al_2O_6$.

2.7 The BaO-Al_2O_3 system

The optimized phase diagram of the system is shown in Fig. 2.7.1 and optimized thermodynamic parameters are presented in Table 2.7.1. The optimized MQM parameters (and the coordination numbers) for the liquid phase are presented in Table 2.7.1. For these parameters, the same notations were used as used by Pelton and coworkers [Pelton, et al. (2000)]. Ye, Zhuang, Deng, Yuan, and Qiao (2006) optimized this system treating the liquid phase by a two-sublattice model for ionic solutions. In this work, however, the thermodynamic data by Bokeriya, Tsagareishvili, and Gvelesiani (1970a) and mass spectrometric data of Hilpert, Beske, and Naoumidis (1975) and Hilpert, Naoumidis, and Wolff (1975) were not taken into account.

In the BaO-Al_2O_3-SiO_2 system, to obtain the optimal fit of the available data, an additional component in the form of $BaAl_2$ associate was added to the liquid phase, i.e. $BaAl_2O_4$ was considered a separate component in the binary BaO-Al_2O_3 system (along with BaO and Al_2O_3). The optimized Gibbs energy of this component ($BaAl_2$ associate) and its coordination number in the liquid phase is presented in Table 2.7.1. Practically, these $BaAl_2$ associates are not stable in the binary BaO-Al_2O_3 system. They are stable in the ternary BaO-Al_2O_3-SiO_2 system, especially in the SiO_2-rich corner. In the BaO-Al_2O_3 system, at 2000 °C and at $X_{Al2O3} = 0.5$, the mole fraction of these associates is only 4.2×10^{-4} mole.

Purt (1960), by thermal analysis and XRD, and Toropov and Galakhov (1952), by quenching techniques, studied the system and reported $3BaO.Al_2O_3$ (B_3A), $BaO.Al_2O_3$ (BA) and $BaO.6Al_2O_3$ (BA_6) as stable compounds. The difference in the calculated phase diagram (Fig.

2.7.1) from these findings is discussed below. F. P. Glasser (1974) reported a polymorphic transformation of B_3A phase at 450 °C. The enthalpy of transformation could not be found in the literature. In the present work, this transformation is shown in Fig. 2.7.1 on the assumption that the thermodynamic properties for the high-temperature form are identical to the low-temperature form. Bokeriya, et al. (1970a) by thermal analysis, reported a polymorphic transformation of BA at 327 ºC. Recently, Rodehorst, et al. (2003) summarized the reported data on this transformation and studied the transformation by infrared powder absorption spectroscopy. They reported this transformation as about 127 °C. Mateika and Laudan (1979) studied the BA_6-Al_2O_3 region of the system by microscopic visual observation of the melting points and identification of the phases by XRD. There are various investigations [Haberey, Oehlschlegel, and Sahl (1977);S. Kimura, Bannai, and Shindo (1982);Iyi, Takekawa, Bando, and Kimura (1983);Iyi, Inoue, Takekawa, and Kimura (1984);Iyi, Inoue, Takekawa, and Kimura (1985)] which report that, in the aluminum-rich region, instead of a single BaA_6 phase there are two distinct phases on either side of the stoichiometric composition BaA_6, i.e. one with more Al_2O_3 and other deficient in it (called here as Al_2O_3-rich and Al_2O_3-deficinet phases). The stoichiometries of these compounds reported in these references differ slightly. Stevels (1978) and Mateika and Laudan (1979) reported that there is one phase but with a range of solid solubility. Gobbels, Kimura, and Woermann (1998) while studying the BaO-MgO-Al_2O_3 system showed two distinct phases in their phase diagrams with chemical formulae $Ba_{1.21}Al_{11}O_{17.71}$ and $Ba_{0.75}Al_{11}O_{17.25}$. Iyi, et al. (1983) reported hexagonal structure for the Al_2O_3-rich phase with space group $P6_3/mmc$ and also a hexagonal structure for the Al_2O_3-deficient phase but different space group $P\bar{6}$. The SrA_6 ($SrAl_{12}O_{19}$) and CA_6 ($CaAl_{12}O_{19}$) phases are also reported [K. Kimura, Ohgaki, Tanaka, Morikawa, and Marumo (1990); Kang, Park, Kim, and Choi (2009); Utsunomiya, Tanaka, Morikawa, Marumo, and

Kojima (1988)] to have hexagonal structure with the space group $P6_3/mmc$. Kadyrova and coworkers [Kadyrova and Daminova (1997; Kadyrova, Syrazhiddinov, and Tuganova (1996)] by quenching and XRD reported the BA_6 as the only stable phase in this region while studying the BA_6-CA_6 and BA_6-SA_6 sections. They reported complete solubility among the BA_6-CA_6 and BA_6-SA_6 phases. In the present work instead of considering an Al_2O_3-rich phase, close to the BA_6 composition, as stable, stoichiometric BA_6 phase was considered stable as it helped in fitting the higher-order phase diagram data of Kadyrova and coworkers. The Al_2O_3-deficient compound was taking into account in the present work as stoichiometric $Ba_{11}Al_{100}O_{161}$. This stoichiometry corresponds to the chemical formula $Ba_{1.21}Al_{11}O_{17.71}$ for this compound as reported by Gobbels, et al. (1998) in their phase diagrams for the BaO-MgO-Al_2O_3 systems. It must be noted that this stoichiometry is tentative and more experimental work is required to correctly establish it.

Pietro Appendino (1971) by XRD studied the most basic region, BaO-B_3A, of the phase diagram and reported five compounds, $4BaO.Al_2O_3$ (B_4A) stable above 940°, $5BaO.Al_2O_3$ (B_5A) stable below 940°, $7BaO.Al_2O_3$ (B_7A) stable below 1050°, $8BaO.Al_2O_3$ (B_8A) stable above 1050°, and $10BaO.Al_2O_3$ ($B_{10}A$) stable below 1130°. Kovba, Lykova, Antipov, Paromova, and Rozanova (1987) by XRD also reported all these phases as stable. They also reported a congruent melting point of 1560 ºC for the compound B_4A. In the present work also, all these phases were calculated as stable as shown in Fig. 2.7.1. The decomposition temperatures of these phases into other solid phases were calculated based upon the temperature ranges of stability reported by Pietro Appendino (1971). Much experimental work is, however, required to establish these data accurately. The present calculated congruent melting temperature for B_4A is 1575 °C.

Hilpert, Beske, et al. (1975) and Hilpert, Naoumidis, et al. (1975) reported the equilibrium partial pressures of BaO gas, by mass spectrometry at different compositions over a range of temperatures which are compared with the present calculations in Figs. 2.7.2 to 2.7.4. The thermodynamic data for BaO gas were taken from JANAF thermochemical tables [Stull and Prophet (1985)]. Experimental data in Fig. 2.7.2 show no evidence for the appearance of the liquid phase until 1820 °C (no change in the slope of experimental points). However, if liquidus data of Purt (1960) and Toropov and Galakhov (1952) are respected then the liquid phase appears below this temperature. Also, Mateika and Laudan (1979) reported that the eutectic lies in this region at about 1860 °C. Hence, no liquid phase can lie below this temperature, which is consistent with the data of Hilpert, Naoumidis, et al. (1975). Moreover, seeing the inconsistency of the two sets of liquidus data, preference was given in the present work to fit the data of Mateika and Laudan (1979) and mass spectrometric data of Hilpert, Beske, et al. (1975) and Hilpert, Naoumidis, et al. (1975). The optimal fit of these data gives the melting temperature of the BA phase as 2285 °C. If the experimental melting temperatures for the BA phase in Fig. 2.7.1 were fitted, then it would cause the liquid phase to appear below 1820 °C which was inconsistent with the liquidus data of Mateika and Laudan (1979) and mass spectrometric data of Hilpert and coworkers. As preference was given to these liquidus and mass spectrometric data and there is no other experimental datum on the melting temperature of the BA phase, it was tentatively calculated (shown as dashed line in Fig. 2.7.1) as 2285 °C. Similarly, Hilpert, Beske, et al. (1975) reported partial pressures of BaO gas at the composition $1.1BaO + 0.9Al_2O_3$ (Fig. 2.7.3). The present calculations are consistent with these data at temperatures where only solid phases (B_3A and BA) are in equilibrium. However, at temperatures greater than 1580 °C, temperatures at which the liquid phase is in equilibrium with the BA phase, reported partial pressures of BaO are

inconsistent with the present calculations (Fig. 2.7.3). Hilpert, Beske, et al. (1975) acknowledged the loss of BaO due to vaporization at this composition and at temperature greater than 1580 °C. It must be noted that the experimental partial pressures in Fig. 2.7.3 at temperature greater than 1580 °C are identical to the one reported for the composition $0.9BaO + 1.1Al_2O_3$. Possibly, because of excessive vaporization of BaO, Hilpert, Beske, et al. (1975) could not keep the starting composition of $1.1BaO + 0.9Al_2O_3$ fixed which led them to measure the decreased partial pressure of BaO. The drastic change in the experimental vapor pressure of BaO (at temperatures greater than 1580 °C) due to melting of B_3A and appearance of liquid phase is not possible. And, it can be said that more work is required to corroborate these data. Hilpert, Beske, et al. (1975) reported partial pressure of BaO gas for the composition $1BaO + 6.4\ Al_2O_3$ which are reasonably well fitted in Fig. 2.7.4.

Peppler and Newman (1951) by solution calorimetry determined the standard enthalpy of formation (ΔH^0_{298}) for the BA and B_3A phases. These data were used as enthalpy of formation for these compounds as shown in Table 2.7.1. Bokeriya, et al. (1970a) performed calorimetric measurements to determine heat contents ($H_T - H_{298}$) for the BA phase. These data are compared with the present calculations, in two difference scales, in Figs. 2.7.5 and 2.7.6. The temperature and enthalpy of transformation from low-temperature to high-temperature BA was obtained by fitting the data shown in Fig. 2.7.6 as were heat capacity (C_p) values for these phases in Table 2.7.1. The optimized heat capacity for BA was found to be close to the heat capacity obtained from adding the heat capacities of constituent oxides (C_p (BA) = Cp (BaO, solid) + C_p (Al_2O_3, corrundum). The optimized standard entropy (S^0_{298}) and entropy of formation with oxides as

reference standards (ΔS^0_{298}) are presented in Table 2.7.1. The data of Hilpert, Beske, et al. (1975) and Hilpert, Naoumidis, et al. (1975) were used to optimize the entropies of the BA, B_3A and BA_6 phases. The ΔS^0_{298} values of other phases are always less than 8 J/(atom of metal) which is quite reasonable.

No data on the mutual solubility among the BaO and Al_2O_3 phases could be found in the literature. Moreover, their different crystal structures and the very large difference in the ionic radii of Ba and Al (Ba = 149 pm and Al = 67.5 pm, [www.webelements.com (2012)]) also mitigate against any appreciable mutual solubility among them. Also, no data on the solid solubility in the solid phases appearing in the BaO-Al_2O_3 system were found. They were modeled as stoichiometric phases.

The enthalpy of mixing and entropy of mixing at 3000 ºC in the liquid phase in the alkaline-earth oxide-alumina systems are compared in Figs. 2.7.7 and 2.7.8 respectively. The enthalpy of mixing follows the trend that it is expected to be more negative in the series CaO to BaO.

Table 2.7.1 Optimized thermodynamic parameters (in Joules/mol) for the BaO-Al_2O_3 system.

Liquid phase (Quasichemical model parameters)

Z^{Al}_{AlAl} = 2.06616563; Z^{Ba}_{BaBa} = 1.37744375; $Z^{BaAl_2}_{BaAl_2BaAl_2}$ = 5.50977500; Z^{Ba}_{BaAl} = 2.75488750; Z^{Al}_{AlBa} = 1.37744375

$\Delta g_{BaAl} = (-150624 + 16.736\ T) - 112968\ X_{BaBa}$

$g^0_{BaAl2} = g^0(BaO,Liq.) + g^0(Al_2O_3,Liq.) - 138072 + 2.092\ T$

Solid Phases

ΔH^0_{298} (kJ/mole)

Compound	Calculated from elements	Calculated oxides (stable at room-temperature) as reference	Experimental, (calculated) oxides (stable at room-temperature) as reference
$Ba_{10}Al_2O_{13}$	–7350.532	–193.792	
$Ba_8Al_2O_{11}$	–6180.905	–120.373	
$Ba_7Al_2O_{10}$	–5705.000	–192.572	
$Ba_4Al_2O_7$	–4036.020	–167.904	
$Ba_5Al_2O_8$	–4608.012	–191.792	
$Ba_3Al_2O_6$	–3504.317	–184.305	–184.305 [Peppler and Newman, '51]
LT-$BaAl_2O_4$	–2324.178	–100.374	–100.374 [Peppler and Newman, '51]
HT-$BaAl_2O_4$	$\Delta H_{trans}{}^{*}$ = 1.400 (at 327 ºC)		
$BaA_{12}O_{19}$	–10732.000	–129.696	
$Ba_{11}Al_{100}O_{161}$	–91201.047	–1386.903	

S^0_{298}, ΔS^0_{298} and C_p (J/mol/K)

Compound	S^0_{298}	ΔS^0_{298} oxides (stable at room-temperature) as reference	C_p
$Ba_{10}Al_2O_{13}$	777.600	6.091	C_p (HT-$BaAl_2O_4$) + 9 C_p (BaO)
$Ba_8Al_2O_{11}$	693.000	65.628	C_p (HT-$BaAl_2O_4$) + 7 C_p (BaO)
$Ba_7Al_2O_{10}$	562.100	6.798	C_p (HT-$BaAl_2O_4$) + 6 C_p (BaO)
$Ba_4Al_2O_7$	369.000	29.905	C_p (HT-$BaAl_2O_4$) + 3 C_p (BaO)
$Ba_5Al_2O_8$	418.200	7.036	C_p (HT-$BaAl_2O_4$) + 4 C_p (BaO)
$Ba_3Al_2O_6$	280.000	12.974	C_p (HT-$BaAl_2O_4$) + 2 C_p (BaO)
LT-$BaAl_2O_4$	158.000	35.112	$170.5 + 0.022\ T - 5613450\ T^{-2}$ ($298.15 < T < 610$ K)

HT-$BaAl_2O_4$	ΔS_{trans}^{**} = 2.500 (at 327 ºC)		138 + 0.032 *T* (610 < *T* < 2500 K)
$BaA_{12}O_{19}$	400.200	23.211	C_p (HT-$BaAl_2O_4$) + 5 C_p (Al_2O_3, Corrundum)
$Ba_{11}Al_{100}O_{161}$	3595.060	261.301	11 C_p (HT-$BaAl_2O_4$) + 39 C_p (Al_2O_3, Corrundum)

[*] Enthalpy of transformation from the low-temperature to the high-temperature $BaAl_2O_4$ (kJ/Mole).
[**] Entropy of transformation from the low-temperature to the high-temperature $BaAl_2O_4$ (J/mol/K).

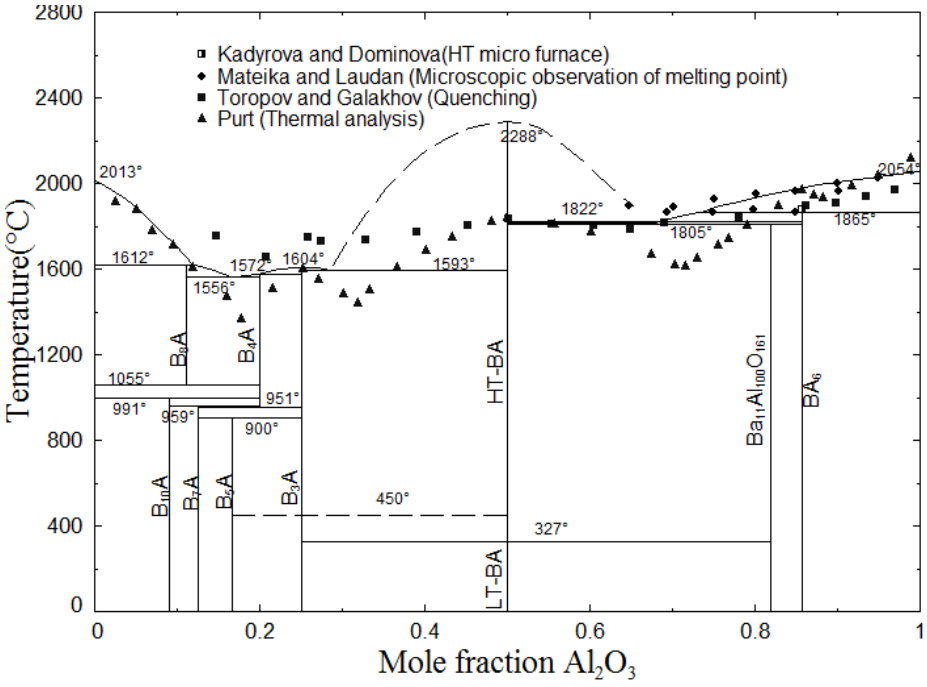

Fig. 2.7.1 Optimized phase diagram of the BaO-Al_2O_3 system.

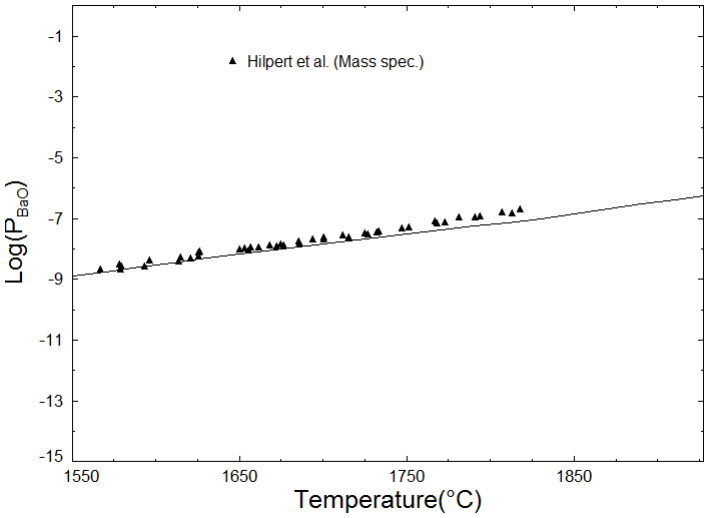

Fig. 2.7.2 Equilibrium partial pressure of BaO (g) at the composition 0.9 BaO + 1.1 Al_2O_3.

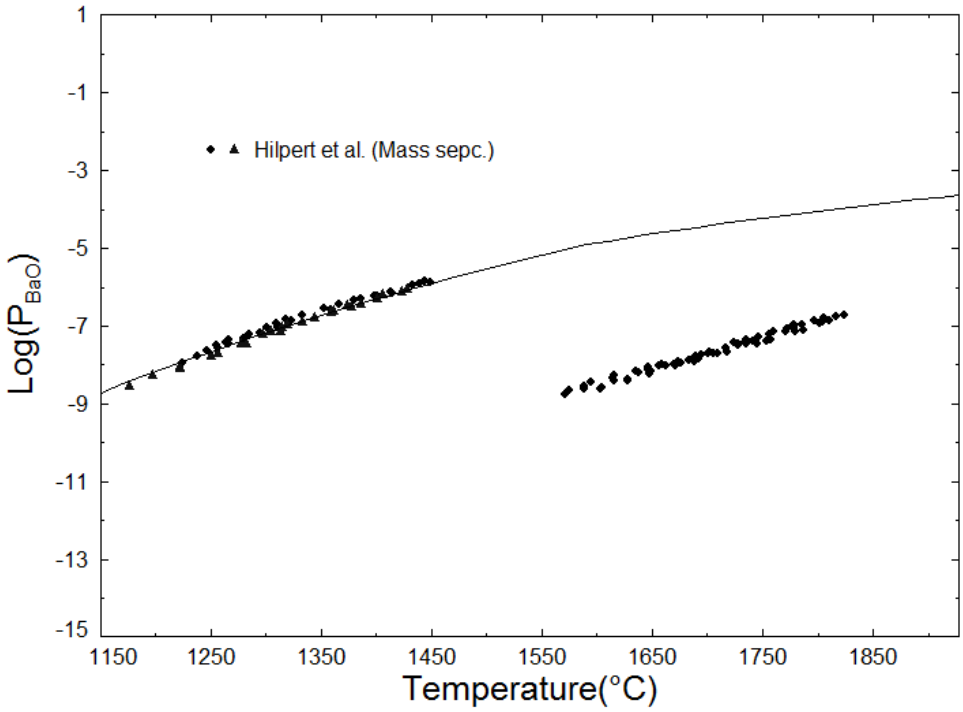

Fig. 2.7.3 Equilibrium partial pressure of BaO (g) at the composition 1.1 BaO + 0.9 Al_2O_3.

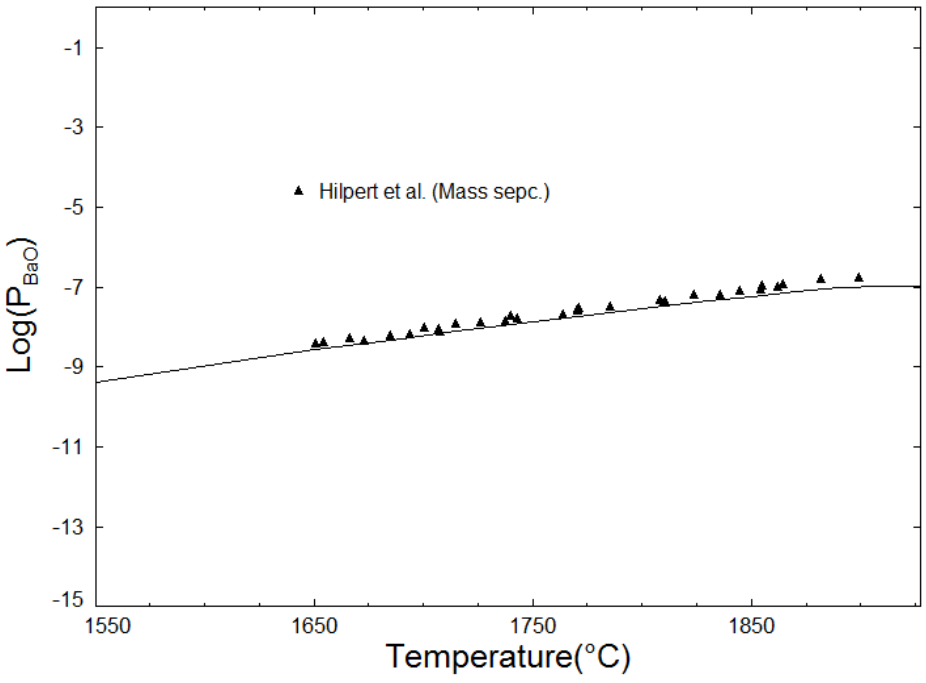

Fig. 2.7.4 Equilibrium partial pressure of BaO (g) at the composition 1BaO + 6.4 Al_2O_3.

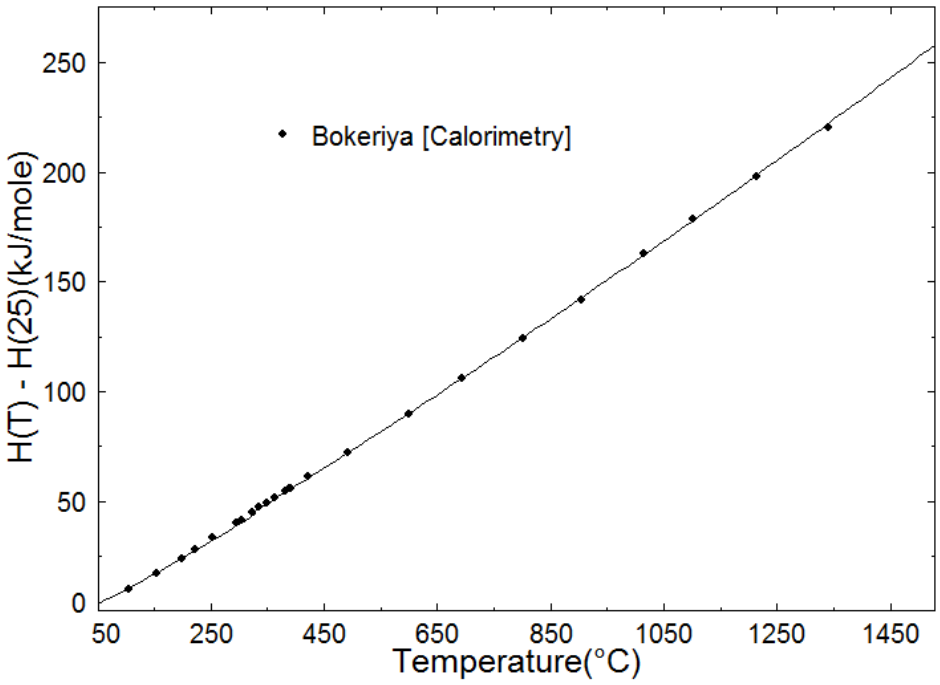

Fig. 2.7.5 Enthalpy increments ($H_{(T)} - H_{(298)}$) for per mole of the $BaAl_2O_4$ phase.

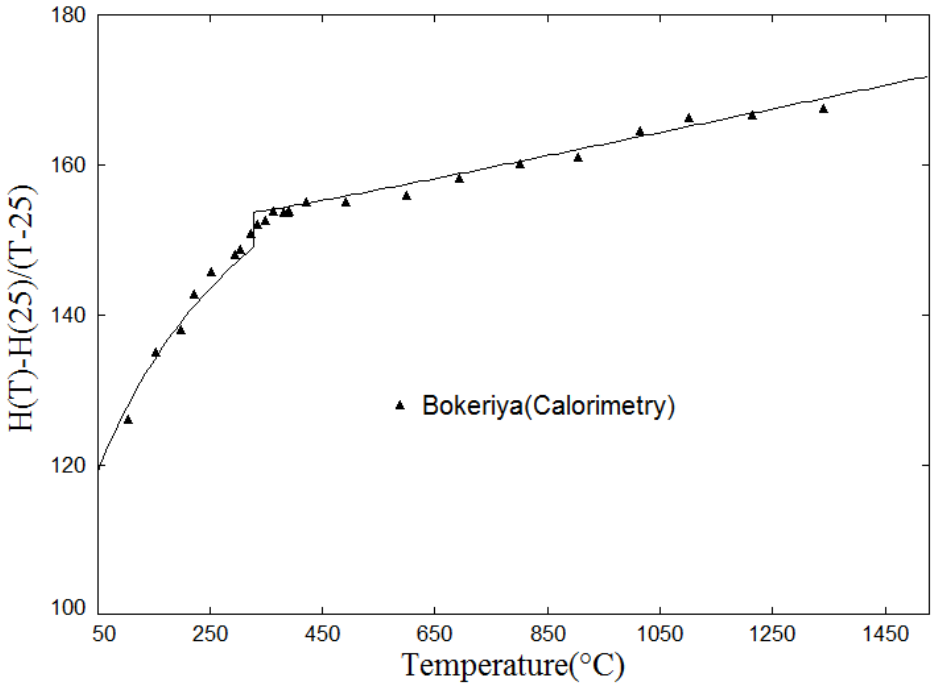

Fig. 2.7.6 Average heat capacity [$(H_{(T)} - H_{(298)})/(T - 298)$] of the $BaAl_2O_4$ phase (per mole).

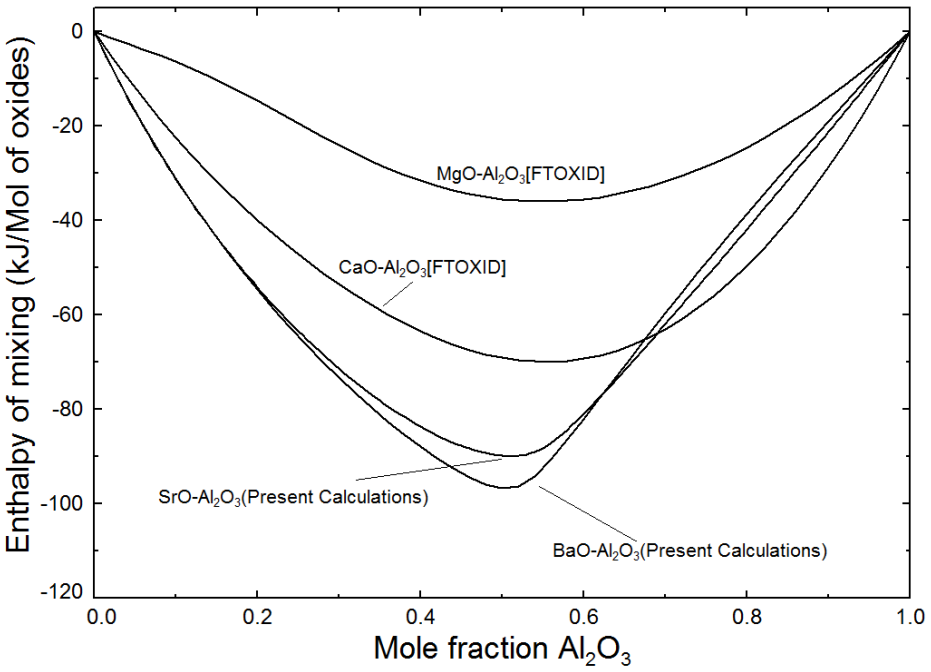

Fig. 2.7.7 Enthalpy of mixing at 2000 ºC in the liquid phase in the alkaline-earth oxide-alumina systems.

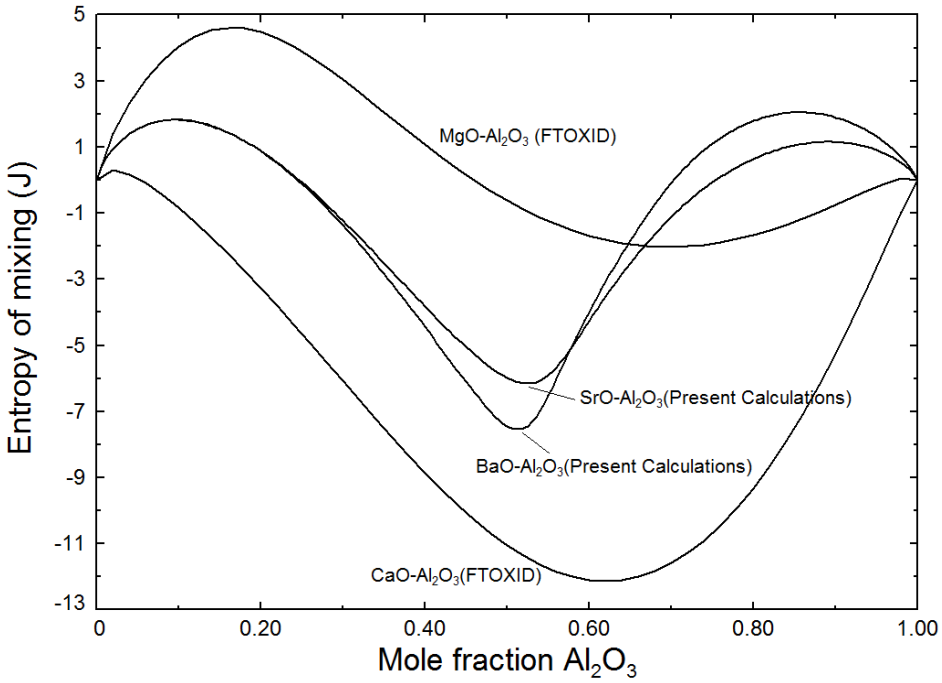

Fig. 2.7.8 Entropy of mixing at 2000 ºC in the liquid phase in the alkaline-earth oxide-alumina systems.

2.8 The BaO-B_2O_3 system

The optimized phase diagram of the system is shown in Fig. 2.8.1 and optimized parameters are presented in Table 2.8.1. The optimized MQM parameters (and the coordination numbers) for the liquid phase are presented in Table 2.8.1. For these parameters, the same notations were used as used by Pelton and coworkers [Pelton, et al. (2000)]. Yu, Chen, and Jin (1999) optimized the system, modeling the liquid phase by two-sublattice ionic solution model.

Guertler (1904) studied the system by cooling curve analysis and reported $3BaO.B_2O_3$ (Ba_3B), $2BaO.B_2O_3$ (Ba_2B), and $BaO.B_2O_3$ (BaB) as equilibrium phases. Carli (1927) also used the same technique to report $BaO.4B_2O_3$ (BaB_4), $BaO.3B_2O_3$ (BaB_3), and $BaO.2B_2O_3$ (BaB_2) as equilibrium phases. Later, Levin and McMurdie (1949), by quenching techniques, reported the phases shown in Fig. 2.8.1. However, they did not find the Ba_2B and BaB_3 phases. Hamilton, Cleek, and Grauer (1958), while studying the ternary system BaO-B_2O_3-SiO_2 by thermal analysis, reported a few melting temperatures in the binary system. Meshalkin and Kaplun (2005) by thermal analysis studied the system from 32 to 67 mol% B_2O_3. They reported the presence of the phase Ba_2B with a peritectic melting point and bounded low-temperature stability. They also reported the presence of a metastable phase $2BaO.3B_2O_3$. Huebner (1969) by XRD reported $2BaO.5B_2O_3$ (Ba_2B_5), Ba_2B and $4BaO.B_2O_3$ (Ba_4B) as stable phases. In the present work, the Ba_2B is included as an equilibrium phase as it was also reported by Guertler (1904) and Meshalkin and Kaplun (2005). Meshalkin and Kaplun (2005) reported the stability range for the phase Ba_2B as 850-1125 °C. The temperature for low-temperature decomposition was tentative. In the present calculations, for an optimal fit of the available liquidus data, the stability of this

phase was calculated as shown in Fig. 2.8.1. Hovhannisyan (2006) studied the system by XRD and DTA and reported all the phases shown in Fig. 2.8.1 as stable. As the Ba_2B_5 phase was reported stable by both Hovhannisyan (2006) and Huebner (1969), this phase was considered as stable in the present calculations also. Wang, Huang, and Liang (1984) while studying the SrO-BaO-B_2O_3 ternary system reported Ba_4B as a stable phase. In their phase diagrams, this phase was found to be stable till 920 °C. No other data on this phase could be found in the literature. In the present calculations, this phase was tentatively calculated to decompose into BaO and Ba_3B phases at around 1000 °C. The BaB_3 phase reported by Carli (1927) was not considered stable, and further experiments are required to confirm its presence. Several authors [Levin and McMurdie (1949);Ohta, Morinaga, and Yanagase (1982);V. B. M. Hageman and Oonk (1979);V. B. M. Hageman and Oonk (1987);Levin and Cleek (1958);Clemens, Yoshiyagawa, and Tomozawa (1981);Crichton and Tomozawa (1997)] studied the liquid immiscibility in the system (Fig. 2.8.1). The boundary of the miscibility gap determined by Ohta, et al. (1982) using a handmade apparatus, for the hot-thermocouple method, and by Hageman and Oonk [V. B. M. Hageman and Oonk (1979) and V. B. M. Hageman and Oonk (1987)], using equilibration and quenching followed by refractive index measurements, were found to agree closely.

Huebner (1969) by XRD, Liang and Huang (1982) by XRD and DTA, and Kouta, Kuwano, Suda, Ishizawa, and Marumo (1994) by high-temperature XRD reported a phase transformation of the BaB phase at about 925 ºC. In the present work, this transformation was neglected because the enthalpy of the transformation could not be found in the literature. A single phase BaB_2O_4, stable up to room temperature, was considered. For the sake of presentation, this transformation

is shown in Fig. 2.8.1 by assuming the thermodynamic properties of the high-temperature phase to be the same as the low-temperature phase.

Cordfunke, Konings, Van der Laan, and Ouweltjes (1993) and Z.-H. Liu, Wang, and Huang (2007) using solution calorimetry reported ΔH^0_{298} for the phases Ba_3B and BaB respectively. The results of Cordfunke, et al. (1993) for ΔH^0_{298} (from elements) of Ba_3B was –2344.2 kJ/mole. ΔH^0_{298} of Ba_3B calculated with reference to oxides (i.e. BaO and B_2O_3), is a positive quantity, 572.048 kJ/mole. Such a positive value is highly unrealistic unless this compound is not stable at room temperature. It is worth mentioning here that for this determination Cordfunke, et al. (1993) required ΔH^0_{298} for $BaCl_2$ as the solution medium taken in the calorimetry was HCl(aq). The value used by them as –1604.2 kJ/mole from the literature is in gross error with the value from the FTSALT database which is –2575.7 kJ/mole. Thus in the present work, the ΔH^0_{298} of Ba_3B was recalculated by using ΔH^0_{298} for $BaCl_2$ from the FTSALT database and all the other required data from Cordfunke, et al. (1993). The value obtained was –3359.9 kJ/mole. This was presented in Fig. 2.8.2 with the label corrected value.

Asano and Kou [Asano and Kou (1989); Asano and Kou (1990)] by the mass-spectrometric/Kudsen effusion method measured the partial pressure of B_2O_3 gas over the BaB liquid, BaB_2 liquid and Ba_3B solid phases. In the present calculations the data for the B_2O_3 gas were taken from JANAF Thermochemical Tables (1985). The present calculations are consistent with these measurements for the BaB and BaB_2 liquids as shown in Figs. 2.8.3 and 2.8.4. However, the present work does not fit these data for the Ba_3B solid phase (Fig. 2.8.5). It was

observed that these data for the Ba_3B phase can be fitted well with a H^0_{298} value which is much less negative than the presently calculated or with a very negative ΔS^0_{298} value. Such a value of H^0_{298} for the Ba_3B phase, and consequently for the BaB phase in an optimal fit, will exacerbate the fit in Fig. 2.8.2. A very negative ΔS^0_{298} is also unreasonable. Hence the data by Asano and Kou for the solid Ba_3B phase were given less weight.

The enthalpy increments ($H_T - H_{25}$) for the phase Ba_3B were measured by Cordfunke, et al. (1993) using drop calorimetry, and are well reproduced in Fig 2.8.6. Stewart and Rindone (1963) by high-temperature calorimetry reported enthalpy increments ($H_T - H_{298}$) for solid and liquid BaB_2 (Fig. 2.8.7) and BaB_4 (Fig. 2.8.8) phases. These enthalpy increments were used to obtain the heat capacities (C_p) for the solid phases presented in Table 2.8.1. In the present calculations, the heat capacity of the liquid phase was calculated by adding the heat capacities of the constituent oxides. Hence, there is disagreement with the data in the liquid region as shown in Figs. 2.8.7 and 2.8.8. The data for the crystals are well reproduced.

Muller and Demirok (1989) measured the integral enthalpy of mixing by dropping samples containing an intimate mixture of crystalline BaO and amorphous B_2O_3 at room temperature into a calorimeter maintained at 1278 ºC. Exact fitting of these enthalpy data gives a larger miscibility gap than calculated in Fig. 2.8.1, which is in disagreement with the available different sets of data. Hence, the enthalpy of mixing was fitted as shown in Fig. 2.8.9. The optimized standard entropy (S^0_{298}) and entropy of formation with oxides as reference standards (ΔS^0_{298}) are presented in Table 2.8.1. The ΔS^0_{298} values are always less than 12 J/(atom of metal), which is reasonable.

No data on the mutual solubility among the BaO and B_2O_3 phases could be found in the literature. Moreover, their different crystal structures and the very large difference in the ionic radii of Ba and B (Ba = 149 pm and B = 25 pm, [www.webelements.com (2012)]) also mitigate against any appreciable mutual solubility among them. Also, no data on the solid solubility in the solid phases appearing in the BaO-Al_2O_3 system were found. They were modeled as stoichiometric phases.

The enthalpy of mixing, at 2500 ºC, and the entropy of mixing, at 1500 °C, in the liquid phase in the BaO-B_2O_3 system is compared with the other alkaline-earth oxide-boron oxide systems in the next section (Figs. 2.9.6 and 2.9.7 respectively). The enthalpy of mixing follows the trend that it is expected to be more negative in the series CaO to BaO.

Table 2.8.1 Optimized thermodynamic parameters (in Joules/mol) for the BaO-B_2O_3 system.

Liquid phase (Quasichemical model parameters)

$Z^{B}_{BB} = 2.06616563$; $Z^{Ba}_{BaBa} = 1.37744375$

$\Delta g_{BaB} = -209200 - 121336\ X_{BB} - 41840\ X_{BB}^4 + (175728 - 48.116\ T)\ X_{BB}^7$

Solid Phases

ΔH^0_{298} (kJ/mole)

Compound	Calculated from elements	Calculated, oxides (stable at room-temperature) as reference	Experimental From elements[a]
$Ba_4B_2O_7$	–3826.104	–361.752	
$Ba_3B_2O_6$	–3276.000	–359.752	–3359.961 ± 5.8 [Cordfunke et al., '93][b]
$Ba_2B_2O_5$	–2576.500	–208.356	
BaB_2O_4	–2004.300	–184.260	–2020.300 ± 1.7 [Liu et al., '07]
$Ba_2B_{10}O_{17}$	–7810.012	–354.124	
BaB_4O_7	–3270.438	–178.462	–3237.899[c]

Compound	S^0_{298}	ΔS^0_{298} calculated, oxides (stable at room-temperature) as reference	ΔS^0_{298} calculated, compounds used to calculate heat capacities as reference	C_p (298.15 < T < 2000 K)
$Ba_4B_2O_7$	380.500	38.274	–1.569	$C_p(BaO) + C_p(Ba_3B_2O_6)$
$Ba_3B_2O_6$	310.000	39.843		$257 + 0.028\ T - 5500000\ T^{-2}$
$Ba_2B_2O_5$	280.000	81.912	64.431	$C_p(BaO) + C_p(BaO.B_2O_3)$
BaB_2O_4	143.500	17.481	–9.0345	$0.5\ (C_p(BaO) + C_p(BaO.2B_2O_3))$
$Ba_2B_{10}O_{17}$	538.550	124.662	18.600	$C_p(B_2O_3) + 2\ C_p(BaO.2B_2O_3)$
BaB_4O_7	233.000	53.031		$223 + 0.048\ T - 6000000\ T^{-2}$
BaB_8O_{13}	390.000	102.131		$400 + 0.102\ T - 14000000\ T^{-2}$

[a] In all these references the enthalpy of formation was reported with reference to elements.
[b] Corrected value (see text).
[c] Calculated from the enthalpy of mixing for the liquid phase (Muller and Demirok (1989)), enthalpy of melting and heat capacity for the respective solid phases (Stewart and Rindone (1963).

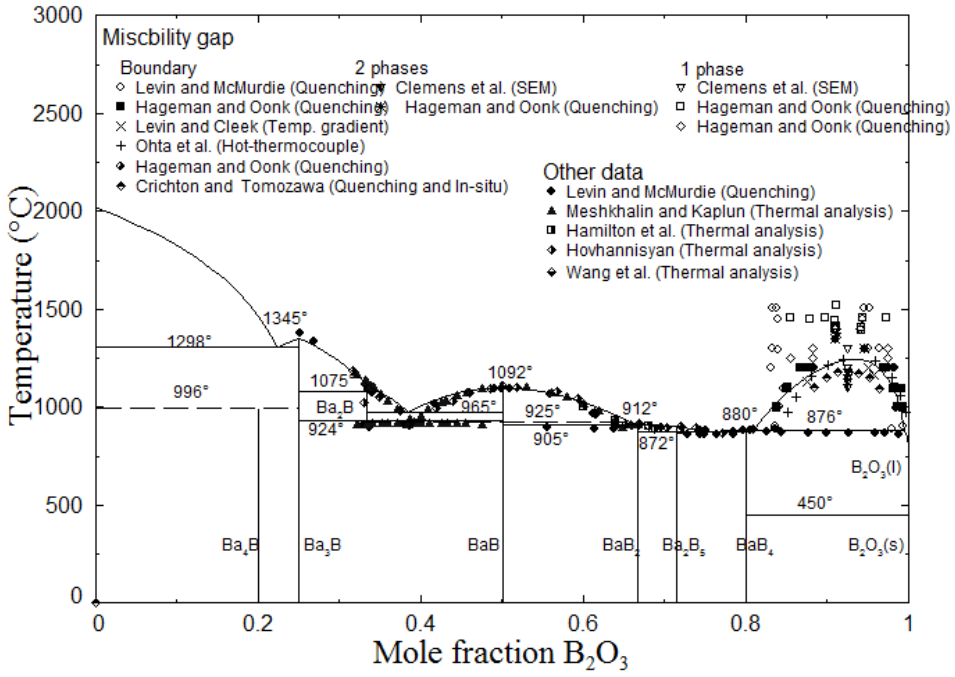

Fig. 2.8.1 Optimized phase diagram of the BaO-B_2O_3 system.

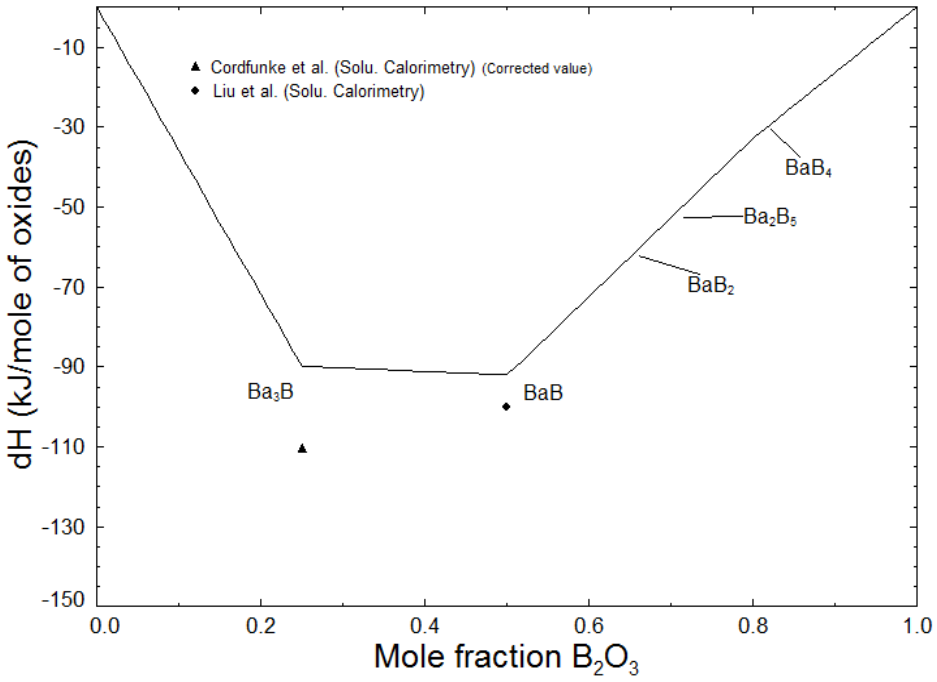

Fig. 2.8.2 Optimized standard enthalpy of formation of intermediate compounds in the BaO-B_2O_3 system.

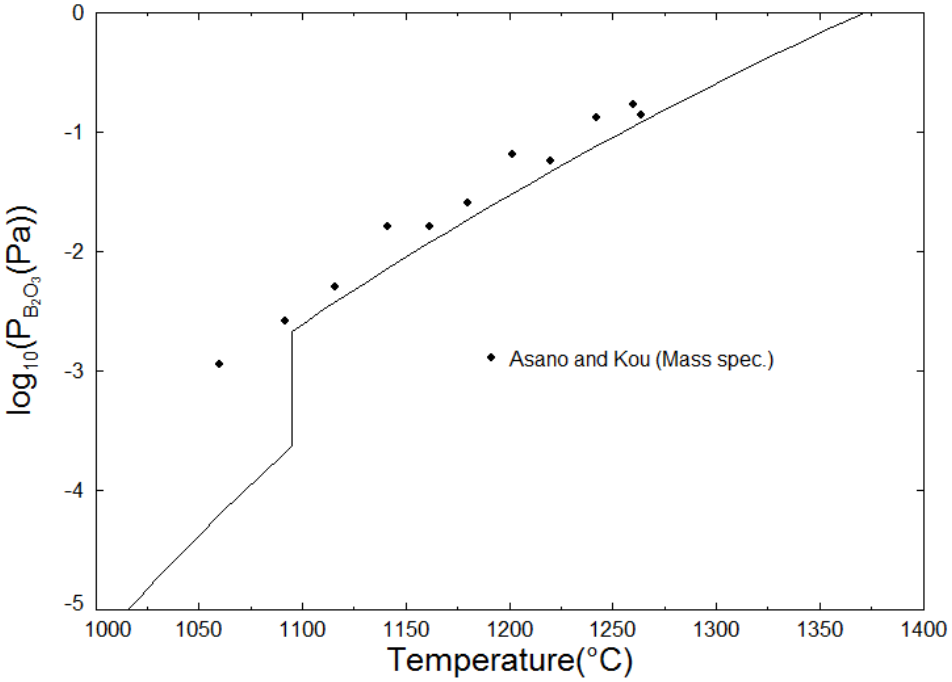

Fig. 2.8.3 Optimized partial pressure of B_2O_3 at the BaB_2O_4 composition.

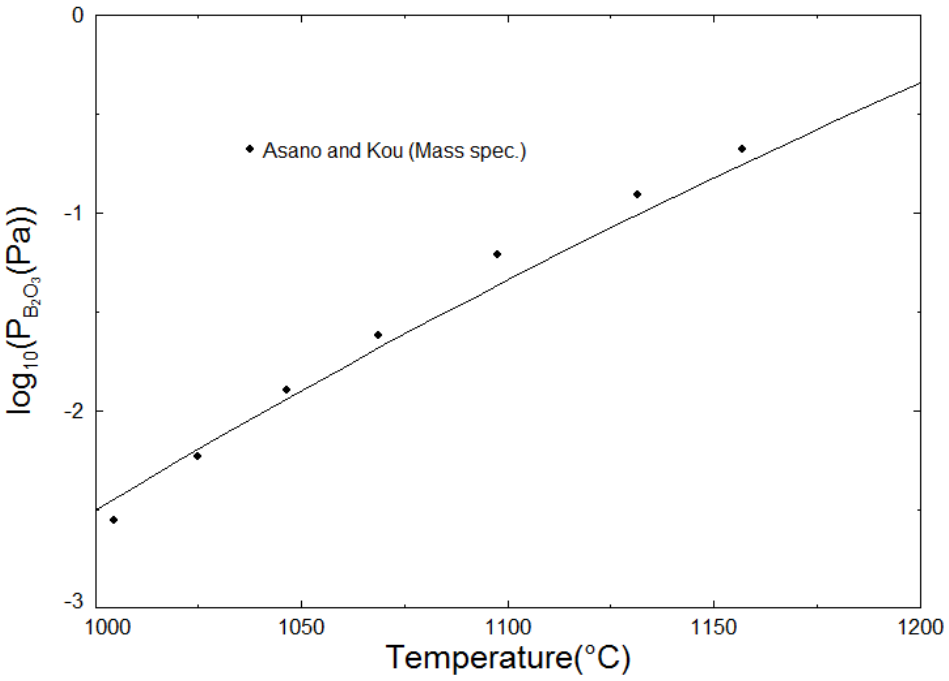

Fig. 2.8.4 Optimized partial pressure of B_2O_3 at the BaB_4O_7 composition.

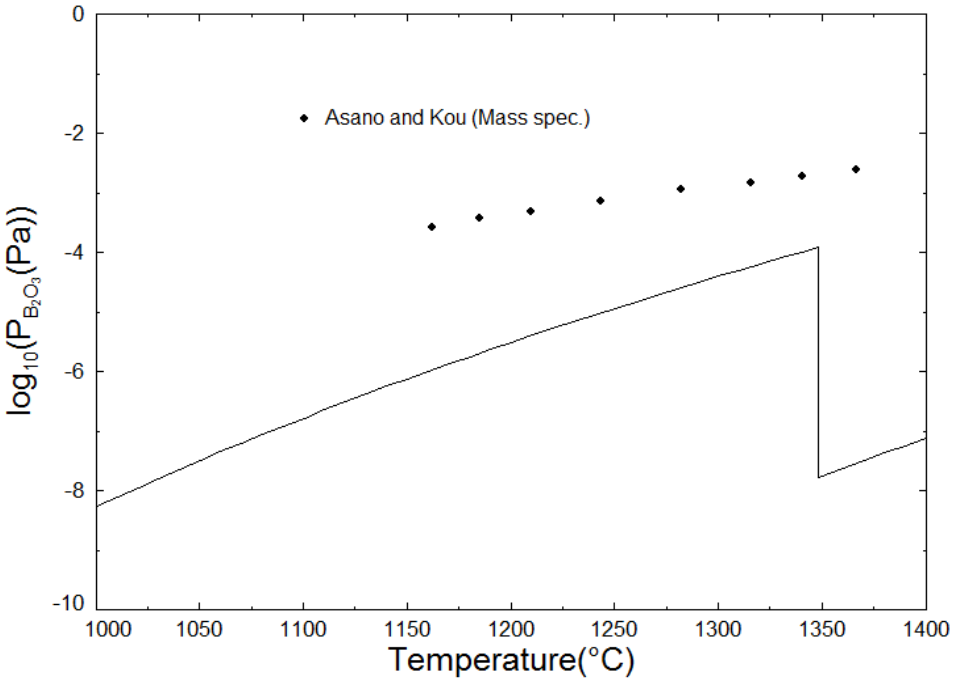

Fig. 2.8.5 Optimized partial pressure of B_2O_3 at the $Ba_3B_2O_6$ composition.

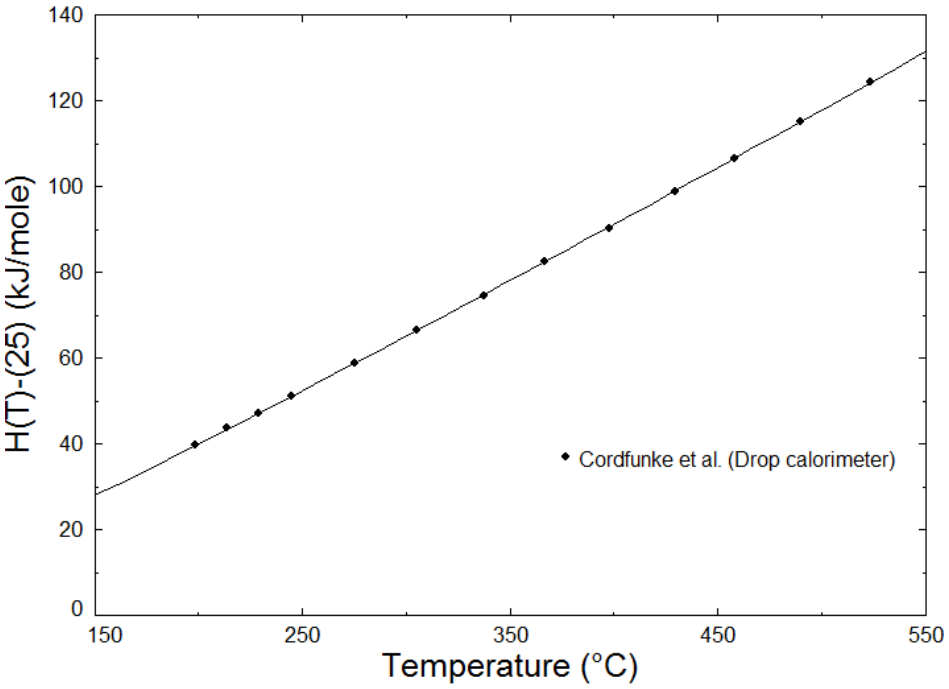

Fig. 2.8.6 Optimized enthalpy increments ($H_{(T)} - H_{(298)}$ for the $Ba_3B_2O_6$ phase.

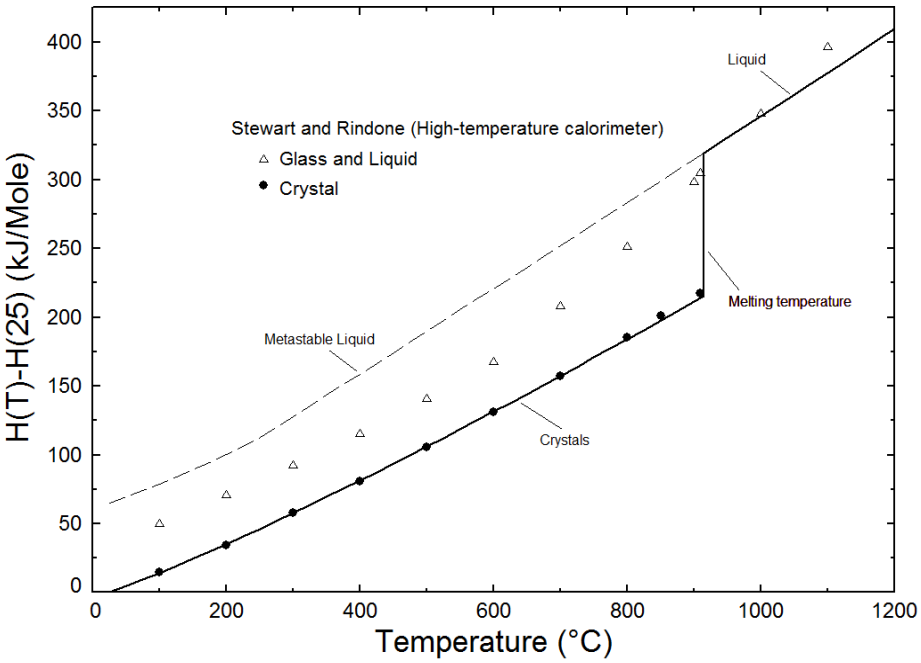

Fig. 2.8.7 Optimized enthalpy increments ($H_{(T)} - H_{(298)}$) (ref. state crystals) for the BaB_4O_7 phase.

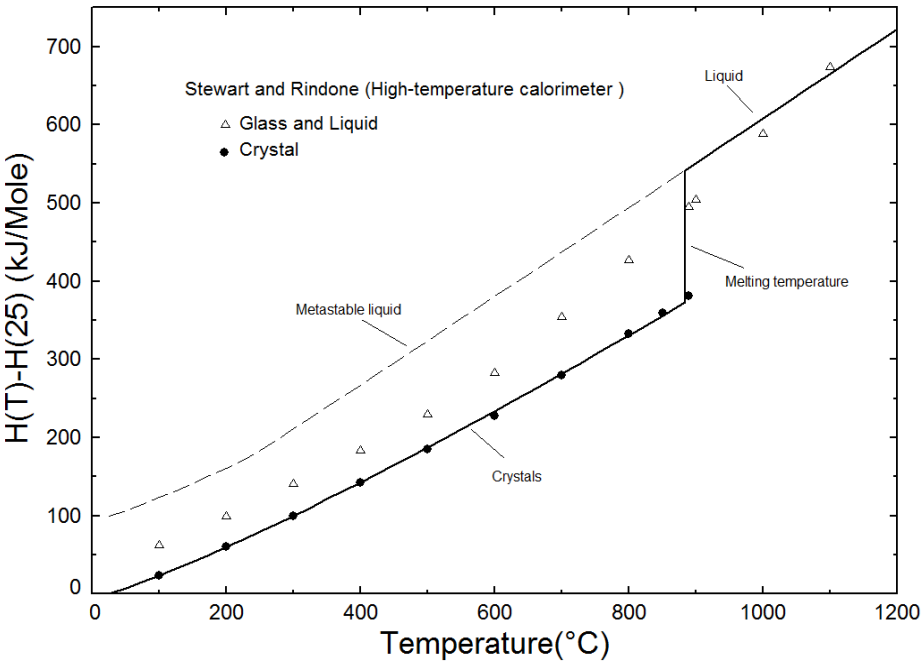

Fig 2.8.8 Optimized enthalpy increments ($H_{(T)} - H_{(298)}$) (ref. state crystals) for the BaB_8O_{13} phase.

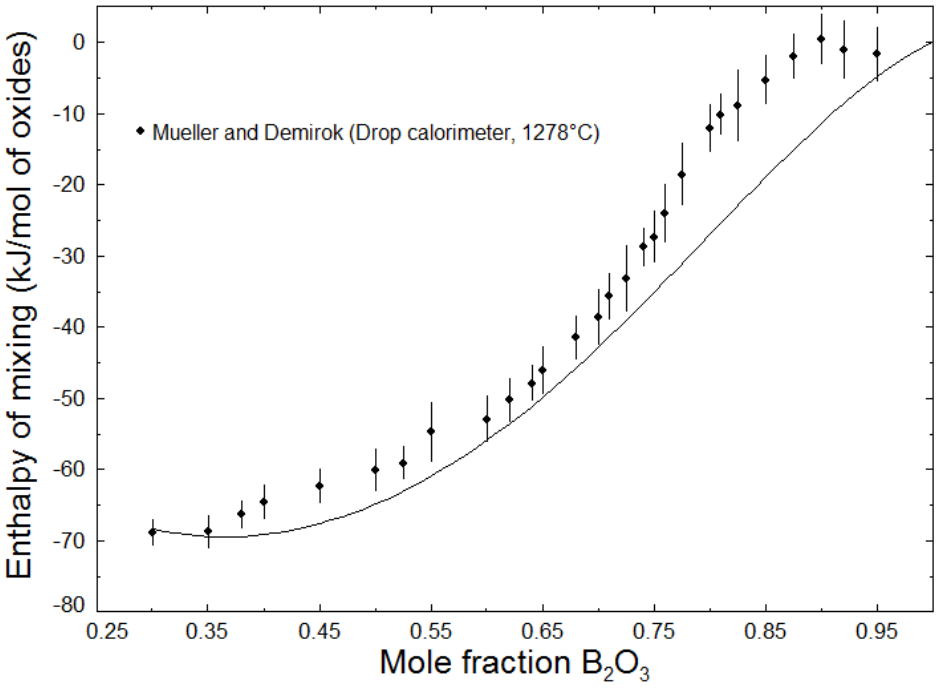

Fig. 2.8.9 Optimized enthalpy of mixing (standard states: solid BaO and liquid B_2O_3) in the liquid phase.

2.9 The $SrO\text{-}B_2O_3$ system

The optimized phase diagram of the system is shown in Fig. 2.9.1 and optimized thermodynamic parameters are presented in Table 2.9.1. The optimized MQM parameters (and the coordination numbers) for the liquid phase are presented in Table 2.9.1. For these parameters, the same notations were used as used by Pelton and coworkers [Pelton, et al. (2000)]. Pan, Wang, and Jin (2004) optimized the system using a two-sublattice ionic solution model for the liquid phase.

Guertler (1904) studied the system by cooling curves and reported $SrO.2B_2O_3$ (SB_2), $SrO.B_2O_3$ (SB) and $2SrO.B_2O_3$ (S_2B) as equilibrium phases. Witzmann and Beulich (1964) and Witzmann and Herzog (1964) by DTA measured the solid-liquid phase equilibria in the system. They reported these solid phases, except $SrO.3B_2O_3$ (SB_3), shown in Fig. 2.9.1 as stable. Hovhannisyan (2006) studied the system by XRD and DTA and reported all the phases shown in Fig 2.9.1 as stable. Chenot (1967) by XRD and DTA reported the presence of the $SrO.3B_2O_3$ phase and reported its peritectic melting at about 890 ºC. Wang, et al. (1984) while studying the BaB-SB section by thermal analysis reported melting point of the SB phase. Ohta, et al. (1982) by a handmade apparatus, for the hot-thermocouple method, V. B. M. Hageman and Oonk (1987) (equilibration and quenching followed by refractive index measurements), Konishi et al. (2000) (in-situ observation of phase separation and microscopic analyses by EPMA) and Crichton and Tomozawa (1997) (equilibration and quenching) measured the immiscibility in the system. Their data are shown in Fig. 2.9.1.

Z.-H. Liu and Huang (2006) by solution calorimetry determined the standard enthalpy of formation (ΔH^0_{298}) for the SB phase. This datum was used as enthalpy of formation for this compound as shown in Table 2.9.1. Asano and Kou (1988) by Knudsen-effusion mass spectrometry reported B_2O_3 vapor pressure over SB solid and liquid phases. These data are compared with the present calculations in Fig. 2.9.2. In the present calculations, the data for pure B_2O_3 gas were taken from JANAF Thermochemical Tables (1985). Stewart and Rindone (1963) by high-temperature calorimetry measured the enthalpy increments (H_T–H_{298}) for the liquid and solid SB_2 phases. The increments for the solid phase in Fig. 2.9.3 were used to obtain the heat capacity (C_p) for the SB_2 phase presented in Table 2.9.1. The optimized heat capacity is close to the one obtained by adding the heat capacities of the constituent oxides. The enthalpy increments for liquid (and glass) SB_2 phases are plotted in Fig. 2.9.4. It should be noted that, as in the BaO-B_2O_3 system, the same authors [Stewart and Rindone (1963)] did not report for this phase the heat of devitrification ($H_{Crystal}$-H_{Glass}) at 25 °C. Thus, the two sets of data could not be plotted on same scale with reference to crystals at room temperature as in the BaO-B_2O_3 system. Nagel, Eagan, and Bergeron (1970) measured the enthalpy of fusion by DTA of the compound SB_2. Their measured value is 139.746 kJ/mole and the present calculate value is 142.170kJ/mole. For the other solid phases in the SrO-B_2O_3 system, the heat capacity was calculated by adding the heat capacities of constituent oxides as shown in Table 2.9.1. No other thermodynamic data on the system could be found in the literature. The optimized standard entropy (S^0_{298}) and entropy of formation with oxides as reference standards (ΔS^0_{298}) are presented in Table 2.9.1. The ΔS^0_{298} values are always less than 9 J/(atom of metal), which is reasonable.

No data on the mutual solubility among the SrO and B_2O_3 phases could be found in the literature. Moreover, their different crystal structures and the very large difference in the ionic radii of Sr and B (Sr = 132 pm and B = 25 pm, [www.webelements.com (2012)]) also mitigate against any appreciable mutual solubility among them. Also, no data on the solid solubility in the solid phases appearing in the SrO-B_2O_3 system were found. They were modeled as stoichiometric phases.

The standard enthalpies of formation for intermediate compounds, enthalpies of mixing (at 2500 °C) and entropies of mixing (at 1500 °C) in the liquid phase in the alkaline-earth oxide-boron trioxide systems are compared in Figs. 2.9.5 to 2.9.7.

Table 2.9.1. Optimized thermodynamic parameters (in Joules/mol) for the SrO-B_2O_3 system.

Liquid phase (Quasichemical model parameters)			
Z_{BB}^{B} = 2.06616563; Z_{SrSr}^{Sr} = 1.37744375 Δg_{SrB} = –188280 –108784 X_{BB} + (154808 – 46.024T) X_{BB}^{8}			
Solid Phases			
ΔH^0_{298} (kJ/mole)			
Compound	Calculated from elements	Calculated, oxides (stable at room-temperature) as reference	Experimental from elements
$Sr_3B_2O_6$	–3350.000	–301.614	
$Sr_2B_2O_5$	–2715.000	–258.764	
SrB_2O_4	–2038.400	–174.314	–2038.400 ± 1.700 [Liu and Huang (‘06)][(a)]
SrB_4O_7	–3310.000	–173.978	
SrB_6O_{10}	–4585.951	–177.993	

S^0_{298}, ΔS^0_{298} and C_p (J/mol/K)			
Compound	S^0_{298}	ΔS^0_{298} calculated, oxides (stable at room-temperature) as reference	C_p
$Sr_3B_2O_6$	230.000	15.310	3 C_p(SrO) + C_p(B_2O_3)
$Sr_2B_2O_5$	165.000	3.890	2 C_p(SrO) + C_p(B_2O_3)
SrB_2O_4	107.550	0.020	C_p(SrO) + C_p(B_2O_3)
SrB_4O_7	193.000	31.520	195 + 0.1 T –7000000 T^{-2}
SrB_6O_{10}	258.000	42.570	C_p(SrO) + 3 C_p(B_2O_3)

[(a)] In this ref. heat of formation was reported with reference to elements only.

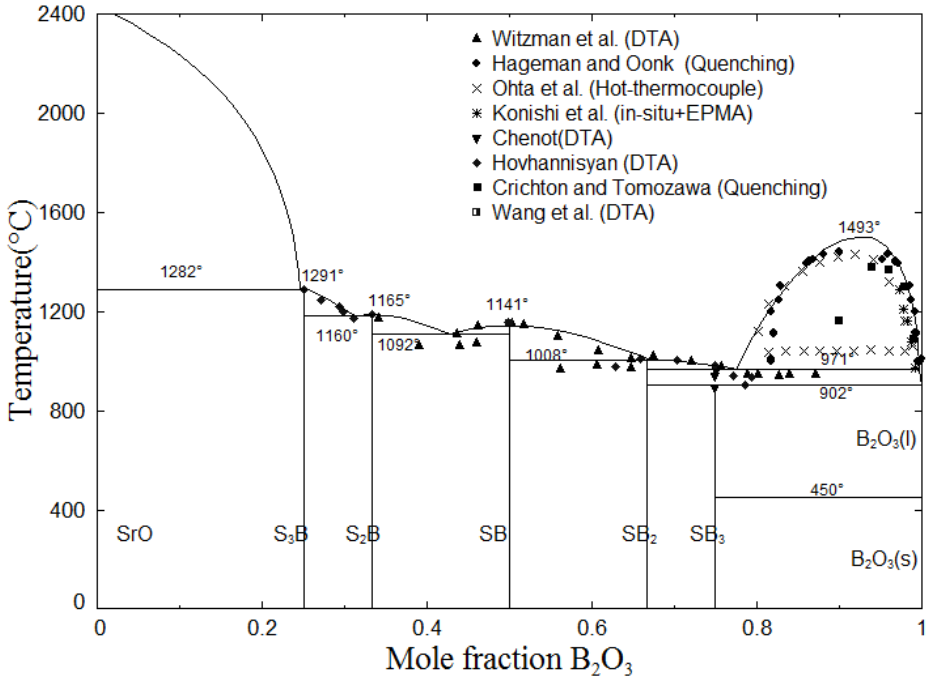

Fig. 2.9.1 Optimized phase diagram of the SrO-B_2O_3 system.

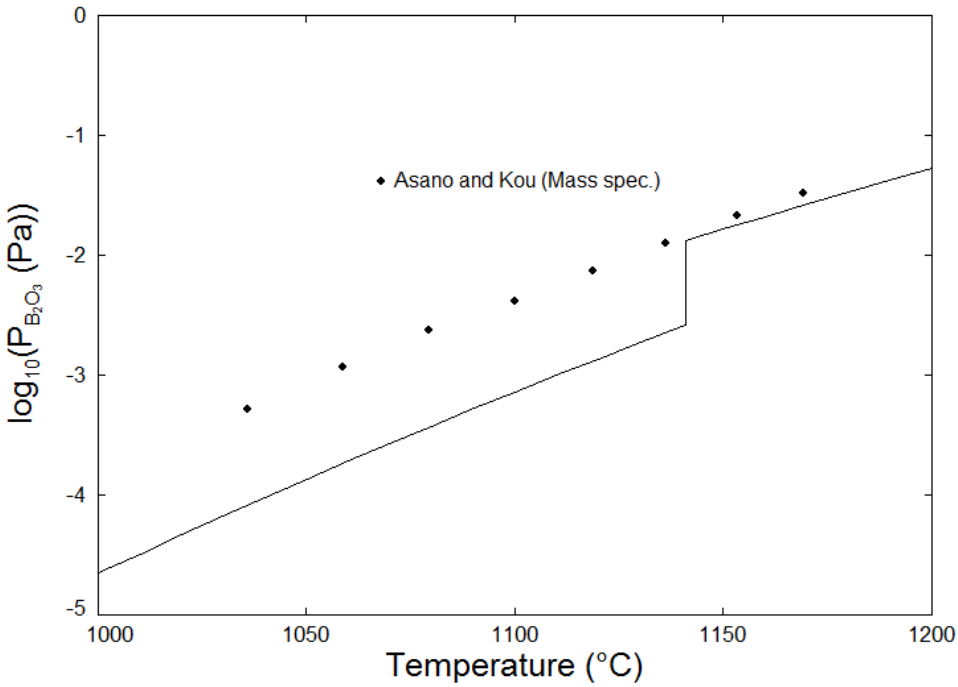

Fig. 2.9.2 Optimized vapor pressure of the B_2O_3 over SrB_2O_4 composition.

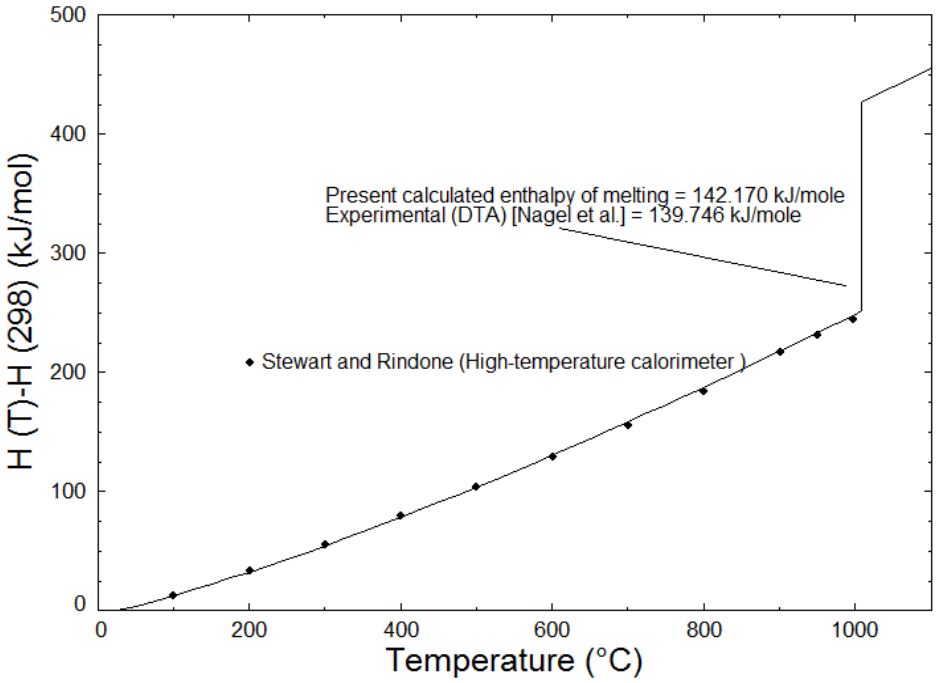

Fig. 2.9.3 Optimized enthalpy increments in the SrB_4O_7 (standard state: crystals) phase.

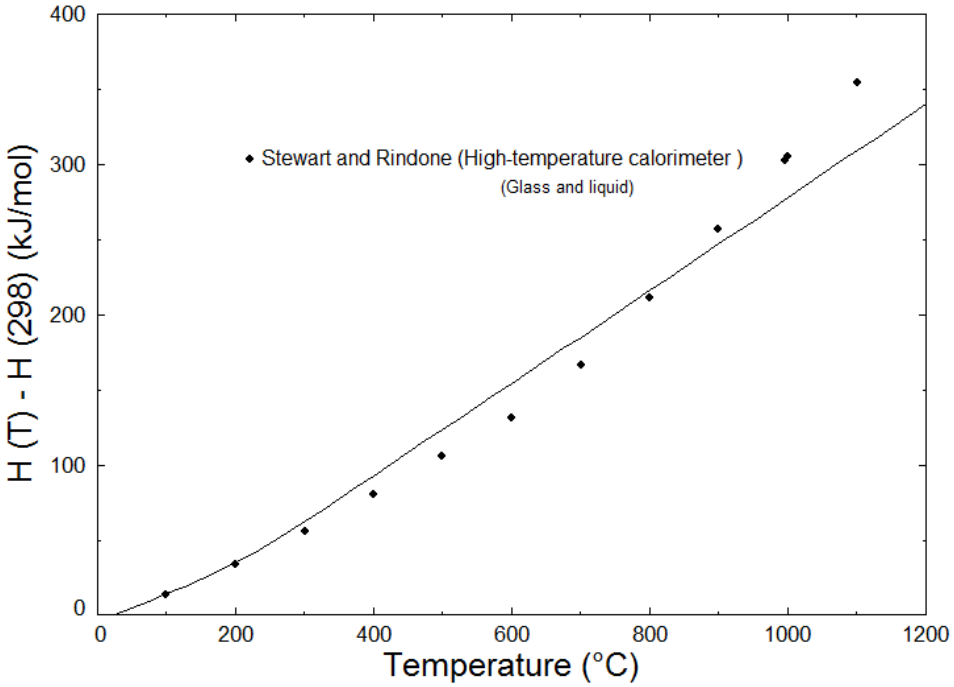

Fig. 2.9.4 Optimized enthalpy increments in the SrB_4O_7 (standard state: liquid at 25 °C) liquid phase.

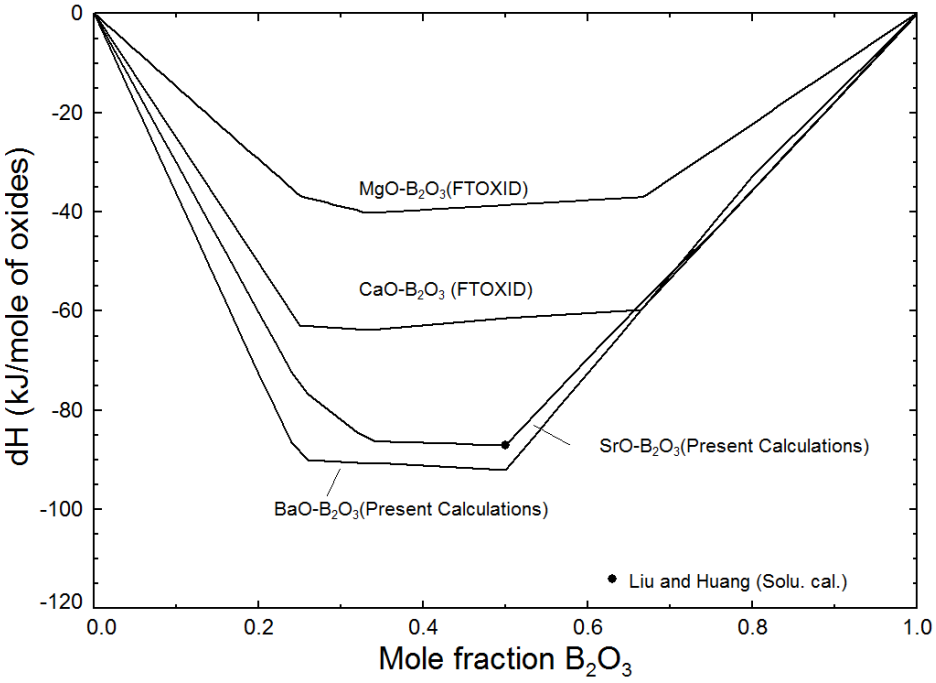

Fig. 2.9.5 Standard enthalpies of formation in alkaline-earth oxide-boron trioxide systems.

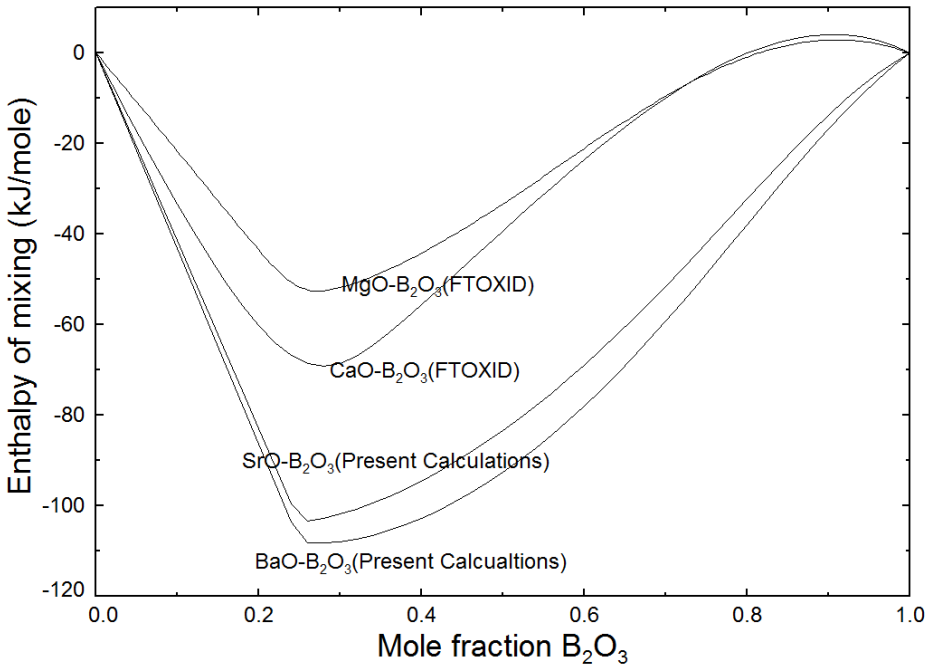

Fig. 2.9.6 Enthalpy of mixing at 2500 ºC in alkaline-earth oxide-boron trioxide systems.

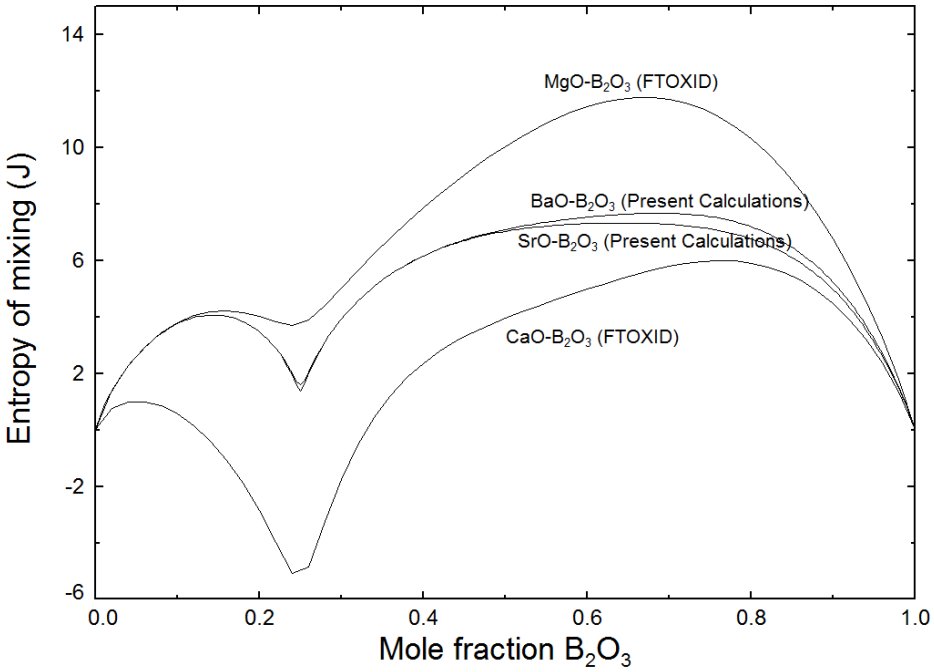

Fig. 2.9.7 Entropy of mixing in the liquid phase at 1500 ºC in alkaline-earth oxide-boron trioxide systems.

3. THE TERNARY AND HIGHER-ORDER SYSTEMS

In the SiO_2-B_2O_3-Al_2O_3-CaO-MgO-BaO-SrO system there are 25 ternary systems which contain either BaO or SrO (or both):

1. BaO-SrO-SiO_2
2. CaO-SrO-SiO_2
3. BaO-CaO-SiO_2
4. SrO-MgO-SiO_2
5. BaO-MgO-SiO_2
6. CaO-SrO-Al_2O_3
7. BaO-CaO-Al_2O_3
8. SrO-BaO-Al_2O_3
9. BaO-MgO-Al_2O_3
10. BaO-Al_2O_3-SiO_2
11. SrO-Al_2O_3-SiO_2
12. BaO-B_2O_3-SiO_2
13. SrO-B_2O_3-SiO_2
14. BaO-B_2O_3-Al_2O_3
15. SrO-B_2O_3-Al_2O_3
16. SrO-BaO-B_2O_3
17. BaO-CaO-B_2O_3
18. SrO-BaO-CaO
19. SrO-BaO-MgO

20.SrO-CaO-B_2O_3

21.SrO-CaO-MgO

22.SrO-MgO-B_2O_3

23.SrO-MgO-Al_2O_3

24.BaO-CaO-MgO

25.BaO-MgO-B_2O_3

Out of these 25, for 17 ternary systems (1 to 17) ternary data were found in the literature. Assessment and optimization of these data is presented in this chapter. For rest of the eight systems (from 18 to 25) no ternary data were found in the literature. Some data were available for the higher-order (quaternary) systems. They are also included in this chapter.

3.1 The BaO-SrO-SiO_2 system

The Gibbs energy of the liquid phase in the ternary system was estimated from the corresponding binary sub-systems by treating SiO_2 as asymmetric component [Pelton and Chartrand (2001)]. No ternary interaction parameter was required to reproduce the available data.

The optimized phase diagram of the SrS-BS section is shown in Fig. 3.1.1 and optimized thermodynamic parameters are presented in Table 3.1.1. The SrS phase has the pseudowollastonite structure [Eskola (1922), Buckner and Roy (1960)], space group, C2/c [Yang and Prewitt (1999)], whereas BS is isotypic with $BaGeO_3$ (space group $P2_12_12_1$) [Grosse, Tillmanns, and Mineral (1974)]. As the two phases are of different structure and Winkle and Muan (1973) also reported the two terminal solid solutions as different phases, in the present

work they were modeled as different phases using single-sublattice simple substitutional models (i.e., (Sr,Ba)SiO_3 and (Ba,Sr)SiO_3). It should be noted that in Table 3.1.1 the Gibbs energies of unstable end-members and excess interaction parameters are presented. The Gibbs energy of stable end-members can be found in the tables in the corresponding binary system.

Fields, et al. (1972) measured the melting and solidus points in the SrS-BS section by DTA, and the points above 1500 ºC by the oxy-acetylene torch method followed by visual observations. Winkle and Muan (1973) measured the phase diagram by quenching techniques followed by identification of phases by XRD and microscopic methods. They suggested the liquid (glass) observed by Fields, et al. (1972) at temperatures far below their liquidus data as metastable supercooled liquid. Later, Huntelaar and Cordfunke (1993) by DTA reported a phase diagram consistent with that of Winkle and Muan (1973).

The B_2S phase is reported [Catti, Gazzoni, and Ivaldi (1983), Pieper, et al. (1972), Hahn and Eysel (1970)] to have an orthorhombic structure, isostructural with α'-Ca_2SiO_4 (C_2S). Hahn and Eysel (1970) predicted the high-temperature polymorphic transformation into high-K_2SO_4 structure (isostructural with α-C_2S) for this phase in line with the structure of similar silicates and germanates. However, no experiments corroborating this prediction in the literature could be found. During experimental investigation on this section Fields, et al. (1972) did not note any α-polymorph for the B_2S and reported only α'- polymorph as stable. In the present work also, only α'- B_2S was considered stable. The Sr_2S phase contains both the α'- and α- polymorphs. Several authors [Fields, et al. (1972), Pieper, et al. (1972), Henning and Paeselt (1965a), O'Daniel and

Tscheischwili (1942), Paeselt and Henning (1968), Grebenshchikov and Shitova (1970)] reported complete solubility in the temperatures corresponding to stability of the α'-phase (orthorhombic) in the Sr_2S-B_2S section.

Fields, et al. (1972) by the oxygen-acetylene torch method reported phase diagram data for this section as shown in Fig. 3.1.2. The slope of the liquidus reported by them is dubious. Moreover, keeping in view the inconsistency of their data with other available data in Fig. 3.1.1, the data in Fig. 3.1.2 are questionable. Hence, further experimental work is required to establish the phase diagram for this section. The present calculated phase diagram for this section is shown in Fig. 3.1.3. In the present calculations, an ideal solution between the α'-polymorphs was assumed. The solubility of Ba in the α-Sr_2S was calculated tentatively. The lattice stability of B_2S in the α-phase was fixed from the B_2S-C_2S phase diagram.

Fields, et al. (1972) by quenching, XRD and optical microscopy reported phase relationships among solid phases (Fig. 3.1.4) in the temperature ranges 1220 to 1275 °C. This can be compared with the present calculated isothermal section at 1250 °C in Fig. 3.1.5 (the calculated phase relationships do not change in the range 1220 to 1275 °C). The phase relationships presented in Fig. 3.1.4 are erroneous because B_2S is shown in equilibrium with SrS which is not possible; tie lines between BS rich solid solution and orthosilicate solution intervene in the B_2S-SrS join, as shown in Fig. 3.1.5. No effort was made, in the absence of any conclusive data, to destabilize the liquid phase appearing at this temperature, contrary to data of Fields, et al. (1972). Fields, et al. (1972) also reported that the ternary compound $BaSrSi_3O_8$ ($BSrS_3$) melts at 1275 °C to Liquid +

SrS phases and decomposes at 1220 °C into BS_2 + SrS phases. The XRD data of this phase was also given. In the present calculations, the melting point of $BSrS_3$ at 1275 °C reported by Fields et al. is reproduced closely at 1272 °C. This compound melts into Liquid+Pseudowoll. and decomposes into BS_2+SrS+SiO_2 at 1184 °C. The present calculated liquidus (polythermal) projection for the BaO-SrO-SiO_2 system is presented in Fig. 3.1.6.

Pietro Appendino and Appendino Montorsi (1969) by quenching and XRD reported the phase B_2SrS_3 as stable on the BS-SrS section. However, other investigations [Fields, et al. (1972), Winkle and Muan (1973)] did not report this phase as stable. Therefore, in the present calculations this phase was neglected. They reported another ternary compound SrB_5S_{10}. Later investigation of Fields, et al. (1972) in the range 1220-1275 °C did not report this phase as stable. In the literature, no other experimental data on this phase could be found. More experimental work is required to prove the presence of this phase. Hence, SrB_5S_{10} was not considered stable in the present calculations.

The phases B_2S_3 and $BSrS_3$ have the same stoichiometry and some amount of mutual solubility among these solid phases can be expected because of similarity between Ba and Sr atoms. No experimental data on such solubility could be found in the literature. The similarity in the structure of these two phases will further enhance the possibility of mutual solid solubility. There are data on crystal structure [Hesse and Liebau (1980)] for the phase B_2S_3; however, no such data could be found for the $BSrS_3$ phase. In the absence of sufficient experimental data the mutual solubility among these phases was neglected. The B_3S and Sr_3S phases also have the same

stoichiometry. Pietro Appendino and Appendino Montorsi (1969) by XRD reported about 20 mol% solubility of Sr at 1100 °C in the B_3S phase. However, they did not report Sr_3S as a stable compound. Fields, et al. (1972) presented references reporting Sr_3S to be isostructural with B_3S (tetragonal structure with space group P4/mmc). Tillmanns and Grosse (1978) also reported tetragonal structure for the B_3S phase. Therefore, in the present calculations also these phases were considered isostructural. An ideal solution was assumed between the Sr_3S and B_3S phases. This assumption reproduced the extent of solubility of Sr_3S in B_3S at 1100 °C (20 mol%) as reported by Pietro Appendino and Appendino Montorsi (1969).

Table 3.1.1 Optimized thermodynamic parameters, in Joules, (Gibbs energies of hypothetical end-members and excess interaction parameters) in the BaO-SrO-SiO_2 system.

$BaSrSi_3O_8$
ΔH^0_{298} = –4141085 J/mol S^0_{298} = 271.000 J/mol/K ΔS^0_{298}[(a)] = 20.971 ΔS^0_{298}[(b)] = 22.409 $C_p = C_p(BaSiO_3) + C_p(SrSiO_3) + C_p(SiO_2(S2))$ T_m[(c)] = 1272 ºC
Pseudowollastonite $G^0(BaSiO_3, \text{Pseudowoll.}) = G^0(BaSiO_3) + 15481$
$BaSiO_3$ solid solution (ss) $G^0(SrSiO_3, \text{ss}) = G^0(SrSiO_3) + 8368$
α'-Sr_2SiO_4 (α'-C_2S)[(d)] $q_{BaSr} = 0$
α-Sr_2SiO_4 (α-C_2S)[(d)] $G^0(Ba_2SiO_4, \alpha) = G^0(Ba_2SiO_4, \alpha') + 8786$
$(Ba\text{-}Sr)_3SiO_5$ solid solution $q_{BaSr} = 0$
Monoxide $q^{11}_{BaSr} = 35698 - 8.870\,T$; $q^{21}_{BaSr} = -3138$

*Here $G^0(A,x)$ refers to Gibb energy of A with *x* as reference state.
[(a)] from oxides (stable at room-temperature) as reference [(b)] from compounds used to calculated heat capacity[(c)] congruent melting[(d)] these α- and α'- phases are same as the α-C_2S and α'-C_2S

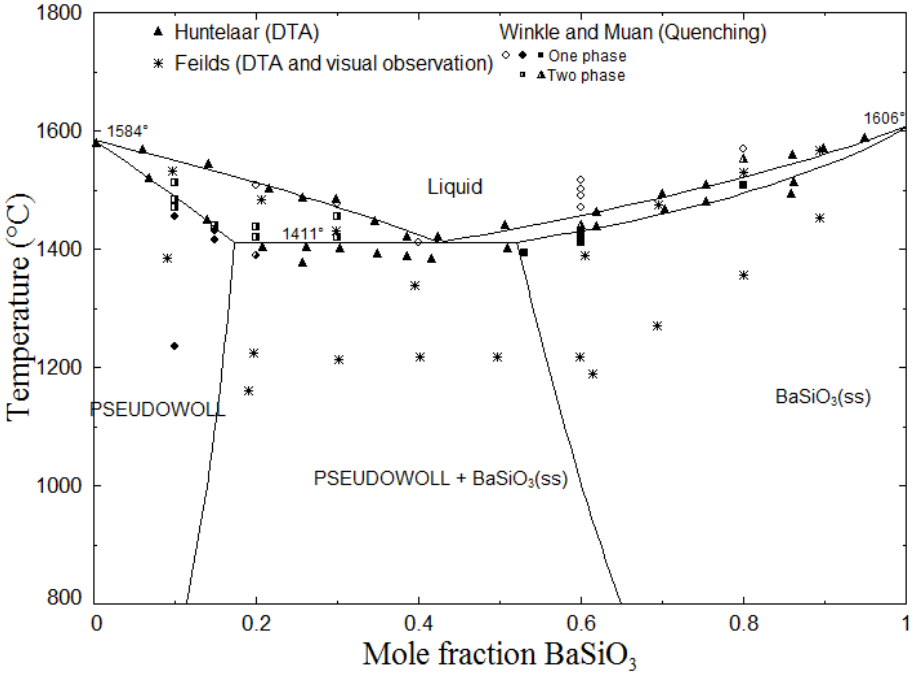

Fig. 3.1.1 Optimized phase diagram for the $SrSiO_3$-$BaSiO_3$ system.

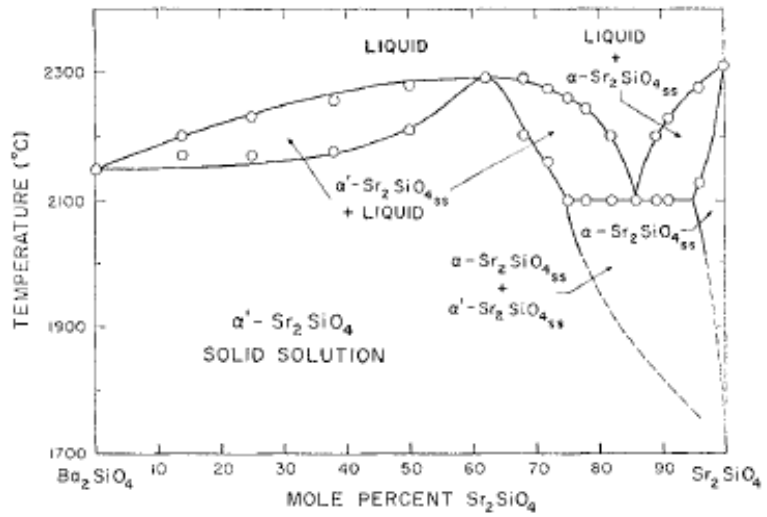

Fig. 3.1.2 The Ba_2SiO_4-Sr_2SiO_4 section as reported by Fields et al.

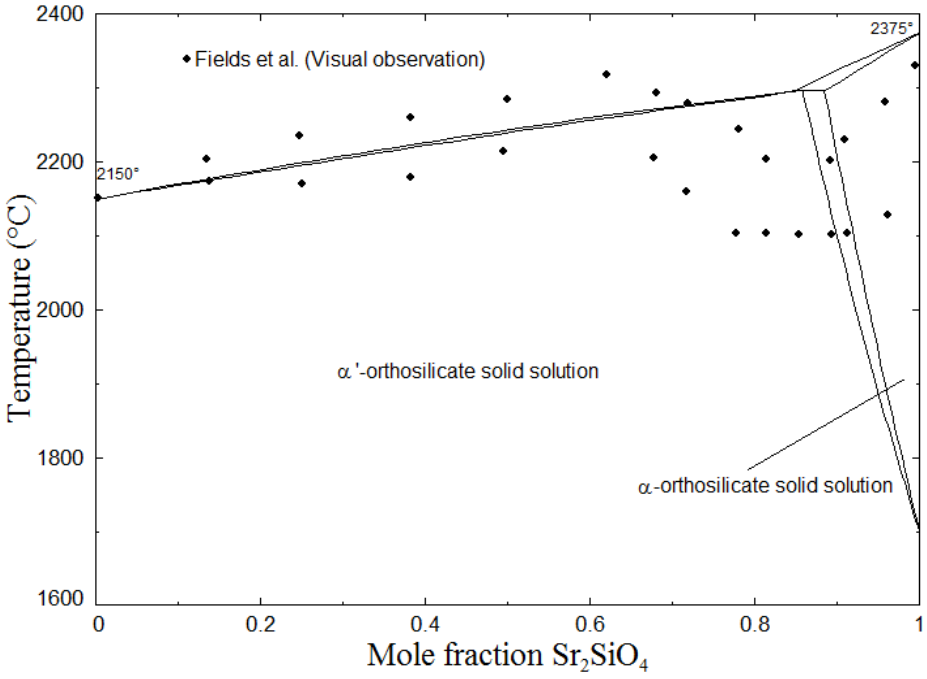

Fig. 3.1.3 Optimized phase diagram for the section Ba_2SiO_4-Sr_2SiO_4.

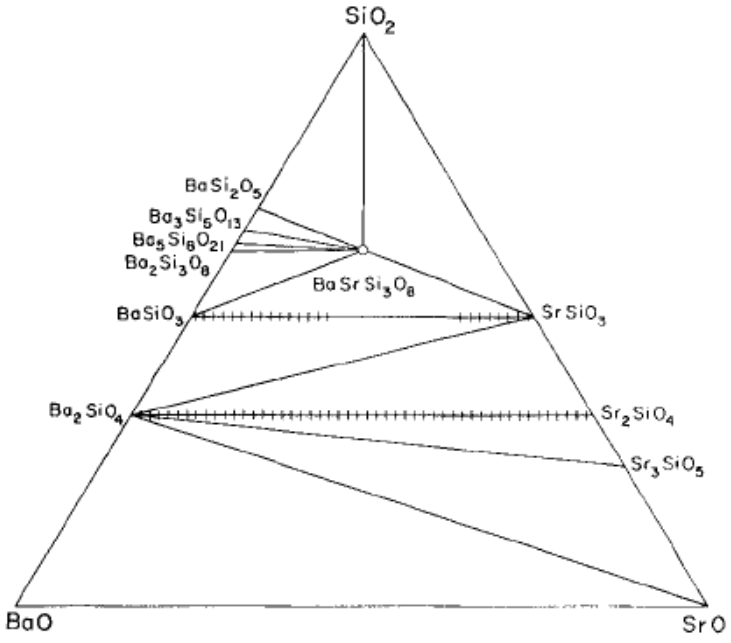

Fig. 3.1.4 Compatibility relations determined by Fields et al. in the temperature ranges 1220-1275 °C.

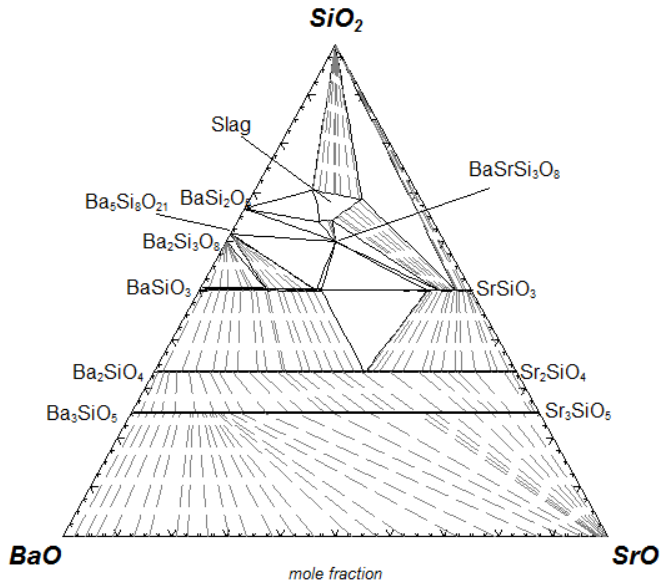

Fig. 3.1.5 Present calculated isothermal section at 1250 °C in the BaO-SrO-SiO_2 system.

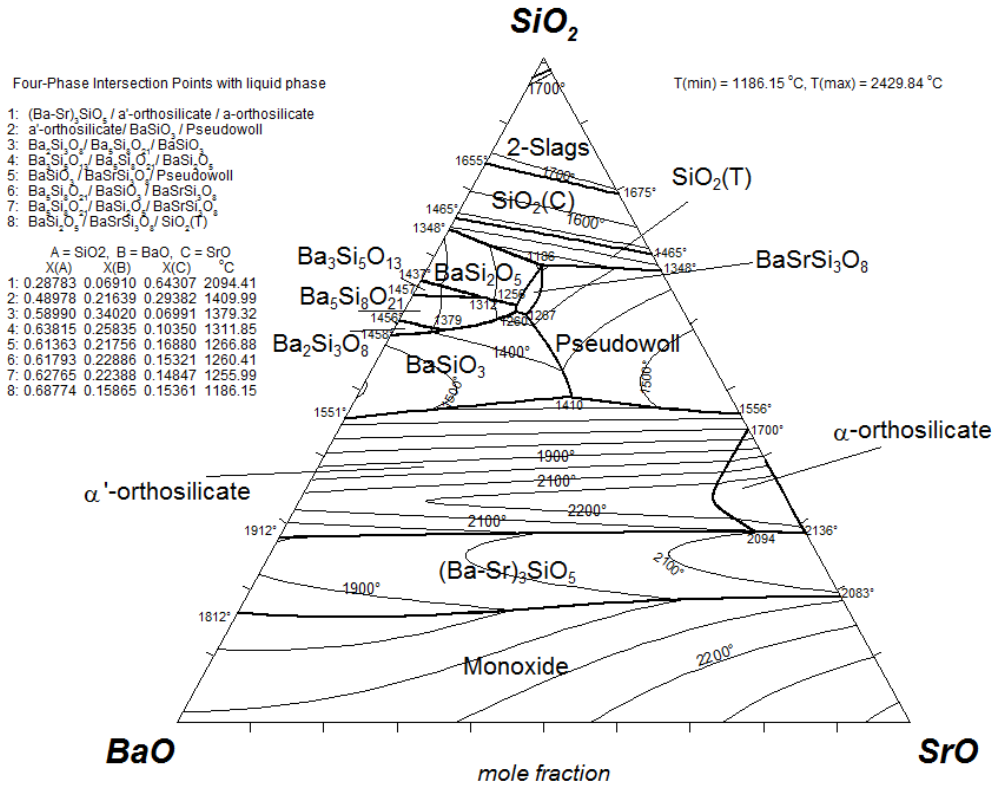

Fig. 3.1.6 Present calculated liquidus (polythermal) projection for the BaO-SrO-SiO_2 system (isotherms were drawn at the interval of 100 °C).

3.2 The CaO-SrO-SiO_2 system

The Gibbs energy of the liquid phase in the ternary system was estimated from the corresponding binary sub-systems by treating SiO_2 as asymmetric component [Pelton and Chartrand (2001)]. Small ternary interaction parameters presented in Table 3.2.1 were used to reproduce the available data. This term was required to obtain an optimal fit in the $CaSiO_3$-$SrSiO_3$-$BaSiO_3$ system (Sec. 3.4).

As reported earlier (in the SrO-SiO_2 binary system) Ca_2SiO_4 and Sr_2SiO_4 have isostructural polymorphs (α- and α'-Ca_2SiO_4). Hence, solubility between corresponding phases in the two end-members is expected. Several authors [Massazza (1955), Toropov and Konovalov (1943), Catti, et al. (1984), Paeselt and Henning (1968), Henning and Paeselt (1965b) reported complete solubility (in the temperature ranges corresponding to stability of orthorhombic (α'-Ca_2SiO_4) phase) in this section but no data establishing phase boundaries could be found in the literature. In the present calculations, ideal solutions were assumed for both the α' and α phases.

The optimized phase diagram of the system is shown in Fig. 3.2.1 and optimized thermodynamic parameters are presented in Table 3.2.1. Eskola (1922) first studied the system by quenching techniques and optical microscopy and reported the liquidus and solidus points. Eskola (1922) reported only one form of $SrSiO_3$ isomorphous with pseudowollastonite-$CaSiO_3$. Winkle and Muan (1973) corroborated Eskola's data of complete solubility between the two metasilicates at 1300 °C. Moir, Gard, and Glasser (1975) reported that $SrSiO_3$ exists in two different polytypes (polytypism is a special case of polymorphism where compounds have nearly identical structure

and composition but differ only in their stacking sequence). The form which is thermodynamically less stable is isomorphous with pseudowollastonite. They also reported the presence of two-polytype regions between the compositions 50-60% $CaSiO_3$. However, they could not establish the exact phase boundary for this two-polytype region. In the present calculations, this polytypism was ignored and one form of $SrSiO_3$ isomorphous with pseudowollastonite-$CaSiO_3$, as also reported by Eskola (1922) and Winkle and Muan (1973), was considered. As these polytypes differ very slightly in their structure their Gibbs energies are supposed to be practically the same. Buckner and Roy (1960) reported subsolidus phase equilibria which are compared with the present calculations in Fig. 3.2.1. They also suggested the presence of a phase, below 700 ºC, named μ-$(Ca,Sr)SiO_3$. More evidence and exact phase diagram data are required to model this phase. In the present work, any presence of such phase was neglected and the system was modeled as shown in Fig. 3.2.1. The solid solutions in Fig. 3.2.1 were modeled using single-sublattice simple substitutional model (i.e., $(Ca,Sr)SiO_3$ and $(Sr,Ca)SiO_3$).

Butt, Timashev, and Kaushanskii (1965) by XRD reported the solubility limit of Sr in the C_3S phase at 1450 °C as 0.035 mole. Boikova, Paramonova, and Domanskii (1972) by XRD reported the solubility limit of Ca in the Sr_3S phase at about 1600 °C phase as 0.11 mole. C_3S is known to exist in different crystal structures [Emanuelson, Solberg, Evju, and Hansen (2001)] but all of them are different from the crystal structure of Sr_3S phase (tetragonal structure, space group P4/mmc). These mutual solid solubilities in the C_3S-Sr_3S section was reproduced by treating both the end-members as different phases and modeling the solution using single-sublattice simple

substitutional model(i.e., $[Ca,Sr]_3SiO_5$, $[Sr,Ca]_3SiO_5$). The optimized parameters for these solutions are presented in Table 3.2.1.The present calculated liquidus (polythermal) projection for the $CaO\text{-}SrO\text{-}SiO_2$ system is presented in Fig. 3.2.2.

Table 3.2.1 Optimized thermodynamic parameters, in Joules, (Gibbs energies of hypothetical end-members and excess interaction parameters) in the $CaO\text{-}SrO\text{-}SiO_2$ system.

Pseudowollastonite $q^{11}_{CaSr} = 5439$
Wollastonite $G^0(SrSiO_3, \text{Woll.}) = G^0(SrSiO_3, \text{Pseudowoll.}) + 33472$
α'-Ca_2SiO_4 (α'-C_2S) $q_{CaSr} = 0$
α-Ca_2SiO_4 (α-C_2S) $q_{CaSr} = 0$
Sr_3S solid solution $G^0(Ca_3SiO_5, Sr_3S) = G^0(Ca_3SiO_5) + 14226$
C_3S solid solution $G^0(Sr_3SiO_5, C_3S) = G^0(Sr_3SiO_5) + 4184$
Liquid $g^{001}{}_{CaSi(Sr)} = -4184$; $g^{001}{}_{SrSi(Ca)} = -4184$
Monoxide $q^{11}_{CaSr} = 27748 - 6.359\,T$; $q^{12}_{CaSr} = -1674$

**Here $G^0(A,x)$ refers to Gibb energy of A with *x* as reference state.

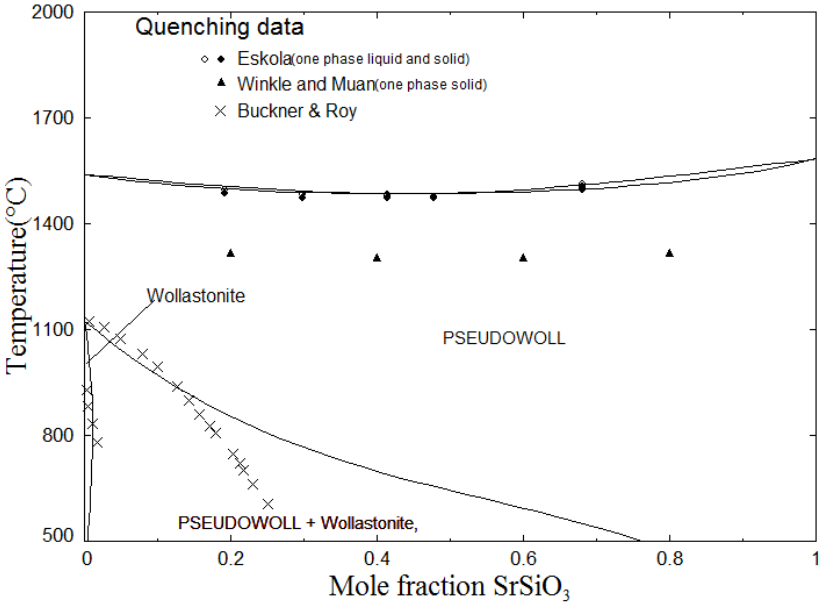

Fig. 3.2.1 Optimized phase diagram for the $CaSiO_3$-$SrSiO_3$ system.

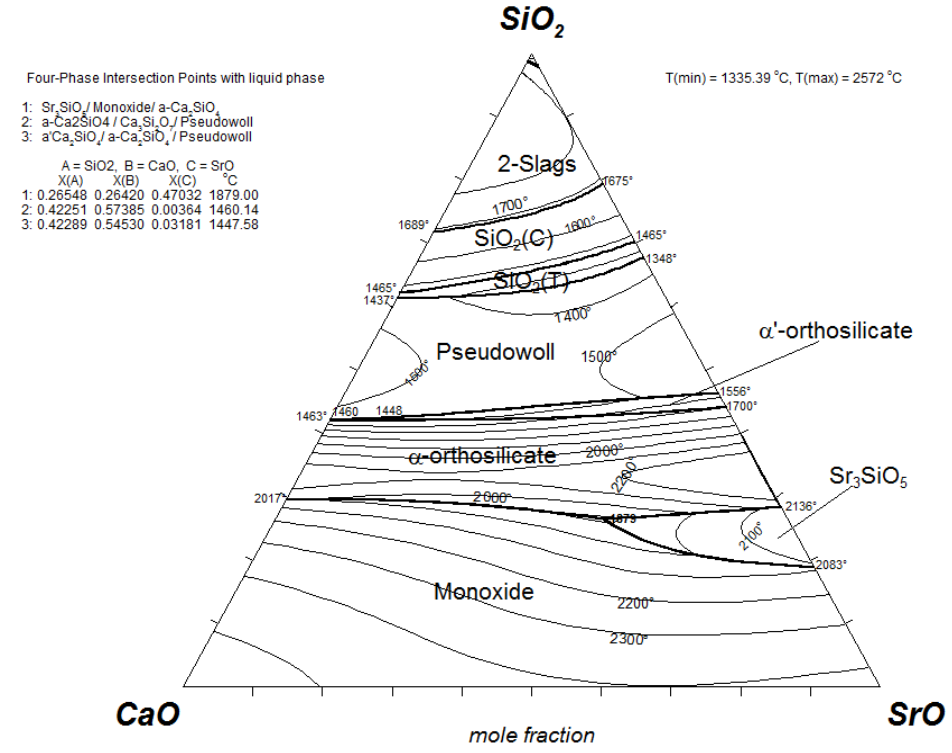

Fig. 3.2.2 Present calculated liquidus (polythermal) projection of the CaO-SrO-SiO_2 system (isotherms were drawn at the interval of 100 °C).

3.3 The BaO-CaO-SiO_2 system

The Gibbs energy of the liquid phase in the ternary system was estimated from the corresponding binary sub-systems by treating SiO_2 as asymmetric component [Pelton and Chartrand (2001)]. The small ternary interaction parameters used for the liquid phase are presented in Table 3.3.1.

The optimized phase diagram of the system CS-BS is shown in Fig. 3.3.1 and optimized thermodynamic parameters are presented in Table 3.3.1. Eskola (1922) reported the presence of a stoichiometric compound $BaCa_2Si_3O_9$ from quenching techniques followed by optical microscopy. Later, Winkle and Muan (1973) by quenching techniques and XRD studied the section. They reported the presence of terminal solid solutions along with a range of homogeneity for the compound $BaCa_2Si_3O_9$ (which were not reported by Eskola (1922)). L. S. D. Glasser and Glasser (1968) reported a triclinic structure (space group $P\bar{1}$) for this compound. They reported three distinct cation sublattices, two for Ca and one for Ba. This compound is also a naturally occurring mineral (walstromite). Doersam, Liebscher, Wunder, Franz, and Gottschalk (2009) reported the crystal structure for the (Ca,Sr)-walstromite phase, which is stable only at high pressures. They also reported three distinct cation sublattices for this compound, two predominantly filled by Ca and Sr each, and the third one by both. Following these findings, in the present work, the $BaCa_2Si_3O_9$ phase was also modeled having three distinct cation sublattices, one filled by Ca only and two others by both Ba and Ca. The phase was modeled as $[Ba,Ca][Ba,Ca]CaSi_3O_9$ using the compound energy formalism (This phase is labelled I-phase in Fig. 3.3.1). It is clear in Fig. 3.3.1 that non-stoichiometry of this phase is present on both sides of the $BaCa_2Si_3O_9$ composition. Hence, Ba and Ca are expected to be present on two of the other

sublattices, if the third one is filled by Ca only. Since $CaSiO_3$ and $BaSiO_3$ have different crystal structures, the terminal solid solutions in Fig. 3.3.1 were modeled as different solid solutions using the single sublattice simple substitutional model (i.e., $(Ca,Ba)SiO_3$ and $(Ba,Ca)SiO_3$).

The optimized phase diagram for the C_2S-B_2S join is shown in Fig. 3.3.2. As reported earlier, the C_2S phase exists in α- and α'- polymorphs, whereas only the α'- phase is stable for B_2S. The α- and α'- solid solutions in Fig. 3.3.2 were modeled using the single-sublattice simple substitutional model, i.e. $[Ca,Ba]_2SiO_4$. All the authors listed below who investigated the C_2S-B_2S solid phase relationships below 1500 °C did not find any appreciable solubility of Ca in the B_2S phase. Hence, as shown in Fig. 3.3.2, practically no solubility of Ca in B_2S phase was assumed below 1500 °C. However, according to the present calculation (Fig. 3.3.2) a small solubility of Ca in the B_2S was calculated above 1500 °C. There are, however, no experimental data in the literature to corroborate this solubility.

Brisi and Appendino [Brisi and Appendino (1965); Brisi (1963)] by quenching and XRD, reported 21 mol% solubility at 1200 °C and 28 mol% solubility at 1350 °C of Ba in Ca_2SiO_4 phase. (They did not specify α- and α'- phases). They also reported the presence of a ternary compound on the C_2S-B_2S join with a range of homogeneity (shown by experimental points in Fig. 3.3.2) which they called T phase. Following Brisi and Appendino (1965) this phase was named T in Fig. 3.3.2. Nadachowski and Grylicki (1959) by quenching and metallography studied the B_2S-C_2S section and their data are shown in Fig. 3.3.2. They reported the T phase as $B_5C_3S_4$ (it is unclear in the publication what led them to conclude this stoichiometry). Toropov

and Fedorov (1964) studied the C_2S-B_2S section by quenching followed by optical microscopy and XRD. These data are shown in Fig. 3.3.2. They reported the T phase as $B_6C_4S_5$, solely based on the maximum in their liquidus data. Matkovic, Popovic, Grzeta, and Halle (1986) by XRD and DTA studied the C_2S-B_2S section. They reported a new orthorhombic phase which they called "X phase" with composition $Ba_{0.48}Ca_{1.52}S$. They also reported eutectoid decomposition of this phase at 1140 °X. Thompson, Withers, and Hyde (1987) by XRD and electron diffraction studied the section. They corroborated the presence of the X phase and reported another new phase, with distorted hexagonal crystal structure, which they call "Y phase". They showed Y phase to be stable around 1150 to 1325 °C in their phase diagram. Thompson, et al. (1987) also reported a small range of homogeneity (2 mol%) for these X and Y phases. No other experimental data on crystal structures or stoichiometries of these two phases could be found in the literature. In the present calculations, the X phase was modeled as stoichiometric $B_2C_6S_4$, which very closely corresponds to the composition of the X phase as reported by Matkovic, et al. (1986). Thompson, et al. (1987) reported the Y phase as stable at 30-32 mol% of Ba_2SiO_4. In the present work, this compound was molded as stoichiometric $B_2C_4S_3$. However, these stoichiometries are approximate and more experiments are required to establish them correctly. Matkovic, et al. (1986), Thompson, et al. (1987) and Fukuda, Maki, and Adachi (1992) by XRD reported that the T phase has a crystal structure derived from hexagonal α-Ca_2SiO_4. Fukuda, et al. (1992) also suggested a probable space group of $P\bar{3}m1$ for the T phase, the same as for α-Ca_2SiO_4. No experimental data on the number of sublattices and cation distributions among the different sublattices in the T phase could be found in the literature. However, α-Ca_2SiO_4 is known [Mumme, Cranswick, and Chakoumakos (1996)] to have three distinct sublattices for Ca ions with site occupancy 2,1,1 in a unit cell. Following these data and the similarity between the T

phase and α-Ca_2SiO_4, the T phase was also modeled having three distinct cation sublattices with site occupancy 2,1,1 as $Ba_2Ca[Ba,Ca]Si_2O_8$.

Brisi and Appendino (1967) reported an isothermal section (Fig. 3.3.3 at 1100 °C which is compared with the present calculations in Fig. 3.3.4. They reported a compound with approximate composition $C_{0.1}B_{0.9}S$ as stable on the BS-CS join. The presence of this compound was not reported by Eskola (1922), Winkle and Muan (1973) and Toropov, Galakhov, and Bondar (1956). No other experimental data on the stability of this compound could be found in the literature. As the present calculations in Fig. 3.3.4 show, it is the T phase which is in equilibrium with the B_2S_3 and BS phases close to this composition. In the present calculations the presence of the compound $C_{0.1}B_{0.9}S$ was neglected. Also, the present calculations disagree with Brisi and Appendino (1967) on the equilibrium of the $2CaO.BaO.3SiO_2$ (Fig. 3.3.3; in the present calculations $2CaO.BaO.3SiO_2$ was modeled as T-phase) with C_2S and C_3S_2 phases along with extent of stability of the C_2S solid solution at 1100 °C. The exact reproduction of these data with the other experimental data on the B_2S-C_2S and BS-CS join was found very difficult. The present calculated liquidus (polythermal) projection for the BaO-CaO-SiO_2 ternary system is presented in Fig. 3.3.5.

No data on the mutual solubility between the C_3S and B_3S phases could be found in the literature. Moreover, as reported previously, there is not much solubility between the C_3S and Sr_3S phases. The bigger size difference between the Ca and Ba atoms would further mitigate against any appreciable solid solubility between the C_3S and B_3S phases. Brisi and Appendino (1967) also at

1100 °C did not report any solubility of Ca in the B_3S phase. In the present, solubility between these phases was ignored.

Table 3.3.1 Optimized thermodynamic parameters, in Joules, (Gibbs energies of hypothetical end-members and excess interaction parameters) in the BaO-CaO-SiO_2 system**.

Pseudowollastonite (Pseudo.)
$G^0(BaSiO_3, \text{Pseudowoll.}) = G^0(BaSiO_3) + 15481$
$q_{BaCa} = 25104$
Wollastonite (Woll.)
$G^0(BaSiO_3, \text{Woll.}) = G^0(BaSiO_3) + 37656$
$BaSiO_3$ solid solution (ss)
$G^0(CaSiO_3, \text{ss}) = G^0(CaSiO_3) + 45229 - 19.018\ T$
α'-Ca_2SiO_4 (α'-C_2S)
$q^{11}_{BaCa} = 41840$
$q^{21}_{BaCa} = -135980 + 58.576\ T$
α-Ca_2SiO_4 (α-C_2S)
$G^0(Ba_2SiO_4, \alpha) = G^0(Ba_2SiO_4, \alpha') + 8786$
Monoxide
$q^{11}_{CaBa} = 58600$
I-phase $[Ca,Ba][Ca,Ba]CaSi_3O_9$
$G^0([Ca][Ca]CaSi_3O_9) = 3\ G^0(CaSiO_3, \text{Woll.}) + 12552$
$G^0([Ca][Ba]CaSi_3O_9) = 2\ G^0(CaSiO_3, \text{Woll.}) + G^0(BaSiO_3) - 6579$
$G^0([Ba][Ca]CaSi_3O_9) - G^0([Ca][Ba]CaSi_3O_9) = 30543$
$G^0([Ca][Ca]CaSi_3O_9) + G^0([Ba][Ba]CaSi_3O_9) = G^0([Ca][Ba]CaSi_3O_9) + G^0([Ba][Ca]CaSi_3O_9)$
T-phase ($Ba_2Ca[Ba,Ca]Si_2O_8$)
$G^0(Ba_2Ca[Ba]Si_2O_8) = -57831 + 6.973\ T$
$G^0(Ba_2Ca[Ba]Si_2O_8) = 32342 - 48.116\ T$
Liquid
$g^{001}_{BaSi(Ca)} = -4602$; $g^{001}_{CaSi(Ba)} = -4937$
X phase ($B_2C_6S_4$)
$\Delta H^0_{298} = -9298830$ $S^0_{298} = 535.126$ J/mol/K $\Delta S^0_{298}{}^{(a)} = -1.352$ $\Delta S^0_{298}{}^{(b)} = 0$
$C_p = C_p(Ba_2SiO_4) + 3\ C_p(Ca_2SiO_4, \gamma)$
$T_d{}^{(c)}$= 1140 ºC, Exp: 1140 °C [Matkovic et al., '86]
Y phase ($B_2C_4S_3$)
$\Delta H^0_{298} = -6902850$ $S^0_{298} = 460.450$ J/mol/K $\Delta S^0_{298}{}^{(a)} = 40.932$ $\Delta S^0_{298}{}^{(b)} = -11.273$
$C_p = C_p(Ba_2SiO_4) + 2\ C_p(Ca_2SiO_4, \alpha')$

**Here $G^0(A,x)$ refers to Gibb energy of A with x as reference state. [(a)] oxides (stable at room-temperature) as reference.[(b)] compounds used to calculated heat capacity as reference. [(c)] eutectoid decomposition

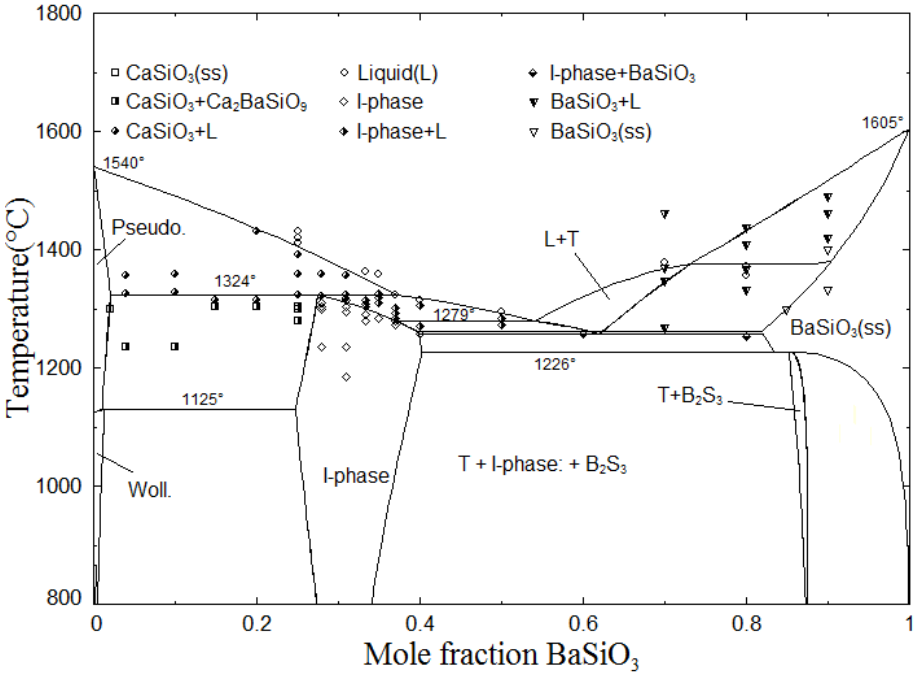

Fig. 3.3.1 Optimized phase diagram for the $CaSiO_3$-$BaSiO_3$ system.

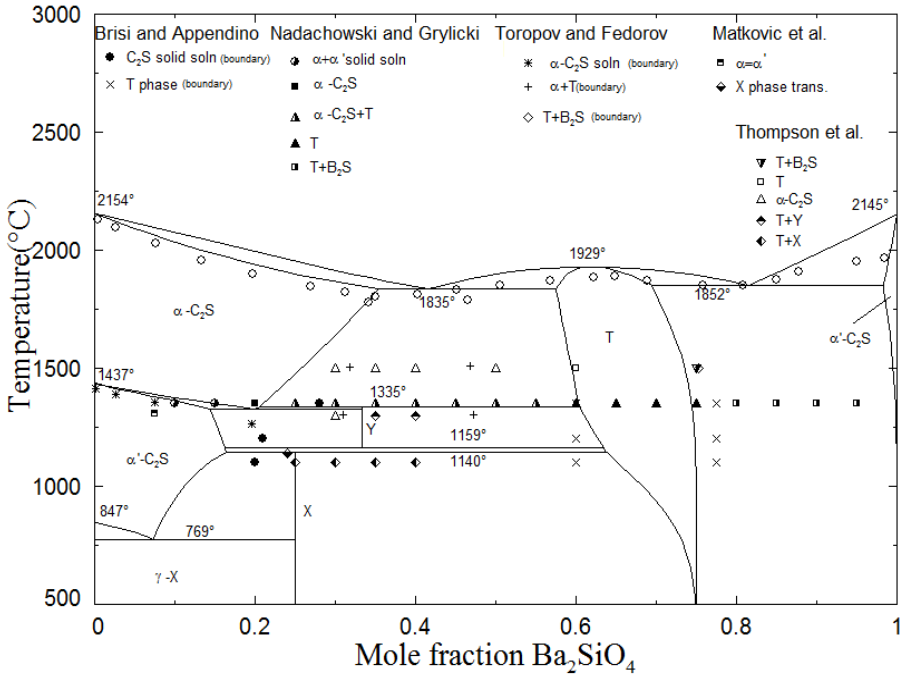

Fig. 3.3.2 Optimized phase diagram for the Ca_2SiO_4-Ba_2SiO_4 system.

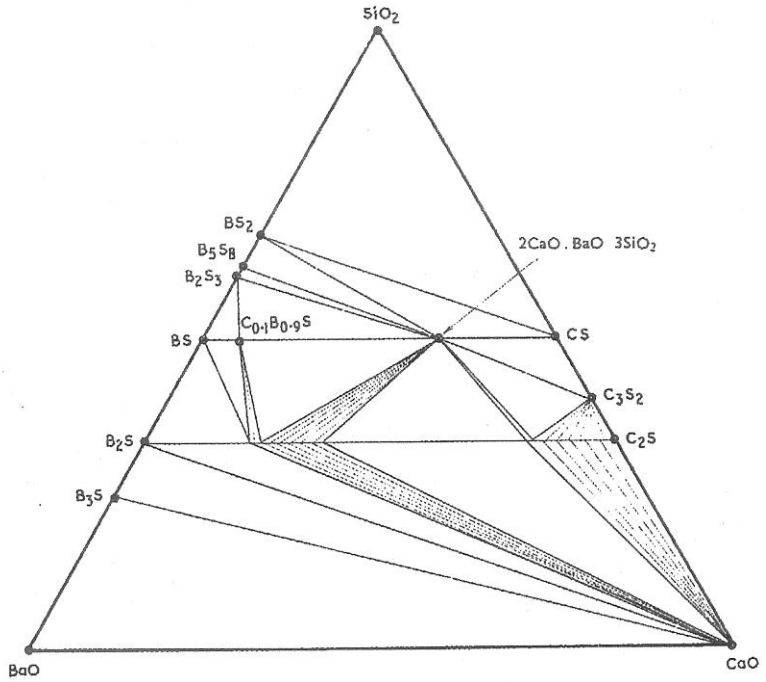

Fig. 3.3.3 An isothermal section at 1100 °C as reported by Brisi and Appendino.

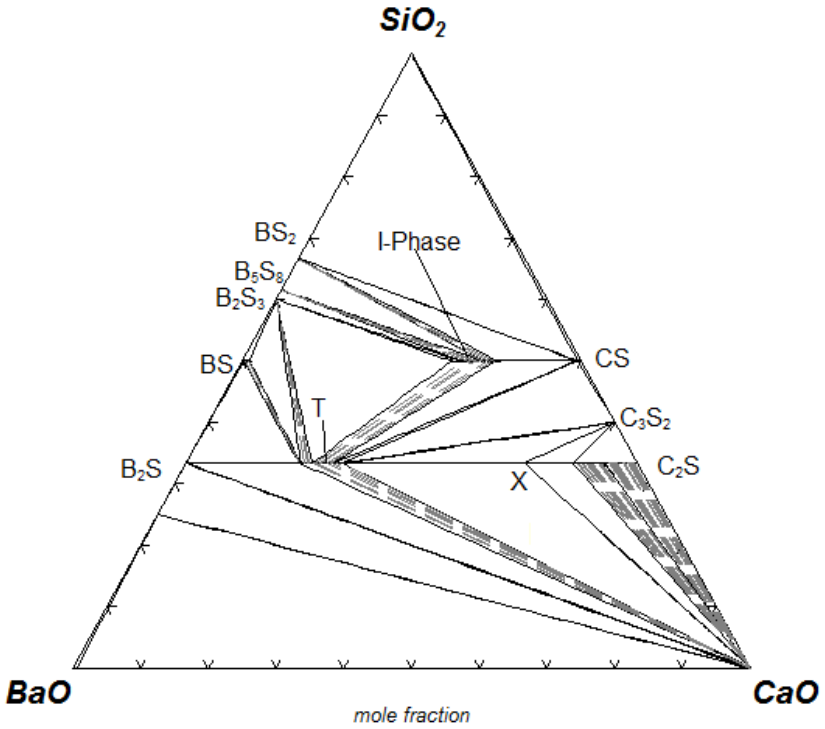

Fig. 3.3.4 Optimized isothermal section in the BaO-CaO-SiO_2 ternary system.

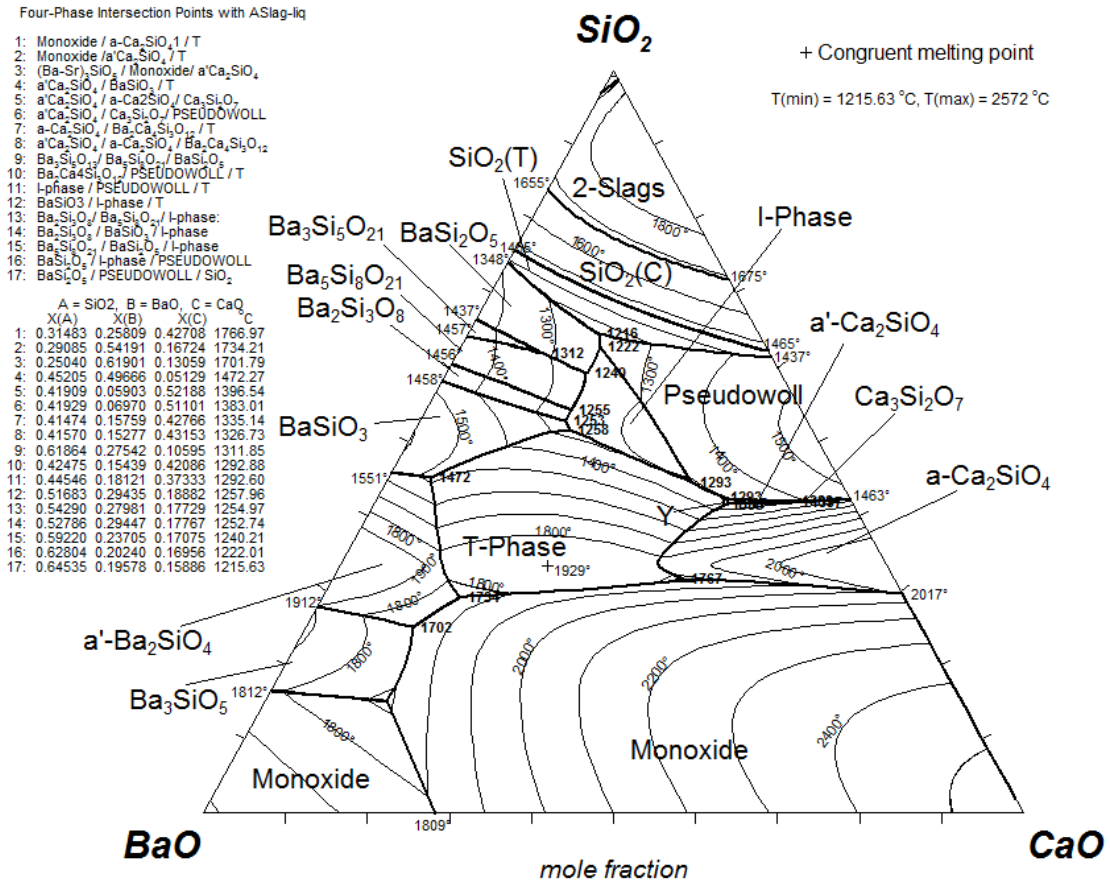

Fig. 3.3.5 Present calculated liquidus (polythermal) projection for the BaO-CaO-SiO_2 system (isotherms were drawn at the interval of 100 °C).

3.4 The $CaSiO_3$-$SrSiO_3$-$BaSiO_3$ system

Winkle and Muan (1973) by quenching techniques and XRD reported phase relations in the temperature range 1225-1275 °C in the $CaSiO_3$-$SrSiO_3$-$BaSiO_3$ system. These data are reasonably well reproduced in the present calculated isothermal section at 1250 °C in Fig. 3.4.1. The Gibbs energy of the liquid phase was estimated from the corresponding binary subsystems treating silica as the asymmetric component [Pelton and Chartrand (2001)]. As can be seen in Fig

3.4.1, the data of Winkle and Muan (1973) show solubility of Sr in the $BaCa_2Si_3O_9$ phase. In the present calculations, the solubility was taken into account by introducing Sr into both the sublattices filled by Ba and Ca, i.e. the phase was modeled as [Ba,Ca,Sr][Ba,Ca,Sr]$CaSi_3O_9$. The optimized parameters of this phase are presented in Table 3.4.1. The primary phase fields region reported by Winkle and Muan (1973) are well reproduced in Fig. 3.4.2. Winkle and Muan (1973) reported a ternary eutectic at 1275 ºC with liquid composition of 20 mol% $CaSiO_3$, 39 mol% $SrSiO_3$ and 41 mol% $BaSiO_3$. The present calculated eutectic temperature is 1303 °C and composition is 24.3 mol% $CaSiO_3$, 34.2 mol% $SrSiO_3$ and 41.5 mol% $BaSiO_3$.

Table 3.4.1 Optimized thermodynamic parameters, in Joules, for the I-Phase: [Ba,Ca,Sr][Ba,Ca,Sr]$CaSi_3O_9$.*

I-phase [Ca,Ba][Ca,Ba]$CaSi_3O_9$
$G^0([Ca][Sr]CaSi_3O_9) = 2\ G^0(CaSiO_3, Woll.) + G^0(SrSiO_3) + 7326$
$G^0([Sr][Ca]CaSi_3O_9) - G^0([Ca][Sr]CaSi_3O_9) = 1674$
$G^0([Ba][Sr]CaSi_3O_9) - G^0([Sr][Ba]CaSi_3O_9) = -20920$
$G^0([Ca][Ca]CaSi_3O_9) + G^0([Sr][Sr]CaSi_3O_9) = G^0([Ca][Sr]CaSi_3O_9) + G^0([Sr][Ca]CaSi_3O_9)$
$G^0([Sr][Sr]CaSi_3O_9) + G^0([Ba][Ba]CaSi_3O_9) = G^0([Ba][Sr]CaSi_3O_9) + G^0([Sr][Ba]CaSi_3O_9)$ + 33472

* Only the Gibbs energy of the end-members containing Sr are presented here; the Gibbs energies of other end-members are presented in the CaO-BaO-SiO_2 section

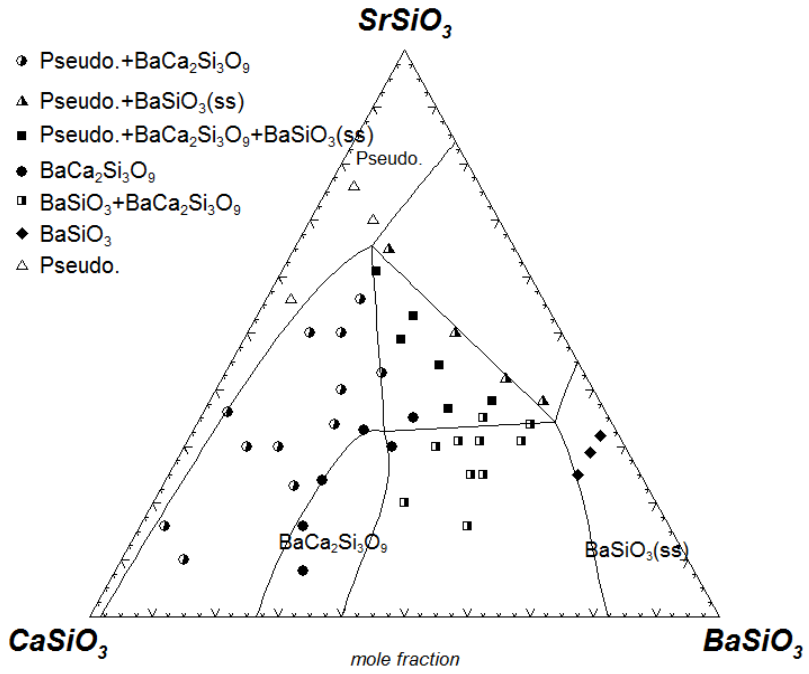

Fig. 3.4.1 Calculated isothermal section at 1250 °C in the $SrSiO_3$-CaSiO3 -$BaSiO_3$ system.

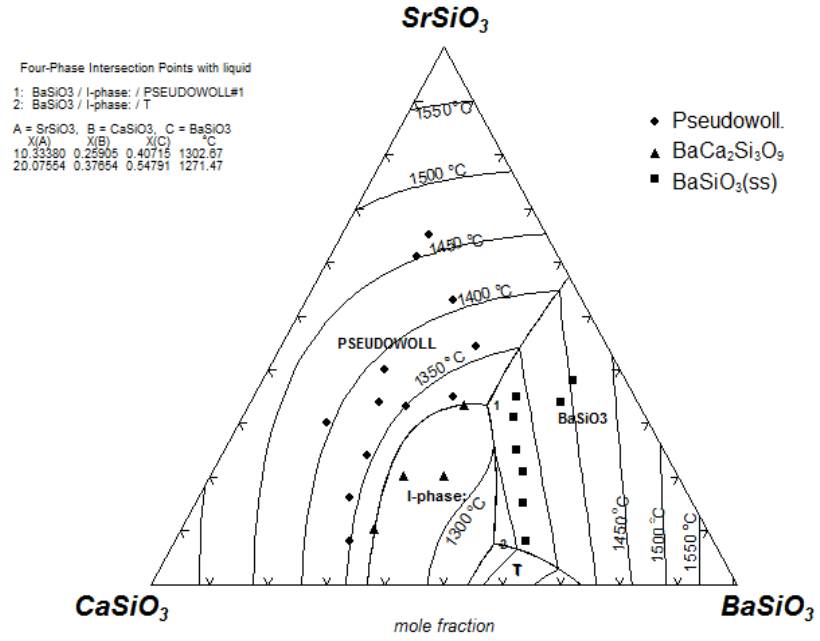

Fig. 3.4.2 The polythermal projection of the $SrSiO_3$-$CaSiO_3$-$BaSiO_3$ system.

3.5 The SrO-MgO-SiO_2 system

Ghanbari-Ahari and Brett (1988) by XRD coupled with optical microscopy and EPMA studied this ternary system and reported isothermal sections over a range of temperature from 1200 and 1700 ºC. The present calculated isothermal sections between 1200 and 1700 ºC are reasonably well reproduced in Figs. 3.5.1-3.5.6. The Gibbs energy of the liquid phase in the ternary system was estimated from the corresponding binary systems by treating SiO_2 as asymmetric component [Pelton and Chartrand (2001)]. The liquid interaction parameters presented in Table 3.5.1 were also used to reproduce these isothermal sections. Ghanbari-Ahari and Brett (1988) confirmed the presence of two ternary compounds $Sr_2MgSi_2O_7$ (Sr_2MS_2), incongruent melting point of 1560 ± 15 ºC, shown as T1 and $Sr_3MgSi_2O_8$ (Sr_3MS_2), melting point above 1700 ºC, shown as T2 in Figs. 3.5.1-3.5.6. In the present calculations, both these phases were modeled as stoichiometric and the optimized parameters for these compounds are presented in Table 3.5.1. Massazza (1962) by quenching reported melting of the $SrMS_2$ phase as 1625 °C. Klasens, Hoekstra, and Cox (1957) while studying ultraviolet fluorescence of some ternary silicates also reported these two compounds. They reported XRD data for the Sr_2MS_2 and Sr_3MS_2 compounds which were indexed by them to the isomorphous $Ca_2MgSi_2O_7$ (akermanite) and $Ca_3MgSi_2O_8$ (merwinite) structures respectively. Ghanbari-Ahari and Brett (1988) also mentioned that analogues of diopside ($CaMgSi_2O_6$) and monticellite ($CaMgSiO_4$) do not exist in the SrO-MgO-SiO_2 system. The EPMA data of Ghanbari-Ahari and Brett (1988) at 1500 and 1600 °C show negligible (< 1wt.%) solid solubility among the Mg_2SiO_4-Sr_2SiO_4 and the $MgSiO_3$-$SrSiO_3$ phases. The different crystal structures (Mg_2SiO_4 has olivine, Sr_2SiO_4 has α'-Ca_2SiO_4, $MgSiO_3$ has various pyroxenes, and $SrSiO_3$ has pseudowollastonite structures) and large difference between ionic radii of Mg and Sr mitigate against any appreciable mutual solid solubility among

these phases. Hence, in the present calculations as well these mutual solubilities were calculated as negligible at all the temperatures.

Huntelaar, Booij, Cordfunke, and Van der Laan (1998) by low-temperature heat capacity measurement reported S^o_{298} and by solution calorimetry reported ΔH^o_{298} for the Sr_3MS_2 phase which are well reproduced as shown in Table 3.5.1. They also reported by high-temperature drop calorimetry the enthalpy increments ($H_T - H_{298}$) in the range 250-650 ºC for this phase. These enthalpy increments were used to optimize the heat capacity of the Sr_3MS_2 phase presented in Table 3.5.1. These enthalpy increments are compared with the present calculations in Fig. 3.5.7. The optimized heat capacity function for the temperature range 250-650 ºC was also used at temperatures above this. The optimized heat capacity is shown in Fig. 3.5.8 where it is also compared with the heat capacity obtained by adding the heat capacities of corresponding orthosilicates. No thermodynamic data for the Sr_2MS_2 phase were found in the literature. The present calculated liquidus (polythermal) projection for the SrO-MgO-SiO_2 system is presented in Fig. 3.5.9.

Table 3.5.1 Optimized thermodynamic parameters, in Joules, in the SrO-MgO-SiO_2 system.

$Sr_3MgSi_2O_8$		
ΔH^0_{298} = –4578300 J/mol	ΔH^0_{298}, Experimental = –4575300 ± 5100 J/mol [Huntelaar et al., '98]	
S^0_{298} = 280.150 J/mol/K	S^0_{298}, Experimental = 280.150 ± 0.600 J/mol/K [Huntelaar et al., '98]	ΔS^0_{298}[(a)] = 9.539
$C_p = 303 + 0.06\ T - 6040000\ T^2$	T_m[(c)] = 1774 ºC; Exp.> 1700 °C [Ghanbari-Ahari and Brett, '88]	
$Sr_2MgSi_2O_7$		
ΔH^0_{298} = –3897000J/mol		
S^0_{298} = 230.879 J/mol/K	ΔS^0_{298}[(a)] = 13.858	ΔS^0_{298}[(b)] = 0
$C_p = C_p\ (SrSiO_3) + C_p\ (MgSiO_3$,protoenstatite) $+ C_p(SrO)$	T_m[(c)] = 1584 ºC; Exp. = 1560 ± 15 °C [Ghanbari-Ahari and Brett, '88] Exp. = 1625 ± 10 °C [Massazza, '62]	
Monoxide (in Joules)		
q^{11}_{SrMg} = 117000		
α'-Mg_2SiO_4[(e)]		
$G^0(Mg_2SiO_4, \alpha') = G^0(Mg_2SiO_4) + 85772$		
α-Mg_2SiO_4[(e)]		
$G^0(Mg_2SiO_4, \alpha) = G^0(Mg_2SiO_4) + 83680$		
Liquid phase (Ternary interaction parameters) (in Joules)		
$q^{101}_{SiMg(Sr)} = -14644 - 26.3592\ T$		
$q^{041}_{SiMg(Sr)}$ = 627600		

[(a)] oxides (stable at room temperature) as reference
[(b)] compounds used to calculate heat capacity as reference
[(c)] incongruent melting temperature
[(e)] Mg_2SiO_4 is an end-member in the α' and α orthosilicate phases

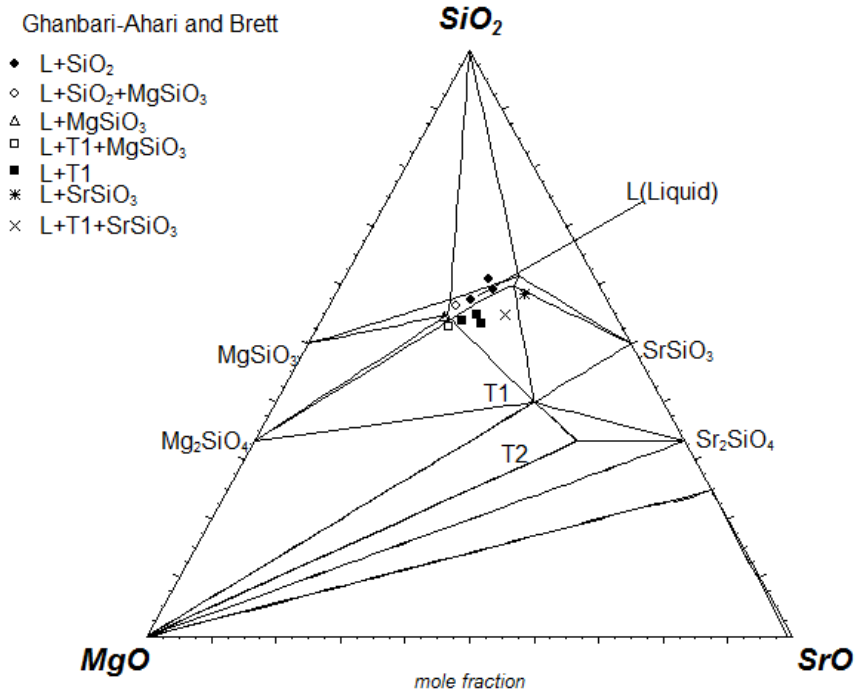

Fig. 3.5.1 Calculated isothermal section at 1200 ºC.

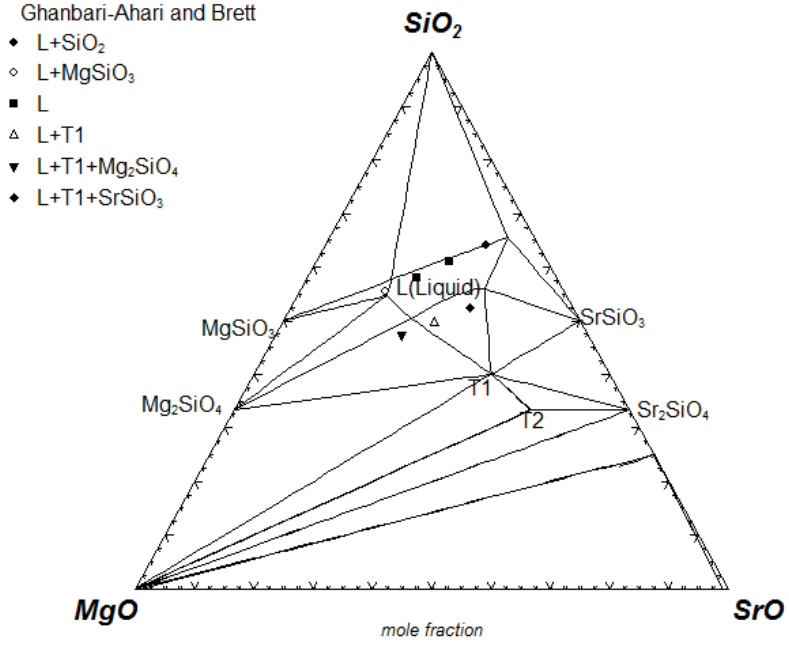

Fig. 3.5.2 Calculated isothermal section at 1300 ºC.

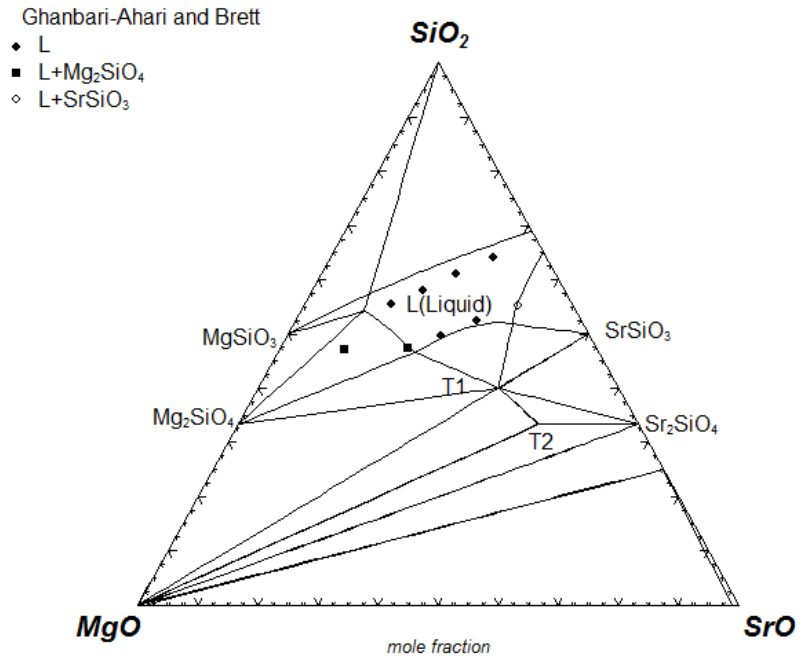

Fig. 3.5.3 Calculated isothermal section at 1400 ºC.

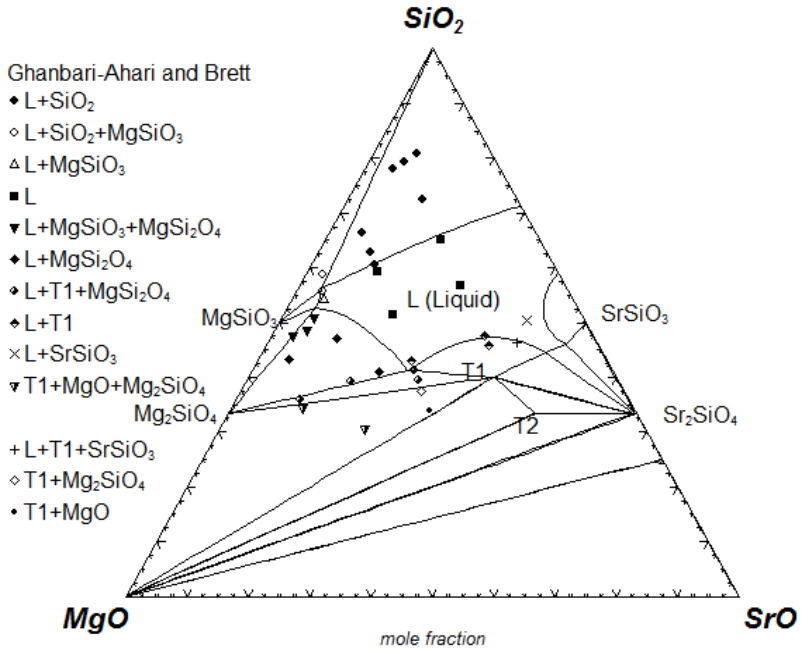

Fig. 3.5.4 Calculated isothermal section at 1500 ºC.

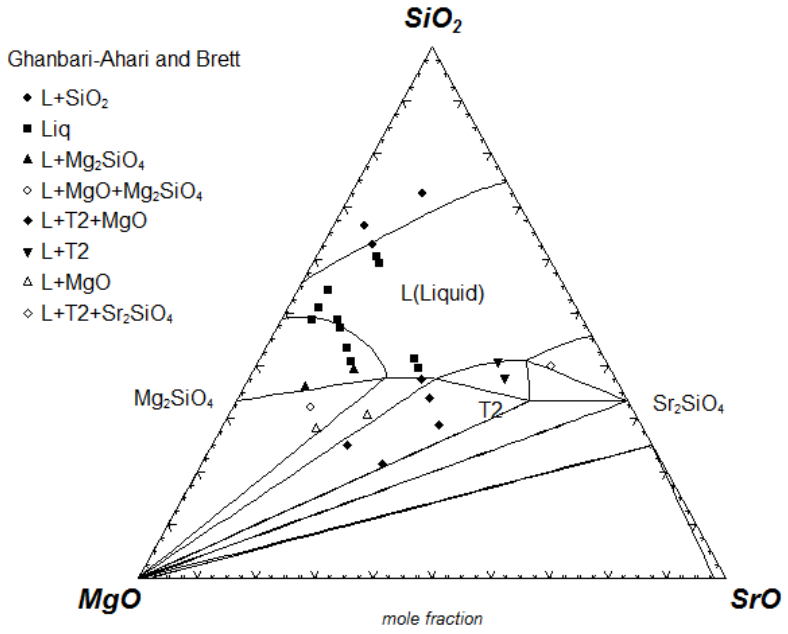

Fig. 3.5.5 Calculated isothermal section at 1600 ºC.

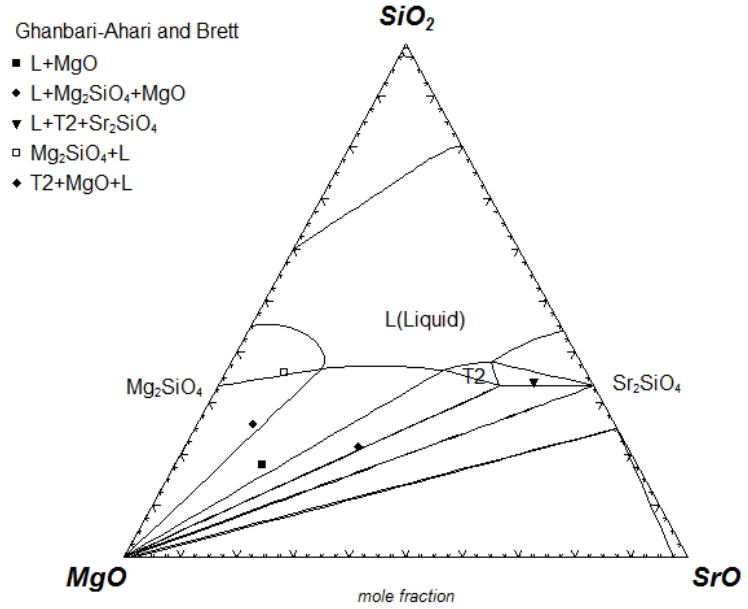

Fig. 3.5.6 Calculated isothermal section at 1700 ºC.

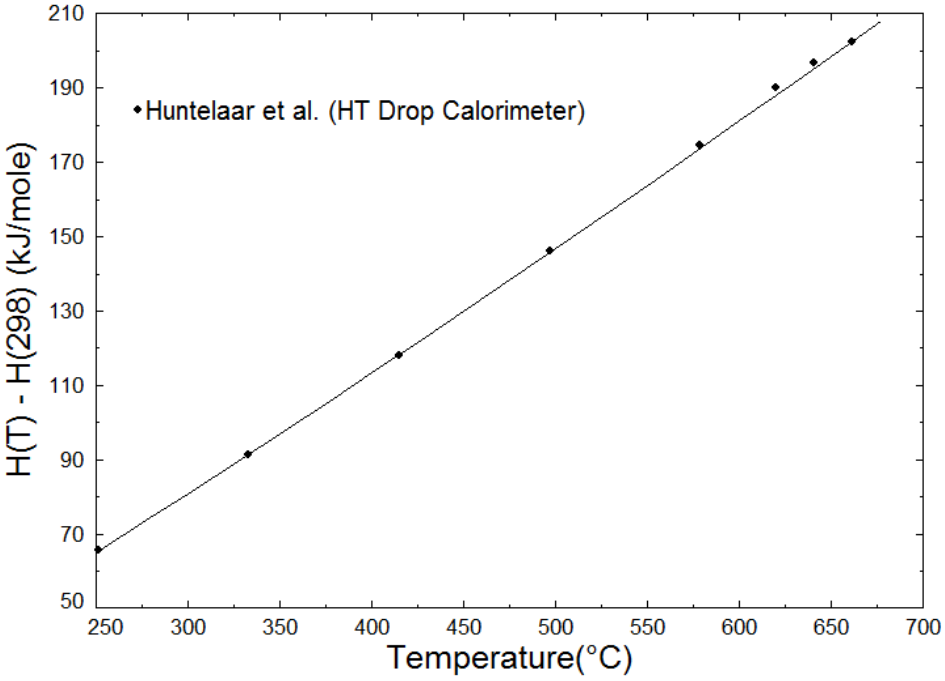

Fig. 3.5.7 Enthalpy increments ($H_{(T)} - H_{(298)}$) in the $Sr_3MgSi_2O_8$ phase.

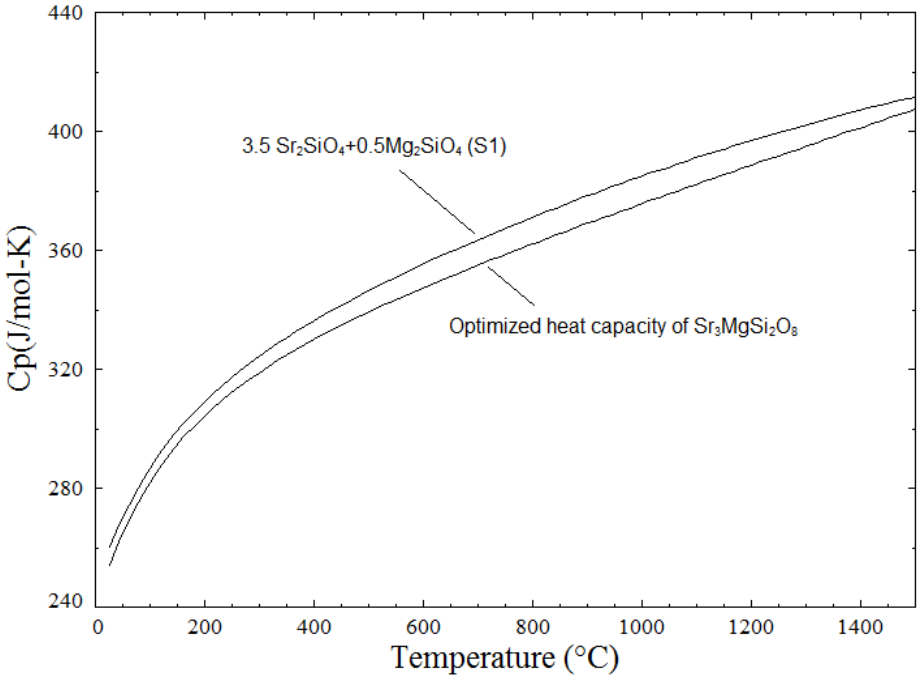

Fig. 3.5.8 Optimized heat capacity of the $Sr_3MgSi_2O_8$ phase compared with the sum of the heat capacity of the orthosilicates.

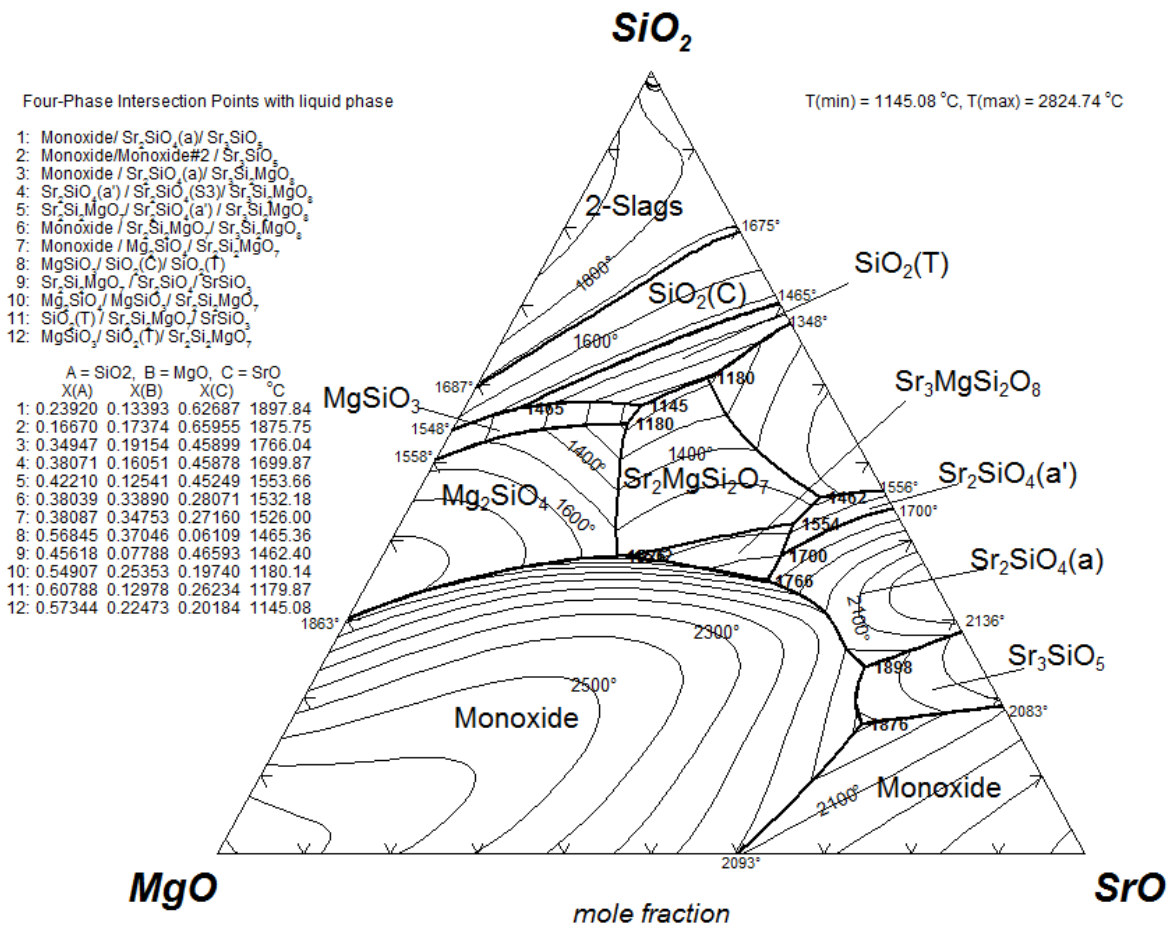

Fig. 3.5.9 Present calculated liquidus (polythermal) projection for the SrO-MgO-SiO_2 system (isotherms were drawn at the interval of 100 °C).

3.6 The CaO-SrO-MgO-SiO_2 system

Massazza and Fadda (1964) and Massazza (1962) studied the $Ca_2MgSi_2O_7$-$Sr_2MgSi_2O_7$ (C_2MS_2-Sr_2MS_2) and $Ca_3MgSi_2O_8$-$Sr_3MgSi_2O_8$ (C_3MS_2-Sr_3MS_2) sections in this quaternary system. As reported in the SrO-MgO-SiO_2 system, Sr_2MS_2 is isostructural with C_2MS_2 and Sr_3MS_2 is isostructural with C_3MS_2. Massazza and Fadda (1964), Barry (1968) and Ruez (1971) reported complete solubility among the C_3MS_2 and Sr_3MS_2 phases but did not report any phase diagram points in this section. Massazza (1962) reported complete solubility among the C_2MS_2 and

Sr_2MS_2 phases and reported phase diagram points on the C_2MS_2-Sr_2MS_2 section. The optimal fit of these data is presented in Fig. 3.6.1. An ideal solution was assumed between the C_3MS_2-Sr_3MS_2 phases. The solid solutions among the C_2MS_2-Sr_2MS_2 and C_3MS_2-Sr_3MS_2 phases were modeled using the single sublattice substitutional random-mixing model. Interaction parameters presented in Table 3.6.1 were also used for the C_2MS_2-Sr_2MS_2 solid solution. In Fig. 3.6.1 the present calculations disagree with the experimental data on the appearance of the merwinite phase [$(Ca,Sr)_3MgSi_2O_8$ in Fig. 3.6.1]. The Gibbs energies of the end-members (C_3MS_2-Sr_3MS_2) for this phase are fixed from the optimizations of the respective ternary systems. During calculations, in an effort to stabilize the merwinite phase, a negative interaction parameter was used but it did not help in fitting the stability of the merwinite phase in Fig. 3.6.1. It can be said that more experimental work is required to corroborate Massazza's data on the stability of merwinite phase in the C_2MS_2-Sr_2MS_2 section. Also, some phase diagram data on the C_3MS_2-Sr_3MS_2 section will also be helpful in fixing the stability of the merwinite phase.

Benna and co-workers [Benna (1982); Benna, Chiari, and Bruno (1987)] by quenching and XRD studied the Sr substitution in the diopside ($CaMgSi_2O_6$, clinopyrexene structure, C2/c) phase. As previously stated, the Sr analogue of diopside phase does not exist in the SrO-MgO-SiO_2 system. The data by Benna and co-workers are compared with the present calculations in Fig. 3.6.2. In our previous studies, the diopside phase was modeled as $[Ca,Mg][Mg]Si_2O_6$. Benna, et al. (1987) also reported that Sr enters the site with Ca and Mg and the second sublattice is filled by Mg only. Therefore, the diopside solution in Fig. 3.6.2 was modeled as $[Ca,Mg,Sr][Mg]Si_2O_6$. The optimized parameters are presented in Table 3.6.1. In the region where Benna, et al. (1987)

reported one phase diopside as stable (black triangles in Fig. 3.6.2), the present calculations show limited amounts of wollastonite and pseudowollastonite phases as stable, together with diopside. The reason for this is that the diopside phase, at the higher temperatures, on the $CaSiO_3$-$MgSiO_3$ join does not exactly lie on the 50-50 ($CaMgSi_2O_6$) composition (This can be seen in our previous study of the CaO-MgO-SiO_2 system) and is slightly off from it. Therefore, when the phase diagram is drawn on the $CaMgSi_2O_6$-$SrMgSi_2O_6$ join these two phases appear in very small amounts. Benna, et al. (1987), probably, could not detect the presence of small amounts of wollastonite and pseudowollastonite phases in their investigations.

Table 3.6.1 Optimized thermodynamic parameters, in joules, in the CaO-SrO-MgO-SiO_2 system.

$(Ca,Sr)_3MgSi_2O_8$
$q^{11} = 0$
$(Ca,Sr)_2MgSi_2O_7$
$q^{21} = 5021$
Diopside ($[Ca,Mg,Sr][Mg]Si_2O_6$)[(a)]
$G^0([Sr][Mg]Si_2O_6 = G^0(SrSiO_3) + G^0(MgSiO_3$,proto-enstatite)
y^{00}_{Sr-Mg} [(b)] = 25304 + 2.358 T
y^{01}_{Sr-Mg} [(b)] = 3019

[(a)] The Gibbs energy of the end-member containing Sr only is presented here; the Gibbs energy of the other end members can be found in the previous work by Jung (2003) on CaO-MgO-SiO_2 system.

[(b)] These are the same parameters as used for the Ca-Mg interaction in the previous work by Jung (2003).

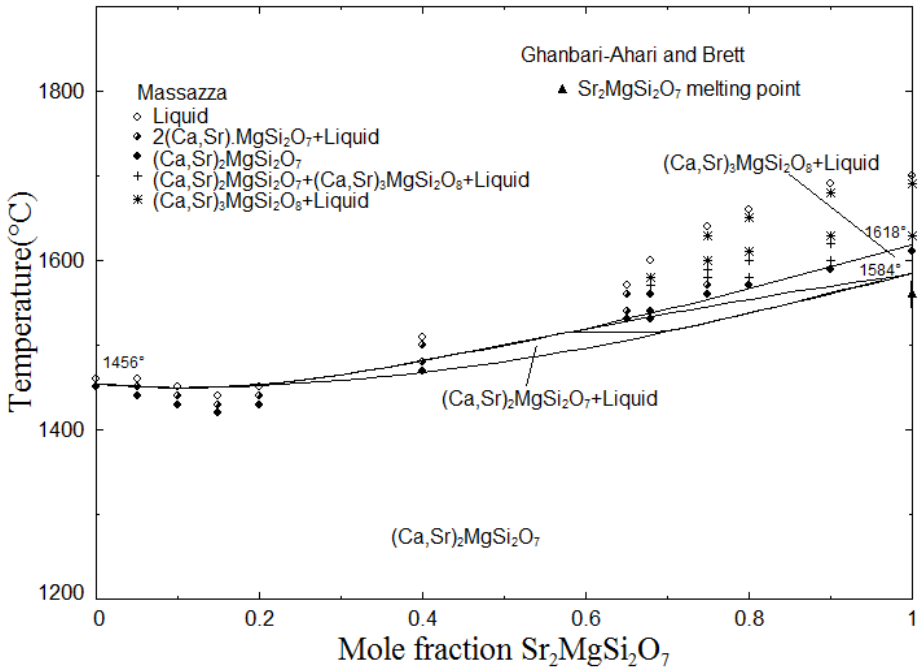

Fig. 3.6.1 Optimized phase diagram of the $Ca_2MgSi_2O_7$-$Sr_2MgSi_2O_7$ system.

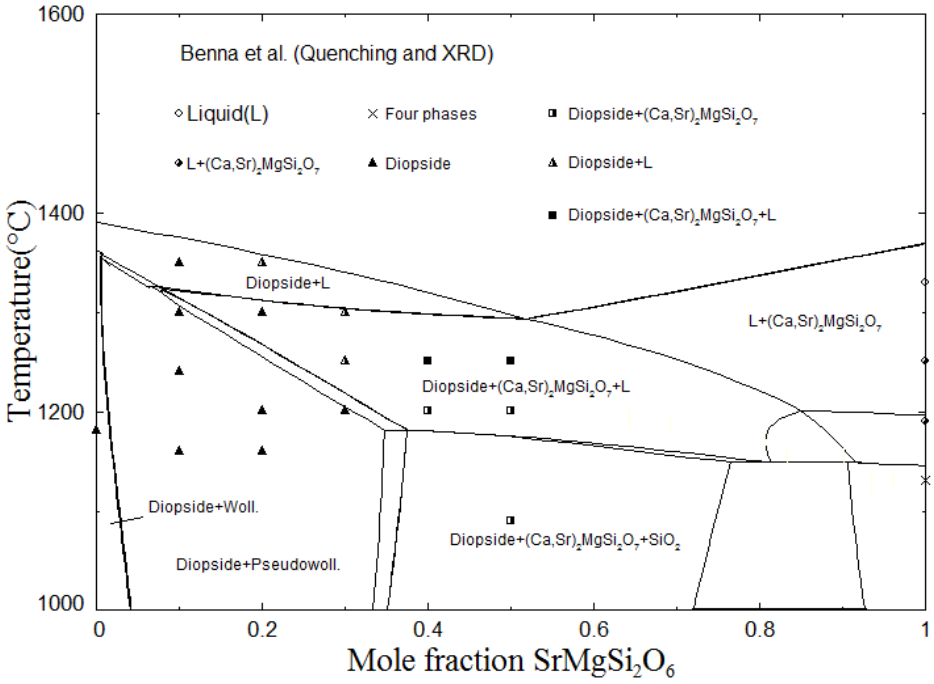

Fig. 3.6.2 Optimized phase diagram for the $CaMgSi_2O_6$-$SrMgSi_2O_6$ join.

3.7 The BaO-MgO-SiO_2 system

The Gibbs energy of the liquid phase in this ternary system was estimated from the corresponding binary systems by treating SiO_2 as asymmetric component [Pelton and Chartrand (2001)]. The liquid interaction parameters presented in Table 3.7.1 was also used to obtain the optimal fit of the available data.

Klasens, et al. (1957) studied ultraviolet fluorescence in some ternary silicate compounds activated by lead. They reported four compounds in the system BaO-MgO-SiO_2: BaO.MgO.SiO_2 (BMS), BaO.2MgO.2SiO_2 (BM_2S_2), 2BaO.MgO.2SiO_2 (B_2MS_2), 3BaO.MgO.2SiO_2 (B_3MS_2). Barry (1968) also studied luminescence in the compound B_3MS_2 (along with 3SrO.MgO.2SiO_2 (Sr_3MS_2) and 3CaO.MgO.2SiO_2 (C_3MS_2)). Klasens, et al. (1957) indexed B_3MS_2 as having the merwinite (C_3MS_2) structure. Shimizu, Kimata, and Iida (1995) indexed B_2MS_2 as millilitre ($Ca_2MgSi_2O_7$) structure. For the BMS phase B. Liu and Barbier (1993) reported a hexagonal crystal structure (with space group $P6_3$). Argyle and Hummel (1965) by quenching studies reported all those phases reported by Klasens, et al. (1957) as stable along with one extra compound, $BaMgSi_3O_8$ (BMS_3).

Nadachowski and Grylicki (1959) studied the Ba_2SiO_4-Mg_2SiO_4 (B_2S-M_2S) section and reported it as a true binary join with BMS and BaO.3MgO.2SiO_2 (BM_3S_2) compounds. Vulkov, Stavrakeva, and Ivanova (1981) also reported it as a binary join with all three BMS, B_3MS_2 and BM_3S_2 as stable compounds. However, Klasens, et al. (1957) and Argyle and Hummel (1965) did not report this section as a true binary join, neither did they report BM_3S_2 as stable compound. No

other experimental data on stability of the BM_3S_2 phase could be found in the literature. In the present work, this phase was not considered as stable.

Argyle and Hummel (1965) by quenching studies reported sub-solidus phase equilibria. Their data are presented in Table 3.7.1 and compared with the present calculations. Argyle and Hummel (1965) presented an isothermal section, based on these data, as shown in Fig. 3.7.1. However, they did not specify the temperature for this section. Presumably, they believed the phase assemblages did not change in the temperature range of their study. However, the present calculations show that phase assemblages change with temperature. For example, they reported BMS_3 to be in equilibrium with the MS phase (Fig. 3.7.1). As can be seen in Table 3.7.1, the only data to corroborate this equilibrium are at 950 °C. The present calculated isothermal section at 950 °C shows this phase to be in equilibrium (Fig. 3.7.2) but at a higher temperature (1000 °C) this is not the case as shown in Fig. 3.7.3 (the exact change occur at about 980°C). However, more experimental data are required to corroborate this change. Also, Argyle and Hummel (1965) and Klasens, et al. (1957), based on experimental data below 1100 °C, reported BM_2S_2 to be in equilibrium with MgO (Fig. 3.7.1). According to the present calculations, MgO is in equilibrium with BM_2S_2 at 1200 °C. However, at and above 1250 °C, instead of these two, BMS and M_2S are in equilibrium (Fig. 3.7.4) and B_2S-M_2S behaves as a true binary join. It should be noted that Nadachowski and Grylicki (1959) and Vulkov, et al. (1981) reported B_2S-M_2S as a true binary join, with an extra compound BM_3S_2 whose presence is neglected here, and all their investigations were above 1200 °C. So it is possible that B_2S-M_2S behaves as a true binary join, with the BM_3S_2 phase stable only at the higher temperatures. Below 1200 °C, the BM_3S_2 phase

decomposes into BM_2S_2 and MgO as shown in Fig. 3.7.4. However, more experimental evidence is required to prove this and the presence of BM_3S_2 was neglected in the present work. No experimental evidence on the mutual solid solubility among the phases of the same stoichiometry, i.e. the Mg_2SiO_4-Ba_2SiO_4 and the $MgSiO_3$-$BaSiO_3$ phases, could be found in the literature. Also, the different crystal structures (Mg_2SiO_4 has the olivine structure, Ba_2SiO_4 has the α'-Ca_2SiO_4 structure, $MgSiO_3$ has the various pyroxene structures, and $BaSiO_3$ has $BaGeO_3$ structure.) and large difference between ionic radii of Mg and Ba mitigate against any appreciable mutual solid solubility among these phases. Hence, in the present calculations as well these mutual solubilities were neglected. The present calculated liquidus (polythermal) projection for the BaO-MgO-SiO_2 system is presented in Fig. 3.7.5.

Argyle and Hummel (1965) also reported the nature and temperatures of melting for these ternary compounds along with low-temperature decomposition for BMS and BMS_3. These data can be compared with the present obtained results in Table 3.7.2. The Gibbs energy of the liquid phase in the ternary system was estimated from the corresponding binaries treating Si as asymmetric component [Pelton and Chartrand (2001)]. A small ternary interaction parameter, presented in Table 3.7.2., in the liquid phase was also used. The standard enthalpies (H^0_{298}) and standard entropies (S^0_{298}) for the solid phases presented in Table 3.7.2 were optimized based on the sub-solidus phase equilibrium data in Table 3.7.1. No thermodynamic data for these solid phases could be found in the literature. The heat capacities for these phases were estimated as the sums of the constituent compounds and oxides, as shown in Table. 3.7.2. All the reported decomposition temperatures (Table. 3.7.2) are reasonably well reproduced except for the B_2MS_2

and BMS_3 phases. It was observed during the calculations that the values of H^0_{298} and S^0_{298} for the B_2MS_2 and BMS_3 phases, which reproduce the data in Table 3.7.1, invariably gave a high melting point and no low-temperature decomposition for the BMS_3 phase. For the BMS_3 phase, the X-ray reflections obtained by Argyle and Hummel (1965) were relatively weak. Argyle and Hummel (1965) at first thought this compound to be metastable. The only evidence based on which they concluded stability of this phases was that they heated a sample of this composition at 340 atm. (5000 psi) and 600 °C for 24 hours to obtain crystalline aggregates of BM_2S_2 and $BaSi_2O_5$ (BS_2). However, the same composition heated at 800 °C for 24 hours at 340 atm. (5000 psi) gave only BMS_3. It should be noted that they did not prove stability of this compound at 1 atm. pressure. In view of the difficulty faced in the present calculations, it can be said that more evidence is required to prove the stability of this phase. Moreover, some thermodynamic data for any of the ternary compounds in the BaO-MgO-SiO_2 system will also help in optimization by restricting the various degrees of freedom. The calculated standard entropies of formation (Table 3.7.2) for these compounds are quite reasonable as they are always less than 6 J/mol of metals.

Table 3.7.1 Experimental data of Argyle and Hummel (1965) compared with the present calculations.

SiO_2	BaO	MgO	Temp.	Exp.	Present calculations (only those points are reported where present calculations differ from the experimental point) (tr=trace)
0.8	0.1	0.1	950	BMS_3+SiO_2	
0.7	0.2	0.1	950	$BMS_3+SiO_2+BS_2$	
0.66	0.17	0.17	950	BMS_3+SiO_2	
0.65	0.1	0.25	950	BMS_3+SiO_2+MS	
0.62	0.25	0.13	950	BMS_3+BS_2	BMS_3+BS_2+tr-$BaSi_2Mg_2O_7$
0.6	0.25	0.15	950	$BMS_3+BS_2+BM_2S_2$	
0.6	0.2	0.2	689	$BM_2S_2+BS_2$	BMS_3
0.6	0.2	0.2	699	BMS_2+BS_2+tr BMS_3	BMS_3
0.6	0.2	0.2	704	BMS_3	
0.6	0.2	0.2	723	BMS_3	
0.6	0.2	0.2	770	BMS_3	
0.6	0.2	0.2	950	BMS_3	
0.6	0.2	0.2	1015	BMS_3+tr glass	BMS_3
0.58	0.29	0.13	1100	$BM_2S_2+BS_2$	
0.57	0.33	0.1	1075	$BM_2S_2+B_3S_5$	$BS_2+BM_2S_2+B_5S_8$ (B_3S_5 decomposes at 1304 °C, see $BaO-SiO_2$ section)
0.56	0.34	0.1	1100	$BM_2S_2+B_5S_8$	$BM_2S_2+B_5S_8+B_2S_3$
0.55	0.2	0.25	950	$BMS_3+BM_2S_2$	
0.55	0.1	0.35	950	BMS_3+MS	
0.52	0.28	0.2	1050	$BM_2S_2+B_3S_5+BS_2$	$BM_2S_2+B_5S_8+BS_2$(B_3S_5 decomposes at 1304 °C, see $BaO-SiO_2$ section)
0.51	0.19	0.3	950	$BM_2S_2+BMS_3$	$BM_2S_2+BMS_3+MgSiO_3$
0.5	0.4	0.1	1000	$B_2MS_2+B_2S_3$	
0.5	0.33	0.17	1050	BM_2S_2+tr$B_2MS_2+B_2S_3$	
0.5	0.3	0.2	1100	$BM_2S_2+B_2S_3$	
0.5	0.25	0.25	1050	$BM_2S_2+BS_2$	
0.5	0.12	0.38	950	$BMS_3+BM_2S_2$+MS	
0.5	0.05	0.45	950	BM_2S_2+trBMS_3+MS	
0.46	0.15	0.39	950	$BM_2S_2+BMS_3$+MS	
0.45	0.45	0.1	1100	$BS+B_2MS_2$	
0.45	0.35	0.2	1100	$B_2MS_2+BM_2S_2+B_2S_3$	
0.45	0.1	0.45	1100	BM_2S_2+MS	
0.43	0.28	0.29	1050	$BM_2S_2+B_2MS_2+B_2S_3$	
0.42	0.5	0.08	1050	$B_2MS_2+BS+B_2S$	

0.4	0.4	0.2	1050	B_2MS_2	
0.4	0.4	0.2	1401	B_2MS_2	
0.4	0.4	0.2	1425	B_2MS_2	
0.4	0.4	0.2	1428	B_2MS_2+trBMS+trGlass	B_2MS_2
0.4	0.3	0.3	1050	B_2MS_2+BM_2S_2	
0.4	0.2	0.4	1200	BM_2S_2	
0.4	0.1	0.5	1200	M_2S+MS+BM_2S_2	
0.4	0.05	0.55	1100	BM_2S_2+M_2S+MS	
0.38	0.5	0.125	1050	B_2MS_2+B_2S	
0.38	0.375	0.25	1050	B_2MS_2+BMS	
0.37	0.45	0.185	1050	B_2MS_2+B_3MS_2	B_2MS_2+B_3MS_2+BMS
0.37	0.27	0.365	980	B_2MS_2+BM_2S_2+MgO	BMS+BM_2S_2
0.37	0.27	0.365	1100	BMS+BM_2S_2	
0.36	0.09	0.55	1100	M_2S+BM_2S_2	M_2S+BM_2S_2+MgO
0.35	0.5	0.15	1050	B_2MS_2+B_3MS_2+B_2S	
0.35	0.4	0.25	1050	B_2MS_2+B_3MS_2+BMS	
0.35	0.3	0.35	1100	BM_2S_2+BMS	
0.33	0.567	0.1	1100	B_3MS_2+B_2S	B_3MS_2+B_2S+tr MgO
0.33	0.5	0.167	1100	B_3MS_2	B_3MS_2+trMgO+ trB_2S)
0.33	0.267	0.4	980	B_3MS_2+B_2MS_2+tr MgO	BMS+BM_2S_2+MgO
0.33	0.4	0.267	1050	B_3MS_2+BMS	B_3MS_2+BMS+ tr MgO
0.33	0.333	0.333	980	B_2MS_2+MgO	BMS + tr BM_2S_2+ tr B_3MS_2
0.33	0.333	0.333	1010	B_2MS_2+MgO	BMS + tr BM_2S_2+ tr B_3MS_2
0.33	0.333	0.333	1016	BMS+trB_2MS_2+trMgO	BMS + tr BM_2S_2+ tr B_3MS_2
0.33	0.333	0.333	1022	BMS	BMS + tr BM_2S_2+ tr B_3MS_2
0.33	0.333	0.333	900	BM_2S_2+MgO	B_2MS_2+MgO+B_3MS_2
0.33	0.27	0.4	1100	BM_2S_2+BMS+MgO	
0.33	0.22	0.45	980	B_2MS_2+BM_2S_2+trMgO	BMS+MgO+BM_2S_2
0.33	0.17	0.5	1100	BM_2S_2+MgO	BMS+MgO+trBMS
0.33	0.11	0.56	1100	BM_2S_2+M_2S+MgO	
0.25	0.5	0.25	1200	B_2S+MgO	
0.25	0.3	0.45	1100	B_3MS_2+BMS+MgO	
0.25	0.25	0.5	1100	BMS+MgO	
0.25	0.18	0.57	1100	BMS+BM_2S_2+MgO	
0.25	0.05	0.7	1100	BM_2S_2+M_2S+MgO	
0.23	0.45	0.325	1100	B_2S+MgO	
0.2	0.4	0.4	1200	B_2S+MgO	
0.2	0.35	0.45	1100	B_3MS_2+B_2S+MgO	
0.2	0.3	0.5	1100	B_3MS_2+MgO	
0.2	0.1	0.7	1100	BM_2S_2+MgO	
0.1	0.5	0.4	1300	B_2S+BaO+MgO	

Table 3.7.2 Optimized thermodynamic parameters, in Joules, in the BaO-MgO-SiO_2 system.

$BaMgSiO_4$ (BMS)		
ΔH^0_{298} = –2198050 J/mol	S^0_{298} = 173.400 J/mol/K	ΔS^0_{298} [(a)] = 19.632
T_m [(c)] = 1642 ºC, Exp.[(b)] = 1640 [Argyle and Hummel, '65]	$C_p = C_p$ ($MgSiO_3$, proto-enstatite) + Cp (BaO)	ΔS^0_{298} [(e)] =32.92
LT [(d)] (T,phases)= 1026, $MgO+B_2MS_2+BM_2S_2$	Exp. LT [(d)] (T,phases)=1020, $MgO+B_3MS_2$ [Argyle and Hummel, '65]	
$Ba_3MgSi_2O_8$ (B_3MS_2)		
ΔH^0_{298} = –4528000 J/mol	S^0_{298} = 323.400 J/mol/K	ΔS^0_{298} [(a)] = 12.180
T_m [(c)] = 1605 ºC, Liq.+B_2S, Exp.[(c)] = 1602 [Argyle and Hummel, '65])		ΔS^0_{298} [(e)] = –2.678
	$C_p = 1.5\ C_p(Ba_2SiO_4) + 0.5\ C_p(Mg_2SiO_4)$	
$Ba_2MgSi_2O_7$ (B_2MS_2)		
ΔH^0_{298} = –3868000 J/mol	S^0_{298} = 257.845J/mol/K	ΔS^0_{298} [(a)] = 0
T_m [(b)] = 1479 ºC Exp.[(c)] = 1428, Liq.+ BMS [Argyle and Hummel, '65]	$C_p = C_p(Ba_2SiO_4) + C_p(MgSiO_3,S3)$	ΔS^0_{298} [(e)] = 3.836
$BaMg_2Si_2O_7$ (BM_2S_2)		
ΔH^0_{298} = –3812000 J/mol	S^0_{298} = 208.200 J/mol/K	ΔS^0_{298} [(a)] = 5.416
T_m [(b)] = 1580 ºC, Exp.[(b)] = 1600 [Argyle and Hummel, '65]	$C_p = C_p(Mg_2SiO_4) + C_p(BaSiO_3)$	ΔS^0_{298} [(e)] = –0.691
$BaMgSi_3O_8$ (BMS_3)		
ΔH^0_{298} = –4087084 J/mol	S^0_{298} = 230.000 J/mol/K	ΔS^0_{298} [(a)] = –4.690
T_m [(c)] = 1259 ºC, Liq.+BM_2S_2	$C_p = C_p$ ($BaSiO_3$) + C_p($MgSiO_3$(S3))	ΔS^0_{298} [(e)] = 6.600
Exp.[(c)] = 1015, Liq.+BM_2S_2 [Argyle and Hummel, '65]	+ C_p (SiO_2(S2))	
LT [(d)] (T,phases)= No decomposition	Exp. LT [(d)] (T,phases)= 700, $BM_2S_2+BS_2$[Argyle and Hummel, '65]	
Monoxide (in Joules)		
q^{11}_{BaMg} = 134000		
Liquid phase (Ternary interaction parameters) (in Joules)		
$g^{001}_{SiBa(Mg)}$ = – 27614		

[(a)] Compounds used to calculate the respective heat capacities as reference
[(b)] Congruent melting temperature
[(c)] Incongruent melting temperature
[(d)] Low-temperature decomposition
[(e)] Oxides (stable at room-temperature) as reference

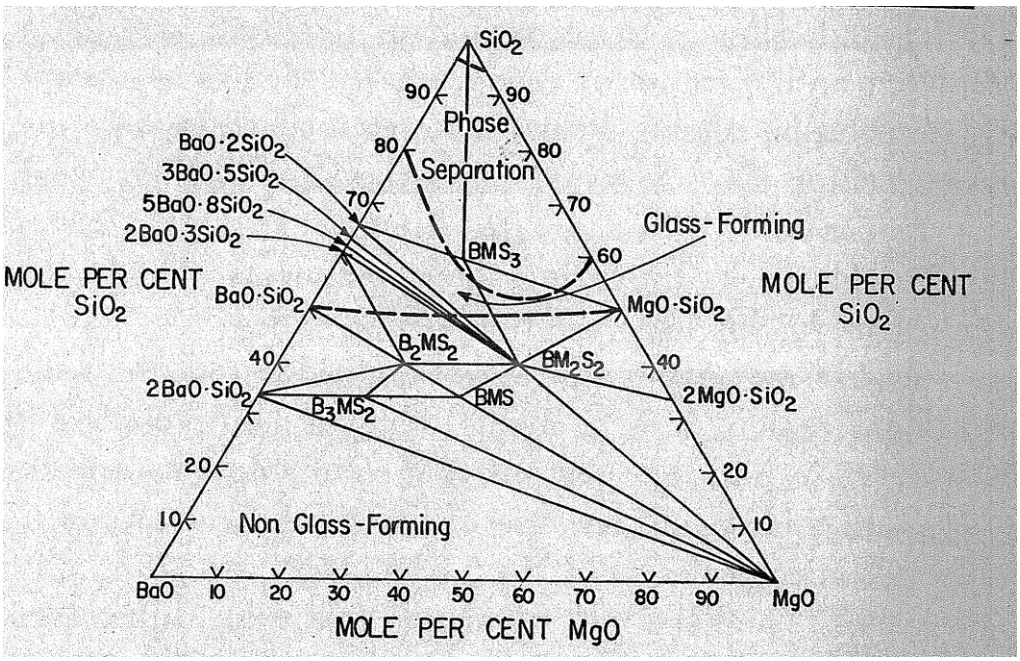

Fig. 3.7.1 Sub-solidus phase equilibria as reported by Argyle and Hummel.

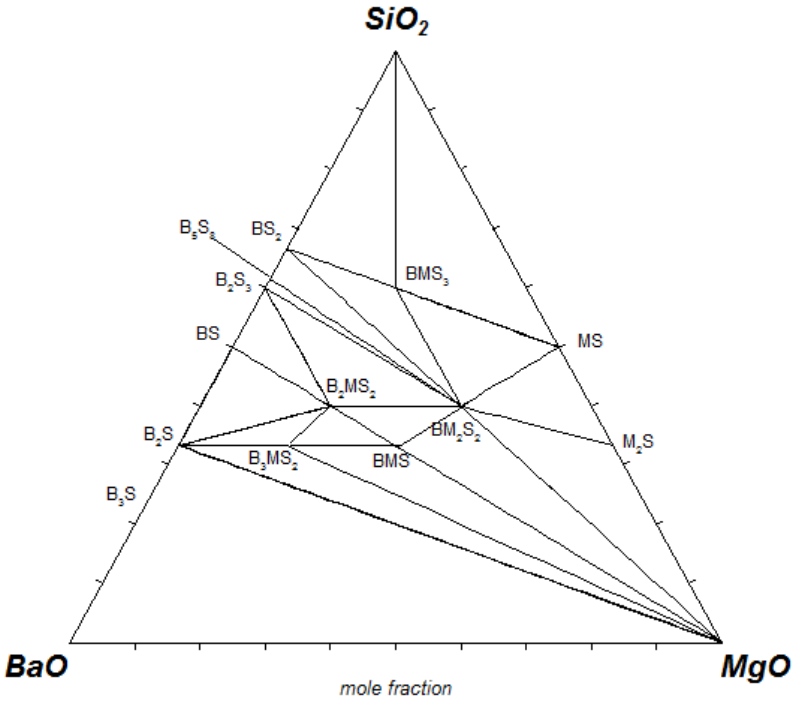

Fig. 3.7.2 Optimized sub-solidus phase equilibria at 950 °C.

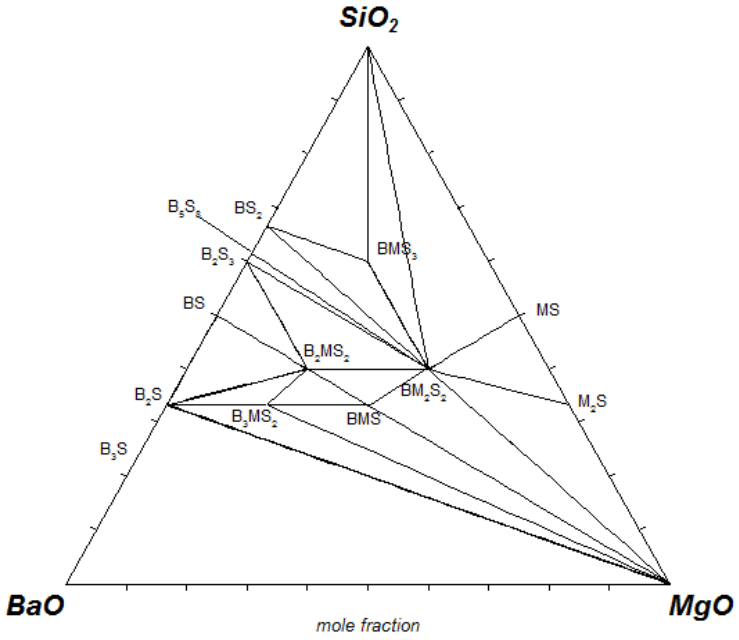

Fig. 3.7.3 Optimized sub-solidus phase equilibria in the temperature range 1000-1200 °C.

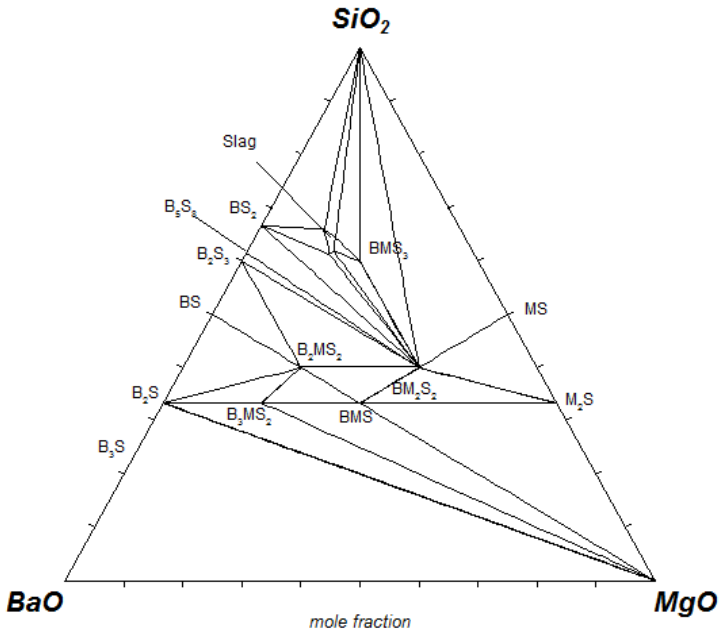

Fig. 3.7.4 Optimized sub-solidus phase equilibria at 1250 °C.

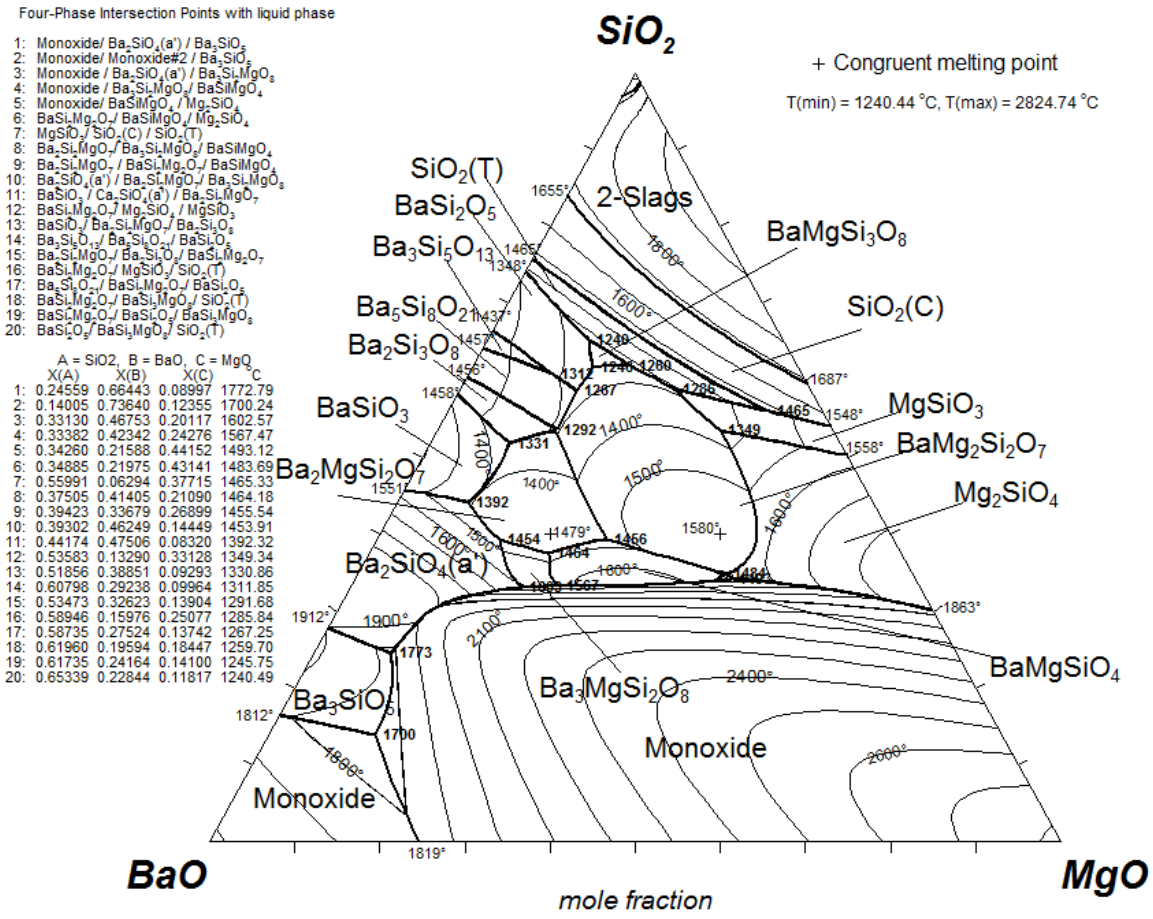

Fig. 3.7.5 Present calculated liquidus (polythermal) projection for the BaO-MgO-SiO_2 system (isotherms were drawn at the interval of 100 °C).

3.8 The BaO-SrO-MgO-SiO_2 system

Barry (1968) reported complete solubility between the isomorphous B_3MS_2 and S_3MS_2 phases (merwinite structure). No phase diagram data on this section could be found in the literature. In the present calculations, an ideal solution was assumed between these phases as also in the similar C_3MS_2-S_3MS_2 system.

Shimizu, et al. (1995) and Mirbabaeva, Sirazhiddinov, and Grebenshchikov (1974) reported B_2MS_2 and Sr_2MS_2 as isomorphous (akermanite structure). Mirbabaeva, et al. (1974) by quenching and XRD also reported a phase diagram for the B_2MS_2-Sr_2MS_2 section. Their phase diagram data are compared with the present calculations in Fig. 3.8.1. As can be seen, these liquidus data are inconsistent with the calculated melting point of Sr_2MS_2. But, the present calculations agree with the melting data of Sr_2MS_2 by Ghanbari-Ahari and Brett (1988). Hence, the experimental data of Ghanbari-Ahari and Brett (1988) and Mirbabaeva, et al. (1974) are inconsistent and cannot be fitted simultaneously. Mirbabaeva, et al. (1974) by XRD also reported, at 1400°C, about 55 mol% solubility of B_2MS_2 in Sr_2MS_2 and about 10 mol% of Sr_2MS_2 in B_2MS_2. They reported, based on the liquidus data only, the presence of a compound $Ba_{1.6}Sr_{0.4}MgSi_2O_7$ on this section. No other reference in the literature stating this compound could be found. In the present calculations, this compound was neglected. More experimental work is required to prove its presence. In the present work, complete solubility between the B_2MS_2 and Sr_2MS_2 was tentatively calculated. The interaction parameter used in the similar C_2MS_2-$SrMS_2$ system was also used. However, more experimental work is required to correctly establish the phase diagram for this section.

Table 3.8.1 Optimized parameters, in joules, in the BaO-SrO-MgO-SiO_2 system.

Merwinite $(Ba,Sr)_3MgSi_2O_8$ $q^{11} = 0$
Akermanite $(Ca,Sr)_2MgSi_2O_7$ $q^{21} = 5021$

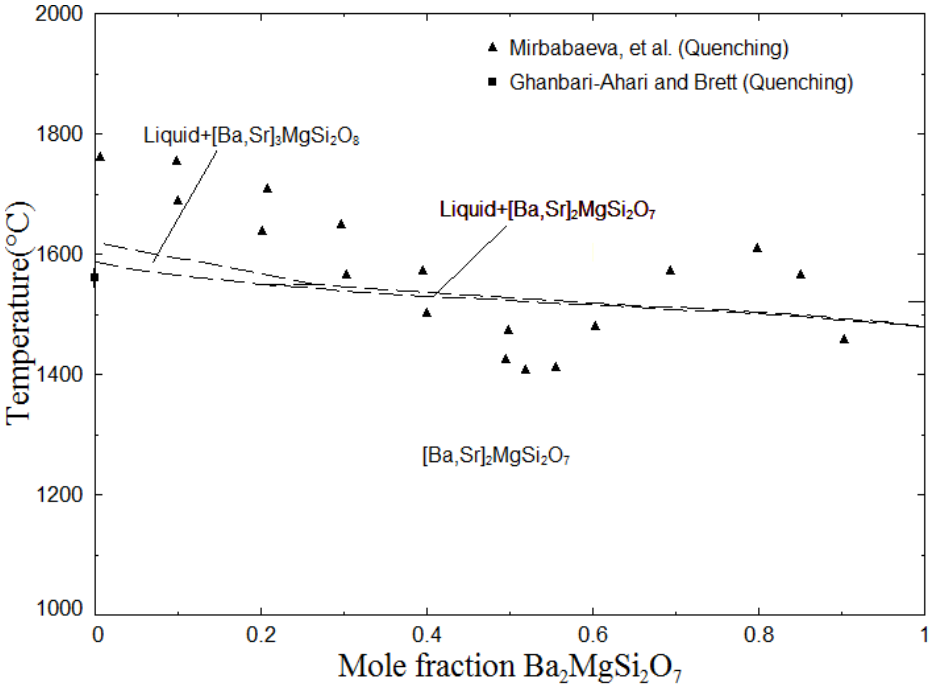

Fig. 3.8.1 Optimized phase diagram of the $Sr_2MgSi_2O_7$-$Ba_2MgSi_2O_7$ system.

3.9 The BaO-CaO-MgO-SiO_2 system

Klasens, et al. (1957) and Barry (1968) by XRD reported B_3MS_2 to be isostructural with C_3MS_2 (merwinite, space group $P2_1/a$). Yonesaki, Takei, Kumada, and Kinomura (2009) by XRD reported that B_3MS_2 has $K_3NaS_2O_8$-type trigonal structure (with space group $P\bar{3}m1$). Park, Hong, and Keszler (2009) by combined X-ray and neutron diffractometry reported that the B_3MS_2 crystal structure is closely related to merwinite, but that it crystallizes in a trigonal structure (with spacegroup $P\bar{3}$). In the present calculations, B_3MS_2 was considered isostructural with C_3MS_2 because, as reported earlier, complete solubility was calculated in the Sr_3MS_2-B_3MS_2 and the C_3MS_2-Sr_3MS_2 systems. Barry (1968), at 1200°C, reported mutual solubility in the system C_3MS_2-B_3MS_2 and the presence of a compound $BaCa_2MgSi_2O_8$ (BC_2MS_2) and its stability region on this join. These data are well reproduced in Fig. 3.9.1. Nadachowski and Grylicki (1959) from

quenching and metallographic techniques, while studying the B_2S-M_2S-C_2S system, also reported the compound BC_2MS_2. In the literature this compound has been widely studied for its luminescence properties. Yonesaki, et al. (2009) by XRD reported the $K_3NaS_2O_8$-type structure (with space group $P\bar{3}m1$) for this phase. Park, et al. (2009) by neutron diffractometry reported a trigonal structure (with space group $P\bar{3}$). Park, et al. (2009) also reported three distinct cation sublattices, one each for Ba, Ca and Mg ions. Experimental data on cation distribution on different sublattices could not be found in the literature. As the data of Barry at 1200 °C show that non-stoichiometry of this phase exists on both the sides of the BC_2MS_2 composition, the phase was modeled as $[Ba,Ca][Ca,Ba]_2MgSi_2O_8$ using the compound energy formalism. The optimized parameters for this phase are presented in Table 3.9.1. No experimental data on the solubility of similar ions like Sr or Mg in this phase could be found in the literature. However, such solubilities cannot be completely ruled out, but in the absence of any experimental data they were neglected.

Nadachowski and Grylicki (1959) by quenching techniques reported an isothermal section at 1350 °C for the B_2S-M_2S-C_2S system as shown in Fig. 3.9.2. The present calculated isothermal section is shown in Fig. 3.9.3. Nadachowski and Grylicki (1959) reported different phase equilibria on the C_2S-M_2S join than those calculated in Fig. 3.9.3 (optimized in our previous study based on numerous later studies). They also did not find the presence of the merwinite phase (B_3MS_2) in their studies. As reported in the ternary BaO-MgO-SiO_2 system the presence of BM_3S_2 was neglected in our calculations. Nadachowski and Grylicki (1959) did not report any appreciable solubility of Mg in the T phase. Hence, solubility of Mg in this phase was ignored.

The solubility of Sr in this phase cannot be completely ruled out. However, in the absence of any experimental evidence, this solubility was also ignored.

Shimizu, et al. (1995) and Mirbabaeva, et al. (1974) reported B_2MS_2 as isostructural with C_2MS_2 phase (akermanite structure). In the literature no data on the mutual solubility between these phases could be found. In the present calculations, an interaction parameter, identical to the one used for the C_3MS_2-Sr_3MS_2 and Sr_3MS_2-B_3MS_2, was used. However, the Ba-Ca interactions in the B_2MS_2 -C_2MS_2 solid solution are supposed to be more positive in value (because of larger size difference between the Ba and Ca atoms) than the interaction between cations in the C_3MS_2-Sr_3MS_2 and Sr_3MS_2-B_3MS_2 systems. But, in the absence of any experimental data to evaluate the Ba-Ca interaction parameter, it was assumed to be the same as for the cations in the C_3MS_2-Sr_3MS_2 and Sr_3MS_2-B_3MS_2 systems.

Table 3.9.1 Optimized thermodynamic parameters, in joules, in the BaO-CaO-MgO-SiO_2 system.

Merwinite $(Ba,Ca)_3MgSi_2O_8$
$q^{11} = 41840$
Akermanite $(Ba,Ca)_2MgSi_2O_7$
$q^{21} = 5021$
$[Ba,Ca][Ca,Ba]_2MgSi_2O_8$ (BC_2MS_2)
$G^0[Ba][Ba]_2MgSi_2O_8 = G^0(Ba_3MgSi_2O_8) + 17154$
$G^0[Ca][Ca]_2MgSi_2O_8 = G^0(Ca_3MgSi_2O_8) + 10878$
$G^0[Ca][Ba]_2MgSi_2O_8 - G^0[Ba][Ca]_2MgSi_2O_8 = 58576$
$G^0[Ba][Ba]_2MgSi_2O_8 + G^0[Ca][Ca]_2MgSi_2O_8 = G^0[Ca][Ba]_2MgSi_2O_8 + G^0[Ba][Ca]_2MgSi_2O_8$

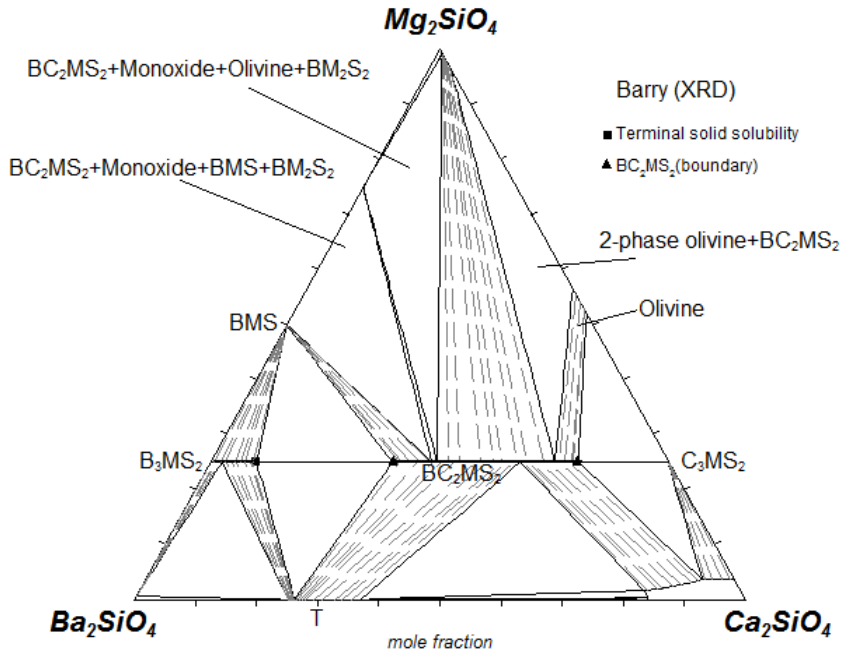

Fig. 3.9.1 Calculated isothermal section at 1200 °C in the BaO-CaO-MgO-SiO_2 system.

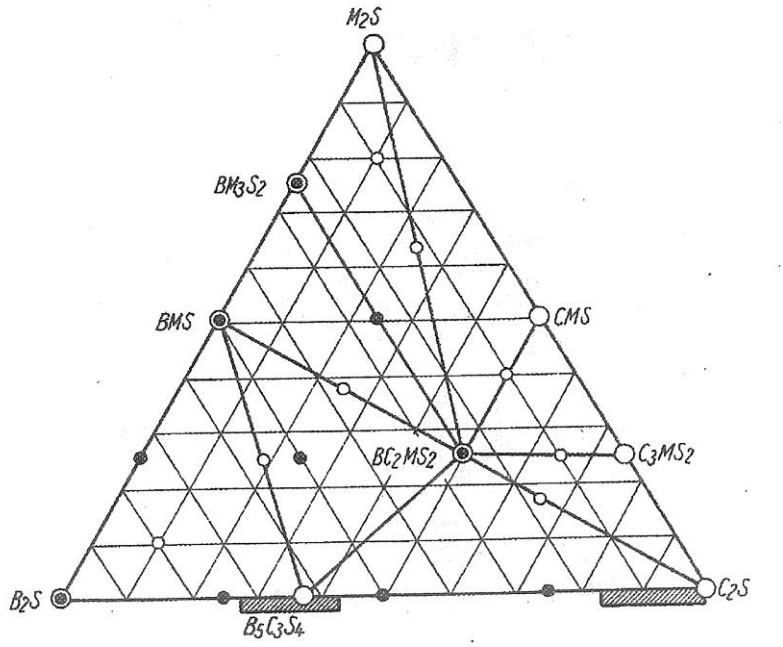

Fig. 3.9.2 Isothermal section at 1350 °C as reported by Nadachowski and Grylicki.

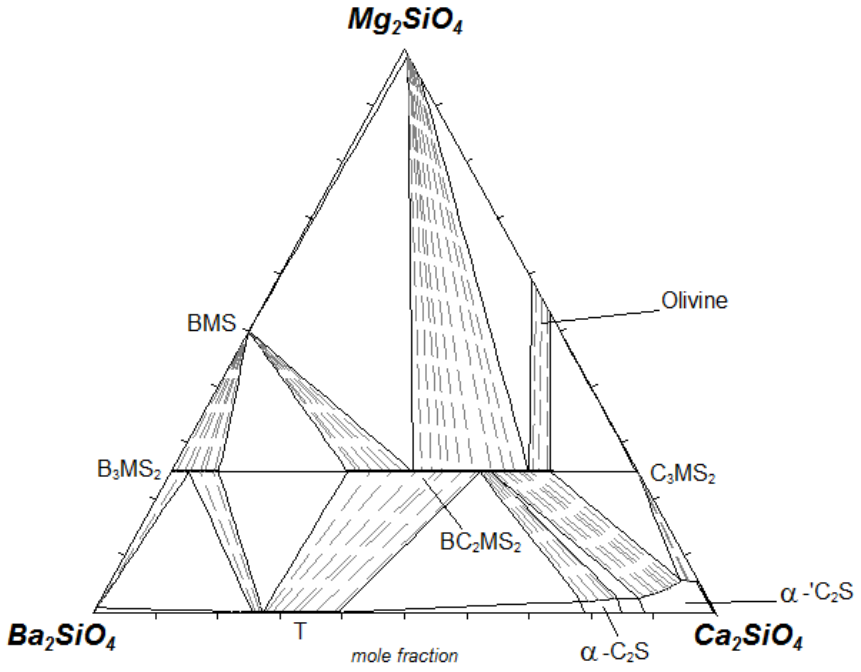

Fig. 3.9.3 Calculated isothermal section at 1350 °C in the BaO-CaO-MgO-SiO_2 system.

3.10 The CaO-SrO-Al_2O_3 system

The Gibbs energy of the liquid phase in the ternary CaO-SrO-Al_2O_3 system was estimated from the corresponding binary systems by treating Al_2O_3 as asymmetric component [Pelton and Chartrand (2001)]. A small liquid interaction parameter presented in Table 3.10.1 was also used. The optimized Gibbs energies of the unstable end-members are presented in Table 3.10.1. The Gibbs energy of the stable end-members can be found from the corresponding binary system.

Massazza and Cannas (1959) by quenching and optical microscopy investigated the ternary system and reported complete solubility at 1400 °C between the $SrO.Al_2O_3$-$CaO.Al_2O_3$ (SA-CA)

phases. However, later findings of Ito, et al. (1977) and of Kuroki, Saito, Matsui, and Morita (2009) by XRD disproved the complete solubility between the SA-CA system. Prodjosantoso and Kennedy (2003) by synchrotron powder diffraction methods reported data similar to Ito, et al. (1977) and Kuroki, et al. (2009). These data are compared with the present calculations in Fig. 3.10.1. The CA phase has a monoclinic crystal structure (space group, P21/n) [Dougill (1957); Fu, Dong, Liu, and Wang (2010)]. The room temperature form of the SA phase is monoclinic (space group, $P2_1$) which transforms at around 650 ºC into $P6_322$ symmetry [Rodehorst, et al. (2003)]. Prodjosantoso and Kennedy (2003) indexed the calcium-rich solid solution in the SA-CA system as P21/n space group and strontium-rich solid solution as $P2_1$ space group. As the two phases are not isostructural, they were modeled differently using single-sublattice substitutional model (i.e. $(Ca,Sr)Al_2O_4$, α in Fig. 3.10.1 and $(Sr,Ca)Al_2O_4$, β in Fig. 3.10.1). The low-temperature SA and the CA phase belong to a different space group; hence they were treated as different phases. An interaction term presented in Table 3.10.1 was used, in the absence of any experimental evidence, to tentatively calculate practically no solubility of Ca in the low-temperature SA phase.

Massazza and Sirchia (1959) by quenching and microscopic observation reported complete solid solubility at about 1500 °C among the phases $3SrO.Al_2O_3$-$3CaO.Al_2O_3$ (S_3A-C_3A). F. P. Glasser (1974) reported that there exist two ordered phases in this section in the ranges 10-60 mol% S_3A and 70-90 mol% S_3A. Later, Prodjosantoso, Kennedy, and Hunter (2000) by synchrotron powder diffraction methods reported complete solubility at 1100 °C among these phases. The S_3A and C_3A phases have cubic crystal structures (space group, Pa3) [Prodjosantoso, et al. (2000);

Mondal and Jeffrey (1975);McMurdie; Chakoumakos, Lager, and Fernandez-Baca (1992)]. In the present work, complete solid solubility between these phases was calculated as shown in Fig. 3.10.2 and this solution was modeled using the single-sublattice substitutional model (i.e. $(Ca,Sr)_3Al_2O_4$), labeled $(S,C)_3A$ in Fig. 3.10.2. Prodjosantoso, et al. (2000) in their experiments prepared the samples through a series of heating in the temperature range 700-1000 °C. They reported that "even prolonged heating contained appreciable amounts of secondary phases and/or unreacted components" (No data on which phases and the amount precipitated were reported). Finally, they annealed the samples at 1100 °C for 72 hours and by XRD found just one phase. According to the present calculations, the $(S,C)_3A$ phase decomposes into the β phase as shown in Fig. 3.10.2 at lower temperatures. In fact, this could be the reason why Prodjosantoso, et al. (2000) obtained intermediate phases in the samples which were annealed at temperatures in the range 700-1000 °C for 24 hours. A small excess interaction term presented in Table 3.10.1 was also used for the $(S,C)_3A$ phase. This term was necessary to make the solid solution stable at 1100 °C. Massazza and Sirchia (1959) reported phase diagram data for the S_3A-C_3A section which are compared with the present calculations in Fig. 3.10.2. In this section, F. P. Glasser (1974) by microscopic observation at 1435 °C between 70 and 95 wt.% S_3A noted signs of incongruent melting. However, the data by Massazza and Sirchia (1959) show a single phase $(S,C)_3A$ solid solution stable at this temperature. The present calculations disagree with the data of Massazza and Sirchia (1959) on the extensive stability of the S_4A phase in this section. The ΔH^0_{298} of the S_4A phase and the stability range for this phase are reproduced quite well in the binary SrO-Al_2O_3 system. Hence, the Gibbs energy of the S_4A phase is fixed and the extensive stability of S_4A phase in this section was not reproduced as reported by Massazza and Sirchia (1959). Probably, more experimental work is required to prove these results.

Massazza and Cannas (1959) by optical microscopy reported complete solubility in the $CaAl_4O_7$-$SrAl_4O_7$ system. There are data [Ponomarev, Kheiker, and Belov (1970), Boyko and Wisnyi (1957)] on the similarity of the structures of these phases. No phase diagram data on this section could be found in the literature. In the present calculations, an ideal solution between these two end-members was assumed.

Massazza and Cannas (1959) by quenching and microscopic observation reported complete solid solubility between the end-members $SrAl_{12}O_{19}$-$CaAl_{12}O_{19}$ (SA_6-CA_6). There are references [K. Kimura, et al. (1990); Kang, et al. (2009); Utsunomiya, et al. (1988)] in the literature proving hexagonal structure with the space group $P6_3/mmc$ for these phases. Kadyrova (1999) also reported complete solubility between these compounds. In the present calculations an ideal solution was assumed between these compounds to calculate the phase diagram shown in Fig. 3.10.3. Kadyrova (1999) using a high-temperature electro vacuum micro-furnace also measured melting temperatures at some compositions (Fig. 3.10.3). His data for the melting of the CA_6 phase are not consistent with the phase diagram for the CaO-Al_2O_3 system from the ftoxide database (L.H.S. of Fig. 3.10.3). Otherwise, these data are consistent with the calculations in Fig. 3.10.3.

Kuroki, et al. (2009) et al. by in-situ observation using CSLM coupled with XRD predicted a part of an isothermal cross section at 1700 ºC as shown in Fig. 3.10.4 (in this figure only the stability region of the liquid, α and β phases were experimentally measured). These results can be

compared with the present calculations in Fig. 3.10.5. Here, the exact reproduction of the three phase region (Liquid + α + β) was found to be very difficult. The extent of solubility at this temperature in the α and β phases is fixed by the phase diagram in Fig. 3.10.1. Moreover, the liquidus boundary is reasonably well reproduced. The present calculated liquidus (polythermal) projection for the CaO-SrO-Al_2O_3 system is presented in Fig. 3.10.6.

Table 3.10.1 Optimized thermodynamic parameters, in Joules, in the SrO-CaO-Al_2O_3 system.

α ([Ca,Sr]Al_2O_4) $G^0(SrAl_2O_4, \alpha) = G^0(SrAl_2O_4, HT) + (15564 - 6.318\ T)$; $q^{11}_{CaSr} = (4184 - 5.021\ T)$
β ([Sr,Ca]Al_2O_4) $G^0(CaAl_2O_4, \beta) = G^0(CaAl_2O_4) + (30125 - 8.368\ T)$; $q^{11}_{CaSr} = (-29288 + 12.594\ T)$
Low-temperature Sr-aluminate solution (LTSrss) $G^0(CaAl_2O_4, LTSrss) = G^0(CaAl_2O_4) + 42000$
$(S,C)_3A$ ($[Ca,Sr]_3Al_2O_6$) $q^{11}_{CaSr} = -6276$
$(S,C)A_2$ ($[Ca,Sr]Al_4O_7$) $q^{11}_{CaSr} = 0$
$(S,C)A_6$ ($[Ca,Sr]Al_{12}O_{19}$) $q^{11}_{CaSr} = 0$
Liquid $\Delta g^{001}_{SrSi(Ca)} = -14644$

** Here $G^0(A, x)$ refers to Gibb energy of A with *x* as reference state.

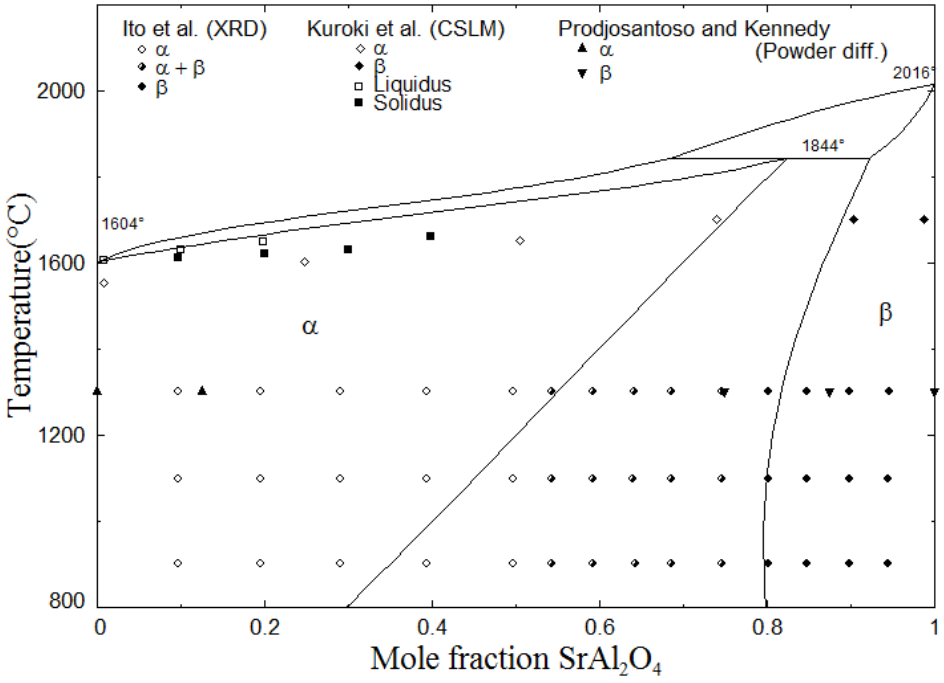

Fig. 3.10.1 Optimized phase diagram of the $CaAl_2O_4$-$SrAl_2O_4$ system.

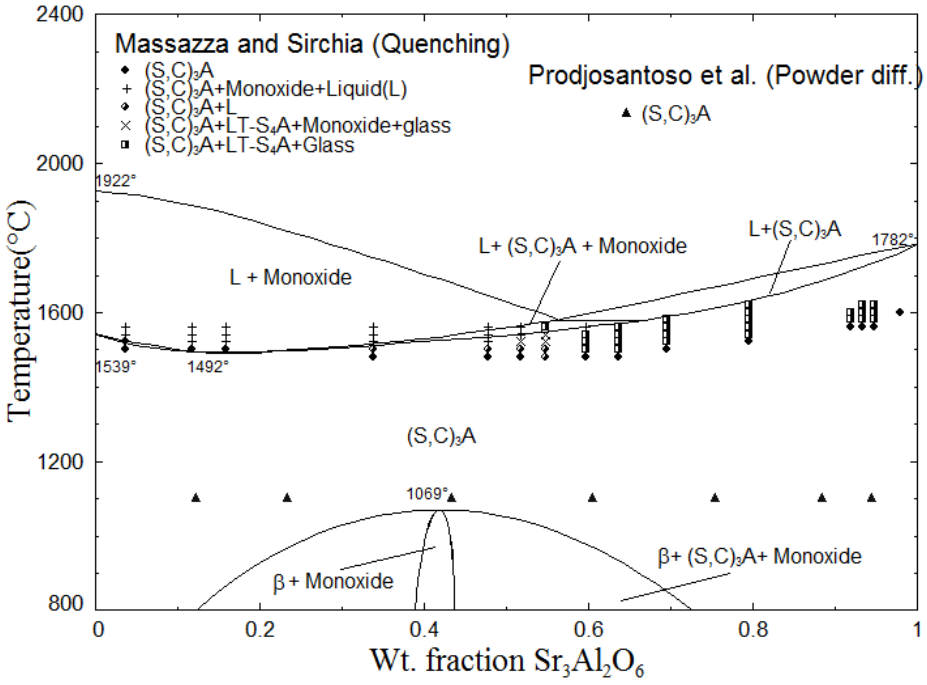

Fig. 3.10.2 Optimized phase diagram of the $Ca_3Al_2O_6$-$Sr_3Al_2O_6$ system.

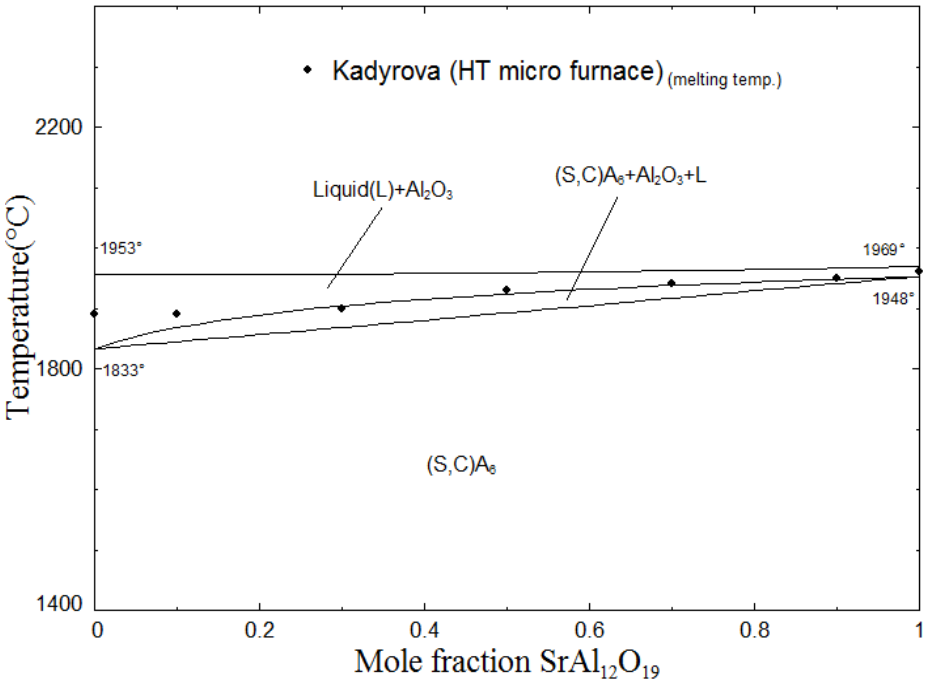

Fig. 3.10.3 Optimized phase diagram of the $CaAl_{12}O_{19}$-$SrAl_{12}O_{19}$ system.

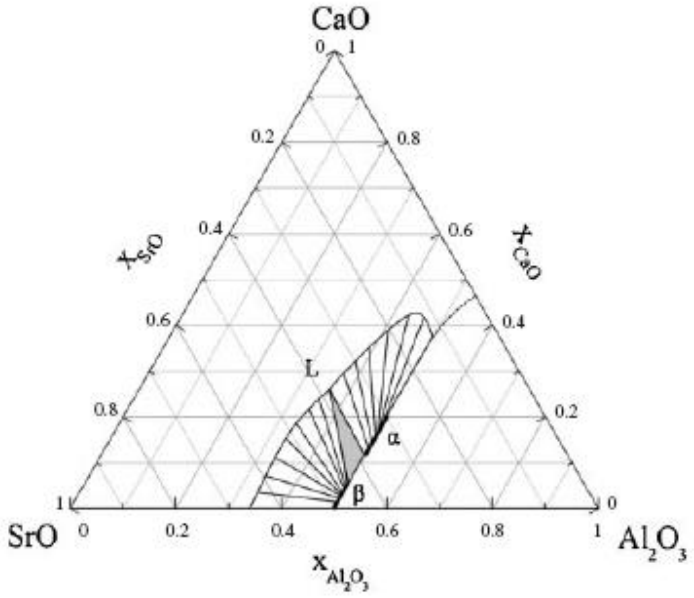

Fig. 3.10.4 The isothermal section at 1700 ºC in the CaO-SrO-Al_2O_3 system as reported by Kuroki et al.

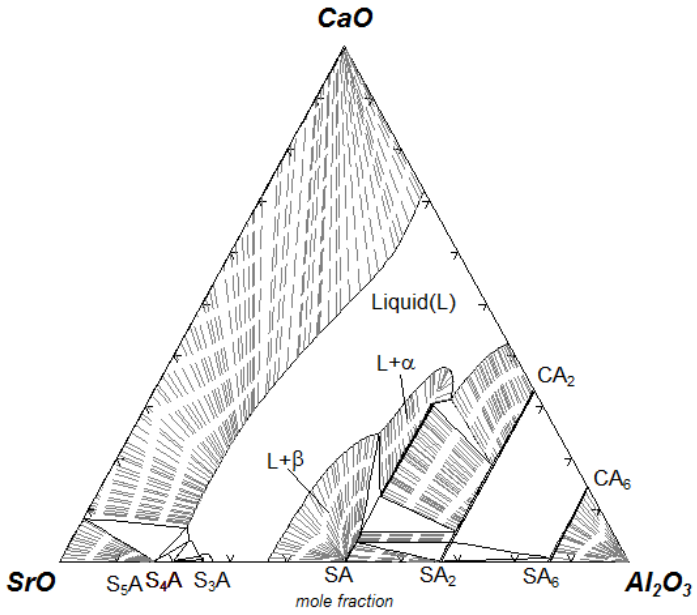

Fig. 3.10.5 Calculated isothermal section of the CaO-SrO-Al_2O_3 system at 1700 ºC.

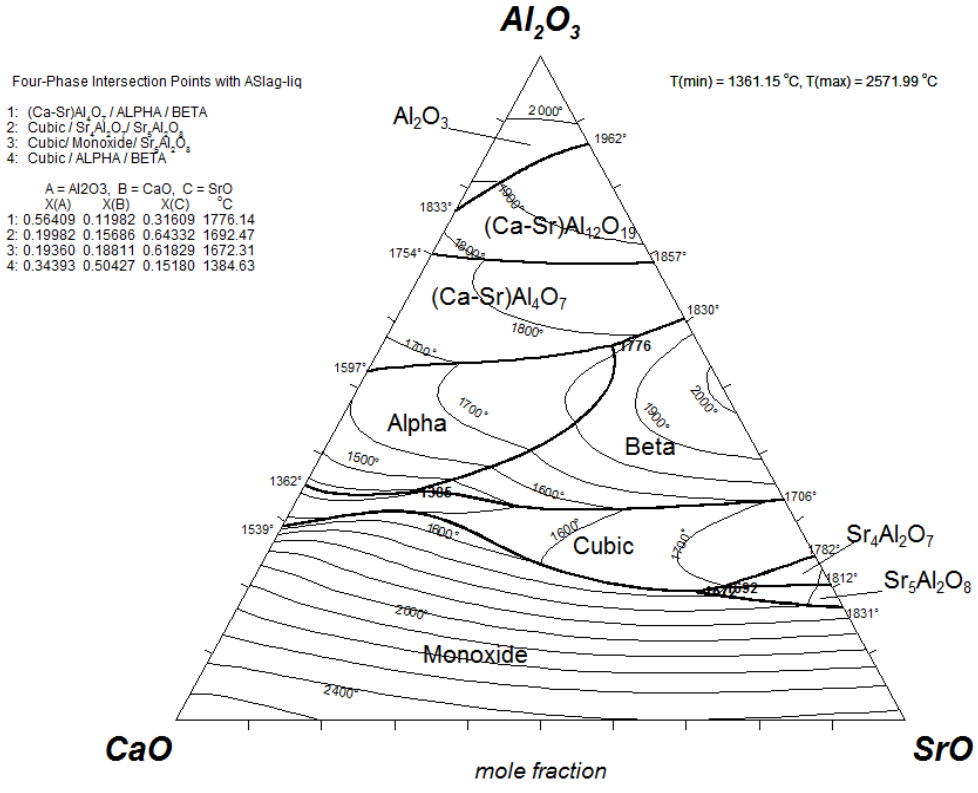

Fig. 3.10.6 Calculated liquidus (polythermal) projection for the CaO-SrO-Al_2O_3 system (isotherms were drawn at the interval of 100 °C).

3.11 The $BaO-CaO-Al_2O_3$ system

The Gibbs energy of the liquid phase in the $BaO-CaO-Al_2O_3$ ternary was calculated from corresponding binary systems by treating Al_2O_3 as asymmetric component [Pelton and Chartrand (2001)]. No ternary interaction parameters were used for the liquid phase. The optimized parameters for the system are presented in Table 3.11.1. For solid solutions, the Gibbs energies of unstable end-members are presented and Gibbs energy of stable end-members can be found in the tables for the corresponding binary systems.

Ito, Banno, Suzuki, and Inagaki (1979) determined the solid solubility in the $BaAl_2O_4$ (BA)-$CaAl_2O_4$(CA) system by lattice parameter measurements (XRD). These data are compared with the present calculations in Fig. 3.11.1.The room-temperature form of BA has hexagonal structure (space group, $P6_3$) which undergoes transformation at about 327 °C into $P6_322$ symmetry [Rodehorst, et al. (2003)]. The CA phase has monoclinic structure (space group, P21/n) [Dougill (1957); Fu, et al. (2010)]. As the two phases have different structures, they were modeled differently using single-sublattice substitution model (i.e. $(Ca,Ba)Al_2O_4$, α in Fig. 3.11.1 and $(Ba,Ca)Al_2O_4$, β in Fig. 3.11.1. The low-temperature BA and the CA phase belong to different space group; hence they were treated as different phases. An interaction term presented in Table 3.11.1 was used, in the absence of any experimental evidence, to tentatively calculate practically no solubility of Ca in the low-temperature BA phase.

Brisi and Montorsi (1962) by XRD reported an isothermal section (Fig. 3.11.2) for the $BaO-CaO-Al_2O_3$ system at 1250 ºC. The present calculated isothermal section at 1250 ºC is shown in Fig.

3.11.3. Appendino (1972b) by equilibration and quenching techniques reported 10% Ca solubility in the $Ba_4Al_2O_7$ (B_4A) phase and 2.5% Ca solubility in the $Ba_8Al_2O_{11}$ (B_8A) phase at 1250 °C. Appendino (1972b) by XRD reported the presence of a ternary compound $Ba_3CaAl_2O_7$ (B_3CA), denoted by T2 in Fig. 3.11.3, and suggested its composition varies in the range 2-3% CaO. In Fig. 3.11.2, Brisi and Montorsi (1962) reported solubility of Ca in B_3A but not of Ba in C_3A. There are different data on the crystal structure of B_3A. Antipov, Lykova, Paromova, Rozanova, and Kovba (1987) reported a cubic structure with space group Pa3. Walz, Heinau, Nick, and Curda (1994) reported an orthorhombic structure, whereas Lazic, Kahlenberg, Kaindl, and Kremenovic (2009) reported cubic structure with space group $P2_13$. As reported earlier, C_3A and S_3A have the same cubic structure with space group Pa3 and form a continuous solid solution. Appendino (1972a) by quenching and XRD reported complete solubility of S_3A and B_3A, which implies that the two are of the same structure. Therefore, in the present work the B_3A phase was considered isostructural with S_3A and C_3A, as also reported by Antipov, et al. (1987). In Fig. 3.11.3, the solid solution between B_3A and C_3A was modeled using the single sublattice substitution model. A negative interaction parameter presented in Table 3.11.1 was used for the $(B,C)_3A$ phase to reproduce the data reported by Brisi and Montorsi (1962).

Massazza (1963) by optical microscopy reported an isothermal section at 1400 ºC (Fig. 3.11.4). The present calculated isothermal section at 1400 ºC is shown in Fig. 3.11.5. The phase equilibria reported by Massazza (1963) were qualitatively the same as reported by Brisi and Montorsi (1962), except that Massazza (1963) reported a range of homogeneity (4-5% CaO) for the ternary compound $Ca_2BaAl_8O_{15}$ (C_2BA_4), denoted by T1 in Fig. 3.11.3. Brisi and Montorsi (1962)

reported this compound as stoichiometric. In the present work, both the ternary phases, C_2BA_4 (T1) and B_3CA (T2), were modeled as stoichiometric phases. The optimized parameters for these phases are presented in Table 3.11.1. The calculated melting temperatures of these compounds are also quite reasonable.

The present calculations at 1400 ºC disagree with Massazza (1963) on account of the appearance of the liquid phase adjacent to the CaO-Al_2O_3 boundary. It was calculated that this liquid phase would not appear had the phase $Ca_{12}Al_{14}O_{33}$, whose stability in the binary CaO-Al_2O_3 is debatable, been included. However, as reported by Eriksson and Pelton (1993) and more recently by Duran et al. (2008), the $Ca_{12}Al_{14}O_{33}$ phase is stable only in humid air. Massazza's work was possibly contaminated by humidity. In the present work, the data for the CaO-Al_2O_3 system are taken from Eriksson and Pelton (1993) which does not contain the $Ca_{12}Al_{14}O_{33}$ phase; hence this phase was also not considered in the ternary calculations.

It can be seen that Brisi and Montorsi (1962) reported no solubility, and Massazza (1963) reported very little, among the $BaAl_{12}O_{19}$ (BA_6)-$CaAl_{12}O_{19}$ (CA_6) phases. However, Kadyrova and Daminova (1997) reported complete solubility among these phases. The CA_6 and BA_6 phases are reported [Kang, et al. (2009);Utsunomiya, et al. (1988); Delacarte, Kahn-Harari, and Thery (1993)] to have hexagonal structure with the space group $P6_3/mmc$. In the present calculations, an ideal solution was assumed (labelled [B,C]A_6) in Fig. 3.11.6) between the phases CA_6 and BA_6 which have the same structure and space group. Kadyrova and Daminova (1997) also measured the melting and liquidus temperatures on the BA_6-CA_6 join. However, the

topology of the phase diagram reported by them is dubious because their data show congruent melting behavior at the BA_6 composition whereas it is most likely peritectic (see Fig. 2.7.1) Their data on the BA_6-CA_6 section are compared with the present calculated phase diagram in Fig. 3.11.6. As is evident, little weight was given to the solidus and liquidus data points. The present calculated liquidus (polythermal) projection for the the BaO-CaO-Al_2O_3 system is presented in Fig. 3.11.7.

Table 3.11.1 Optimized thermodynamic parameters, in Joules, in the BaO-CaO-Al_2O_3 system.*

$Ca_2BaAl_8O_{15}$ (T1)			
$\Delta H^0_{298} = -8680482$	$S^0_{298} = 438.646$ J/mol/K $\Delta S^0_{298}{}^{(a)} = 0$ $\Delta S^0_{298}{}^{(b)} = 87.797$	$C_p = C_p(BA\ (HT)) + C_p(CA)$ $C_p(CA_2)$ J/mol/K	$T_m{}^{(c)} = 1695$ ºC
$Ba_3CaAl_2O_7$ (T2)			
$\Delta H^0_{298} = -4110102$	$S^0_{298} = 343.750$ J/mol/K $\Delta S^0_{298}{}^{(a)} = 0$ $\Delta S^0_{298}{}^{(b)} = 38.973$	$C_p = C_p(B_3A) + C_p(CaO)$ J/mol/K	$T_m{}^{(c)} = 1585$ ºC
β ($[Ba,Ca]Al_2O_4$)			
$G^0(CaAl_2O_4, \beta) = G^0(CaAl_2O_4) + (30125 - 8.368\ T)$ J; $q^{11}_{BaCa} = (50208 - 25.104\ T)$ J			
α ($[Ca,Ba]Al_2O_4$)			
$G^0(BaAl_2O_4, \alpha) = G^0(BaAl_2O_4) + 4184$ J			
Low-temperature Ba-aluminate solution (LTBass)			
$G^0(CaAl_2O_4, LTBass) = G^0(CaAl_2O_4) + 42000$			
$(B,C)_3A$ ($[Ba,Ca]_3Al_2O_6$)			
$q^{21}_{BaCa} = -33472$ J			
B_4Ass ($[Ba,Ca]_4Al_2O_7$)			
$G^0(Ca_4Al_2O_7, B_4Ass) = G^0(Ca_3Al_2O_6) + G^0(CaO) + 83680$ J; $q^{11}_{BaCa} = -41840$ J			
B_8Ass ($[Ba,Ca]_8Al_2O_7$)			
$G^0(Ca_8Al_2O_{11}, B_8Ass) = G^0(Ca_3Al_2O_6) + 5\ G^0(CaO) + 146440$ J			
$[B,C]A_6ss$ ($[Ba,Ca]Al_{12}O_{19}$)			
$q_{BaCa} = 0$			

* Here $G^0(A,x)$ refers to Gibb energy of A with x as reference state.

(a) compounds used to calculate heat capacity as reference

(b) oxides (stable at room-temperature) as reference

(c) incongruent melting temperature

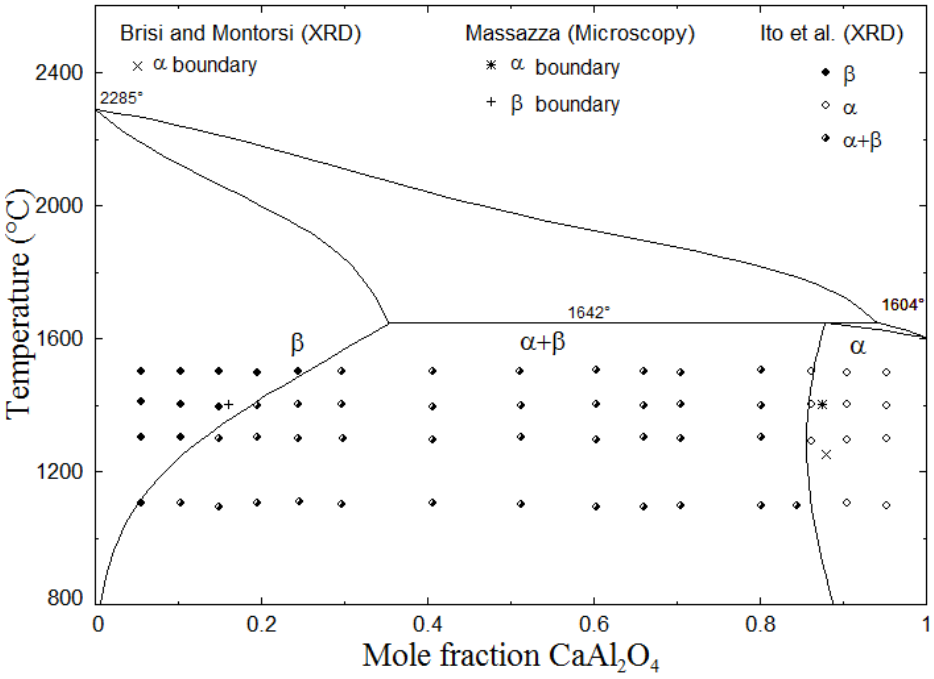

Fig. 3.11.1 Optimized phase diagram of the $BaAl_2O_4$-$CaAl_2O_4$ system.

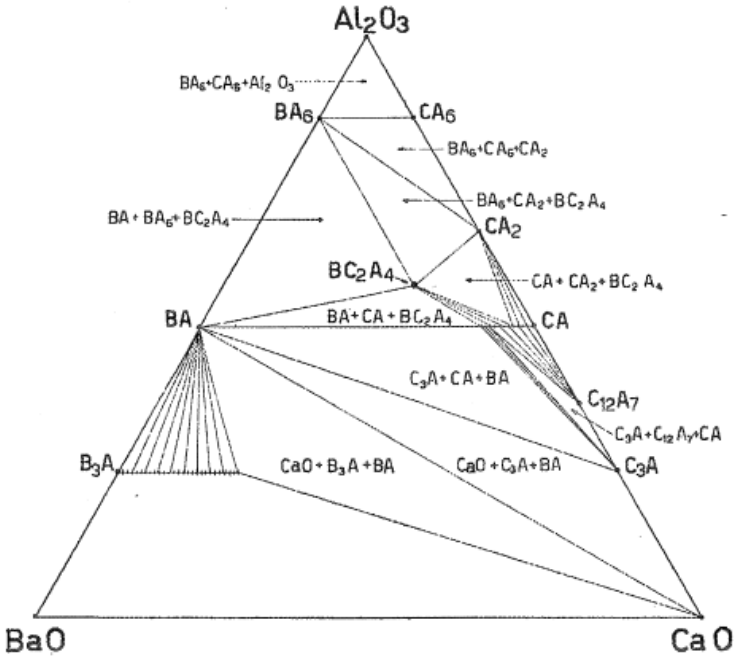

Fig. 3.11.2 Isothermal section at 1250 ºC as reported by Brisi and Montorsi.

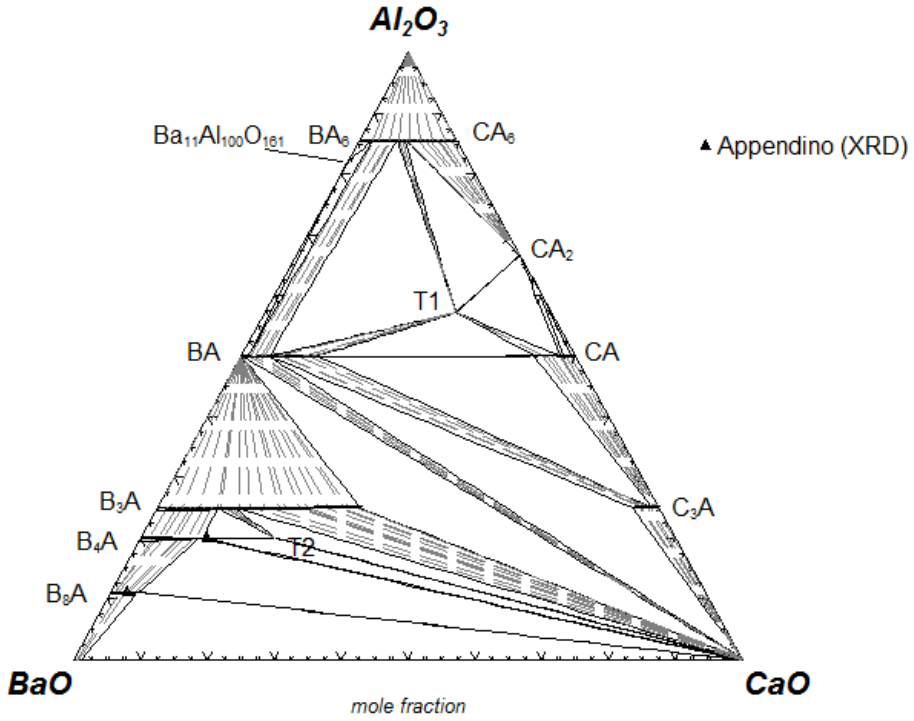

Fig. 3.11.3 Optimized isothermal section at 1250 ºC in the BaO-CaO-Al_2O_3 system.

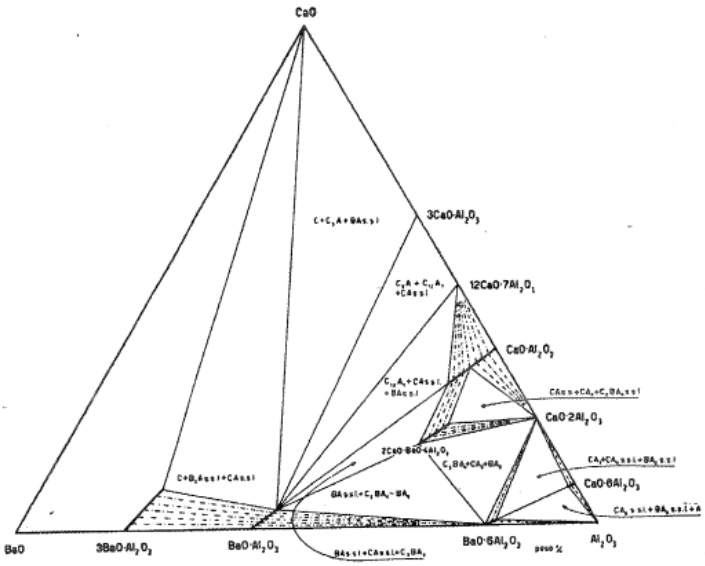

Fig. 3.11.4. Isothermal section at 1400 ºC as reported by Massazza.

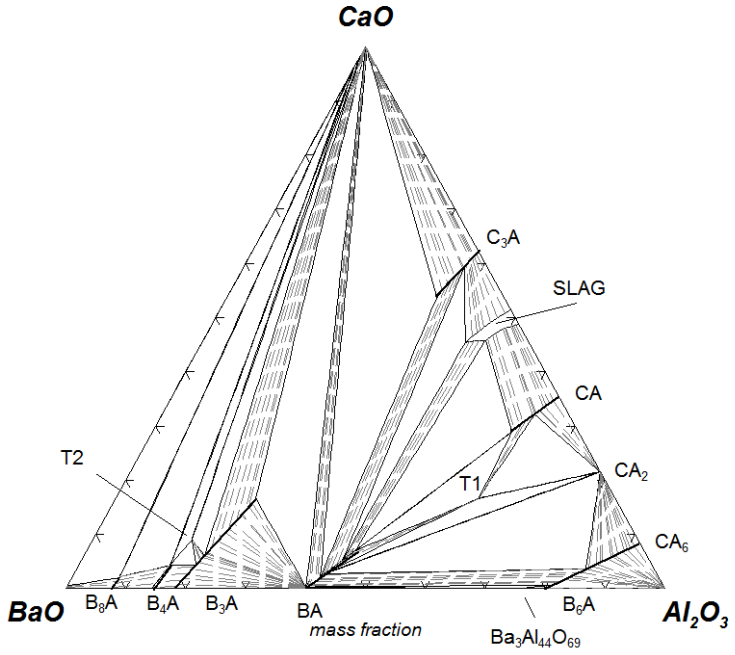

Fig. 3.11.5 Optimized isothermal section at 1400 ºC in the BaO-CaO-Al_2O_3 system.

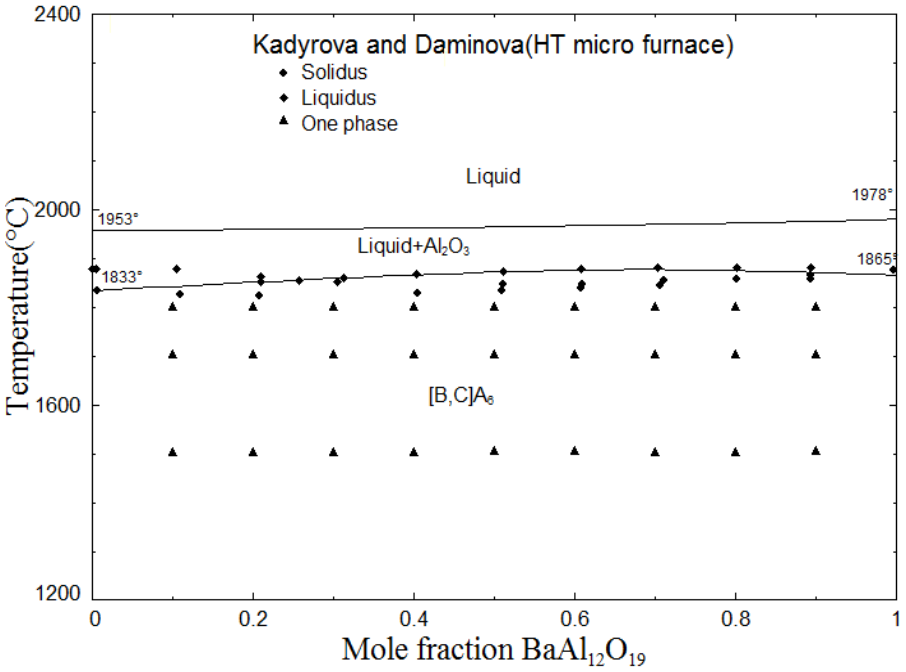

Fig. 3.11.6 Optimized phase diagram of the section $CaA_{12}O_{19}$-$BaAl_{12}O_{19}$.

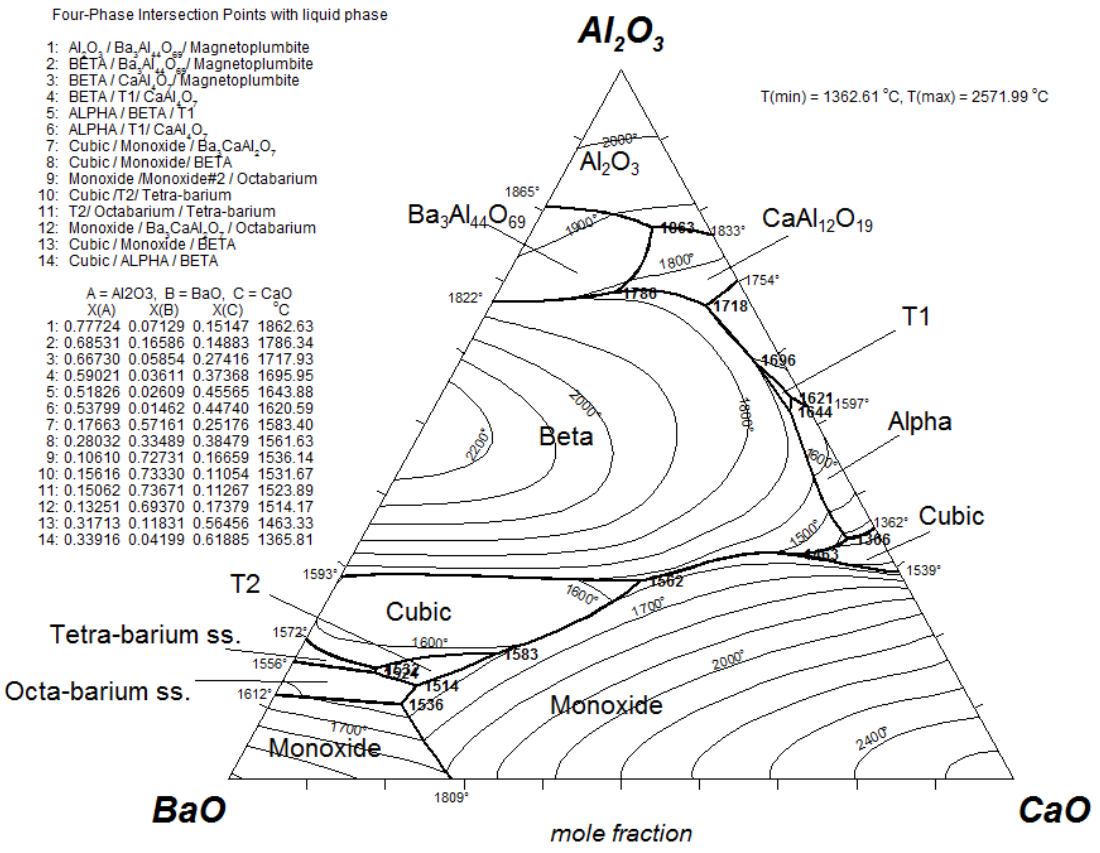

Fig. 3.11.7 Present calculated liquidus (polythermal) projection for the BaO-CaO-Al_2O_3 system (isotherms were drawn at the interval of 100 °C).

3.12 The SrO-BaO-Al_2O_3 system

The Gibbs energy of the liquid phase in the SrO-BaO-Al_2O_3 ternary was calculated from the corresponding binary systems by treating Al_2O_3 as asymmetric component [Pelton and Chartrand (2001)]. No ternary interaction parameters were used for the liquid phase. The optimized parameters for the system are presented in Table. 3.12.1. For solid solutions, the Gibbs energies of unstable end-members are presented and Gibbs energies of stable end-members can be found in the sections on the corresponding binary systems.

Ito, et al. (1979) by XRD reported complete solubility among the high temperature polymorphs in the $BaAl_2O_4$-$SrAl_2O_4$ (BA-SA) section. These high-temperature polymorphs are isostructural and have $P6_322$ symmetry [Rodehorst, et al. (2003)]. Rodehorst, et al. (2003) studied the solubilities in this section by infrared powder absorption spectroscopy and presented a schematic phase diagram depicting the first- and second-order transitions as shown in Fig. 3.12.1. They also reported complete solubility in the BA-SA section at higher temperatures. In the present calculations as well, an ideal solution was calculated among these high-temperature polymorphs as shown in Fig. 3.12.2 (which shows first order transitions only). This solution (β in Fig. 3.12.2) was modeled using a single-sublattice simple substitutional model (i.e., $[Ba,Sr]Al_2O_4$). Henderson and Taylor (1982) by thermal analysis measured the solubility in the low-temperature isomorph of the $SrAl_2O_4$ phase which is monoclinic in structure with space group $P2_1$ [Rodehorst, et al. (2003)]. No data in the literature could be found for the solubility of Sr in low-temperature BA, which has a hexagonal structure with space group $P6_3$ [Rodehorst, et al. (2003)]. In the present calculations, Sr solubility in the low-temperature BA phase was tentatively calculated based on the schematic diagram of Rodehorst, et al. (2003). The low temperature (LT) solid solutions in Fig. 3.12.2 were also modeled using a single-sublattice simple substitutional model (i.e., $[Ba,Sr]Al_2O_4$ and $[Sr,Ba]Al_2O_4$].

Appendino (1972a) by quenching and XRD studies established an isothermal section at 1400 °C in the SrO-BaO-Al_2O_3 system as shown in Fig. 3.12.3. This figure can be compared with the present calculated isothermal section at 1400 °C in Fig. 3.12.4. As reported earlier, B_3A and S_3A phases have a cubic structure with space group Pa3. In the present calculations, complete

solubility was calculated among these phases as reported by Appendino (1972a). The solution was modeled using the single-sublattice substitutional model and an excess interaction parameter, presented in Table 3.12.1, was used to reproduce the data of Appendino (1972a) in Fig. 3.12.3. In the $Ba_3Al_2O_6$-$Sr_3Al_2O_6$ (B_3A-S_3A) section, F. P. Glasser (1974) by quenching, XRD and crystallographic studies reported two ordered phases at 1370 °C. The first has a homogeneity range between 10 and 20 mol% B_3A, and the second one from 30 to 90% B_3A. F. P. Glasser (1974) also noted signs of incongruent melting between compositions 70 and 95 mol% S_3A at 1435 °C. According to the present calculations no liquid phase appears on this section until about 1600 °C. As reported earlier, his similar data in the in the $Ca_3Al_2O_6$-$Sr_3Al_2O_6$ (C_3A-S_3A) section are not in agreement with the available data. More experimental work is required to corroborate F. P. Glasser (1974)'s observations of incongruent melting at this temperature.

Appendino (1972a), on the $Ba_4Al_2O_7$-$Sr_4Al_2O_7$ (B_4A-S_4A) join, reported a ternary compound $2BaO.2SrO.Al_2O_3$ (B_2S_2A). No thermodynamic data for this phase could be found in the literature. Appendino (1972a), apart from the terminal solid solutions and the ternary compound, reported one more phase (a solid solution as can be seen in Fig. 3.12.3). No X-ray data for this phase were given by Appendino (1972a). No data on the crystal structure of the S_4A phase could be found in the literature. The B_4A phase is orthorhombic in structure with space group Cmca [Kahlenberg (2001)]. In the present calculations, the S_4A was assumed to be isostructural with the B_4A and complete solubility was calculated between these two phases. This solid solution was modeled using the single-sublattice simple substitutional model (i.e., $[Ba,Sr]_4Al_2O_7$). The ternary compound reported by Appendino was neglected. Terminal solid solubility in the

$Ba_8Al_2O_{11}$ phase at 1400 °C as reported by Appendino (1972a) was reproduced in Fig. 3.12.4. The solid solution was modeled using the single-sublattice simple substitutional model (i.e., $[Ba,Sr]_8Al_2O_{11}$]). Teoreanu and Ciocea (1978) by quenching and XRD studied the $BaAl_2O_4$-$SrAl_2O_4$-Al_2O_3 section of the ternary system at 1700 °C and reported the same phase assemblage as reported by Appendino (1972a). Teoreanu and Ciocea (1978), at 1700 °C, and Appendino (1972a), at 1400 °C, did not report SA_2 and S_4A_7 as stable phases. However, as reported in the binary SrO-Al_2O_3 section, these phases are considered stable in the present calculations; hence they appear in Fig. 3.12.4.

Teoreanu and Ciocea (1978) at 1700 °C, and Appendino (1972a) at 1400 °C, reported no solubility in the ($BaAl_{12}O_{19}$-$SrAl_{12}O_{19}$) BA_6-SA_6 section. However, Kadyrova, et al. (1996) reported complete solubility in this section at 1400 and 1500 °C. As reported earlier, the BA_6 and SA_6 phases have the same hexagonal structure and space group, $P6_3/mmc$. In the present calculations, an ideal solution was assumed between BA_6 and SA_6. Kadyrova, et al. (1996) also measured the melting temperature and liquidus temperatures on the BA_6-CA_6 join. However, the topology of the phase diagram reported by them is dubious because their data show congruent melting behavior at the BA_6 composition, whereas it is most likely peritectic (see Fig. 2.7.1). These data on the BA_6-SA_6 section are compared with the present calculations in Fig. 3.12.5. The present calculated liquidus (polythermal) projection for the SrO-BaO-Al_2O_3 system is presented in Fig. 3.12.6.

Table 3.12.1 Optimized thermodynamic parameters, in Joules, in the SrO-BaO-Al_2O_3 system.

β ($[Sr,Ba]Al_2O_4$) $q^{11}_{BaSr} = 0$
Low-temperature Sr-aluminate solution (LTSrss) ($[Sr,Ba]Al_2O_4$) $G^0(BaAl_2O_4, (LTSrss)) = G^0(BaAl_2O_4) + 4184$ $q^{11}_{BaSr} = -2929$
Low-temperature Ba-aluminate solution (LTBass) ($[Ba,Sr]Al_2O_4$) $G^0(SrAl_2O_4, (LTBass) = G^0(SrAl_2O_4) + 20920$
$(B,S)_3A$ ($[Ba,Sr]_3Al_2O_6$) $q^{11}_{BaSr} = 0$
$(B,S)_4A$ ($[Ba,Sr]_4Al_2O_7$ $q^{11}_{BaSr} = 0$
$(B,S)_8A$ ($[Ba,Sr]_8Al_2O_{11}$ G^0 ($Sr_8Al_2O_{11}$, B_8A ss) = 8 $G^0(SrO)$ + $G^0(Al_2O_3)$ + 4184

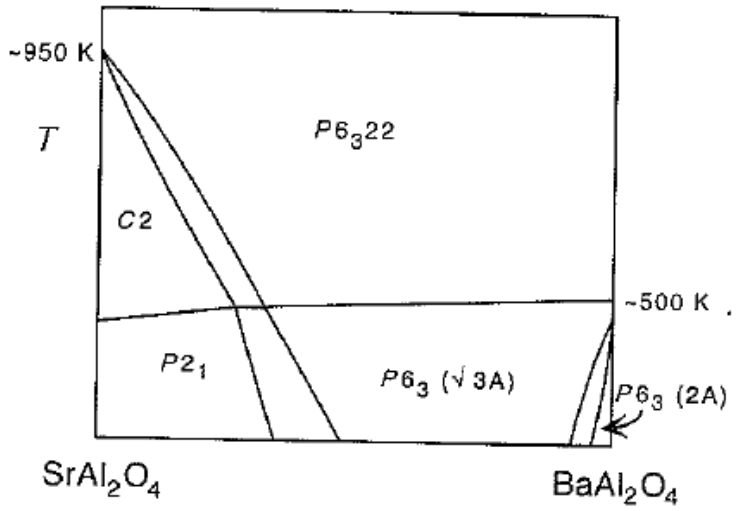

Fig. 3.12.1 A schematic phase diagram for the $SrAl_2O_4$-$BaAl_2O_4$ section as reported by Rodehorst et al. (The transitions from C2 to $P2_1$ and $P6_322$ to $P6_3$ ($\sqrt{3A}$) are of second order character).

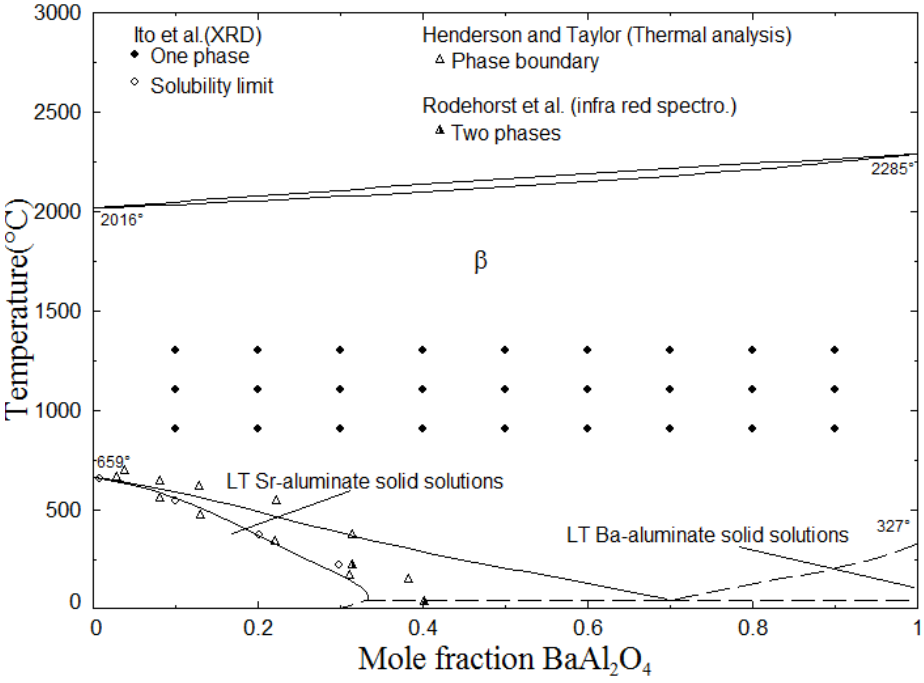

Fig. 3.12.2 Optimized phase diagram of the $SrAl_2O_4$-$BaAl_2O_4$ section.

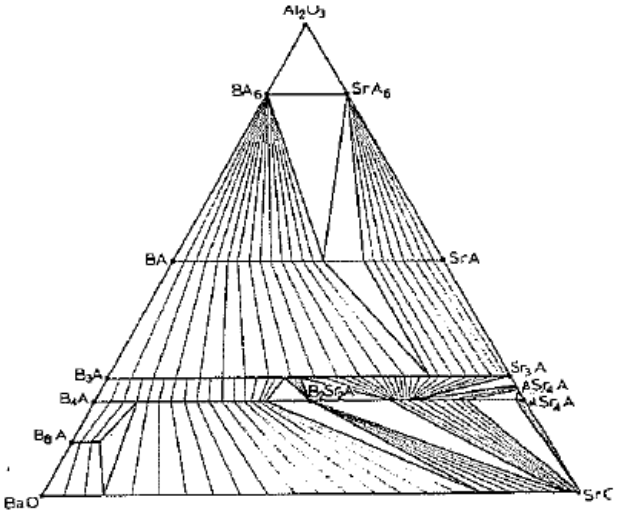

Fig. 3.12.3 Isothermal section of the SrO-BaO-Al_2O_3 system at 1400 °C as reported by Appendino.

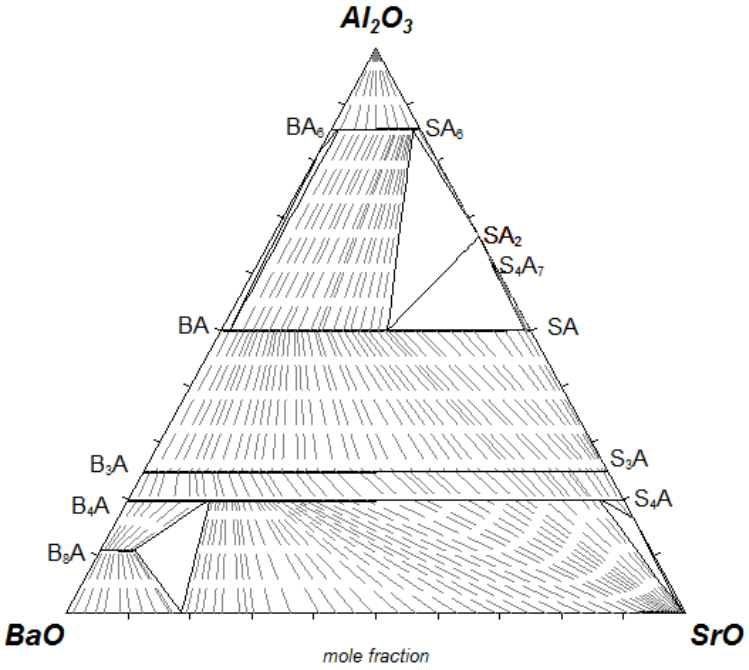

Fig. 3.12.4 Optimized isothermal section of the SrO-BaO-Al_2O_3 system at 1400 °C.

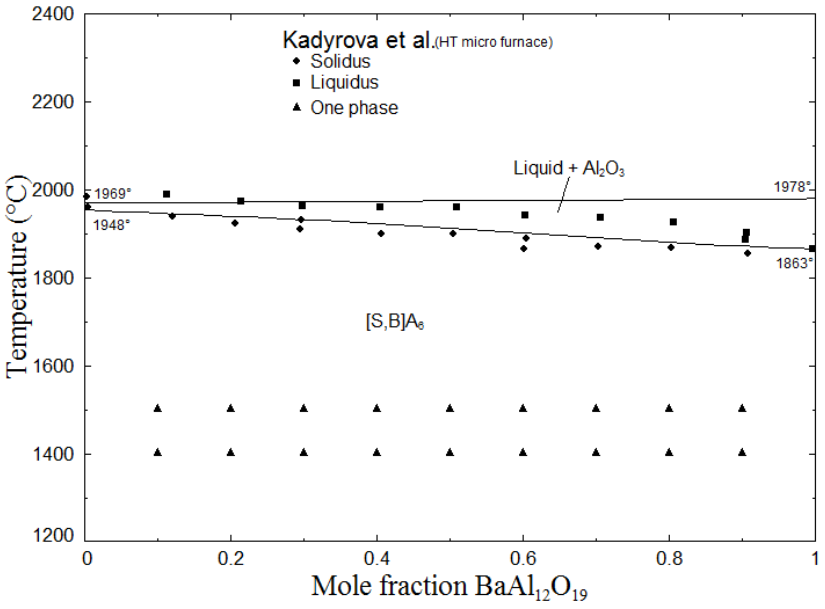

Fig. 3.12.5 Optimized phase diagram of the section $SrAl_{12}O_{19}$- $BaAl_{12}O_{19}$.

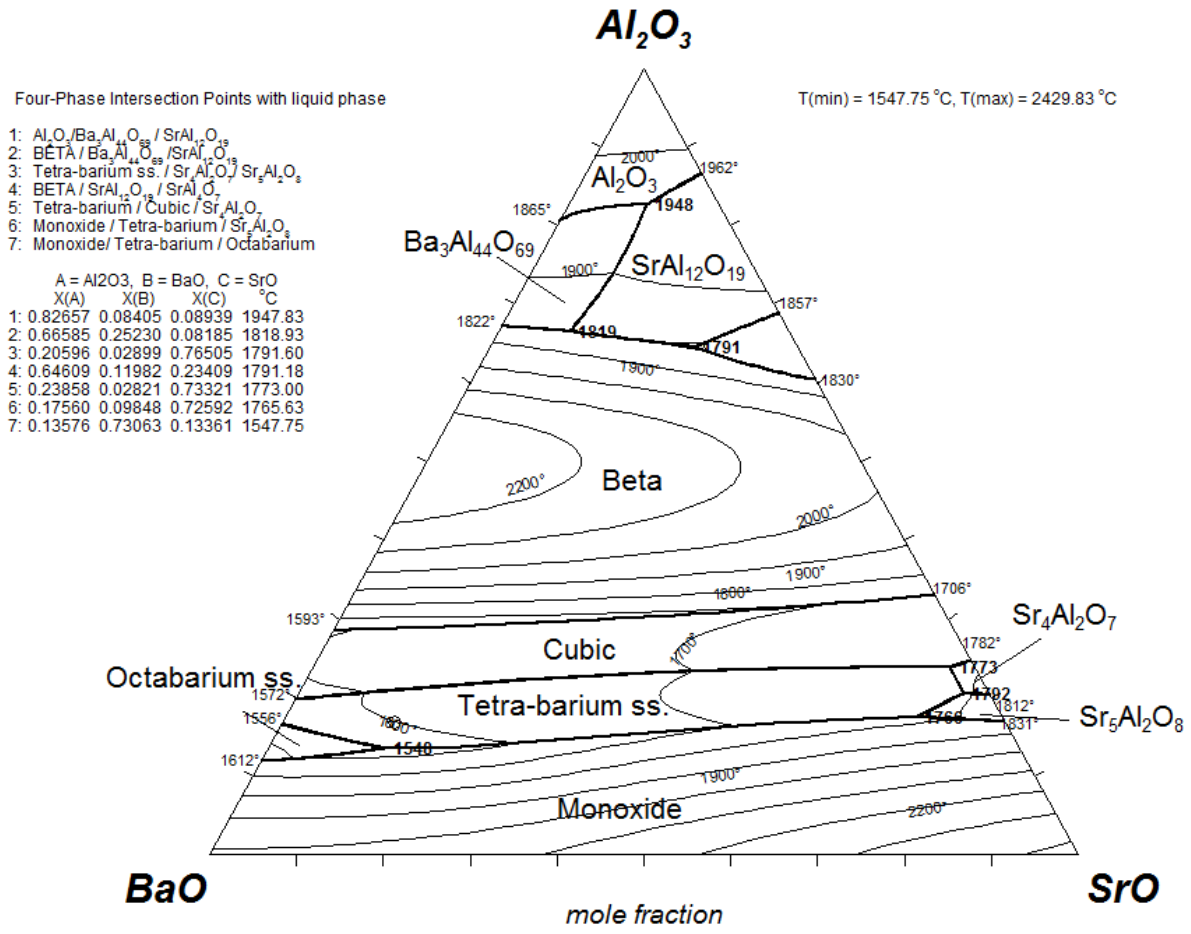

Fig. 3.12.6 Present calculated liquidus (polythermal) projection for the SrO-BaO-Al_2O_3 system (isotherms were drawn at the interval of 100 °C).

3.13 The $CaAl_2O_4$-$SrAl_2O_4$-$BaAl_2O_4$ system

Ito, et al. (1979) by XRD also reported an isothermal section at 1300 °C for the system CA-SA-BA. These data are reasonably well reproduced in Fig. 12.6.

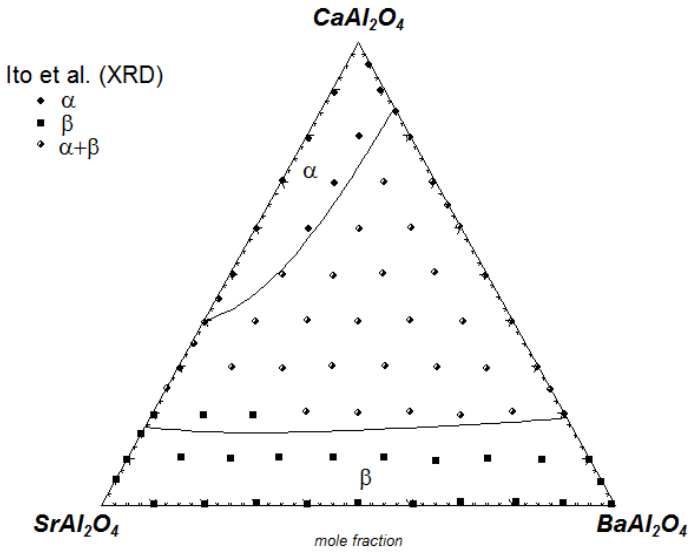

Fig. 3.13.1 Optimized isothermal section at 1300 °C in the $CaAl_2O_4$-$SrAl_2O_4$-$BaAl_2O_4$ system.

3.14 The BaO-MgO-Al_2O_3 system

Gobbels, et al. (1998) by quenching and EPMA determined the phase relationships at 1800 °C in the Al-rich part of the ternary system as shown in Fig. 3.14.1. They reported $BaMgAl_{10}O_{17}$ (BMA_5) as a stable ternary compound and presented references on its similarity of structure (space group, $P6_3/mmc$) with the binary phase close to the BA_6 composition, called Al_2O_3-rich phase in the present work (see BaO-Al_2O_3 section). They also proved experimentally the presence of continuous solid solution (BAM-I_{ss} in Fig. 3.14.1) at 1800 °C among these two phases. As reported earlier, in the present calculations the Al_2O_3-rich phase was taken into account as stoichiometric BA_6 phase. In the present calculations, an ideal single-sublattice substitutional solution was assumed among the BMA_5 and BA_6 phases (the association of BaMg was considered as one particle; replacing Ba in the BA_6 phase). As can be seen in Fig. 3.14.1,

Gobbels, et al. (1998) reported another stable ternary compound as $BaMg_3Al_{14}O_{25}$ (BM_3A_7) with very limited range of solubility (BAM-II_{ss} in Fig. 3.14.1). Nobuo Iyi, Gobbels, and Kimura (1998) reported hexagonal structure (space group, $P\bar{6}m2$) for this compound. In the present calculations, this phase was modeled as stoichiometric. The phase relationships reported by Gobbels, et al. (1998) can be compared with the present calculations in Fig. 3.14.2. Gobbels, et al. (1998) reported incongruent melting behavior for the BAM-II_{ss} phase (they did not report temperature of melting). In the present calculations, the incongruent melting temperature for this phase is 1945 °C. The Gibbs energy of the liquid phase in the ternary BaO-MgO-Al_2O_3 system was estimated from the constituent binary systems by treating Al_2O_3 as asymmetric component [Pelton and Chartrand (2001)]. No ternary parameters were required. The present calculated liquidus (polythermal) projection for the BaO-MgO-Al_2O_3 system is presented in Fig. 3.14.3.

Table 3.14.1 Optimized thermodynamic parameters, in Joules, in the BaO-MgO-Al_2O_3 system.

BMA_5-BA_6 solid solution (BAM-lss)		
g^0 ($BaMgAl_{10}O_{17}$) = g^0 (BA, HT) + g^0 (MA, FACT) + 3 g^0 (Al_2O_3, corr.) – 57218		
$q_{(BMA5\text{-}BA6)}$ = 0		
$BaMg_3Al_{14}O_{25}$ (BM_3A_7)		
ΔH^0_{298} = –14346833 J/Mol	S^0_{298} = 562.329 J/mol/K	ΔS^0_{298} [(a)] = 0
T_m [(b)] = 1945 °C		
C_p = 2 C_p (BA) + 6 C_p(MA, FACT53) + 6 (Al_2O_3, corr.) (298.15 < T < 2000 K)		

[(a)] from the compounds used to calculated the heat capacities
[(b)] incongruent melting temperature

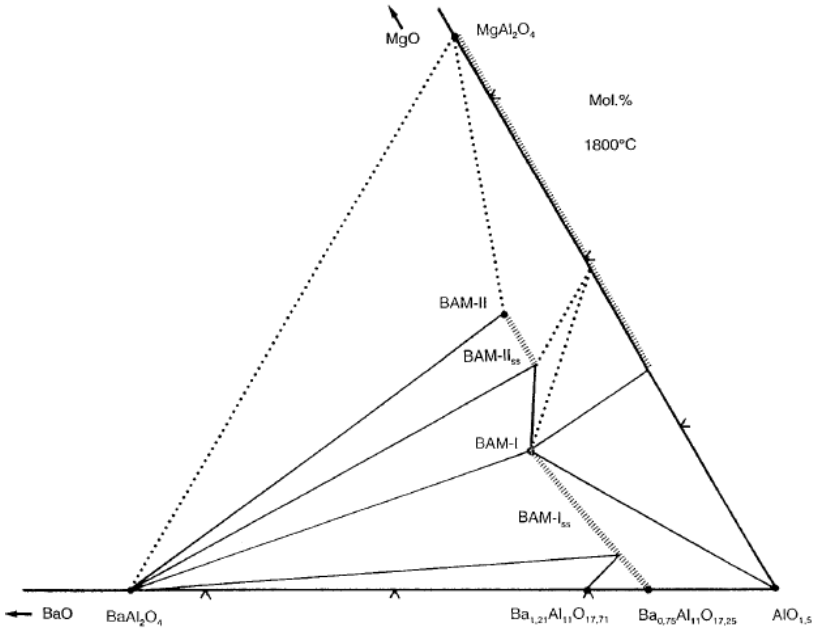

Fig. 3.14.1 Phase equilibria as reported by Gobbels et al.

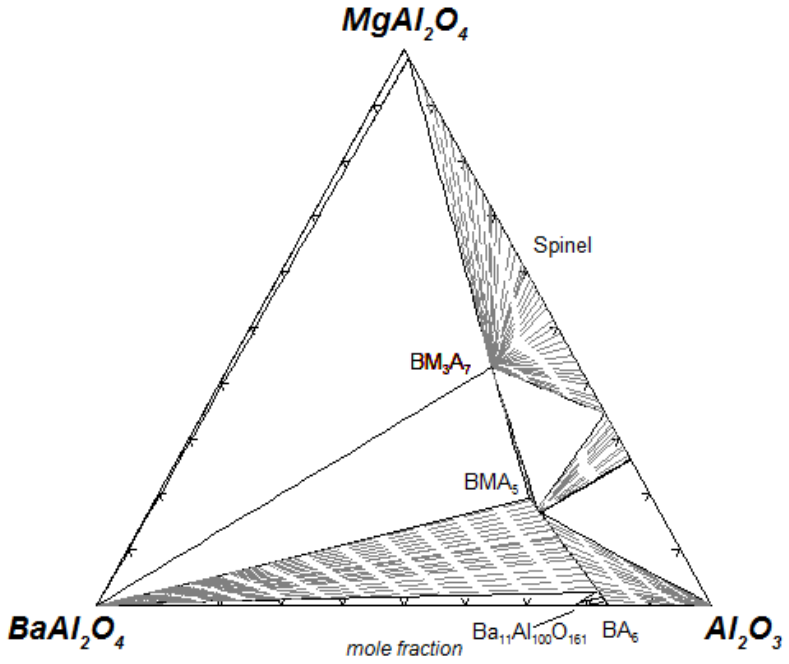

Fig. 3.14.2 A part of the present calculated isothermal section at 1800 °C.

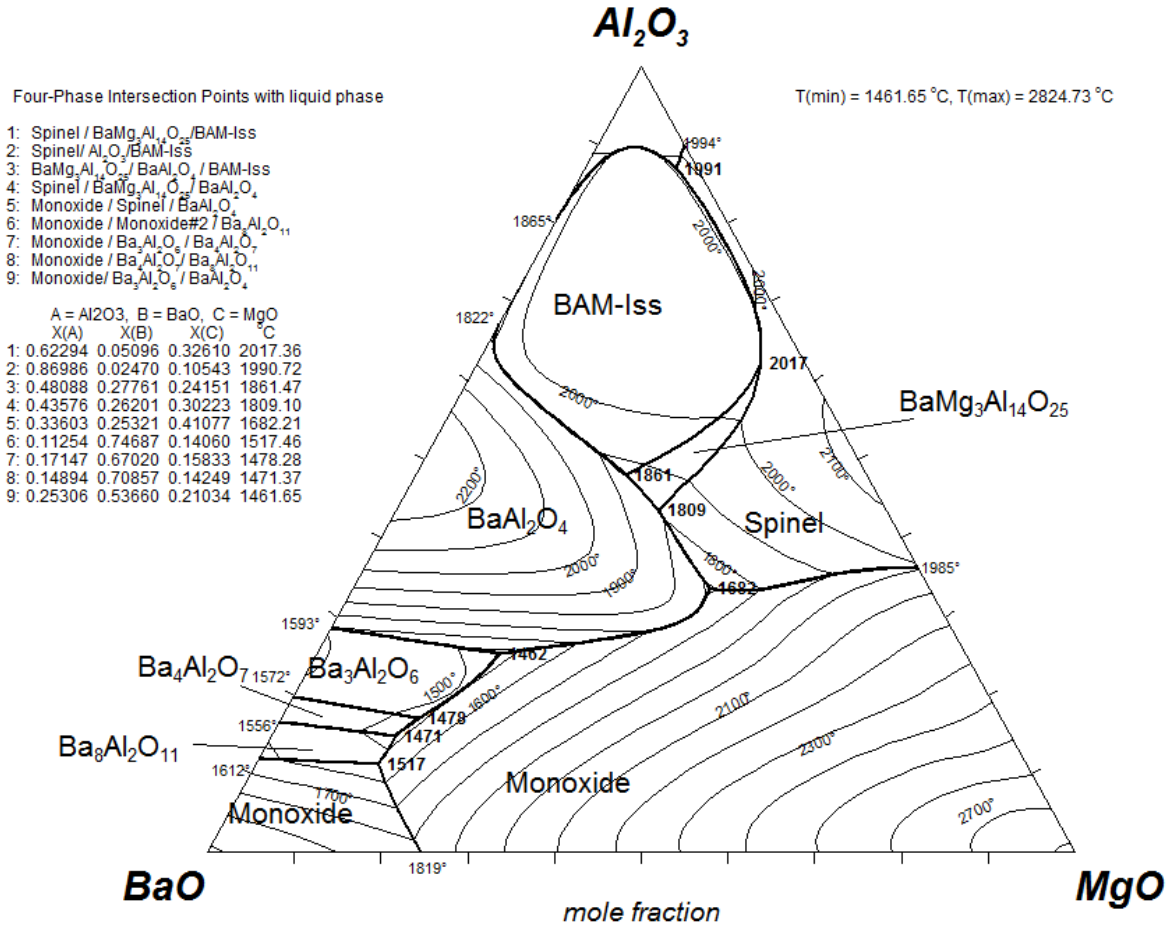

Fig. 3.14.3 Present calculated liquidus (polythermal) projection for the BaO-MgO-Al_2O_3 system (isotherms were drawn at the interval of 100 °C).

3.15 The BaO-Al_2O_3-SiO_2 system

In the BaO-Al_2O_3-SiO_2 system, to obtain the optimal fit of the available data, an additional component in the form of a $(BaAl_2)^{+8}$ associate was added to the liquid phase, i.e. $BaAl_2O_4$ was considered a separate component in the binary BaO-Al_2O_3 system (along with BaO and Al_2O_3). The introduction of these associates can be interpreted as the method to take the charge compensation effect (Chartrand and Pelton, 1999) into account. Chartrand and Pelton (1999)

introduced $(NaAl)^{+4}$ associates to model the Na_2O-Al_2O_3-SiO_2 solutions. They explained that the dissolution of alumina in silica by the replacement of Si^{+4} in the tetrahedral network by Al^{+3} is energetically unfavourable because it results in a negative charge centre. However, upon addition of Na_2O this negative charge can be compensated by a Na^+ ion placed next to the aluminum. In the BaO-Al_2O_3-SiO_2 system, replacement of one Si^{+4} in the tetrahedral network by one Al^{+3} and compensation by Ba^{+2} will result in energetically unfavourable positive charge centre. This can be avoided by substituting two Si^{+4} ions next to each other by two Al^{+3} ions and Ba^{+2} placed next to these aluminium ions. Thus, $(BaAl_2)^{+8}$ associates were treated as separate component of the liquid phase. The ternary solution was then formally treated as a quaternary solution with components BaO, Al_2O_3, SiO_2 and $BaAl_2O_4$. The standard Gibbs energy of the hypothetical pure component $BaAl_2O_4$, $g^0_{(BaAl2O4)}$, was fixed during optimization so that the $(BaAl_2)^{+8}$ associates are practically unstable in the BaO-Al_2O_3 binary system. In the BaO-Al_2O_3 system, at 2000 °C and at $X_{Al2O3} = 0.5$, the mole fraction of these associates is only 4.2×10^{-4}. These associates were stabilized in the SiO_2-rich region of the ternary system by the help of a similar kind of Gibbs energies of formation model parameters as presented in Sec. 1.2.2 for the $(NaAl)^{+4}$ associates. The present optimized parameters for the BaO-Al_2O_3-SiO_2 liquid phase are presented in Table 3.15.1. The Gibbs energy of the liquid phase in the BaO-Al_2O_3-SiO_2 system was calculated from the corresponding binary systems by treating SiO_2 as an asymmetric component i.e. BaO, Al_2O_3 and $BaAl_2O_4$ were kept in the same group (Pelton and Chartrand, 2001).

Thomas (1950) reported the primary phase fields in the composition ranges containing less than 30% Al_2O_3 and more than 20% SiO_2 by weight in the BaO-Al_2O_3-SiO_2 system by quenching,

petrography and XRD. Toropov, et al. (1954) studied the system by quenching and reported a polythermal liquidus projection for the ternary system. Foster and coworkers in a series of articles [Lin and Foster (1968); Foster and Lin (1969); Lin and Foster (1969); Semler and Foster (1969); Lin and Foster (1970); Semler and Foster (1970)] reported phase relationships in this ternary system mainly from quenching. Von Oehlschlegel and Ohnmacht (1975) studied the system by thermal analysis and quenching. All these studies agree on the presence of the ternary compound $BaAl_2Si_2O_8$ (BAS_2) as a stable phase. Lin and Foster (1968) presented a good literature review and performed experiments to study the polymorphism of BAS_2. They concluded that BAS_2 is monoclinic at room temperature, inverting reversibly to a hexagonal structure at 1590 °C. The hexagonal form is stable to the melting point at about 1760 °C. This polymorphic transformation at 1590 °C was taken into account by assuming, as no experimental data could be found in the literature, this enthalpy of transformation to be 100 J. However, more experimental work is required to accurately establish it.

Foster and Lin (1969) studied the BAS_2-SiO_2 section and presented its phase diagram. Foster and Lin (1969 also deduced the phase diagram of this section from the data of Thomas (1950) and Toropov, et al. (1954), who did not study this section separately. This deduced phase diagram showed SiO_2 to be incompatible with BAS_2. Foster and Lin (1969) presented arguments on the compatibility of silica with BAS_2. Later, Von Oehlschlegel and Ohnmacht (1975) also studied the BAS_2-SiO_2 system and proved the compatibility of silica with BAS_2. The data of Foster and Lin (1969) and Von Oehlschlegel and Ohnmacht (1975) are reasonably well reproduced in Fig. 3.15.1. The g^{00} and g^{05} parameters in Table 3.15.1 were used to fit this section.

In a different work, Lin and Foster (1969) studied the $BaSi_2O_5$ (BS_2)-BAS_2 system. Lin and Foster (1969), from the data of Thomas (1950) and Toropov, et al. (1954) - who did not study this section separately - deduced a simple eutectic phase diagram for this section with substantial solid solution of BAS_2 in BS_2 close to the eutectic temperature. Lin and Foster (1969) also reported a simple eutectic phase diagram for this section but stated that there is no solubility of BAS_2 in BS_2 for compositions greater than 6% BAS_2; for smaller compositions they were unable to conclude anything from the experimental techniques employed. Von Oehlschlegel and Ohnmacht (1975) measured phase diagram for this section, in which phases $Ba_3Si_5O_{13}$ (B_3S_5) and $Ba_5Si_8O_{21}$ (B_5S_8) also appeared, contrary to the data of Lin and Foster (1969). Von Oehlschlegel and Ohnmacht (1975) also did not report any mutual solubility among these phases. The data of Lin and Foster (1969) and Von Oehlschlegel and Ohnmacht (1975) are reasonably well reproduced in Fig. 3.15.2. No mutual solubility among the terminal phases was considered in the present work. The g^{001} parameter in Table 3.15.1 was used to fit the BS_2-BAS_2 section. The positive enthalpy and temperature dependent entropy terms in the g^{001} parameter were required to simultaneously fit the eutectic temperature and liquidus data on this section.

Von Oehlschlegel and Ohnmacht (1975) also reported phase diagram for the sections BAS_2-$Ba_2Si_3O_8$ (B_2S_3) and BAS_2-$Ba_5Si_8O_{21}$ (B_5S_8). They reported a simple eutectic phase diagram for the section BAS_2-B_2S_3, whereas in the BAS_2-B_5S_8 section the B_2S_3 phase also appeared. Their data are reasonably well reproduced in Figs. 3.15.3 and 3.15.4.

Semler and Foster (1969) studied the sections BAS_2-Al_2O_3 and BAS_2-mullite. These data are well reproduced in Figs. 3.15.5 and 3.15.6 respectively. The mullite phase appearing in the Al_2O_3-SiO_2 system was modeled as a non-stoichiometric phase [Swamy, Jung, and Decterov (2009)]. In the present calculations, to obtain an optimal fit of the available data, the BAS_2-mullite section was calculated at the mullite composition $(Al_2O_3)_{0.65}(SiO_2)_{0.35}$.

Lin and Foster (1970) studied the primary phase field regions in the ternary sub-system BS_2-BAS_2-SiO_2. These data are compared with the present calculations in Fig. 3.15.7 which also contains data by Thomas (1950) and Toropov, et al. (1954). With the help of these data, Lin and Foster (1970) reported a ternary eutectic at 1122±7 °C and a composition of BaO 35.2, Al_2O_3 9.5, and SiO_2 55.3 wt.%. The present calculated ternary eutectic temperature is 1116 °C and composition of BaO 38.4, Al_2O_3 7.2, and SiO_2 54.8 wt.%. In a different work, Semler and Foster (1970) studied the ternary sub-system BAS_2-SiO_2-Al_2O_3. They reported primary phase fields for these phases and an isothermal section at 1400 °C. These data are compared with the present calculations in Figs. 3.15.7 and 3.15.8 respectively. Semler and Foster (1970) reported a ternary eutectic in this ternary-subsystem at 1296±3 °C and of composition BaO 19, Al_2O_3 15, and SiO_2 66 wt%. The present calculated ternary eutectic temperature is 1230 °C and composition BaO 17.0, Al_2O_3 18.5, SiO_2 64.5 wt%. As evident in Fig. 3.15.7, there is also disagreement with the data by Semler and Foster (1970) on the primary phase region of mullite phase in this region. In the present calculations, simultaneous fitting of this eutectic temperature, with the primary phase region and experimental data in Figs. 3.15.1 and 3.15.6 by Foster and coworkers, was found to be very difficult. The g^{101} and g^{102} parameters were used to simultaneously fit the experimental data

in Fig. 3.15.6 and the ternary eutectic temperature reported by Semler and Foster. The positive enthalpy and negative entropy terms in these parameters were required to simultaneously fit the ternary eutectic temperature, which lie at comparatively lower temperature, and the liquids data in Fig. 3.15.6.

Toropov, et al. (1954), apart from BAS_2, reported another ternary compound of composition $3BaO.3Al_2O_3.2SiO_2$ ($B_3A_3S_2$). They reported this compound as non-stoichiometric, melting incongruently at 1550 °C into BA and liquid. There are data in the literature [Gebert (1968); Kockel and Oehlschlegel (1969)] for the presence of another ternary compound, $BaAl_2SiO_6$ (BAS). However, Toropov, et al. (1954) did not report this phase as stable. No other evidence in the literature on the presence of the $B_3A_3S_2$ phase could be found. In the present work, the BAS phase was included as stoichiometric phase and the presence of the $B_3A_3S_2$ phase, close to the BAS composition, was neglected.

Lapina, Semenov, and Khodakovskii (1989) performed calorimetric measurements to report a standard heat of formation (H^0_{298}) and enthalpy increment at 700 °C ($H_{973}–H_{298}$) for the BAS_2 compound. As shown in Table 3.15.1, this value of ΔH^0_{298} was used for the BAS_2 phase. Chernyshova et al. (1991) by DSC measured the heat capacity for the compound in the temperature range 39-439 °C. Therefore, up to 439 °C the heat capacity equation reported by Chernyshova, et al. (1991) was used. Above this temperature, the heat capacity was extrapolated as shown in Fig. 3.15.9 where it is also compared with the sum of the heat capacities of constituent compounds. With the optimized heat capacity of the BAS_2 phase, the $H_{973}–H_{298}$ value

reported by Lapina, et al. (1989) is well reproduced, as shown in Table 3.15.1. Other than these, no thermodynamic data for the ternary compounds were found in the literature. The calculated standard entropies of formation for the ternary compounds are less than 8 J/(mol of metal) which is quite reasonable.

Table 3.15.1 Optimized thermodynamic parameters, in Joules, in the BaO-Al_2O_3-SiO_2 system.

LT-$BaAl_2Si_2O_8$ (BAS_2(LT))	
ΔH^0_{298} = –4244300 J/mol	Exp. = –4244300 ± 1200 J/mol [Lapina et al., '89]
H_{973}–H_{298} = 191.885 kJ/mol	Exp. = 190.600 ± 2.2 kJ/mol [Lapina et al., '89]
S^0_{298} = 246.500, ΔS^0_{298}[(a)] = 40.691	
C_p = 261.05 + 0.0664 T –5256000 T^{-2} (298 < T < 712 K) [Chernyshova et al., '91]	
C_p = 234 + 0.108 T– 2.5E-5 T^2 (712 < T < 2200 K)	
HT-$BaAl_2Si_2O_8$ (BAS_2(HT))	
ΔH^{tr} = 100 J (at 1590 °C)	
Cp = same as LT-BAS_2	
T_m[(b)] = 1763 ºC, Experimental = 1760 [Lin and Foster, '68]	
$BaAl_2SiO_6$ (BAS)	
ΔH^0_{298} = –3333000 S^0_{298} = 171 ΔS^0_{298}[(a)] = 6.651	
C_p = C_p (BaO)+C_p (Al_2O_3)+ C_p (SiO_2,S2) (298 <T < 2000 K)	T_m[(b)] = 1673
Liquid phase (Ternary interaction parameters) (in Joules)	
$g^0_{BaAl2O4}$ = g^0(BaO,l) + g^0(Al_2O_3,l) –138072 + 2.092 T	
$g^{00}_{BaAl2\text{-}Si}$ = –56484 ; $g^{05}_{BaAl2\text{-}Si}$ = 41840 – 14.644 T	
$g^{001}_{BaAl2\text{-}Si(Ba)}$ = 33472 – 41.840 T	
$g^{101}_{BaAl2\text{-}Si(Al)}$ = 25104 – 71.128 T ; $g^{102}_{BaAl2\text{-}Si(Al)}$ = 100416 – 15.899 T	

(a) oxides (stable at room-temperature) as reference
(b) congruent melting temperature

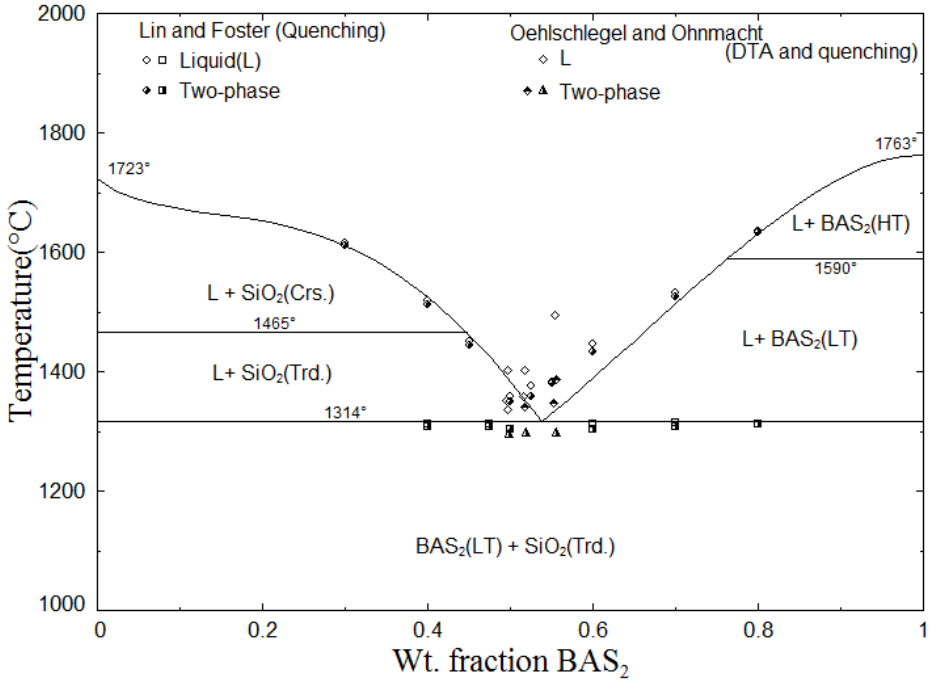

Fig. 3.15.1 Optimized phase diagram of the SiO_2-$BaAl_2Si_2O_8$ (BAS_2) section.

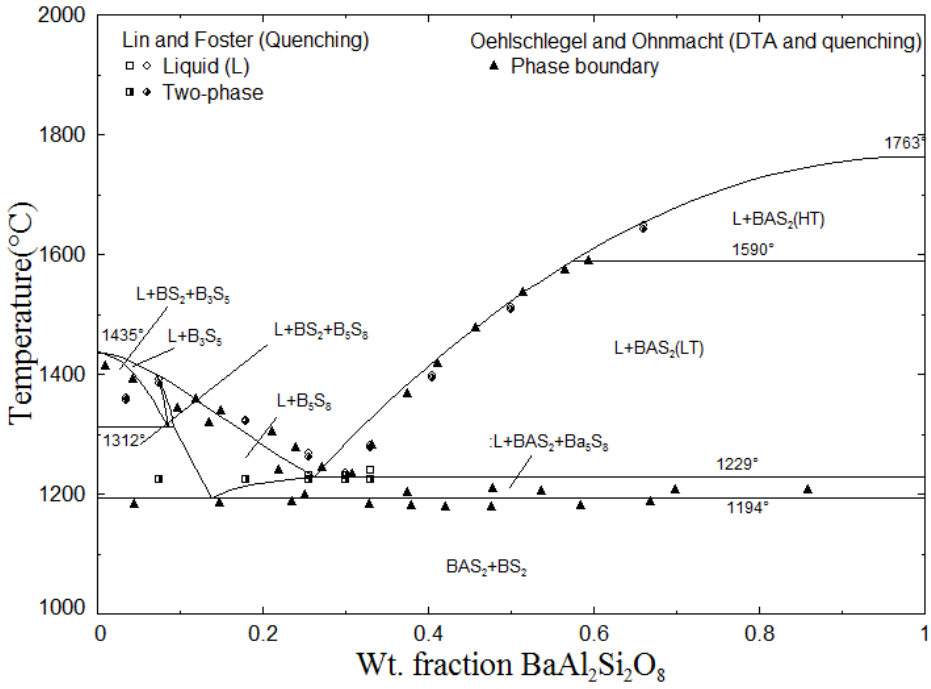

Fig. 3.15.2 Optimized phase diagram of the $BaSi_2O_5$(BS_2)-$BaAl_2Si_2O_8$ (BAS_2) section.

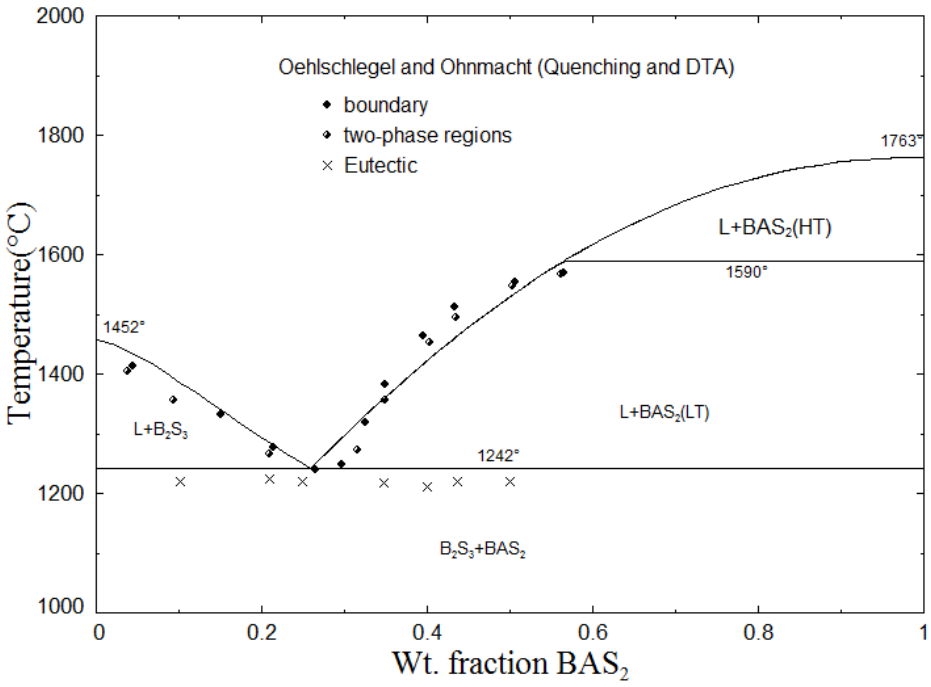

Fig. 3.15.3 Optimized phase diagram of the $Ba_2Si_3O_8(B_2S_3)$-$BaAl_2Si_2O_8$ (BAS_2) section.

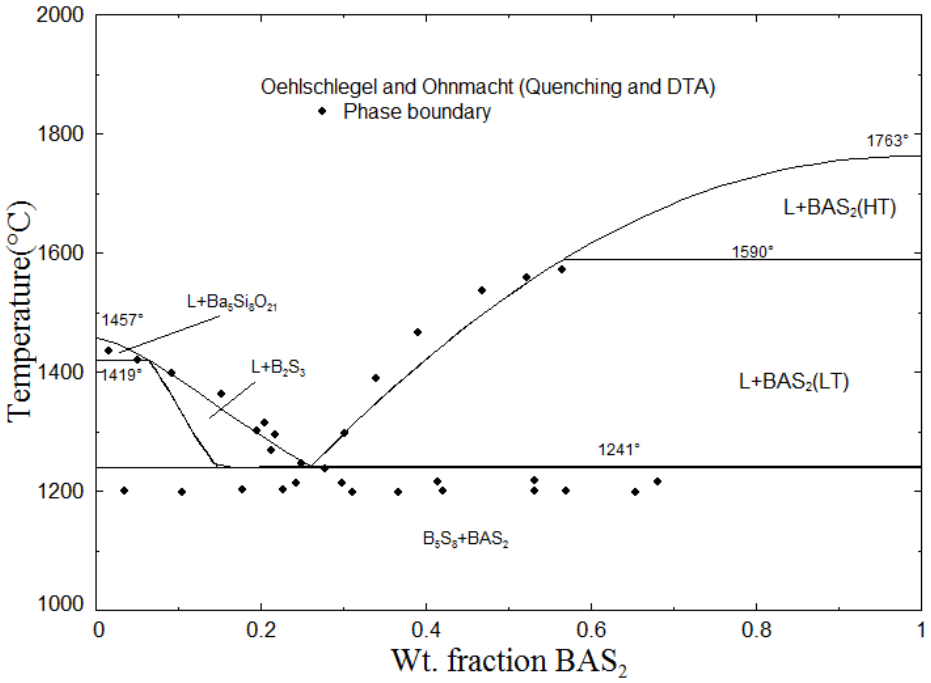

Fig. 3.15.4 Optimized phase diagram of the $Ba_5Si_8O_{21}(B_5S_8)$-$BaAl_2Si_2O_8$ (BAS_2) section.

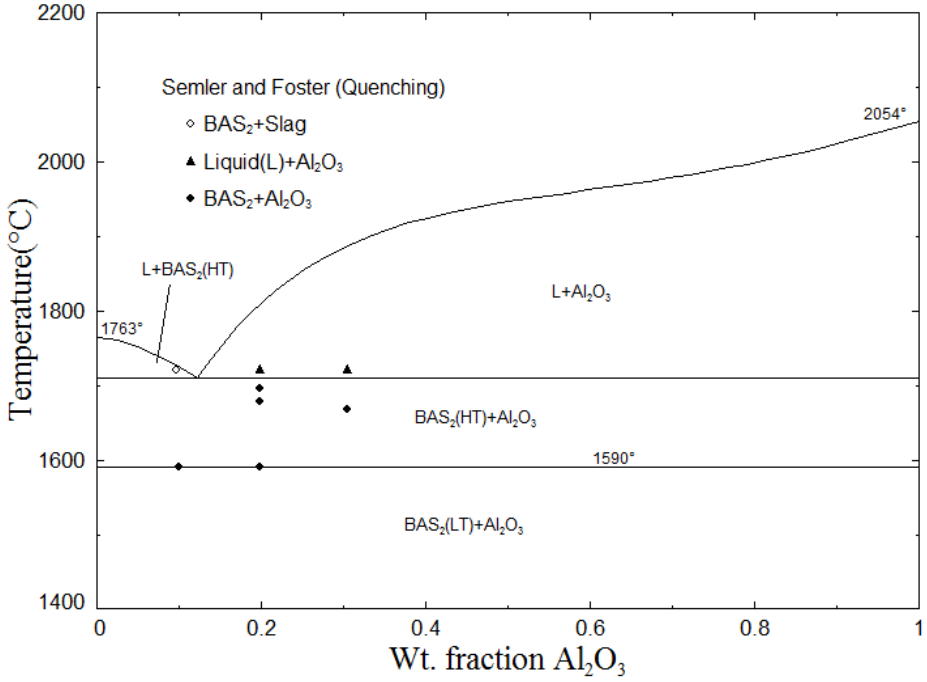

Fig. 3.15.5 Optimized phase diagram of the $BaAl_2Si_2O_8$ (BAS_2)-Al_2O_3 section.

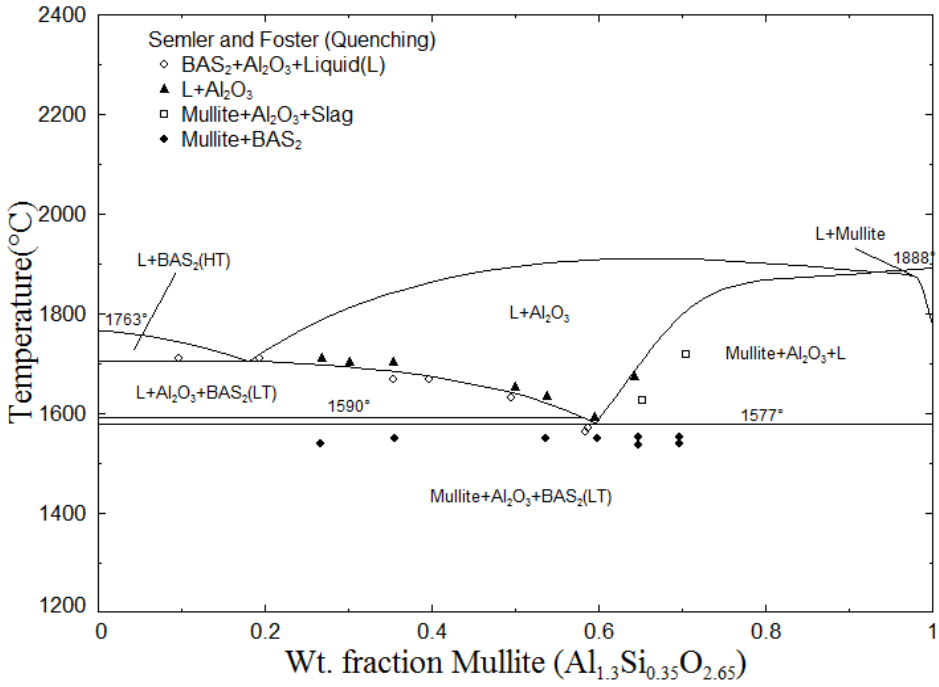

Fig. 3.15.6 Optimized phase diagram of the $BaAl_2Si_2O_8$ (BAS_2)-Mullite ($Al_{1.3}Si_{0.35}O_{2.65}$) section.

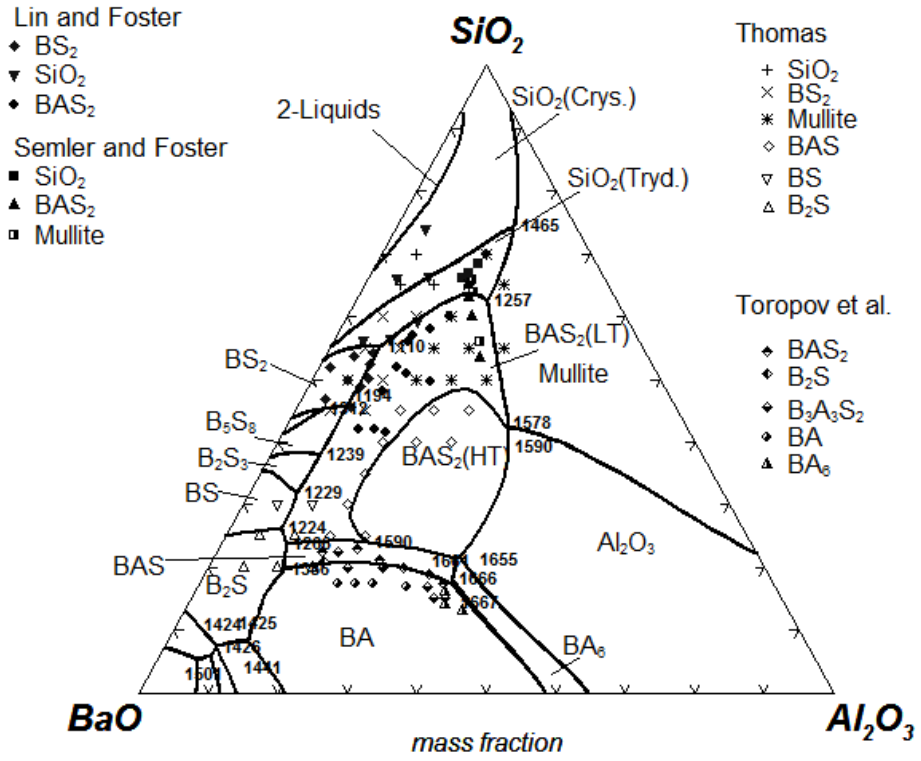

Fig. 3.15.7 Polythermal projection of the BaO-Al_2O_3-SiO_2 system (for clarity, only univariant lines are shown).

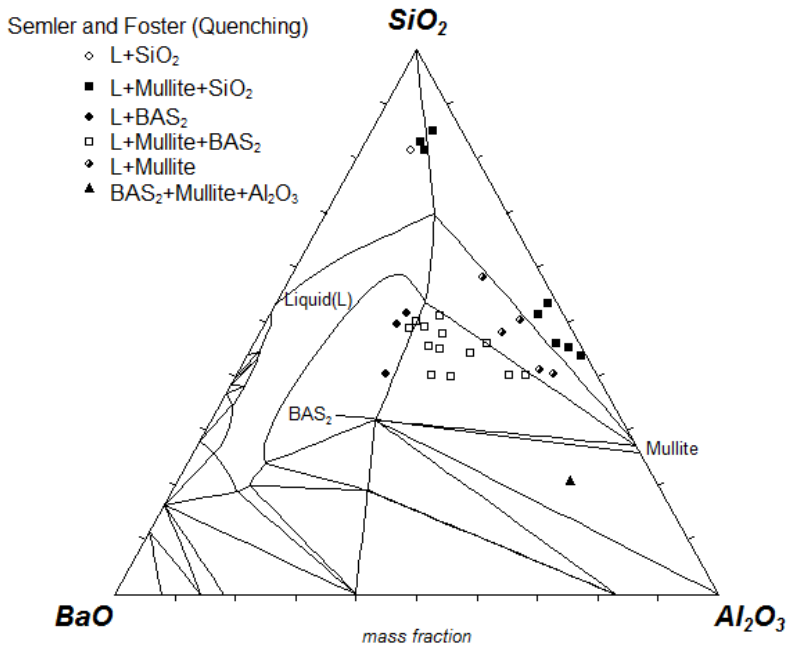

Fig. 3.15.8 Isothermal section at 1400 °C in the BaO-Al_2O_3-SiO_2 system.

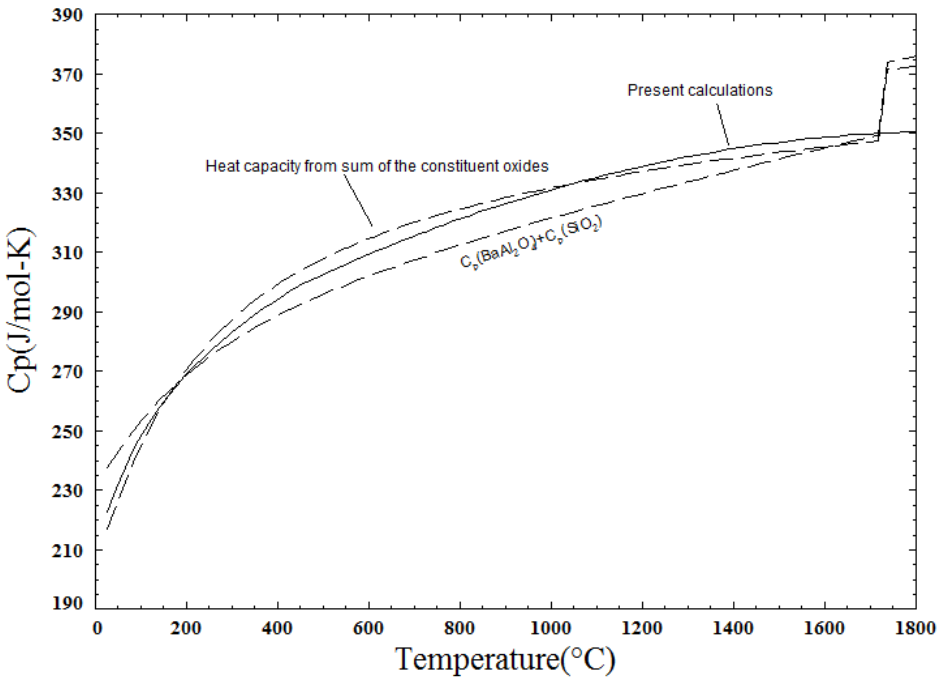

Fig. 3.15.9 Optimized heat capacity of the $BaAl_2Si_2O_8$ phase compared with other heat capacity schemes.

3.16 The SrO-Al_2O_3-SiO_2 system

In the SrO-Al_2O_3-SiO_2 system, to obtain the optimal fit of the available data an additional component in the form of $(SrAl_2)^{+8}$ associates was added to the liquid phase. As explained in the BaO-Al_2O_3-SiO_2 system, the introduction of these associates can be interpreted as the method to take the charge compensation effect (Chartrand and Pelton, 1999) into account. This effect is explained as the substitution of two Si^{+4} ions, next to each other in the tetrahedral network, by two Al^{+3} ions. Sr^{+2} ion can be placed next to these aluminium ions to compensate the charge. Thus, $(SrAl_2)^{+8}$ associates were treated as separate component of the liquid phase. The ternary solution was then formally treated as a quaternary solution with components SrO, Al_2O_3, SiO_2 and $SrAl_2O_4$. The standard Gibbs energy of the hypothetical pure component $SrAl_2O_4$, $g^0_{(SrAl2O4)}$, was fixed during optimization so that the $(SrAl_2)^{+8}$ associates are practically unstable in the SrO-Al_2O_3 binary system. In the SrO-Al_2O_3 system, at 2050 °C and at $X_{Al2O3} = 0.5$, the mole fraction of these associates is only 4.4×10^{-4} mole. The Gibbs energy of the liquid phase in the SrO-Al_2O_3-SiO_2 system was calculated from the corresponding binary systems by treating SiO_2 as an asymmetric component i.e. SrO, Al_2O_3 and $SrAl_2O_4$ were kept in the same group (Pelton and Chartrand, 2001). The optimized parameters for the SrO-Al_2O_3-SiO_2 ternary systems are presented in Table 3.16.1. During simultaneous optimization, effort was made to use parameters for the liquid phase which are similar in form as obtained for the liquid phase in the BaO-Al_2O_3-SiO_2 system. The parameters which gave optimal fit of the available data in the SrO-Al_2O_3-SiO_2 system are presented in Table 3.16.1. It can be seen that all the parameters, except the g^{011}, are same in form as used for the BaO-Al_2O_3-SiO_2 system. The g^{011} parameter was required to obtain good fit in the SrO-rich regions.

Dear (1957a) by quenching techniques reported sub-solidus phase equilibria at 1350 °C, presented in Fig. 3.16.1, in the SrO-Al_2O_3-SiO_2 system. These phase equilibria can be compared with the present calculations in Fig. 3.16.2. The assumption of the low-temperature decomposition of the Sr_3S helped in fitting these data. Hence, this low-temperature decomposition was calculated in the binary SrO-SiO_2 system as shown in Fig. 2.4.1. However, more experimental work is required to corroborate this decomposition. Dear (1957a) did not find the liquid phase to be stable at 1350 °C at any composition. The binary eutectic temperature between the SrS and SiO_2 phases in the binary SrO-SiO_2 system is about 1350 °C. Therefore, the ternary eutectic between SrS, SiO_2 and $SrAS_2$ phase is expected to be below 1350 °C. In fact, similar eutectics in the CaO-Al_2O_3-SiO_2 and BaO-Al_2O_3-SiO_2 systems lie at 1184 and 1116 °C. There are data in the Sci-Glass database on liquidus temperatures at compositions in the subsystem SrS-$SrAS_2$-SiO_2 which show the presence of the liquid phase well below 1350 °C. However, exact fitting of these liquidus data will reproduce a eutectic below 1000 °C in this ternary subsystem. Therefore, these liquidus data were fitted as shown in Table 3.16.2 to reproduce the eutectic at 1179 °C (close to that of CaO-Al_2O_3-SiO_2 system). Moreover, in general, the liquidus temperatures reported in the Sci-Glass database are not true liquidus temperature. They are the temperatures below which solids (crystals) from within a few hours, generally within 6-12 h, and remain in the liquid [Wallenberger and Smrcek (2010)]. These temperatures are to check the resistance to the development of devitrification in the glass manufacturing conditions [Dumbaugh (1992)]. Dear reported three stable ternary phases: $SrAl_2Si_2O_8$ ($SrAS_2$), $Sr_2Al_2SiO_7$ (Sr_2AS), $Sr_6Al_{18}Si_2O_{37}$ ($Sr_6A_9S_2$). The optimized parameters for these phases are presented in Table. 3.16.1. As reported earlier, the S_4A_7 and SA_2 phases, which

were not obtained by Dear (1957a) as equilibrium phases, are considered stable in the binary $SrO\text{-}Al_2O_3$ phase diagram. Hence, they appear in the present calculations at 1350 °C.

Starczewski (1964) by thermal analysis studied various isoplethal sections in the system and reported the data under the name "average temperature of melting". This name suggests that the thermal analysis peaks reported by Starczewski (1964) should correspond to the temperature at which melting starts at a particular composition (solidus or invariant temperature). The optimal fit of these data is presented in Figs. 3.16.3-3.16.18. It can be seen that the thermal peaks obtained by Starczewski (1964) correspond to various phase transitions, not necessarily to solidus or invariant temperatures. It must be noted that Starczewski (1964) reported higher melting temperatures than the other available experimental data by Hanic, et al. (1979) in the SrO-rich region in the binary $SrO\text{-}Al_2O_3$ system (see section $SrO\text{-}Al_2O_3$). The present calculations fit the data by Hanic, et al. (1979) comparatively better in this region. In the ternary isoplethal sections as well there is disagreement between Starczewski's higher melting temperatures at the SrO-rich compositions and the present calculations. In view of the inconsistency of Starczewski's data in the SrO-rich region in the binary $SrO\text{-}Al_2O_3$ system, his experimental data on the melting temperatures at the SrO-rich compositions in the ternary isopleths sections were given less weight. Starczewski (1964) reported congruent melting temperature of 1765 °C for the $SrAS_2$ phase and incongruent melting temperature of 1705 °C for the Sr_2AS phase. Bambauer, Schoeps, and Pentinghaus (1984) reported congruent melting point of the $SrAS_2$ phase at 1656 °C. The present calculated congruent melting temperatures for these phases are 1654 and 1704 °C

respectively. The present calculated liquidus (polythermal) projection for the SrO-Al_2O_3-SiO_2 system is presented in Fig. 3.16.20.

Lapina, et al. (1989) performed calorimetric measurements and reported the standard enthalpy of formation (H^0_{298}) and an enthalpy increment at 700 °C (H_{973}–H_{298}) for the $SrAS_2$ compound. As shown in Table 3.16.1, this value of ΔH^0_{298} was used for the $SrAS_2$ phase. Chernyshova, et al. (1991) by DSC measured the heat capacity for the compound in the temperature range 39-439 °C. Their measured heat capacities were quite close to the heat capacity obtained by adding the heat capacities of constituent oxides. Therefore, up to 439 °C the heat capacity equation reported by Chernyshova, et al. (1991) was used and above this temperature the heat capacity was calculated as sum of the constituent oxides. This scheme of heat capacity is also plotted in Fig. 3.16.19 where it is compared with the heat capacity obtained by adding the heat capacities of constituent compounds. Using this scheme of heat capacity for the $SrAS_2$ phase, the (H_{973}–H_{298}) value reported by Lapina, et al. (1989) is well reproduced as shown in Table 3.16.1. Massazza and Fadda (1966) by solution calorimetry reported the standard heat of formation from oxides (ΔH^0_{298}) for the Sr_2AS phase which is compared with the present calculated value in Table 3.16.1. The present calculated value is more negative than was required to reproduce the data in Fig. 3.16.2 reported by Dear (1957a). The datum by Massazza and Fadda (1966) would make the Sr_2AS phase to decompose at the lower temperatures. The standard entropies of formation from oxides (ΔS^0_{298}) for the three ternary compounds are always less than 7 J/(mol of metal) which is quite reasonable.

Table 3.16.1 Optimized thermodynamic parameters, in Joules, in the SrO-Al_2O_3-SiO_2 system.

$SrAl_2Si_2O_8$ ($SrAS_2$)	
ΔH^0_{298} = –4248000 J/mol	Exp. = –4248000 ± 4700 J/mol [Lapina et al., '89]
H_{973}–H_{298} = 192.840 kJ/mol	Exp. = 185.800 ± 1.8 kJ/mol [Lapina et al., '89]
S^0_{298} = 209.854 J/mol/K	$\Delta S^{0(a)}_{298}$ = 22.534 ΔS^0_{298} (from SA(HT) and SiO_2(S1)) = –0.945
$T_m^{(c)}$ = 1654 ºC, Exp.$^{(c)}$ = 1765 [Starczewski, '64] Exp.$^{(c)}$ = 1656 [Bambauer et al, '84]	
C_p = 269.59 + 0.05784 T –5833000 T^2 (298<T<712 K) [Chernyshova et al., '91]	
$C_p = C_p$ (SrO)+C_p (Al_2O_3) +2 Cp (SiO_2,S2) (712<T<2000 K)	
$Sr_2Al_2SiO_7$ (Sr_2AS)	
ΔH^0_{298} = –3989732 S^0_{298} = 235.700 $\Delta S^{0(a)}_{298}$ = 36.260 $\Delta S^{0(b)}_{298}$ = 12.221	
$\Delta H^{0(a)}_{298}$ = –219032 Exp. = –173050.24 J/mol [Massazza and Fadda, '66]	
$C_p = C_p$ ($SrSiO_3$)+C_p ($SrAl_2O_4$, HT) (298<T<2000 K) $T_m^{(c)}$ = 1704 °C, Exp.$^{(d)}$ = 1705 [Starczewski, 64]	
$Sr_6Al_{18}Si_2O_{37}$ ($Sr_6A_9S_2$)	
ΔH^0_{298} = –21133330 S^0_{298} = 992.000 $\Delta S^{0(a)}_{298}$ = 130.220 $\Delta S^{0(b)}_{298}$ = –8.933	
C_p = 6 C_p ($SrAl_2O_4$, HT)+ 2 C_p (Al_2SiO_5,S1)(FACT)+ 1 C_p (Al_2O_3) (298 < T < 2000 K) $T_m^{(d)}$ = 1760 °C	
Liquid phase (Ternary interaction parameters) (in Joules)	
$g^0_{SrAl2O4} = g^0$(SrO,l) + g^0(Al_2O_3,l) –112968 + 2.092 T	
$g^{00}_{SrAl2\text{-}Si}$ = –42677 ; $g^{05}_{SrAl2\text{-}Si}$ = 33472 – 5.201 T	
$g^{001}_{SrAl2\text{-}Si(Sr)}$ = 39748 – 41.840 T	
$g^{101}_{SrAl2\text{-}Si(Al)}$ = 50208 – 41.840 T	
$g^{011}_{Si\text{-}Al(Sr)}$ = 146440	

[a] oxides (stable at room-temperature) as reference, [b] compounds used to calculate heat capacity as reference
[c] congruent melting temperature, [d] incongruent melting temperature

Table 3.16.2 Calculated liquidus temperature compared with the experimental data from the Sci-Glass database.

GNo	SiO2	Al2O3	SrO	Exp.	Present
62083	61.1	10.0	28.9	1260	1319
62084	61.2	12.8	26.0	1215	1425
62085	60.0	11.3	28.7	1215	1379
62086	60.0	14.1	25.9	1321	1466
62087	58.7	8.4	32.8	1163	1248
62088	58.8	11.2	30.0	1201	1380
62089	58.8	14.0	27.1	1308	1471
62090	57.6	11.2	31.2	1155	1386
62091	56.4	9.7	33.8	1145	1326
62092	56.4	11.1	32.4	1100	1388
62093	55.3	11.0	33.6	1145	1389
62094	56.2	11.0	34.8	1150	1381
62095	54.2	11.7	34.2	1160	1421
62096	51.9	10.8	37.2	1150	1397

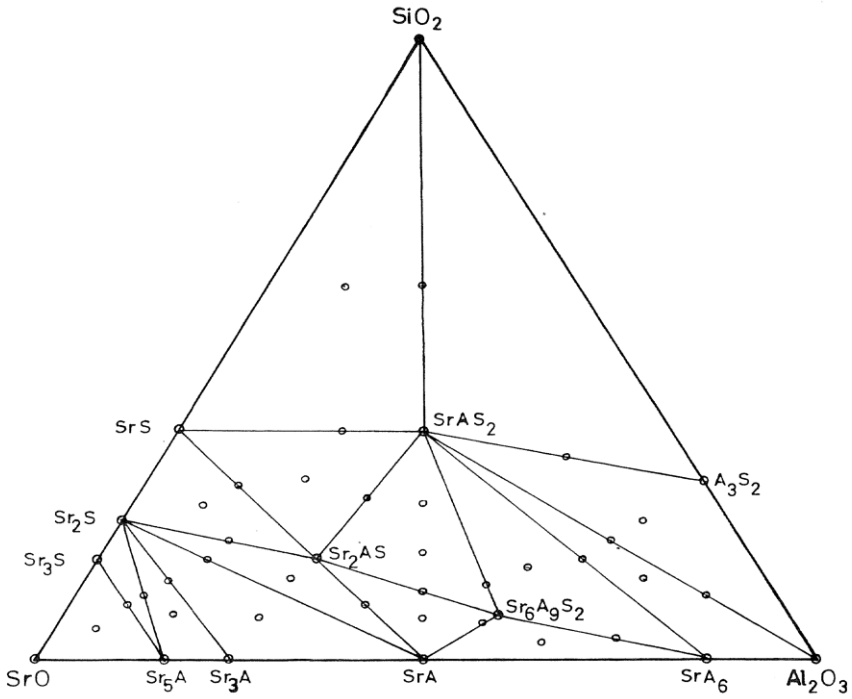

Fig. 3.16.1 Solid-phase relationships at 1350 °C as reported by Dear.

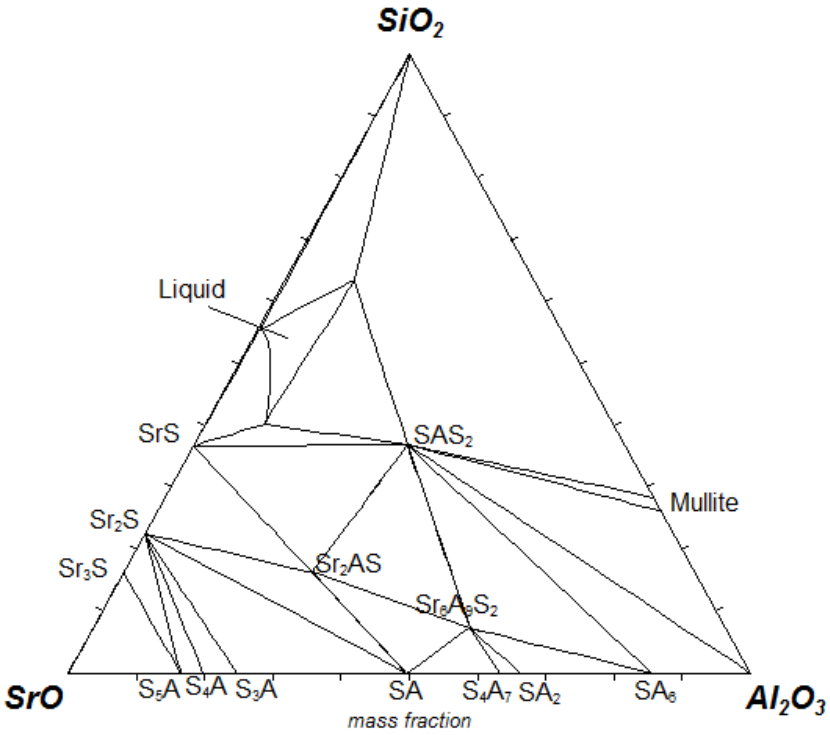

Fig. 3.16.2 Present calculated isothermal section at 1350 °C.

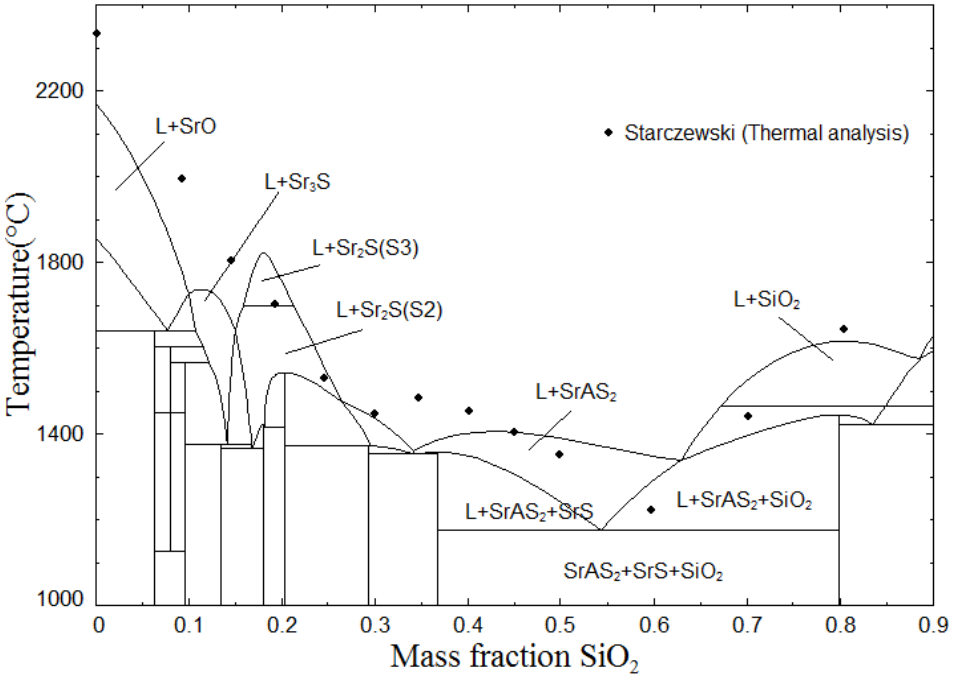

Fig. 3.16.3 Optimized phase diagram of isoplethal section Al_2O_3=0.10 in the SrO-Al_2O_3-SiO_2 system.

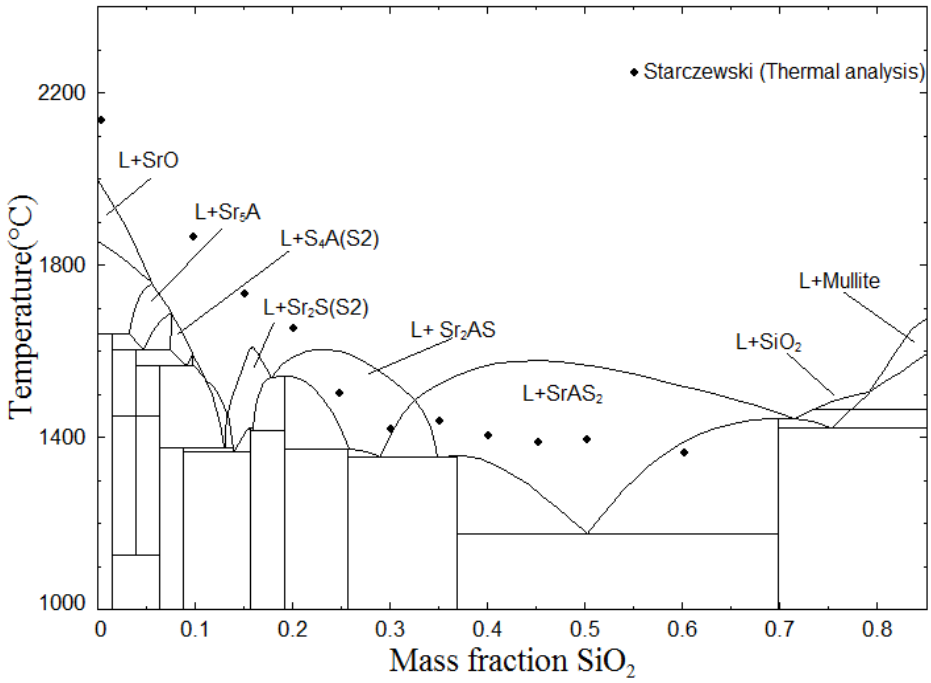

Fig. 3.16.4 Optimized phase diagram of isoplethal section Al_2O_3=0.15 in the SrO-Al_2O_3-SiO_2 system.

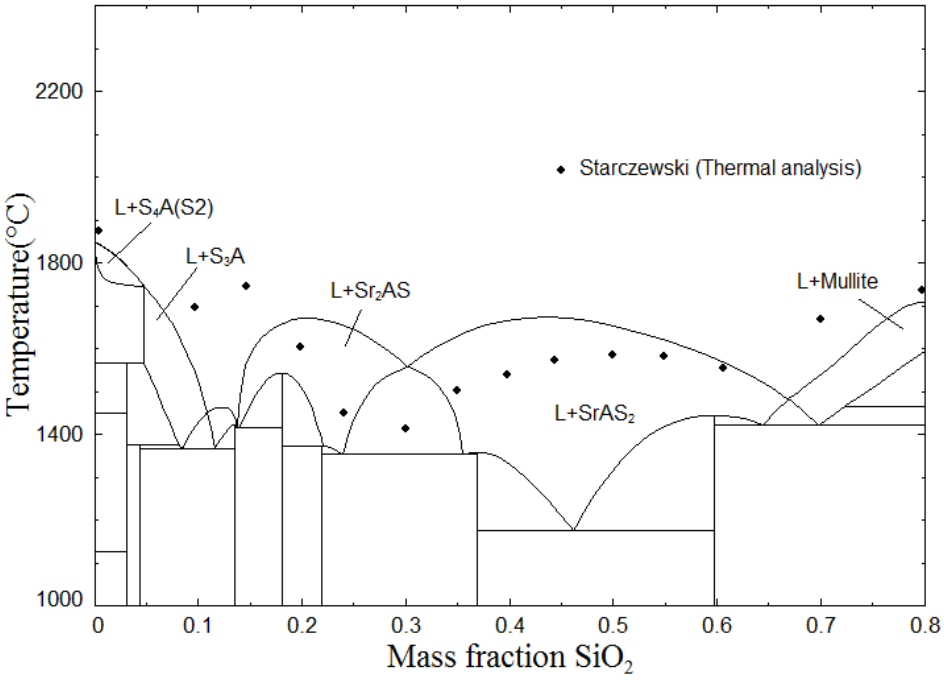

Fig. 3.16.5 Optimized phase diagram of isoplethal section Al_2O_3=0.20 in the SrO-Al_2O_3-SiO_2 system.

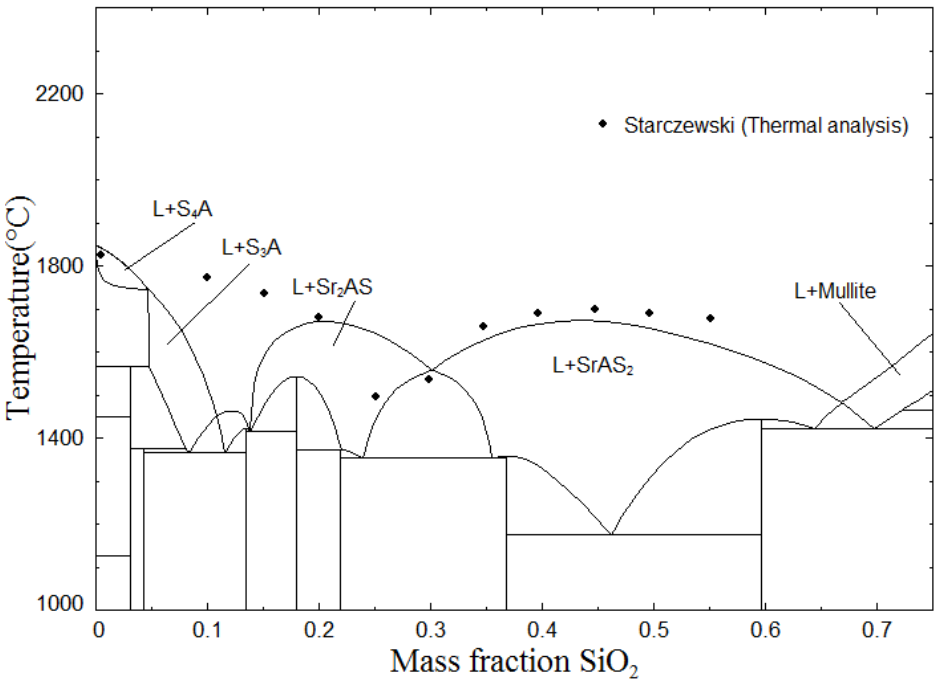

Fig. 3.16.6 Optimized phase diagram of isoplethal section Al_2O_3=0.25 in the SrO-Al_2O_3-SiO_2 system.

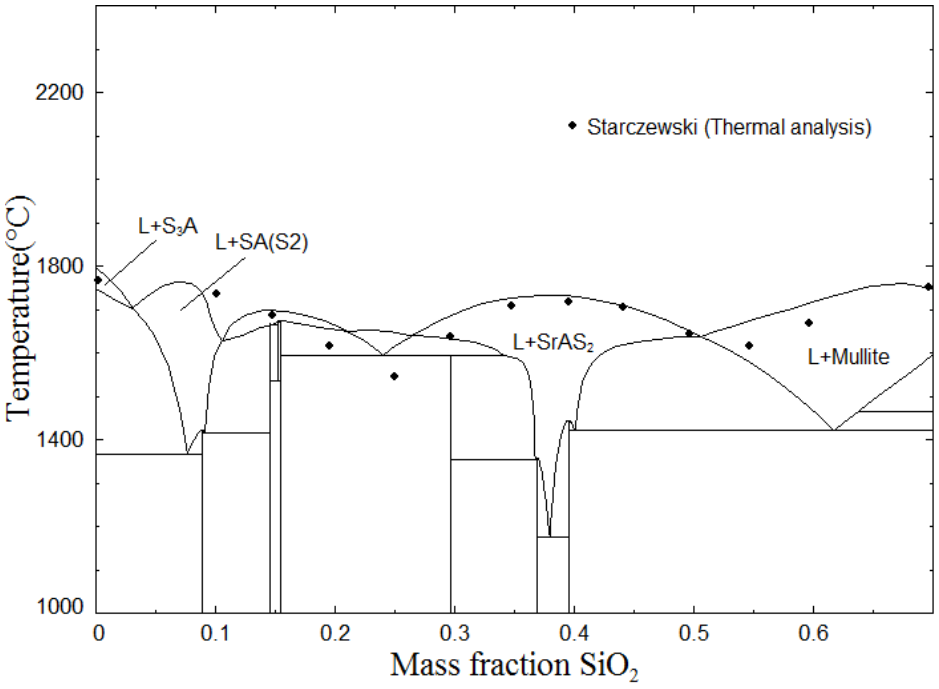

Fig. 3.16.7 Optimized phase diagram of isoplethal section Al_2O_3=0.30 in the SrO-Al_2O_3-SiO_2 system.

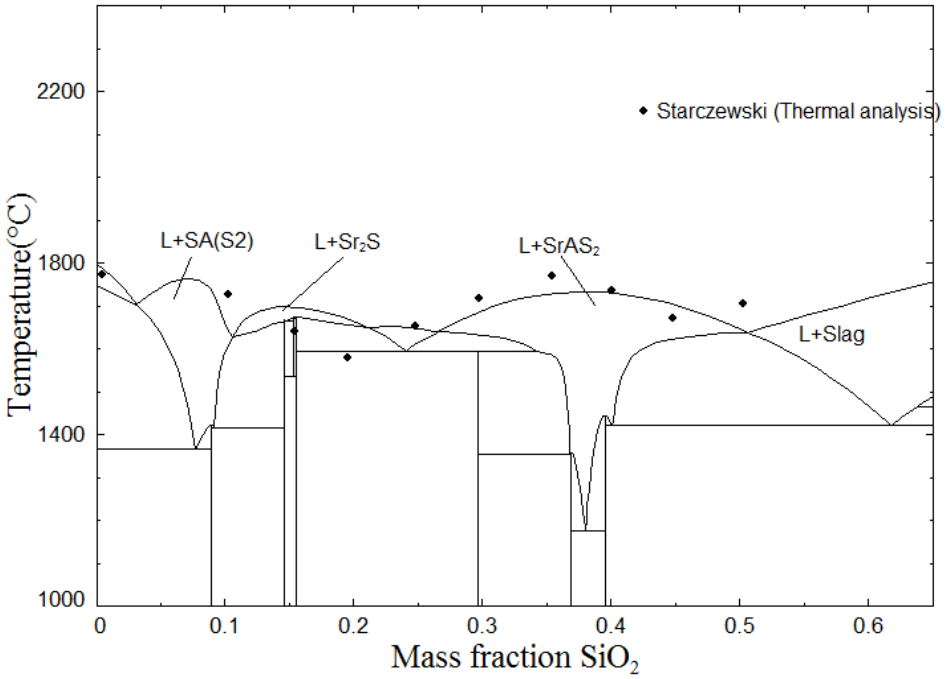

Fig. 3.16.8 Optimized phase diagram of isoplethal section Al_2O_3=0.35 in the SrO-Al_2O_3-SiO_2 system.

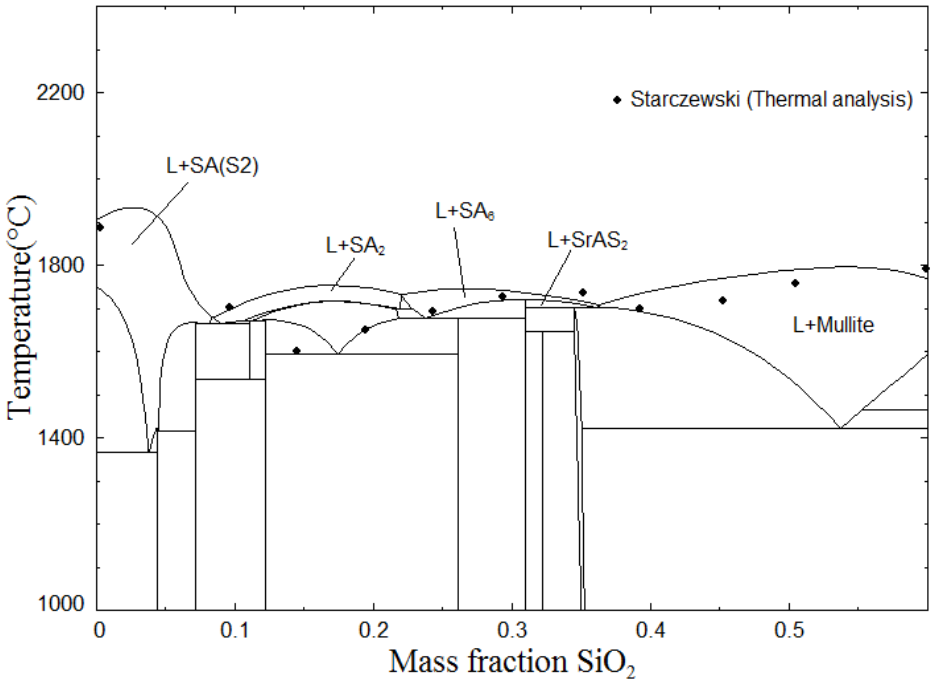

Fig. 3.16.9 Optimized phase diagram of isoplethal section Al_2O_3=0.40 in the SrO-Al_2O_3-SiO_2 system.

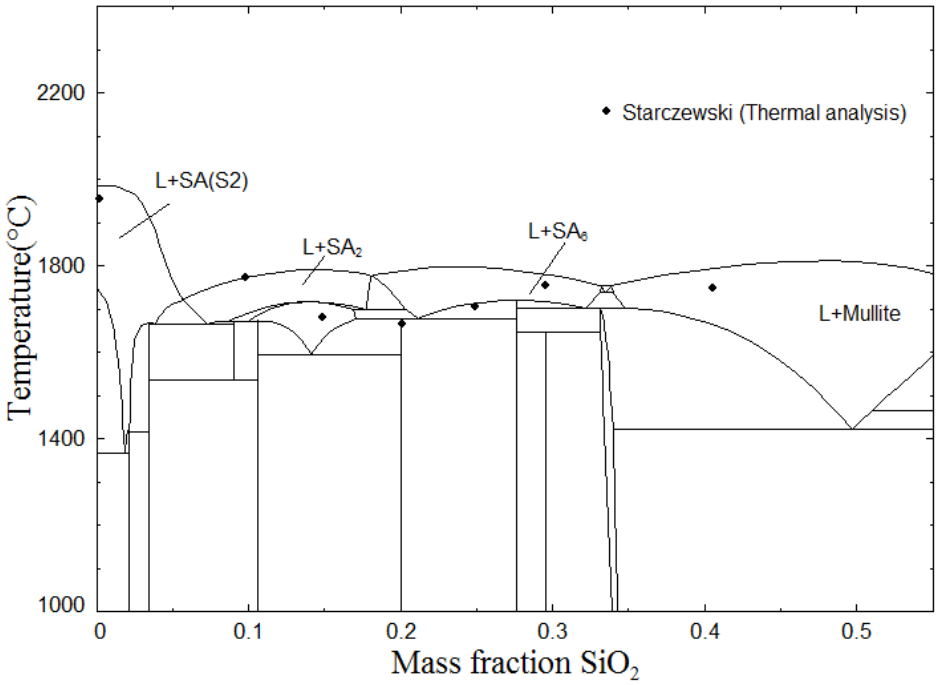

Fig. 3.16.10 Optimized phase diagram of isoplethal section Al_2O_3=0.45 in the SrO-Al_2O_3-SiO_2 system.

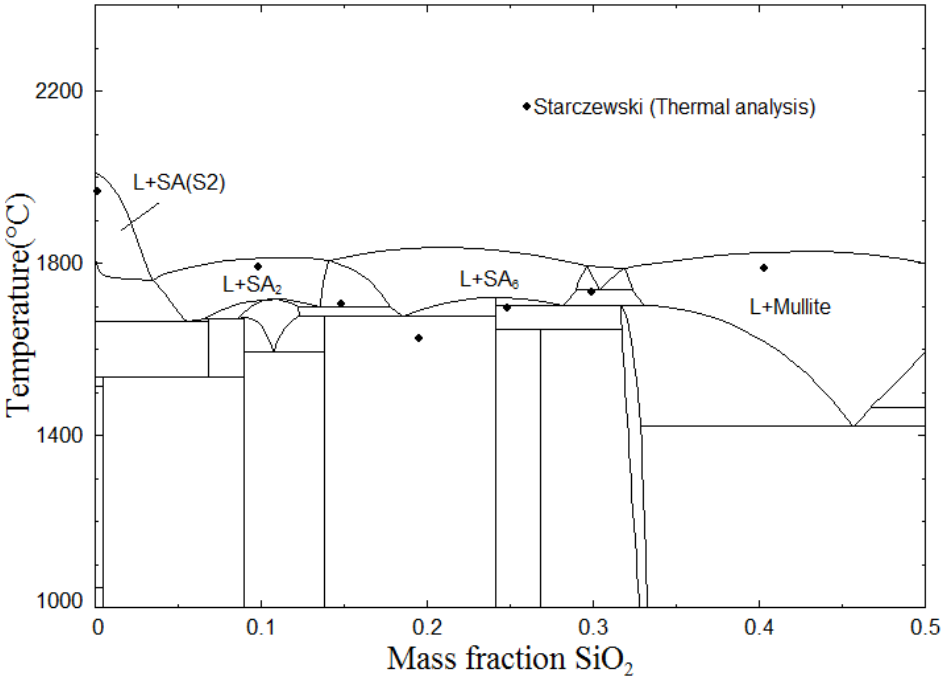

Fig. 3.16.11 Optimized phase diagram of isoplethal section Al_2O_3=0.50 in the SrO-Al_2O_3-SiO_2 system.

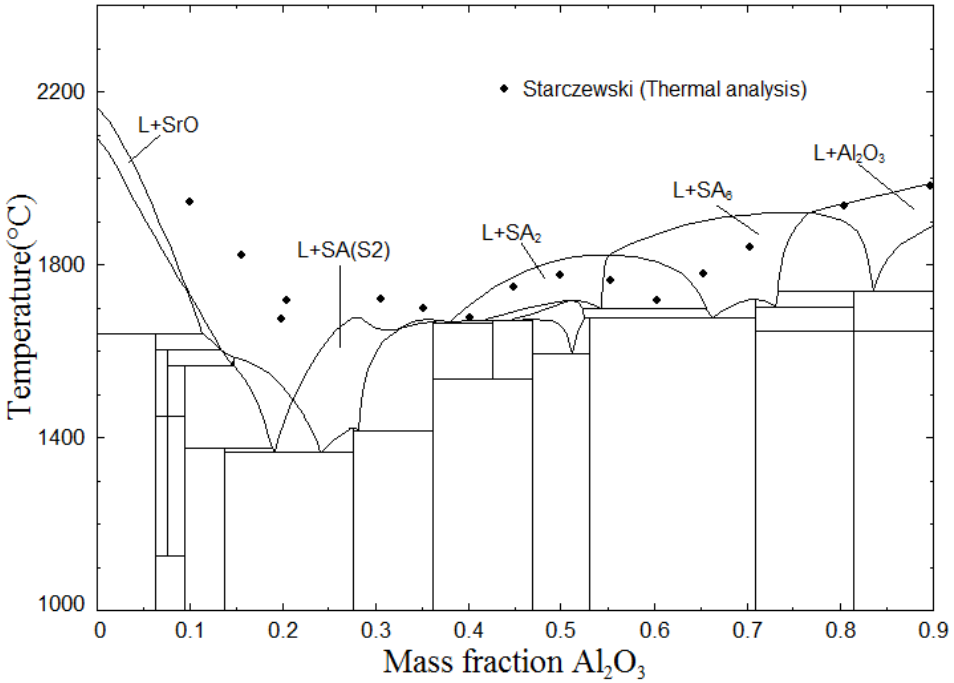

Fig. 3.16.12 Optimized phase diagram of isoplethal section SiO_2=0.10 in the SrO-Al_2O_3-SiO_2 system.

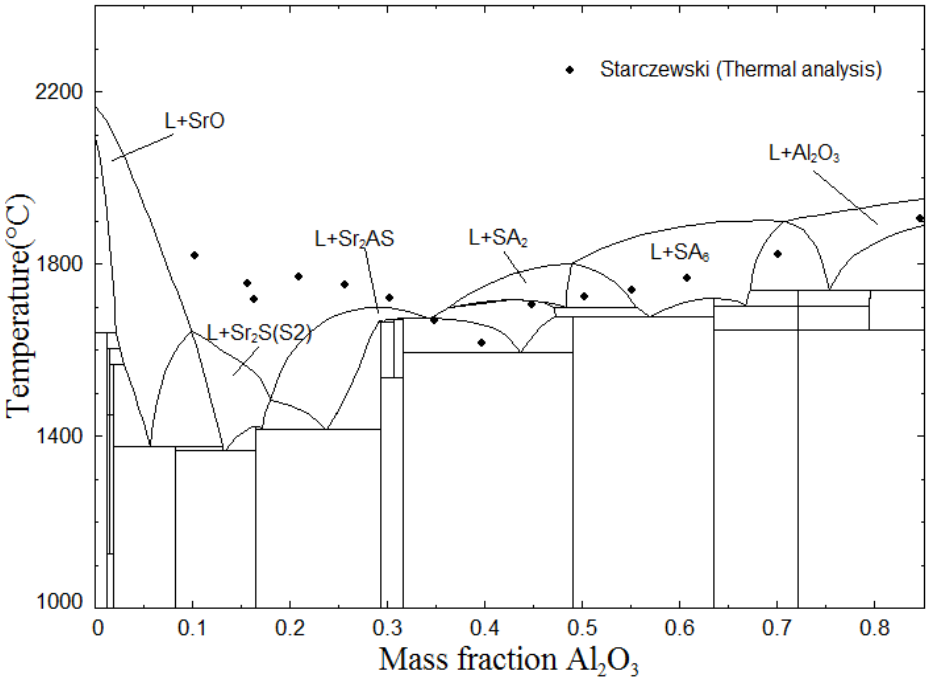

Fig. 3.16.13 Optimized phase diagram of isoplethal section SiO_2=0.15 in the SrO-Al_2O_3-SiO_2 system.

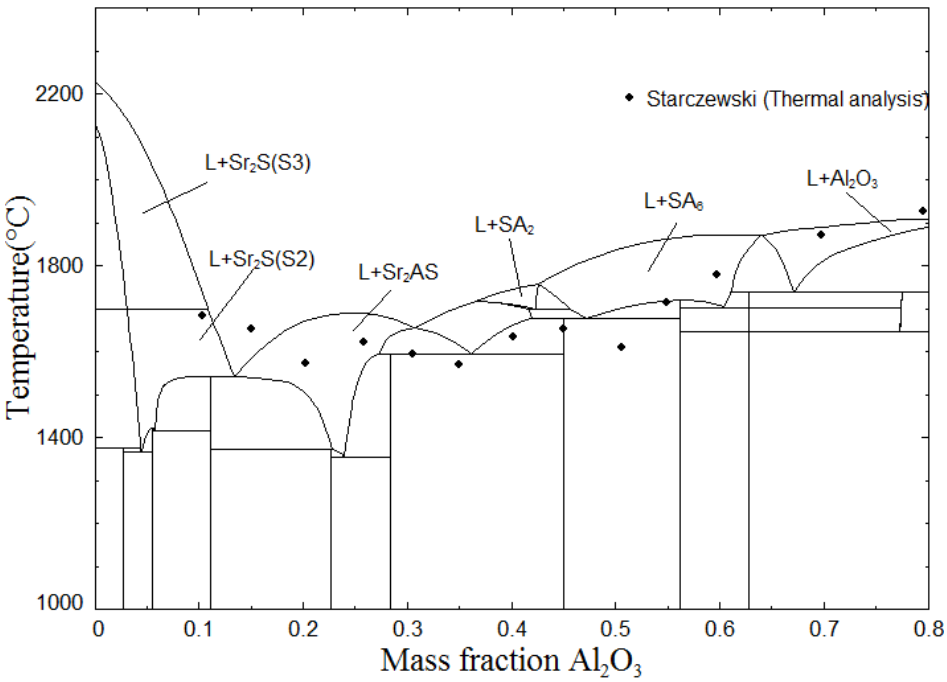

Fig. 3.16.14 Optimized phase diagram of isoplethal section SiO_2=0.20 in the SrO-Al_2O_3-SiO_2 system.

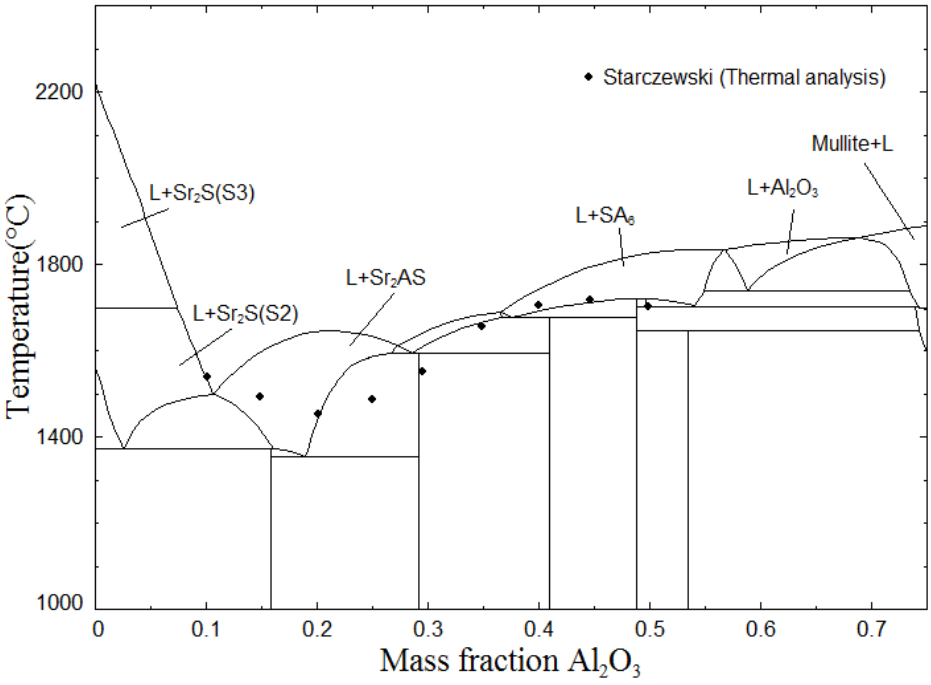

Fig. 3.16.15 Optimized phase diagram of isoplethal section SiO_2=0.25 in the SrO-Al_2O_3-SiO_2 system.

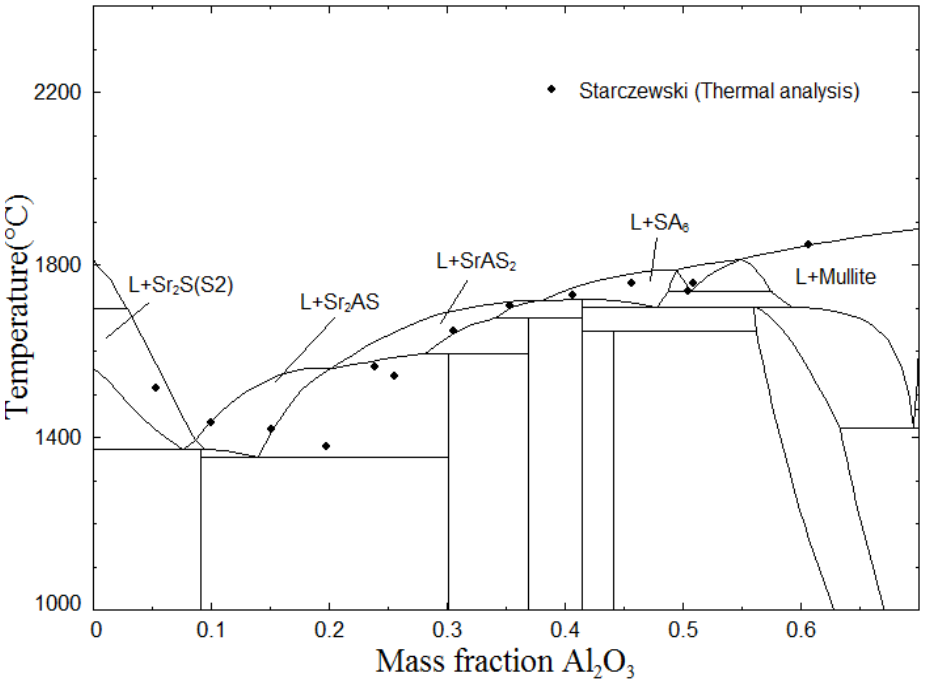

Fig. 3.16.16 Optimized phase diagram of isoplethal section SiO_2=0.30 in the SrO-Al_2O_3-SiO_2 system.

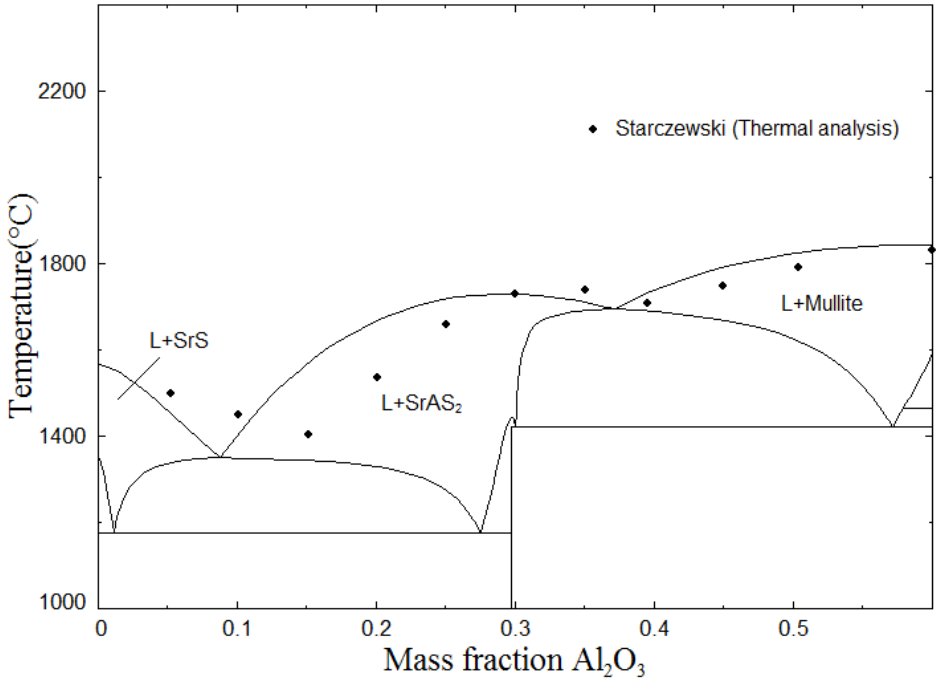

Fig. 3.16.17 Optimized phase diagram of isoplethal section SiO_2=0.40 in the SrO-Al_2O_3-SiO_2 system.

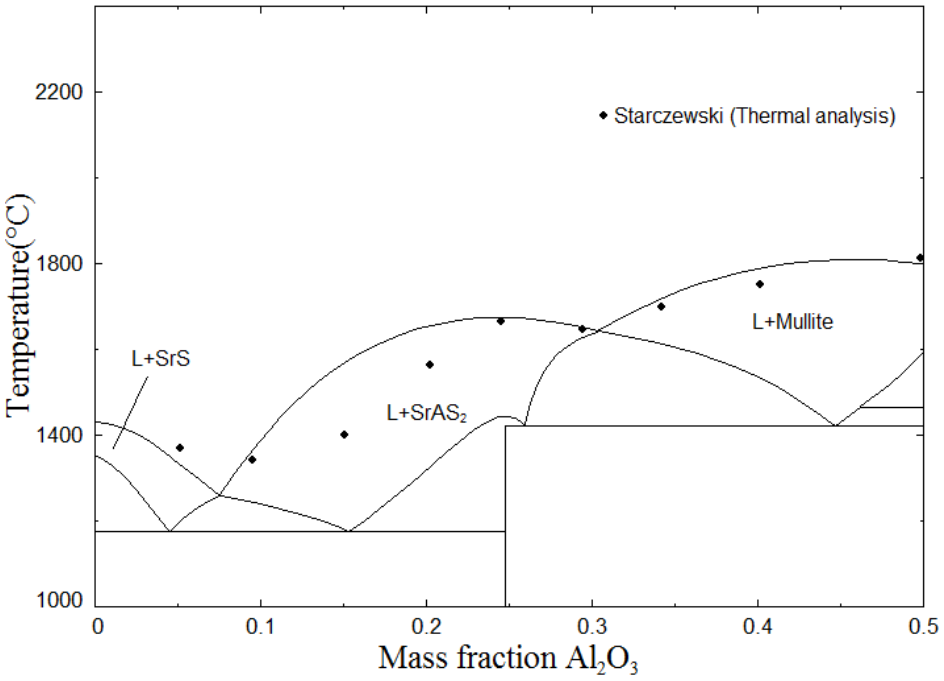

Fig. 3.16.18 Optimized phase diagram of isoplethal section SiO_2=0.50 in the SrO-Al_2O_3-SiO_2 system.

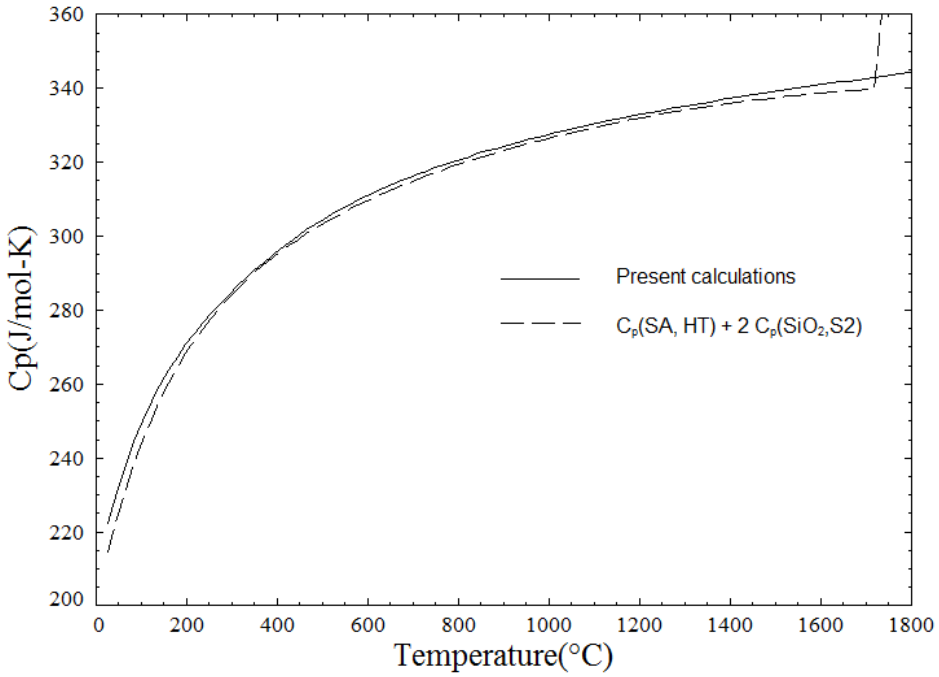

Fig. 3.16.19 Optimized heat capacity of the $SrAl_2Si_2O_8$ phase compared with the other heat capacity scheme.

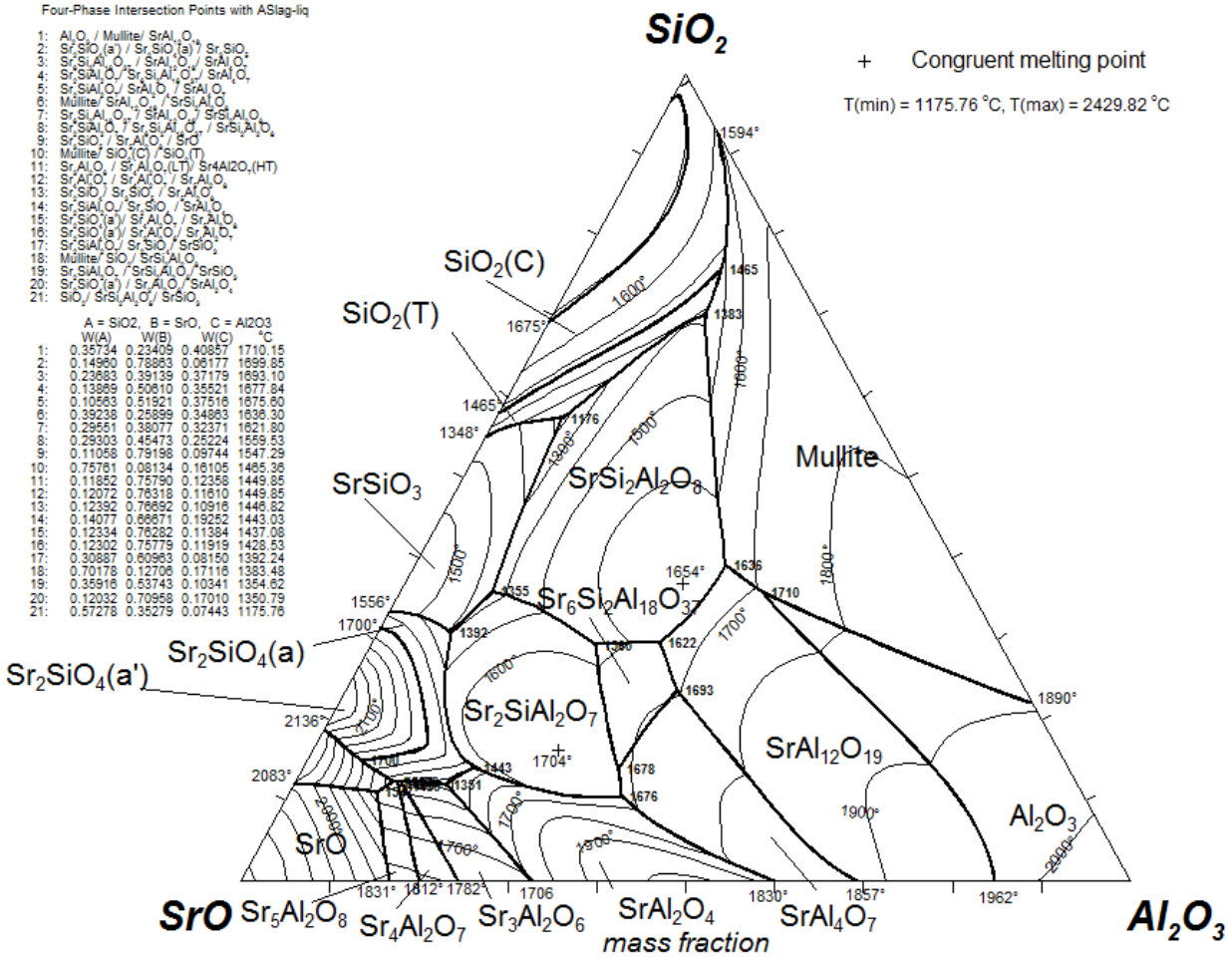

Fig. 3.16.20 Present calculated liquidus (polythermal) projection for the SrO-Al_2O_3-SiO_2 system (isotherms were drawn at the interval of 100 °C).

3.17 The BaO-B_2O_3-SiO_2 system

The Gibbs energy of the liquid phase in the BaO-B_2O_3-SiO_2 ternary system was calculated from the corresponding binary systems by treating BaO as asymmetric component [Pelton and Chartrand (2001)]. The optimized parameters for this ternary system are presented in Table. 3.17.1. For the liquid phase, ternary interaction parameters presented in Table 3.17.1, were also used to obtain the optimal fit of the available data.

Levin and Ugrinic (1953) performed a detailed study on the system by the classical quenching method. Their data are reasonably well reproduced in Figs. 3.17.1 to 3.17.7. Levin and Ugrinic (1953) reported continuous solubility between the binary phases BS_2 and B_2S_3. However, as reported in the BaO-SiO_2 section, this binary system was optimized based on later investigations which disproved this complete solubility, reporting two stoichiometric compounds (B_5S_8 and B_3S_5) between these compositions. Therefore, the solid solubility between the phases BS_2 and B_2S_3 reported by Levin and Ugrinic (1953) does not appear in the present calculations. They also reported the presence of a ternary compound $Ba_3B_6Si_2O_{16}$ ($Ba_3B_2S_2$). No thermodynamic data for this phase could be found in the literature. This phase was modeled as stoichiometric and the optimized properties of this phase are presented in Table. 3.17.1. The liquidus temperature (the temperature at which first solid precipitates from the liquid phase) at various compositions as reported by Levin and Ugrinic (1953) are compared with the present calculations in Table 3.17.2. Hamilton, et al. (1958) by thermal analysis reported isoplethal sections (at constant BaO mol%) in this ternary system. The optimal fit of these data is presented in Figs. 3.17.8-3.17.13. Levin and Cleek (1958) with a temperature gradient apparatus determined dome temperatures (the boundary surface separating the two-liquid region from the one-liquid region). The samples were kept in open cells for 5 to 15 minutes in a horizontal tube furnace maintained in a stable temperature gradient. The quenched samples were then analyzed. The position in the gradient corresponding to the dome temperature was considered to lie midway between the sample-cell showing evidence of single-liquid formation and that showing two-liquid phases in petrographic examinations. In the present modeling, the reproduction of the two liquids region in Fig. 3.17.7, as reported by Levin and Ugrinic (1953), required much higher dome temperatures than reported by Levin and Cleek (1958) as shown in Table 3.17.3. It was observed during calculations that

dome temperatures reported by Levin and Cleek (1958) could be fitted more closely had there be no stable immiscibility region in the binary BaO-SiO_2 system. As reported in the binary BaO-SiO_2 section that there are data reporting both stable and metastable immiscibility region in the silica region part of the BaO-SiO_2 system. But, it was found very difficult to suppress the sable liquid miscibility gap in the SiO_2 region simultaneously with the reproduction of the flat liquidus of SiO_2 as reported by Greig (1927). Hence, it can be said that more experimental work is required to corroborate the dome temperature data of Levin and Cleek (1958). For this ternary immiscibility gap, the monotectic temperature (Table 3.17.2) and monotectic composition (Fig. 3.17.7) are comparatively well reproduced.

Z. G. Tyurnina, Lopatin, and Stolyarova (2008), at 1377 °C and 1457 °C, by high-temperature mass spectrometry measured the activities in the BaO-B_2O_3-SiO_2 melt at constant BaO mol%. These activities are compared with the present calculated activities at 1427 °C (according to the present calculations, the activities at 1377 and 1457 °C are practically the same) in Figs. 3.17.14-3.17.18. (the different experimental points at the same composition in these figures correspond to the two different temperature; in the scale of these figures there is practically no difference in the calculated activities in this temperature range. Therefore the present calculations were performed at 1417 °C). It must be noted that Tyurnina and coworkers measured some of these activities in the two-phase liquid region (for X_{BaO} = 0.1 and 0.2). Achievement of equilibrium in such a highly viscous liquid phase, especially in the two-phase region, is quite sluggish. Tyurnina and coworkers did not mention in their publication the time given to samples to reach equilibrium. Moreover, careful analyses of their data make them dubious. For example, in Figs. 3.17.14-

3.17.18 the silica activity first increases and then decreases with increasing silica content. This is not possible because increasing silica content should increase silica activity. At X_{BaO} = 0.5 (Fig. 3.17.18), the BaO activity is higher than that of SiO_2 and B_2O_3. In the present work, many ternary phase diagram data in this region and temperature range were reproduced quite well. Therefore, it seems unlikely that the present calculated BaO activities can deviate so much from the experimental data. More experimental work is required to corroborate these activities data from Tyurnina and coworkers.

Table 3.17.1 Optimized thermodynamic parameters, in Joules, in the BaO-B_2O_3-SiO_2 system.

$Ba_3B_6Si_2O_{16}$ ($Ba_3B_3S_2$)		
ΔH^0_{298} = –7794000 J/mol	S^0_{298} = 577.500 ΔS^0_{298} [b] = 48.009	ΔS^0_{298} [a] = 116.523
T_m [c] = 1014 °C, Exp.= 1014 °C		
$C_p = C_p(BaB_2) + C_p(BaB) + C_p(BS) + C_p(SiO_2,S_2)$		
Liquid phase (Ternary interaction parameters) (in Joules)		
$g^{301}_{\text{B-Ba(Si)}}$ = 58576		
$g^{102}_{\textit{Si-Ba(B)}}$ = –50208		

[a] oxides (stable at room-temperature) as reference
[b] compounds used to calculate the heat capacity as reference
[c] congruent melting temperature

Table 3.17.2 Liquidus temperature as reported by Levin and Ugrinic (Exp.) compared with the present calculations. (Compositions in wt.%)

S.No.	SiO_2	BaO	B_2O_3	Experimental	Present	Diff.
1	33.77	51.21	15.02	1066	1016	-50
2	35.16	51.89	12.95	1103	1062	-41
3	39.23	53.83	6.94	1243	1224	-19
4	26.49	54.6	18.91	1002	984	-18
5	25.91	54.61	19.48	999	987	-12
6	29.28	54.94	15.78	1055	1021	-34
7	33.14	55.16	11.7	1150	1106	-44
8	37.49	55.58	6.93	1243	1230	-13
9	27.36	55.69	16.95	1050	1002	-48
10	40.76	56.35	2.89	1345	1349	4
11	38.14	56.56	5.3	1277	1288	11
12	28.68	56.71	14.61	1078	1048	-30
13	34.28	56.89	8.83	1214	1183	-31
14	29.91	57.25	12.84	1130	1089	-41
15	24.21	57.73	18.06	1023	992	-31
16	23.33	57.81	18.86	1005	991	-14
17	24.2	58.6	17.2	1048	1012	-36
18	23.22	59.15	17.63	1010	1007	-3
19	24.74	59.47	15.79	1049	1042	-7
20	26.18	59.88	13.94	1085	1080	-5
21	34.01	59.02	6.97	1238	1248	10
22	33.01	59.98	7.01	1244	1251	7
23	23.63	60.21	16.16	1042	1037	-5
24	27.76	60.41	11.83	1125	1128	3
25	24.98	60.49	14.53	1073	1070	-3
26	28.06	61.13	10.81	1152	1154	2
27	20.45	61.42	18.13	1000	1003	3
28	29.64	61.46	8.9	1201	1202	1
29	31.57	61.47	6.96	1245	1255	10
30	30.69	61.68	7.63	1226	1237	11
31	24.86	61.74	13.4	1089	1095	6
32	23	62.29	14.71	1064	1067	3
33	34.61	62.49	2.9	1365	1371	6
34	19.17	62.53	18.3	994	999	5
35	21.05	62.87	16.08	1040	1039	-1
36	19.2	63.42	17.38	1001	1013	12

37	33.36	63.59	3.05	1350	1366	16
38	26.07	64.8	9.13	1182	1192	10
39	18.13	64.92	16.95	1001	1017	16
40	18.78	66.01	15.21	1036	1044	8
41	15.13	66.62	18.25	976	979	3
42	21.23	67.15	11.62	1102	1112	10
43	23.68	67.22	9.1	1164	1173	9
44	14.35	67.52	18.13	947	970	23
45	15.68	67.65	16.67	982	997	15
46	22.31	67.81	9.88	1145	1146	1
47	15.71	68.48	15.81	995	1002	7
48	14.24	68.57	17.19	965	973	8
49	23.45	68.61	7.94	1237	1193	-44
50	12.3	70.02	17.68	964	965	1
51	14.07	70.22	15.71	1016	980	-36
52	21.1	71.04	7.86	1305	1212	-93
53	10.3	72.01	17.69	975	963	-12
54	15.87	72.08	12.05	1189	1074	-115
55	15.96	74.13	9.91	1250	1189	-61
56	6.91	74.93	18.16	961	993	32
57	12.23	75.69	12.08	1160	1188	28
58	5.7	76.06	18.24	950	1012	62
59	8.19	76.11	15.7	1038	1094	56
60	5.29	76.83	17.88	954	1034	80
61	4.86	77.61	17.53	959	1055	96
62	4.64	78.02	17.34	962	1065	103
63	16.04	76.01	7.95	1308	1335	27
64	12.75	76.71	10.54	1263	1276	13
65	10.23	77.99	11.78	1224	1277	53
66	5.48	78.4	16.12	1055	1121	66
67	7.85	78.72	13.43	1274	1235	-39
68	6.41	79.16	14.43	1223	1201	-22
69	2.42	77.82	19.76	910	931	21
70	3.54	80.04	16.42	1077	1098	21
71	1.9	83.05	15.05	1206	1165	-41
72	1.33	54.88	43.79	897	903	6
73	2.16	56.46	41.38	926	934	8
74	9.07	62.8	28.13	1002	1005	3
75	8.11	63.47	28.42	1028	1017	-11
76	6.01	64.93	29.06	1054	1042	-12
77	11.68	65.09	23.23	993	999	6

78	11.12	65.82	23.06	992	1004	12
79	12.94	66.98	20.08	969	984	15
80	11.48	67.22	21.3	984	998	14
81	7.03	69.41	23.56	1025	1035	10
82	4.69	69.58	25.73	1077	1059	-18
83	9.09	69.84	21.07	1003	1008	5
84	11.44	70.24	18.32	962	974	12
85	9.96	71.38	18.66	968	978	10
86	3.07	71.41	25.52	1057	1063	6
87	6.14	74.23	19.63	951	978	27
88	6.45	74.7	18.85	939	969	30
89	3	77	20	925	940	15
90	5.66	39.3	55.04	845	860	15
91	6.94	40.26	52.8	841	858	17
92	3.62	40.57	55.81	858	870	12
93	2.49	42.42	55.09	877	880	3
94	10.1	42.65	47.25	841	851	10
95	11.21	43.49	45.3	840	850	10
96	5.98	44.21	49.81	870	868	-2
97	7.31	46.25	46.44	885	862	-23
98	4.39	48.05	47.56	884	876	-8
99	4.55	48.55	46.9	884	876	-8
100	1.39	52.9	45.71	906	898	-8
101	1.94	53.69	44.37	897	893	-4
102	20	18	62	874	858	-16
103	33.65	23.24	43.11	830	847	17
104	15.38	29.63	54.99	841	857	16
105	7.69	32.33	59.98	861	859	-2
106	4.81	33.34	61.85	870	860	-10
107	2.4	34.18	63.42	875	845	-30
108	3.43	36.7	59.87	864	861	-3
109	5.44	37.62	56.94	854	815	-39
110	4.88	38.71	56.41	845	861	16
111	2.81	39.33	57.86	861	870	9
112	50	17.51	32.49	830	941	111
113	42.97	29.85	27.18	1018	1050	32
114	50.62	34.13	15.25	1350	1292	-58
115	18.55	42.63	38.82	915	930	15
116	8.81	39.28	51.91	826	856	30
117	11.12	40.36	48.52	838	852	14
118	13.2	41.37	45.43	834	847	13

119	14.17	41.81	44.02	860	859	-1
120	15.53	42.46	42.01	860	888	28
121	16.11	43.91	39.98	891	906	15
122	34.83	45.05	20.12	1102	1122	20
123	21.92	45.56	32.52	955	958	3
124	26.39	47.69	25.92	1101	968	-133
125	28.72	48.79	22.49	1008	964	-44
126	27.87	49.79	22.34	1005	967	-38
127	30.98	49.89	19.13	1015	957	-58
128	32.47	50.59	16.94	1032	977	-55
129	26.74	50.64	22.62	1002	975	-27
130	27.9	50.69	21.41	1005	972	-33
131	25.49	51.43	23.08	1000	981	-19
132	13.15	44.98	41.87	850	845	-5
133	14.26	45.8	39.94	897	898	1
134	8.08	47.43	44.49	904	883	-21
135	17.03	47.92	35.05	965	938	-27
136	8.77	48.49	42.74	924	903	-21
137	9.12	49.02	41.86	936	913	-23
138	4.79	49.25	45.96	890	877	-13
139	5.03	49.95	45.02	904	885	-19
140	20.91	50.85	28.24	986	979	-7
141	26.8	52.06	21.14	995	980	-15
142	22.58	52.09	25.33	997	989	-8
143	11.12	52.1	36.78	985	963	-22
144	2.69	53.41	43.9	900	889	-11
145	24.52	53.56	21.92	998	992	-6
146	15.56	53.66	30.78	1003	994	-9
147	18.71	54.11	27.18	1000	1001	1
148	21.31	54.32	24.37	1001	1001	0
149	6.17	54.38	39.45	957	949	-8
150	24.87	54.46	20.67	999	992	-7
151	9.26	55.24	35.5	988	982	-6
152	11.76	55.72	32.52	1002	998	-4
153	13.97	56.56	29.47	1005	1009	4
154	16.06	57.15	26.79	1008	1012	4
155	17.96	57.67	24.37	1008	1012	4
156	7.43	57.72	34.85	985	984	-1
157	18.51	57.83	23.66	1005	1010	5
158	20.06	58.11	21.83	1005	1005	0
159	15.22	58.3	26.48	1013	1014	1

160	21.86	58.63	19.51	1002	994	-8
161	21.75	59.82	18.43	997	996	-1
162	19.21	61.3	19.49	995	987	-8
163	11.07	61.41	27.52	1007	1003	-4
164	14.33	62.44	23.23	996	995	-1
165	15.56	63.13	21.31	998	984	-14
166	17.1	64.2	18.7	978	987	9
167	13.84	64.77	21.39	985	979	-6
168	12.49	65.41	22.1	972	992	20

Table 3.17.3 Dome temperatures as reported by Levin and Cleek (Exp.) compared with the present calculations (Cal.). (Compositions in wt.%).

S.No.	BaO	B_2O_3	SiO_2	Exp.	Cal.
1	31.8	65.5	2.7	864-877	1008
2	30.3	60.7	9	995-1004	1177
3	32.5	56.2	11.3	953	1170.9
4	22.8	64.9	12.3	1178	1342.7
5	10.4	77.2	12.4	1215	1345
6	36.5	46.1	17.4	915-918	1177.51
7	37.8	38.5	23.7	1010-1022	1224.03
8	35.5	40.2	24.3	1090	1298.98
9	22.7	52.8	24.5	1235	1498.04
10	10.4	65	24.6	1230	1458.19
11	42.8	29.3	27.9	960	1063.91
12	10.6	52.9	36.5	1260	1565.56
13	22.4	40.9	36.7	1285	1624.15
14	22.1	17.8	60.1	1370	1805.99

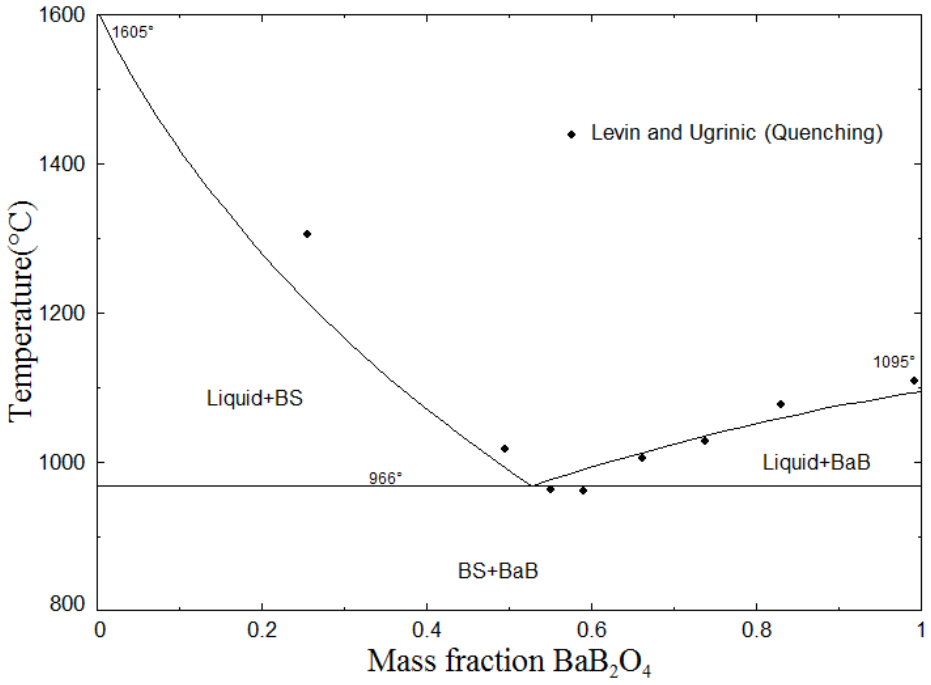

Fig. 3.17.1 Optimized phase diagram of the $BaSiO_3$-BaB_2O_4 section.

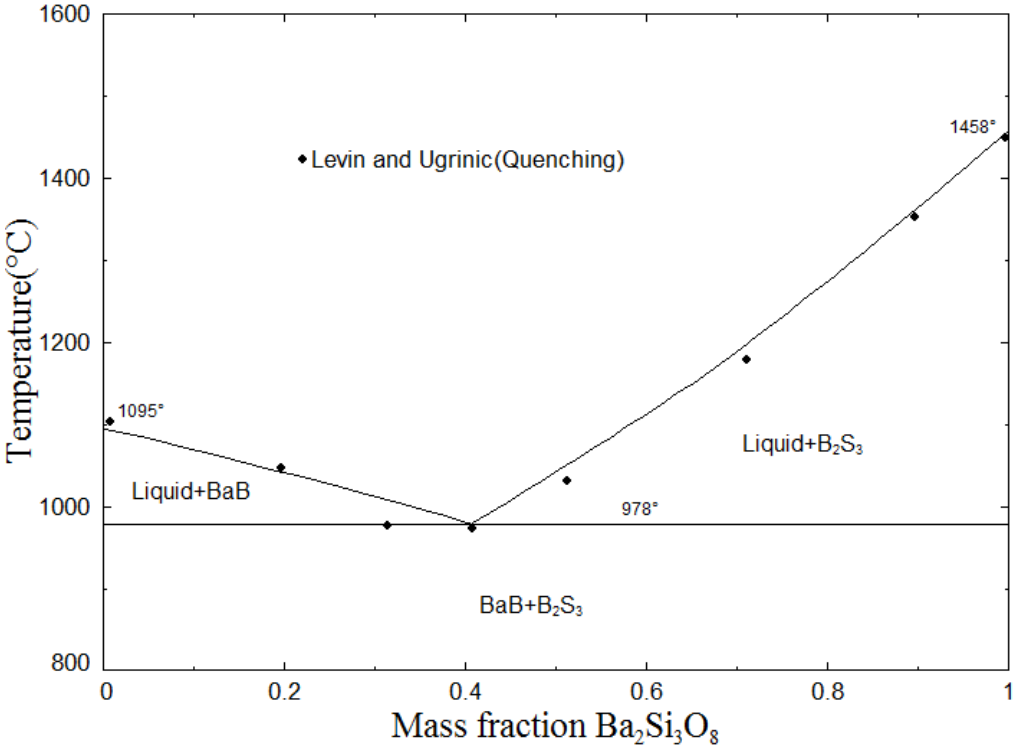

Fig. 3.17.2 Optimized phase diagram of the BaB_2O_4-$Ba_2Si_3O_8$ section.

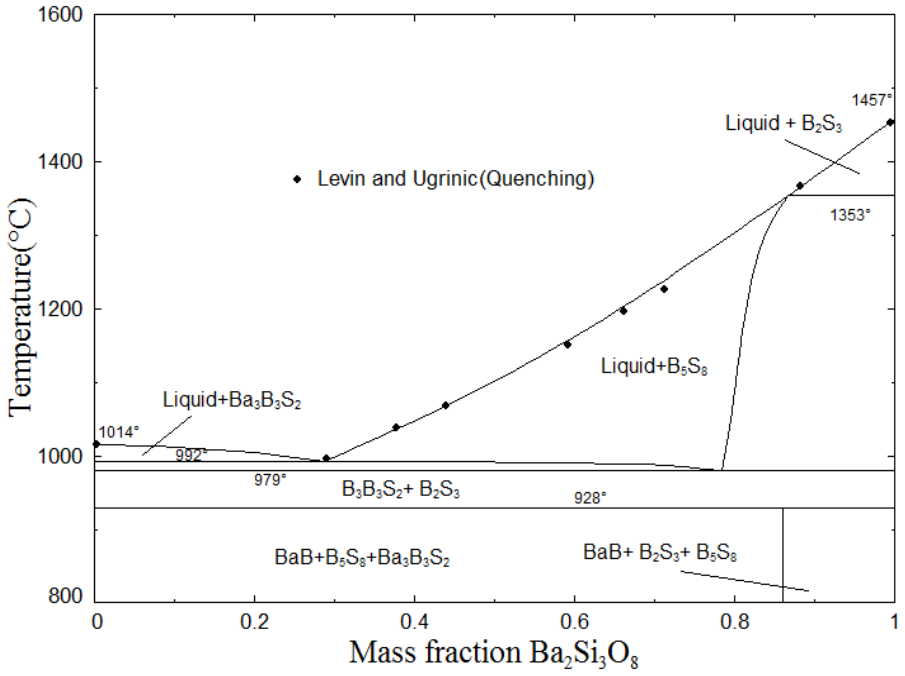

Fig. 3.17.3 Optimized phase diagram of the $Ba_3Si_2B_6O_{16}$-$Ba_2Si_3O_8$ section.

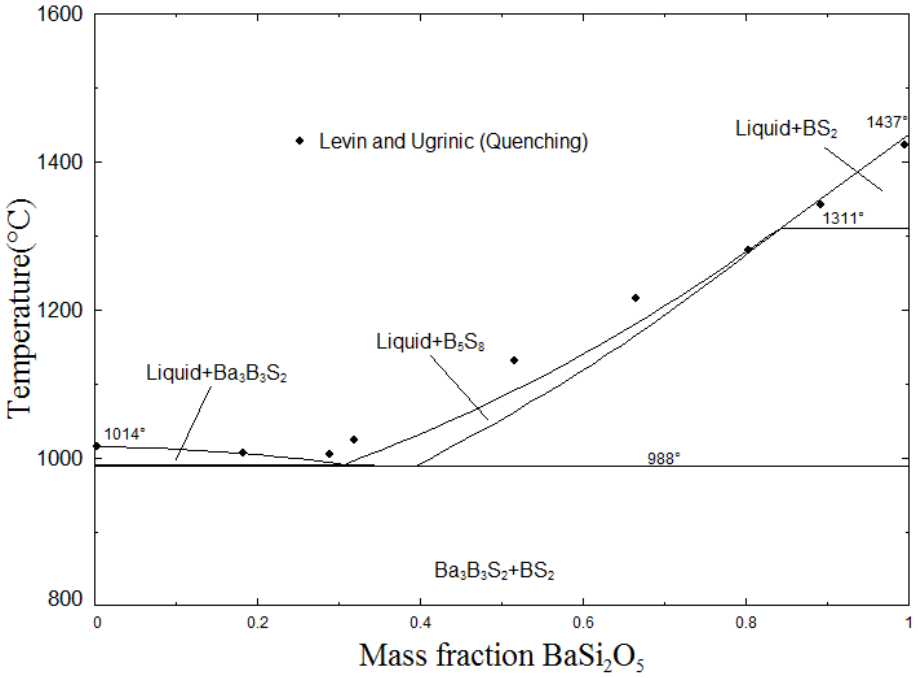

Fig. 3.17.4 Optimized phase diagram of the $Ba_3Si_2B_6O_{16}$-$BaSi_2O_5$ section.

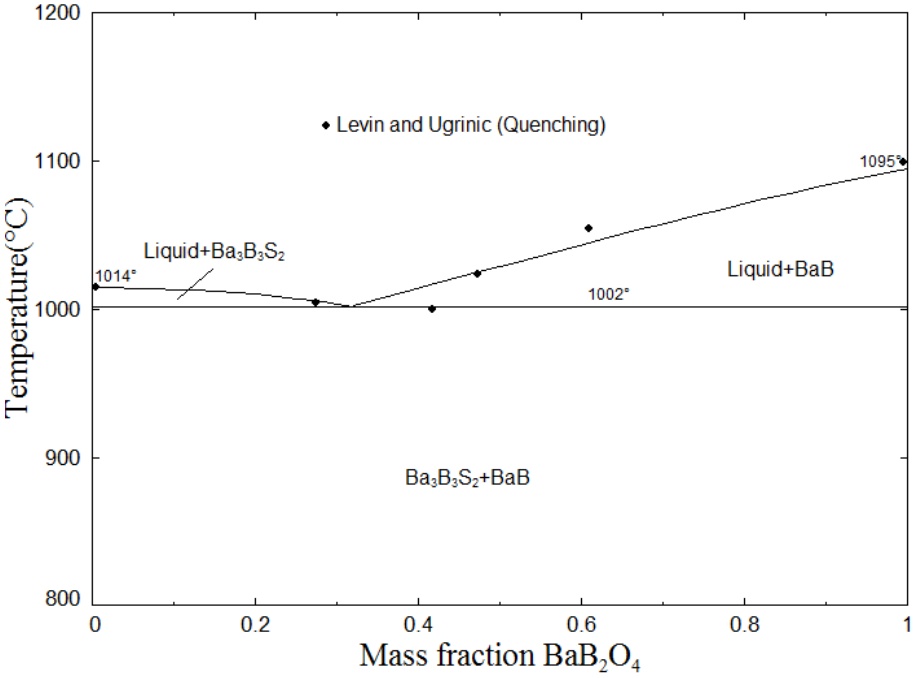

Fig. 3.17.5 Optimized phase diagram of the $Ba_3Si_2B_6O_{16}$-BaB_2O_4 section.

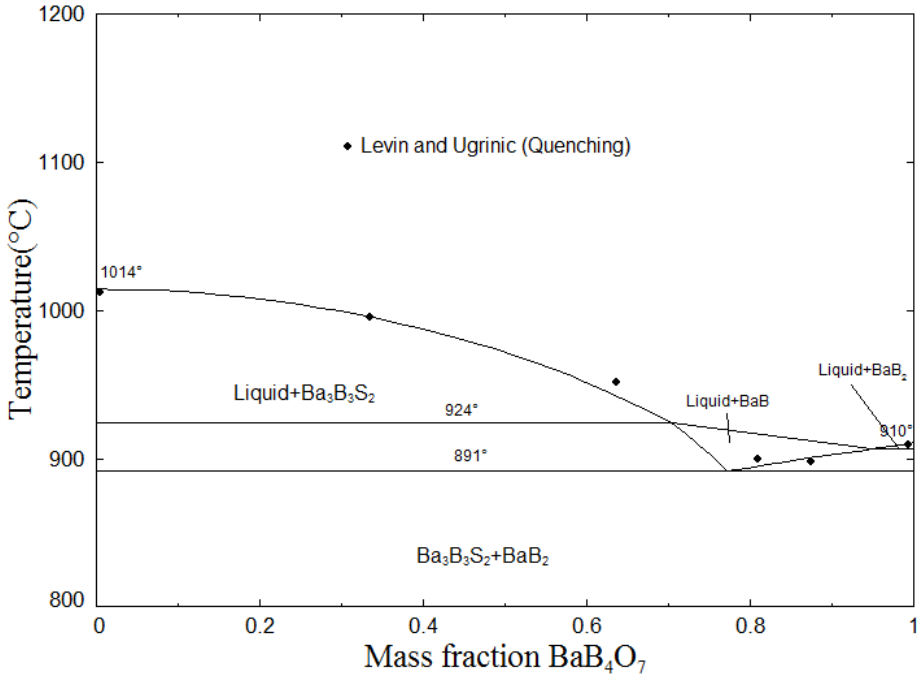

Fig. 3.17.6 Optimized phase diagram of the $Ba_3Si_2B_6O_{16}$-BaB_4O_7 section.

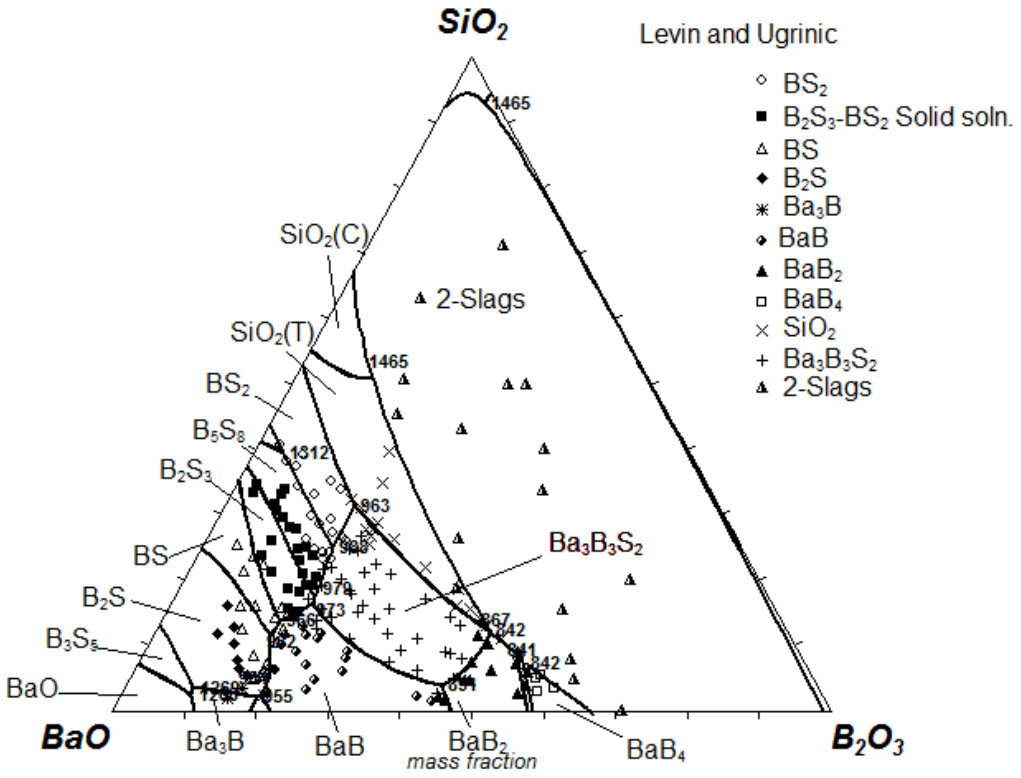

Fig. 3.17.7 The present calculated polythermal projection of the BaO-B_2O_3-SiO_2 system comparing the primary phase regions reported by Levin and Ugrinic.

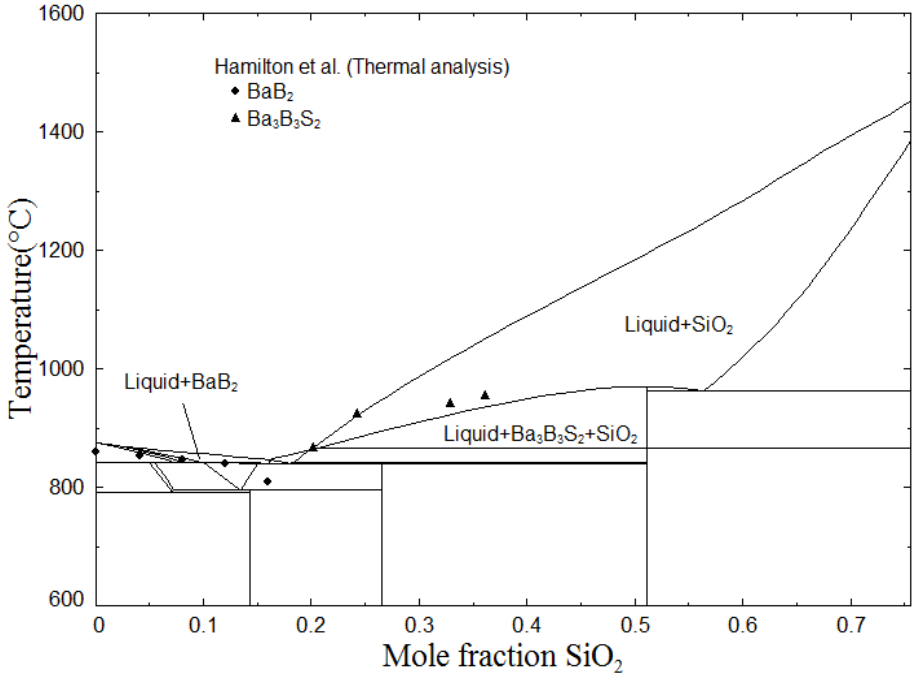

Fig. 3.17.8 Optimized isoplethal section at X_{BaO}=0.245.

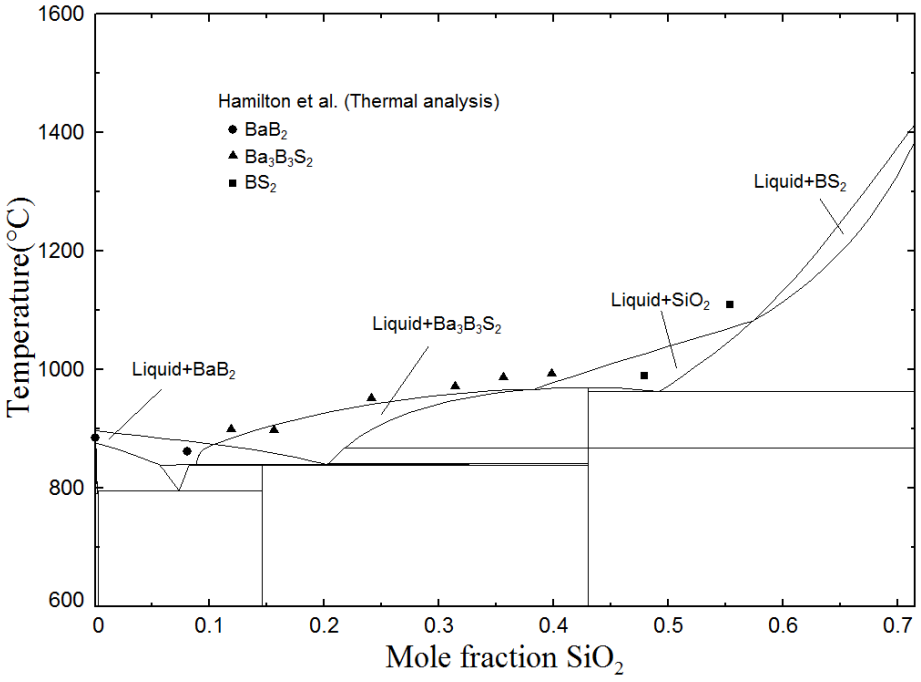

Fig. 3.17.9 Optimized isoplethal section at X_{BaO}=0.285.

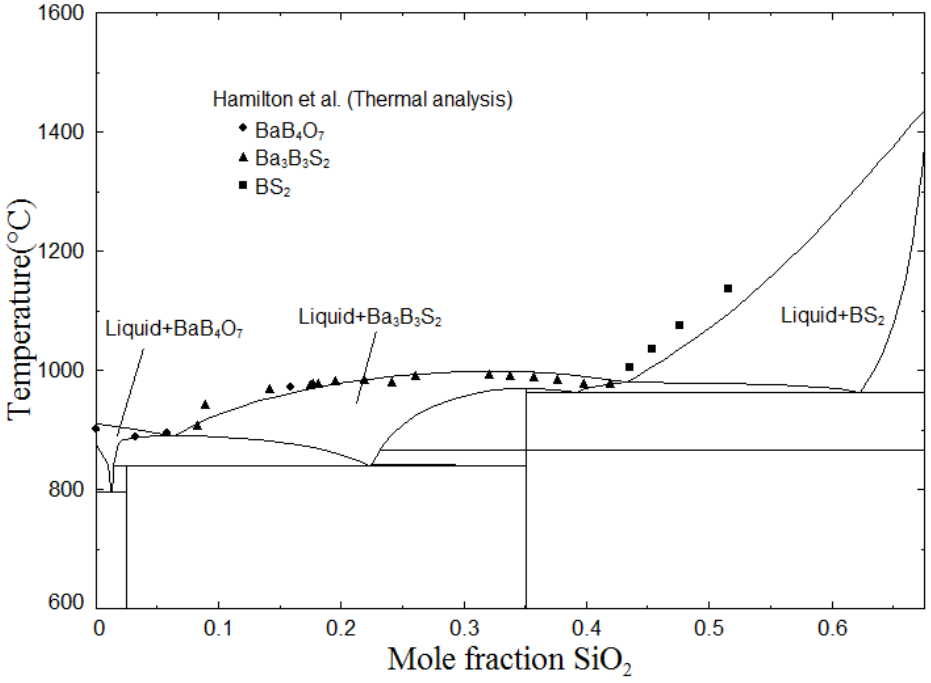

Fig. 3.17.10 Optimized isoplethal section at X_{BaO}=0.325.

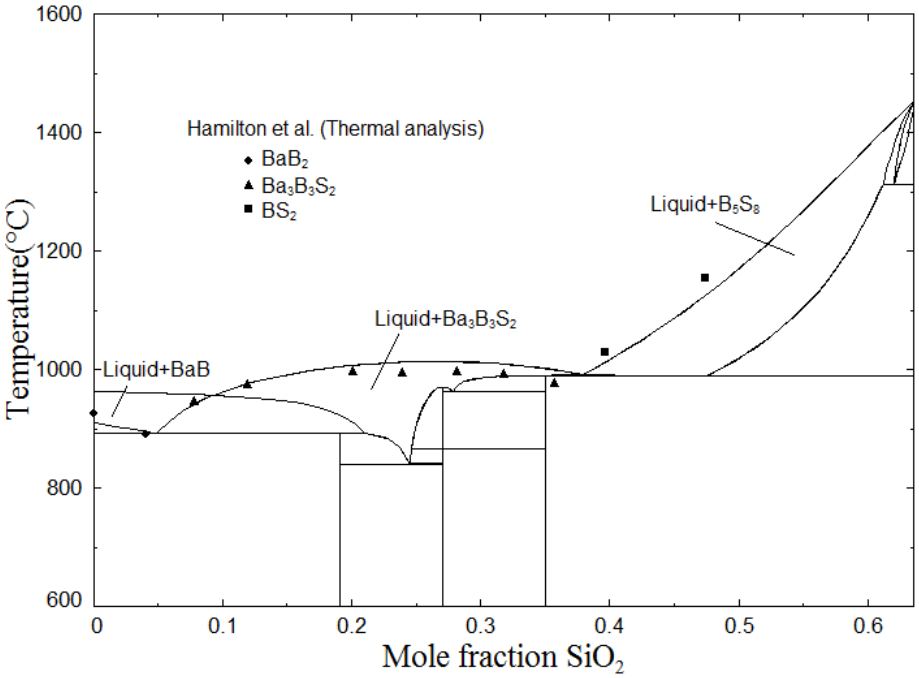

Fig. 3.17.11 Optimized isoplethal section at X_{BaO}=0.365.

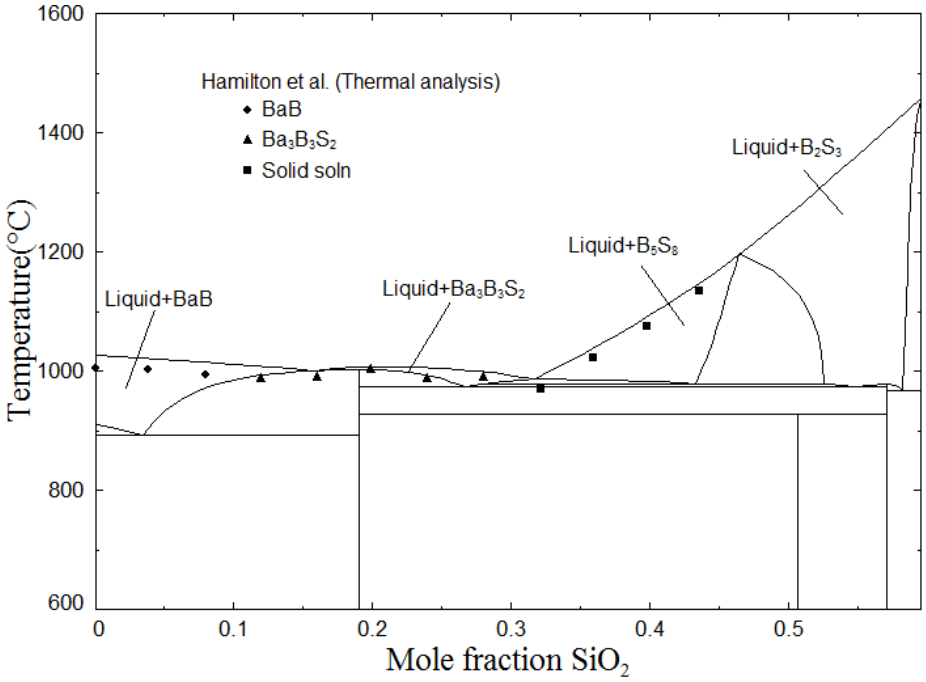

Fig. 3.17.12 Optimized isoplethal section at X_{BaO}=0.405.

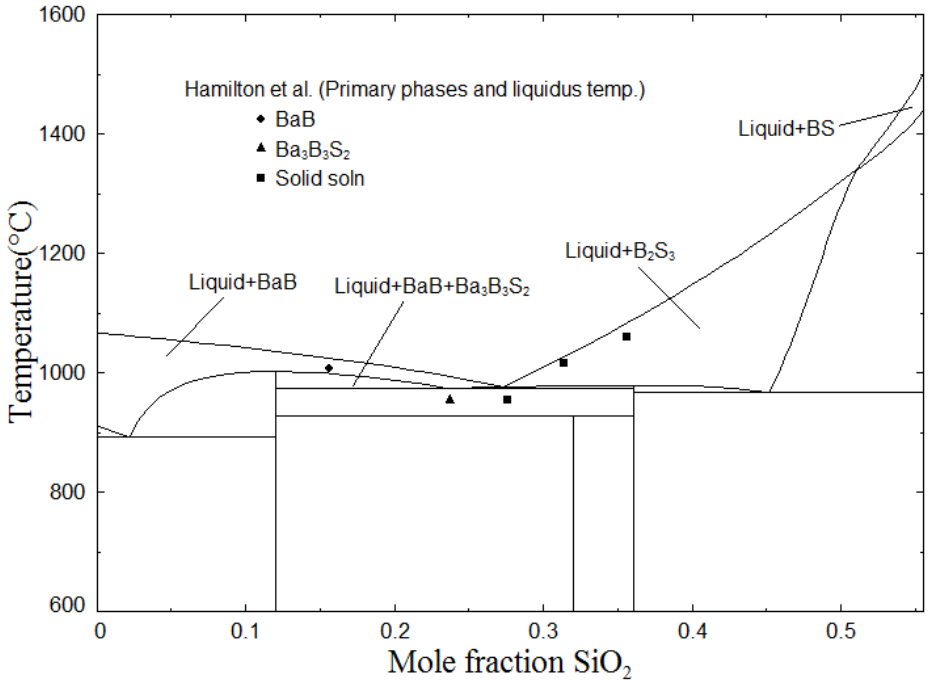

Fig. 3.17.13 Optimized isoplethal section at X_{BaO}=0.44.

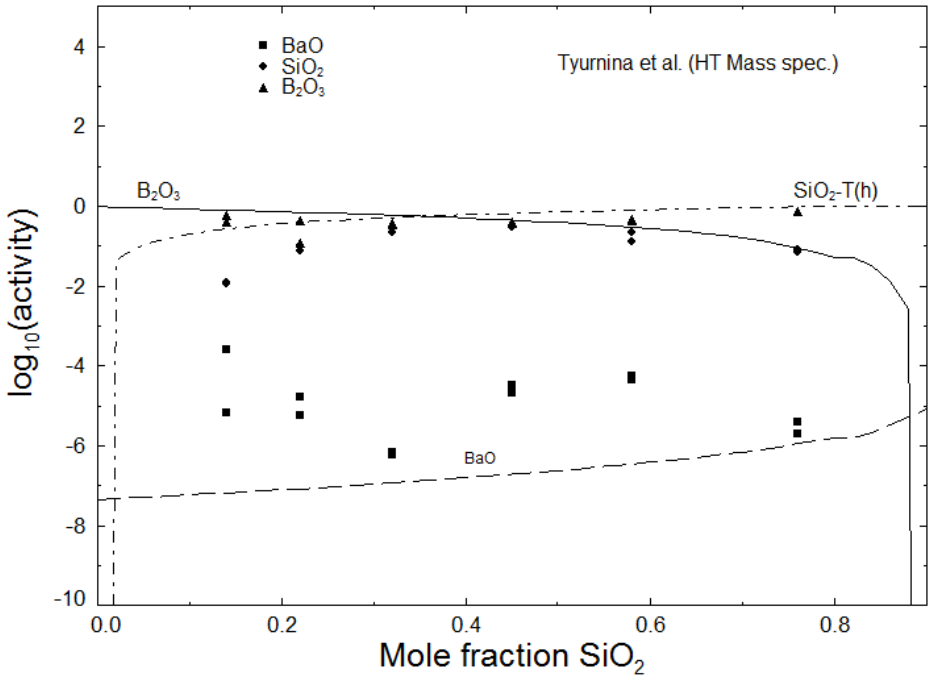

Fig. 3.17.14 Activities on the isoplethal section X_{BaO} =0.1 in the BaO-B_2O_3-SiO_2 system at 1427 °C (Std. states; solid for BaO and SiO_2 and liquid for B_2O_3).

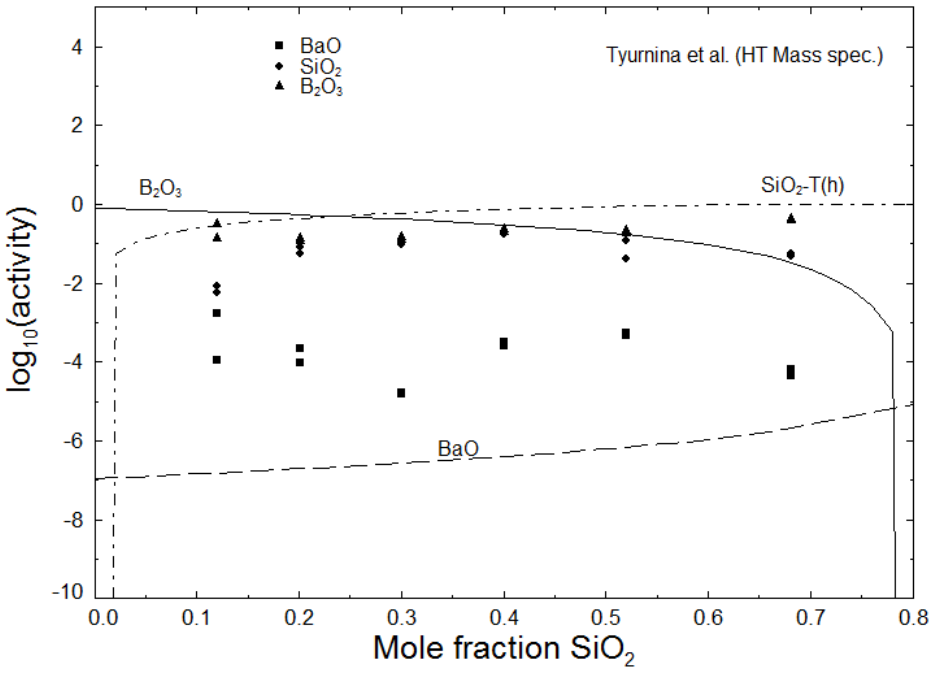

Fig. 3.17.15 Activities on the isoplethal section X_{BaO} =0.2 in the BaO-B_2O_3-SiO_2 system at 1427 °C (Std. states; solid for BaO and SiO_2 and liquid for B_2O_3).

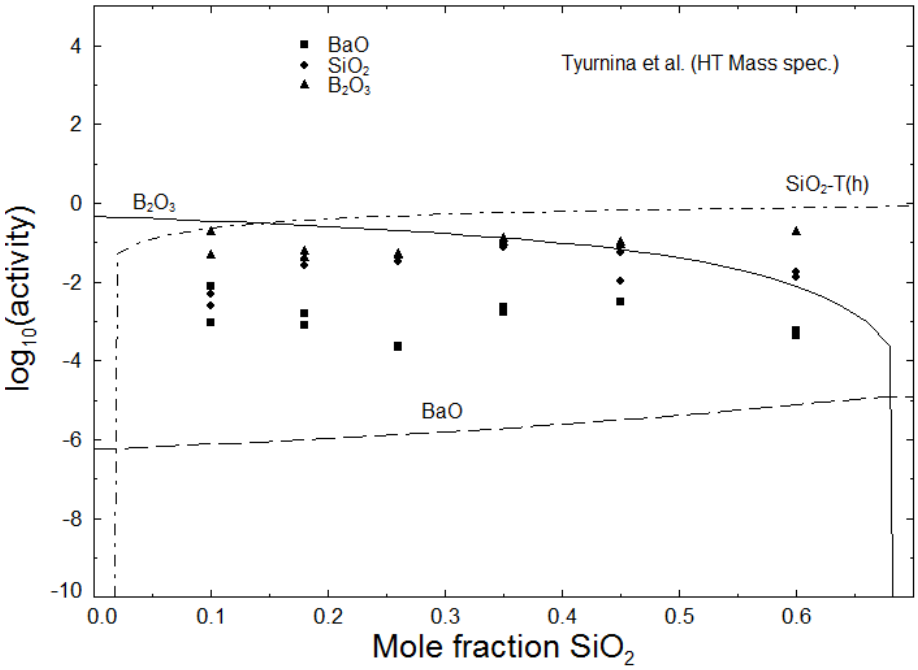

Fig. 3.17.16 Activities on the isoplethal section X_{BaO} =0.3 in the BaO-B_2O_3-SiO_2 system at 1427 °C (Std. states; solid for BaO and SiO_2 and liquid for B_2O_3).

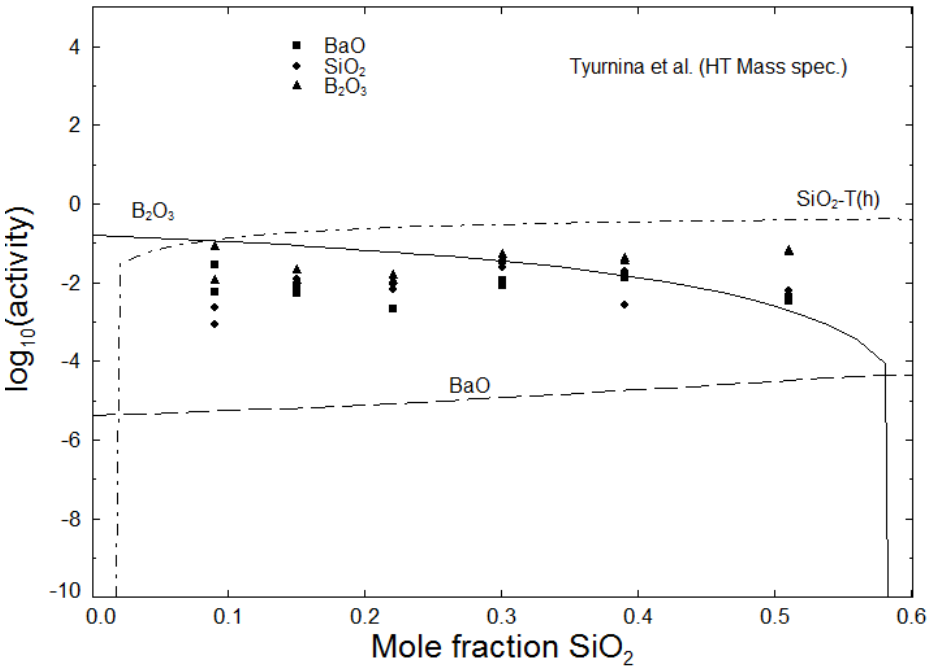

Fig. 3.17.17 Activities on the isoplethal section X_{BaO} =0.4 in the BaO-B_2O_3-SiO_2 system at 1427 °C (Std. states; solid for BaO and SiO_2 and liquid for B_2O_3).

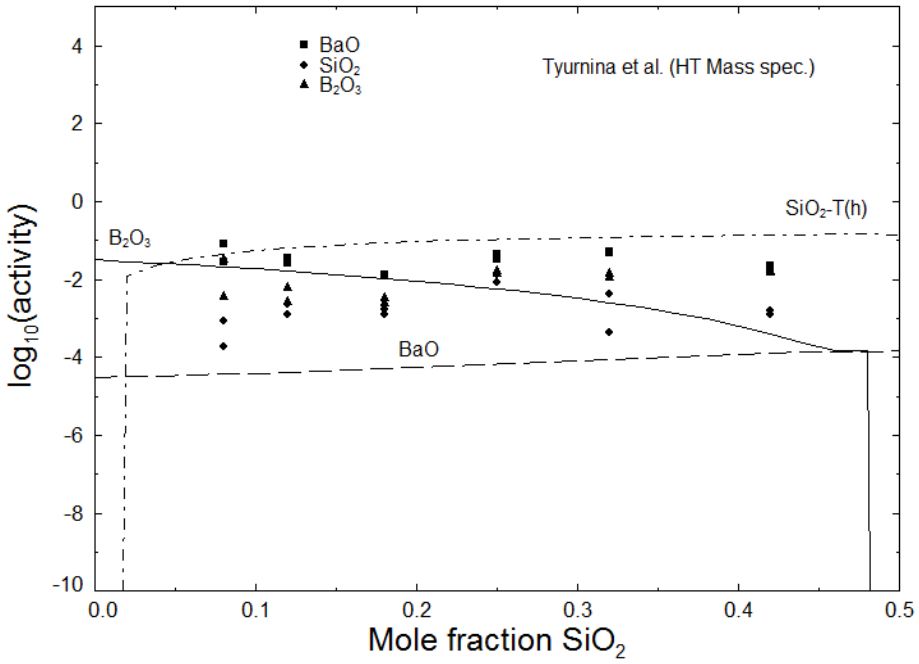

Fig. 3.17.18 Activities on the isoplethal section X_{BaO} =0.5 in the BaO-B_2O_3-SiO_2 system at 1427 °C (Std. states; solid for BaO and SiO_2 and liquid for B_2O_3).

3.18 The $SrO-B_2O_3-SiO_2$ system

The Gibbs energy of the liquid phase in the $SrO-B_2O_3-SiO_2$ ternary system was calculated from the corresponding binary systems by treating SrO as asymmetric component [Pelton and Chartrand (2001)]. The optimized parameters for this ternary system are presented in Table 3.18.1. For the liquid phase, ternary interaction parameters presented in Table 3.18.1, were also used to obtain the optimal fit of the available data.

Baylor and Brown (1976b) reported sub-solidus phase equilibria, as shown in Fig. 3.18.1, in the $SrO-B_2O_3-SiO_2$ system. These phase equilibria can be compared with the present calculations at 400 °C (the temperature at which no liquid phase appears in this system) in Fig. 3.18.2 However, the present calculations give these same phase equilibria from room temperature to higher temperatures, by emitting the liquid phase from calculations at higher temperatures. Baylor and Brown (1976b) reported the presence of a stable ternary compound $Sr_3B_2SiO_8$ (Sr_3BS). No thermodynamic data for this phase could be found in the literature. The optimized parameters for this phase are presented in Table 3.18.1. Krzhizhanovskaya, Bubnova, Krivovichev, Belousova, and Filatov (2010) reported orthorhombic crystal structure with space group *Pnma* for this phase. N. G. Tyurnina, Belousova, Domanskii, Doronina, and Ugolkov (2010) by DTA reported a congruent melting temperature at 1180 °C for this compound. The present calculated congruent melting temperature is 1166 °C.

N. G. Tyurnina, et al. (2010), by DTA and high-temperature microscope melting techniques, measured eutectic and liquidus temperatures on some of the vertical sections in the $SrO-B_2O_3-$

SiO_2 system. The optimal fits of these data are presented in Figs. 3.18.3-3.18.6. In these figures the DTA peaks (Fig. 16.3) are comparatively better reproduced than the liquidus temperatures (Figs. 16.3-16.6) determined by high-temperature microscopic melting. N. G. Tyurnina, et al. (2010), while presenting the phase diagram for this section, acknowledged the inconsistency between their findings and melting temperatures for the binary phases from the literature. This inconsistency is also visible in the present calculated phase diagram for these sections. Moreover, they also reported that in the B_2O_3-rich samples they overestimated the liquidus temperature because of selective evaporation of B_2O_3 oxide. Hence, more experimental work is required to establish correctly the liquidus temperatures on these sections. In the present work, these data were optimized as shown in Figs. 3.18.3-3.18.6.

Baylor and Brown (1976a) by quenching techniques measured the one- and two-phase liquid regions in the temperature range 1100-1525 °C. Their data are reasonably well reproduced in Table 3.18.2. The compositions at which they obtained a two-phase liquid at equilibrium are also plotted in the Fig. 3.18.7 showing the primary phase field regions in the SrO-B_2O_3-SiO_2 system. This figure also contains the data reported by N. G. Tyurnina, et al. (2010), who also used quenching techniques, on the two-phase liquid region.

In the present work (see chapter 4), quenching experiments followed by EPMA analysis were performed to find the composition of the liquid phase in equilibrium with the SrS phase at 1150, 1050 and 1000 °C. The liquid composition obtained at these three temperatures is also plotted in Fig. 3.18.7 and the present optimization fits them reasonably well. In these experiments the

eutectic temperature comprising SrS, SB and SiO_2 phases was bracketed between 950 and 1000 °C. The present calculated eutectic temperature is 991 °C. The details of these experiments and results are presented in Chapter 4.

Stolyarova, Lopatin, and Shilov (2009), at 1447 °C and 1527 °C, by high-temperature mass spectrometry measured the activities in the SrO-B_2O_3-SiO_2 melt at constant SrO mol%. These activities are compared with the present calculations at 1487 °C (according to present calculations, the activities at 1447 and 1527 °C are practically the same) in Figs. 3.18.8-3.18.13 (the different experimental points at the same composition in these figures correspond to the two different temperatures; in the scale of these figures there is practically no difference in the calculated activities in this temperature range. Therefore the present calculations were performed at 1487 °C). It must be noted that Stolyarova and coworkers measured some of these activities in two-phase liquid region (for X_{SrO} = 0.1 and 0.2). Achievement of equilibrium in such a highly viscous liquid phase, especially in the two-phase region, is quite sluggish. Stolyarova and coworkers did not mention in their publication on the time given to samples to reach equilibrium. Also, the rate of increase in the SrO activity with increase in SrO content is too much. At X_{SrO} = 0.5 and 0.6 (Figs. 3.17.17 and 3.17.18), the SrO activity is more than that of SiO_2 and B_2O_3. It is hard to believe that the present optimized parameters which reasonably fit the other available experimental data will deviate so much from the data of Stolyarova and coworkers. More experimental work is required to corroborate the data by Stolyarova and coworkers.

Table 3.18.1 Optimized thermodynamic parameters, in Joules, in the SrO-B_2O_3-SiO_2 system.

$Sr_3B_2SiO_8$ (Sr_3BSi)		
ΔH^0_{298} = –4342000 J/mol	S^0_{298} = 274.000 ΔS^0_{298} [(b)] = 17.850	ΔS^0_{298} [(a)] = 10.254
T_m = 1180 °C[(c)], Exp. = 1179 °C[(c)]		
$C_p = C_p(Sr_2SiO_4, \alpha') + C_p(SrB_2O_4)$		
Liquid phase (Ternary interaction parameters) (in Joules)		
$g^{301}_{B\text{-}Sr(Si)}$ = 66944		
$g^{102}_{Si\text{-}Sr(B)}$ = 54392		
$g^{002}_{Si\text{-}Sr(B)}$ = –33472		

[(a)] from the compounds used to calculate heat capacity
[(b)] from the oxides
[(c)] incongruent melting

Table 3.18.2 1-phase and 2-phase liquid region as determined by Baylor and Brown (Exp.) compared with the present calculations (Cal.) (Compositions in mol).

SiO_2	SrO	B_2O_3	T(C)	Exp.	Cal.
0.103	0.308	0.589	1100	1-liquid	1-liquid
0.104	0.261	0.635	1100	1-liquid	1-liquid
0.205	0.308	0.487	1250	1-liquid	1-liquid
0.206	0.258	0.536	1250	1-liquid	1-liquid
0.307	0.307	0.386	1325	1-liquid	1-liquid
0.405	0.304	0.291	1325	1-liquid	1-liquid
0.217	0.272	0.511	1250	1-liquid	1-liquid
0.404	0.346	0.250	1325	1-liquid	1-liquid
0.105	0.210	0.685	1100	2-liquids	2-liquids
0.103	0.030	0.867	1320	2-liquids	2-liquids
0.207	0.208	0.585	1250	2-liquids	2-liquids
0.307	0.256	0.437	1325	2-liquids	2-liquids
0.311	0.207	0.482	1325	2-liquids	2-liquids
0.303	0.030	0.667	1325	2-liquids	2-liquids
0.408	0.255	0.337	1325	2-liquids	2-liquids
0.409	0.204	0.387	1325	2-liquids	2-liquids
0.219	0.162	0.619	1275	2-liquids	2-liquids
0.221	0.110	0.669	1275	2-liquids	2-liquids
0.257	0.257	0.486	1275	2-liquids	2-liquids
0.272	0.218	0.510	1275	2-liquids	2-liquids
0.335	0.167	0.498	1335	2-liquids	2-liquids

0.400	0.286	0.314	1425	2-liquids	1-liquid
0.385	0.220	0.395	1425	2-liquids	2-liquids
0.388	0.166	0.446	1425	2-liquids	2-liquids
0.385	0.110	0.505	1425	2-liquids	2-liquids
0.541	0.324	0.135	1525	2-liquids	1-liquid
0.525	0.225	0.250	1525	2-liquids	2-liquids
0.642	0.129	0.229	1525	2-liquids	2-liquids
0.678	0.068	0.254	1525	2-liquids	2-liquids

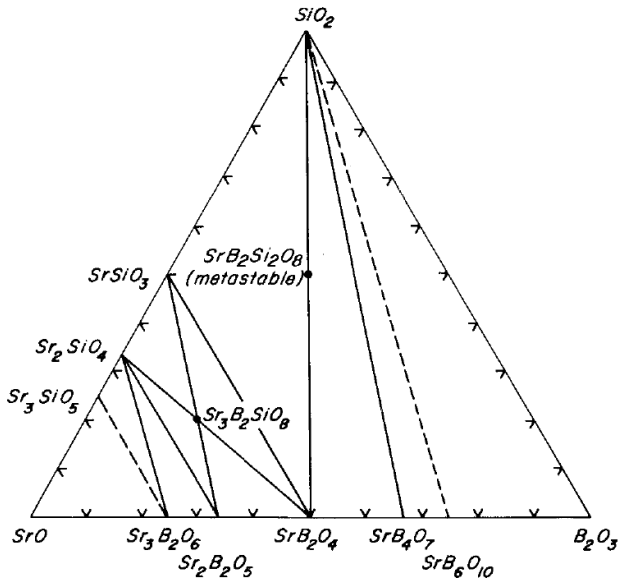

Fig. 3.18.1 Sub solidus phase equilibria as reported by Baylor and Brown.

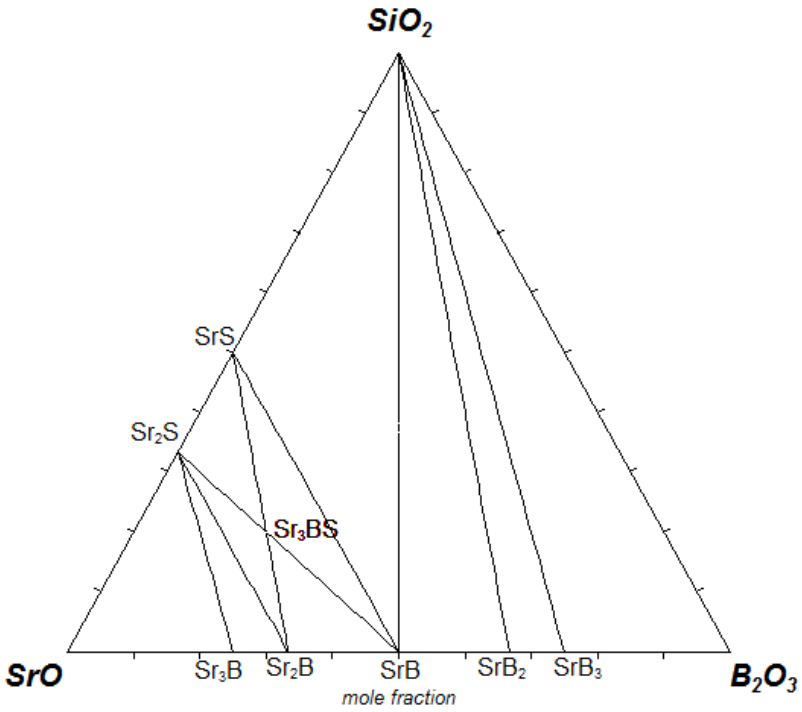

Fig. 3.18.2 Present calculated isothermal section at 400 °C in the SrO-B_2O_3-SiO_2 system.

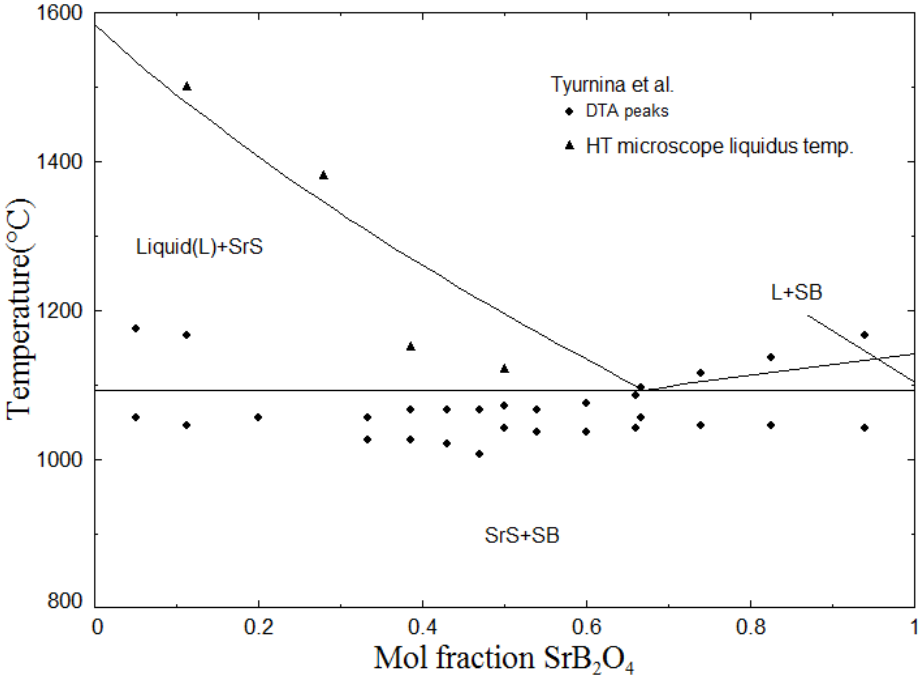

Fig. 3.18.3 Optimized phase diagram of the section $SrSiO_3$-SrB_2O_4.

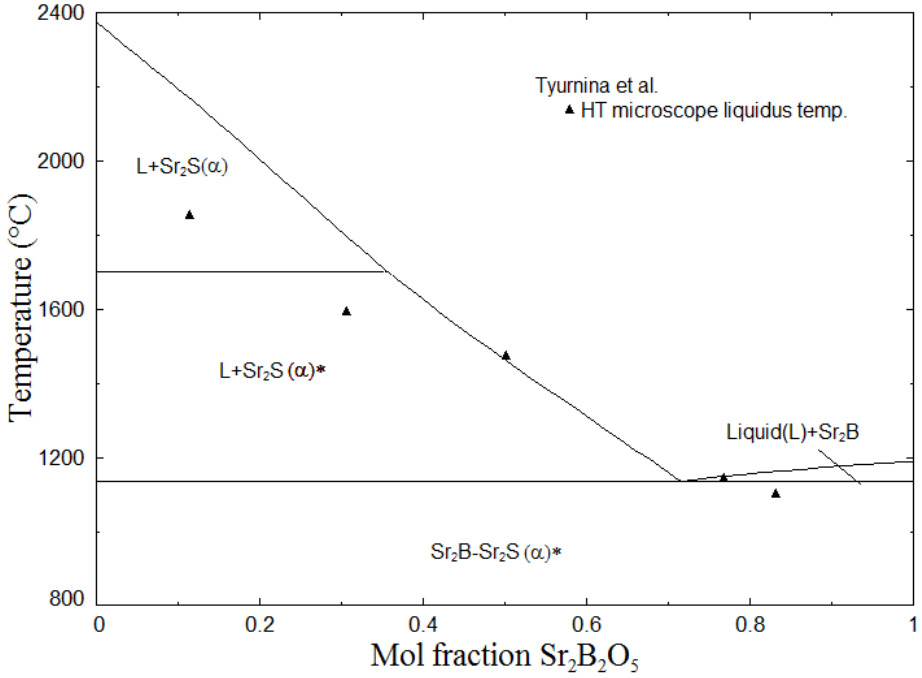

Fig. 3.18.4 Optimized phase diagram of the section Sr_2SiO_4-$Sr_2B_2O_5$.

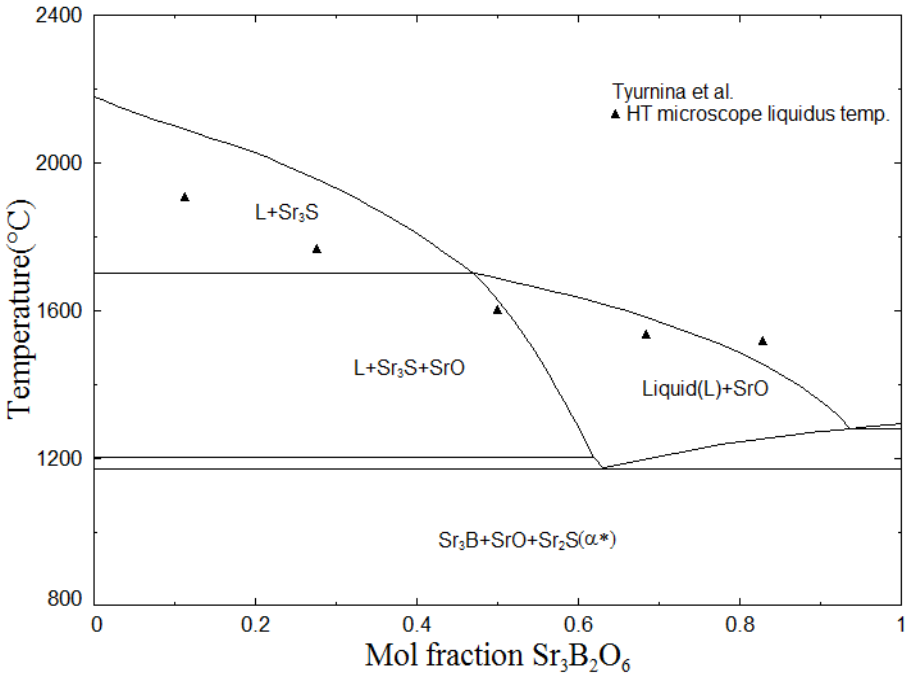

Fig. 3.18.5 Optimized phase diagram of the section Sr_3SiO_5-$Sr_3B_2O_6$.

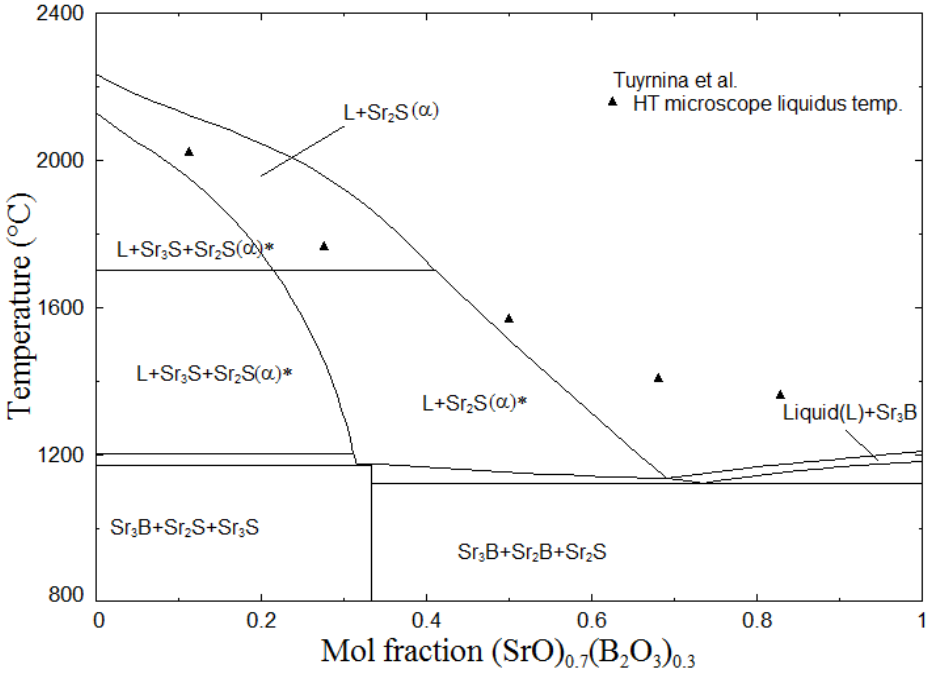

Fig. 3.18.6 Optimized phase diagram of the section $(SrO)_{0.7}(SiO_2)_{0.3}$-$(SrO)_{0.7}(B_2O_3)_{0.3}$.

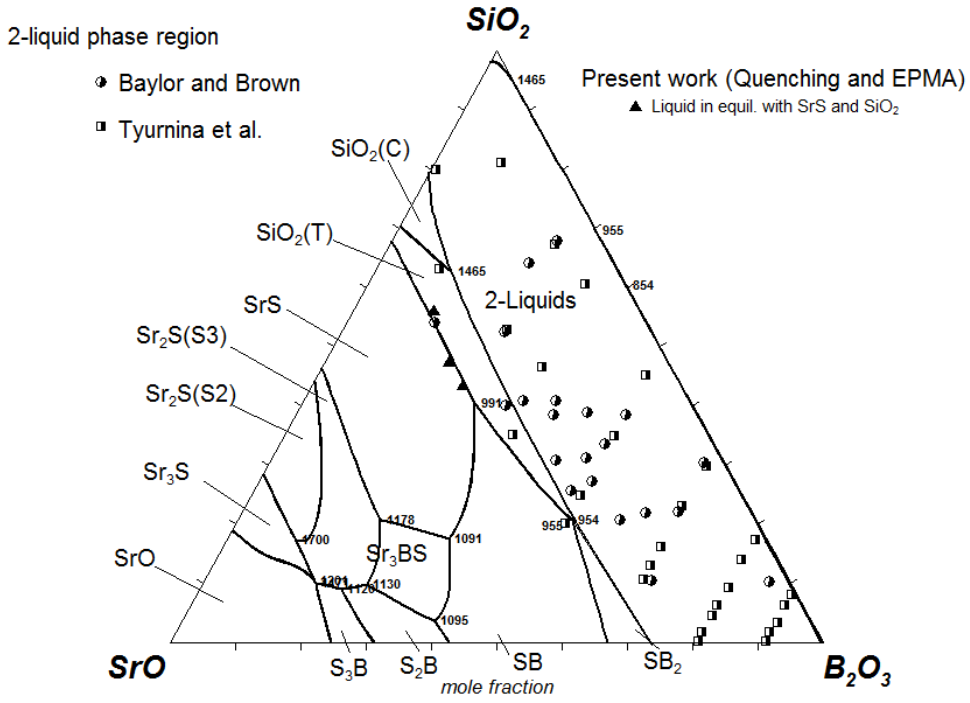

Fig. 3.18.7 Polythermal projection of the SrO-B_2O_3-SiO_2 system.

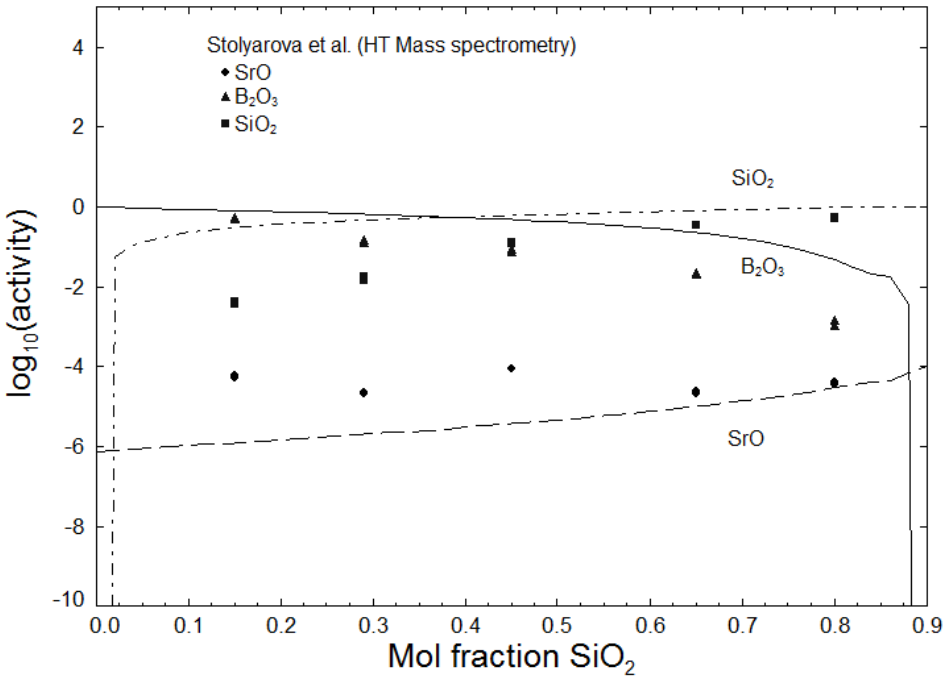

Fig. 3.18.8 Activities on the isoplethal section X_{SrO} =0.1 in the SrO-B_2O_3-SiO_2 system at 1487 °C (Std. states; solid for SrO and SiO_2 and liquid for B_2O_3).

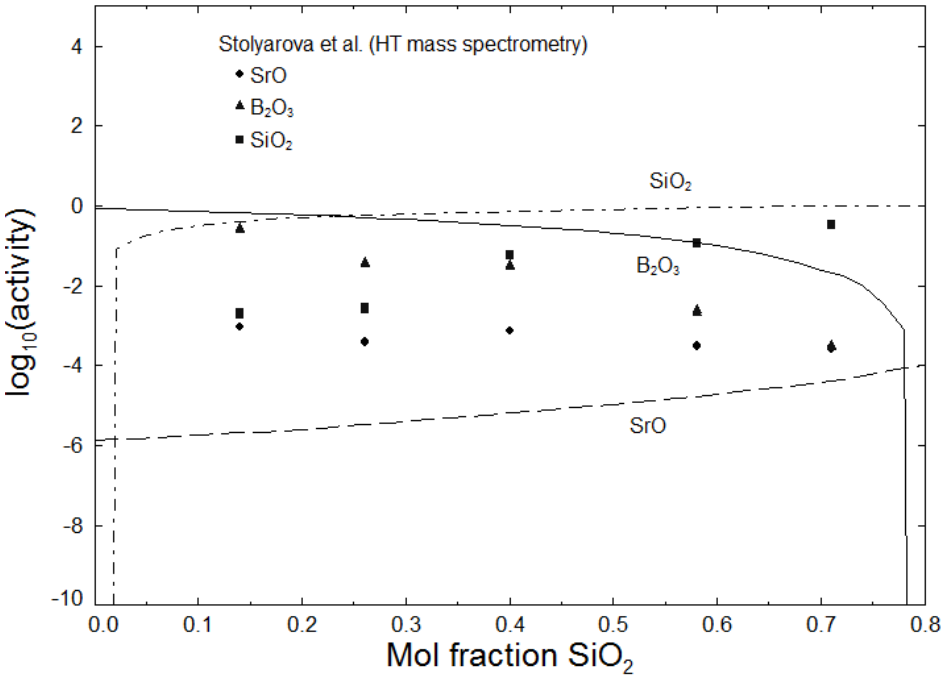

Fig. 3.18.9 Activities on the isoplethal section X_{SrO} =0.2 in the SrO-B_2O_3-SiO_2 system at 1487 °C (Std. states; solid for SrO and SiO_2 and liquid for B_2O_3).

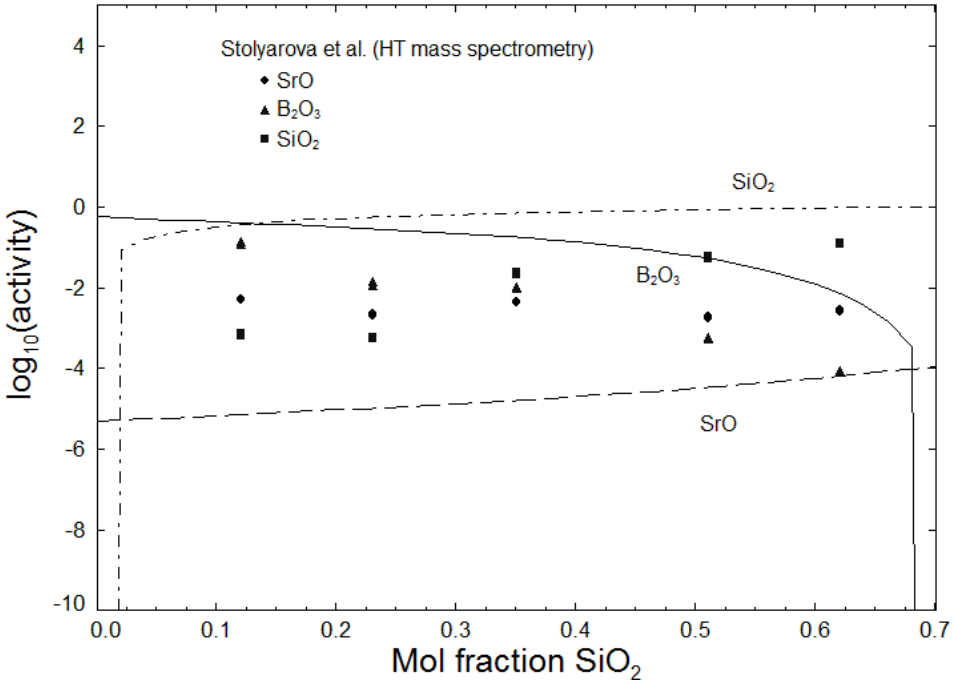

Fig. 3.18.10 Activities on the isoplethal section X_{SrO} =0.3 in the SrO-B_2O_3-SiO_2 system at 1487 °C (Std. states; solid for SrO and SiO_2 and liquid for B_2O_3).

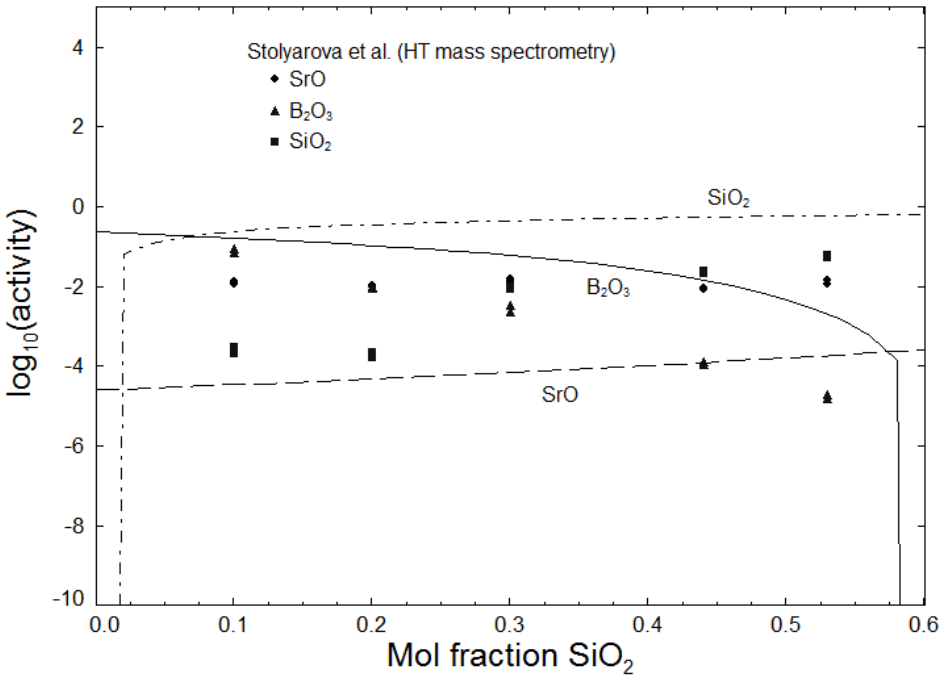

Fig. 3.18.11 Activities on the isoplethal section X_{SrO} =0.4 in the SrO-B_2O_3-SiO_2 system at 1487 °C (Std. states; solid for SrO and SiO_2 and liquid for B_2O_3).

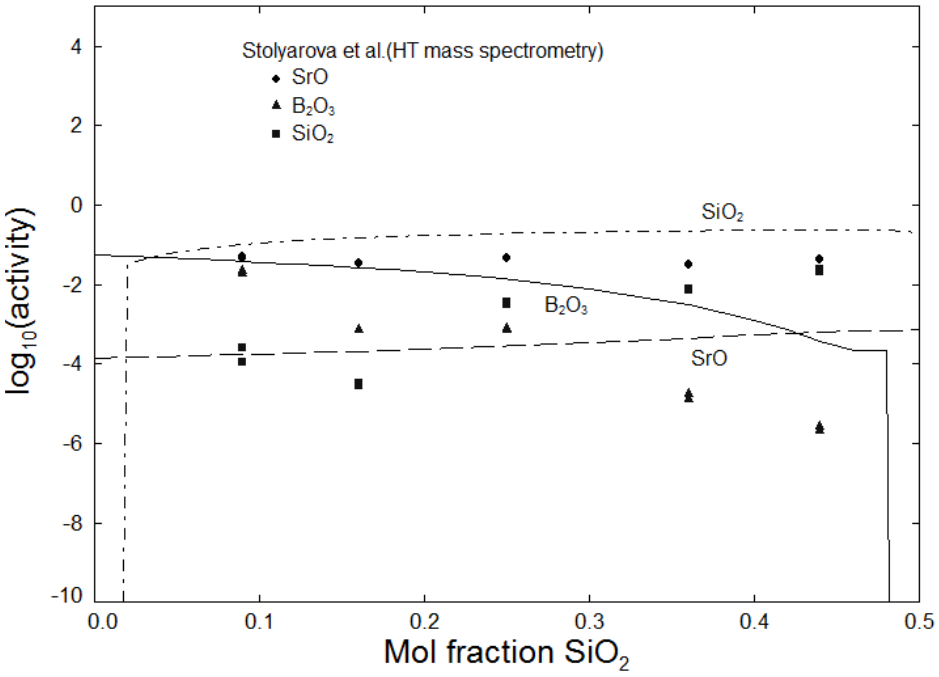

Fig. 3.18.12 Activities on the isoplethal section X_{SrO} =0.5 in the SrO-B_2O_3-SiO_2 system at 1487 °C (Std. states; solid for SrO and SiO_2 and liquid for B_2O_3).

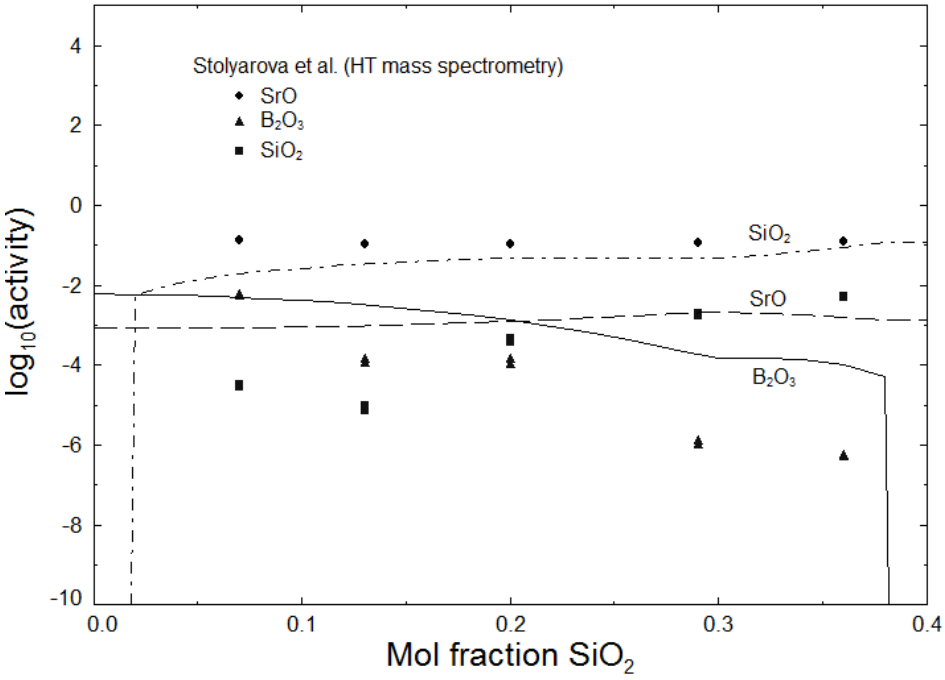

Fig. 3.18.13 Activities on the isoplethal section X_{SrO} =0.6 in the SrO-B_2O_3-SiO_2 system at 1487 °C (Std. states; solid for SrO and SiO_2 and liquid for B_2O_3).

3.19 The BaO-SrO-B_2O_3 system

The Gibbs energy of the liquid phase in the BaO-SrO-B_2O_3 ternary system was calculated from the corresponding binary systems by treating B_2O_3 as asymmetric component [Pelton and Chartrand (2001)]. Small ternary interaction parameters present in Table 3.19.1 were also used to fit the available data. The optimized parameters for this ternary system are presented in Table 3.19.1.

Wang, et al. (1984) studied the system by quenching techniques, DTA and XRD. The data reported by them on the BaB_2-SrO and BaB-SB sections are reasonably well reproduced in Figs. 3.19.1 and 3.19.2. In Fig. 3.19.2, the difference between the calculated melting temperature of the BaB phase and experimental point of Wang, et al. (1984) is about 10 °C. However, the present optimal fit of the binary BaO-B_2O_3 system (Fig. 2.8.1) is very close to the melting point of the BaB phase, 1092 °C, reported by Ernest M. Levin and McMurdie (1949). The crystal structures of the low- and high-temperature forms of the BaB phase belong to R3*c* and $R\bar{3}c$ space group symmetries [Liebertz (1988)], whereas that of the SB phase belongs to the P*bcn* space group symmetry [Kim et al. (1996)]. The BaB and SB solid solutions in Fig. 3.19.2 were treated as different phases using the single-sublattice random mixing model. No data on the solubility of Sr in the low-temperature form could be found in the literature. Moreover, the present calculations were performed by assuming the same thermodynamic properties for the low- and high-temperature forms (see the BaO-B_2O_3 section). Wang, et al. (1984) reported unindexed XRD data of a ternary compound $Ba_5Sr_6B_{10}O_{26}$ ($B_5S_6B_{10}$). No other data for this compound, neither on its

presence nor on its thermodynamic properties, could be found in the literature. In the present calculations, the presence of this compound was neglected.

Wang, et al. (1984) by quenching techniques also reported a part of an isothermal section at 880 °C as shown in Fig. 3.19.3. As evident in Fig. 3.19.3, they reported about 40 % solubility of Sr in the Ba_4B phase. The thermodynamic equilibrium of BaB and Ba_4B solid solutions reported by Wang, et al. (1984) is incorrect as there are other binary phases, Ba_3B and Ba_2B (not shown in Fig. 3.19.3) between the BaB and Ba_4B which appear in the present calculations as shown in Fig. 3.19.4. In the present calculations, in view of this inconsistency in the diagram of Wang, et al. (1984), the solubility of Sr in Ba_4B reported by Wang, et al. (1984) was neglected. Also, there are some other phases in the SrO-BaO-B_2O_3 system which have the same stoichiometries: S_3B-Ba_3B, SB_2-BaB_2. The crystal structure of the S_3B phase belongs to the $R\bar{3}ch$ space group [Wei et al. (2001)]. No data on the crystal structure of the Ba_3B phase could be found in the literature. The S_3B and Ba_3B phases might be isomorphic and completely mutual soluble. During calculations, when an ideal solution was assumed between these two phases, this solid solution appeared in Fig. 3.19.1. However, such a solid solution was not reported by Wang, et al. (1984) in this section. Therefore, the possibility of complete solid solution between these two phases was neglected. If these two phases belong to different crystal structures then also because of chemical similarity between the Ba and Sr atoms some amount of mutual solid solubility between these phases can be expected. However, in the absence of any experimental data on such solubility it was neglected in the present calculations. Similarly, the SB_2 and BaB_2 phases are not isomorphic. The crystal structure of the SB_2 phase belongs to the Pmn21 space group [H. Liu, Guo, Fan, and

Xu (1997)] whereas of that the BaB_2 phase belongs to the P21/c space group [Block and Perloff (1965)]. Here again, because of the absence of any experimental evidence, the possibility of some amount mutual solid solubility between these two phases was neglected. The present calculated liquidus (polythermal) projection for the BaO-SrO-B_2O_3 system is presented in Fig. 3.19.5.

Table 3.19.1 Optimized thermodynamic parameters, in Joules, in the BaO-SrO-B_2O_3 system.

BaB_2O_4 solid solutions (BaB)
g^0 (SrB_2O_4, BaB) = g^0 (SrB_2O_4) + 8786
SrB_2O_4 solid solutions (SrB)
g^0 (BaB_2O_4, SrB) = g^0 (BaB_2O_4) + 13389
Liquid phase (Ternary interaction parameters)
$g^{002}_{\text{B-Sr(Ba)}}$ = 2510
$g^{002}_{\text{B-Ba(Sr)}}$ = 4184

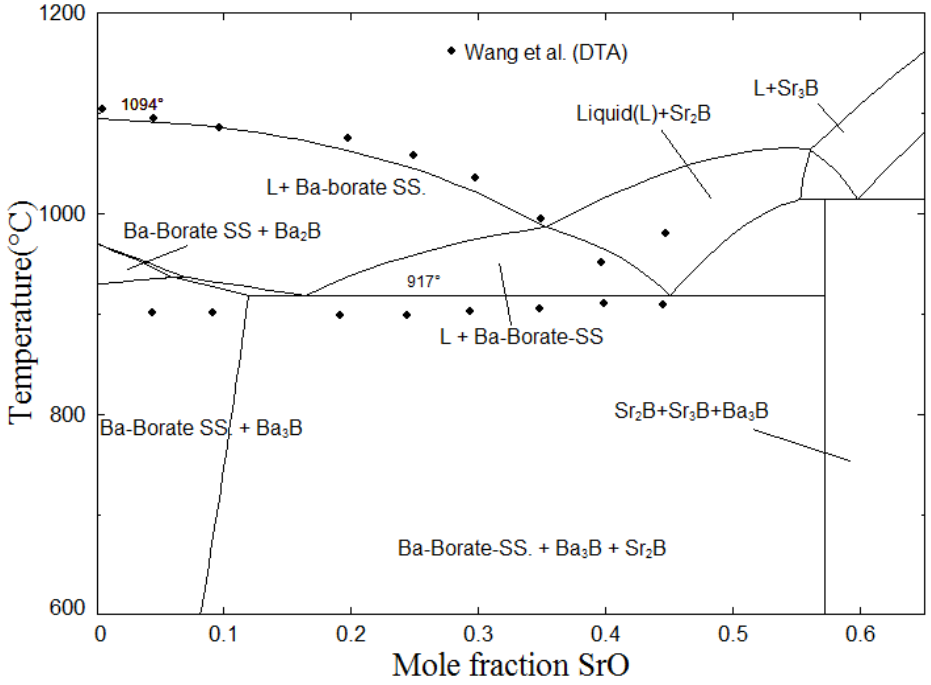

Fig. 3.19.1 Optimized phase diagram of the BaB_2O_4-SrO section.

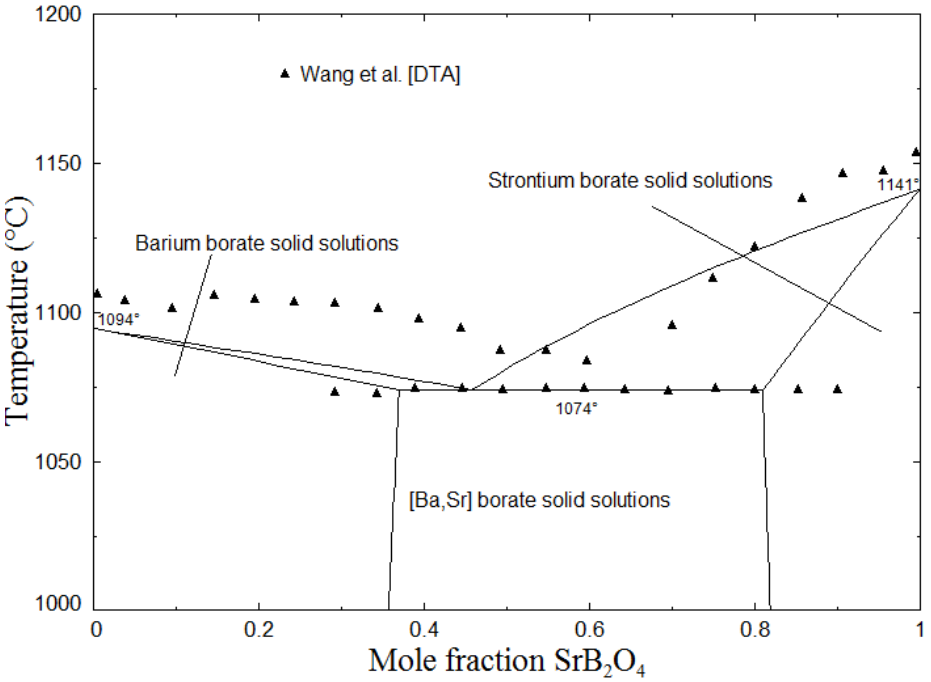

Fig. 3.19.2 Optimized phase diagram of the BaB_2O_4-SrB_2O_4 section.

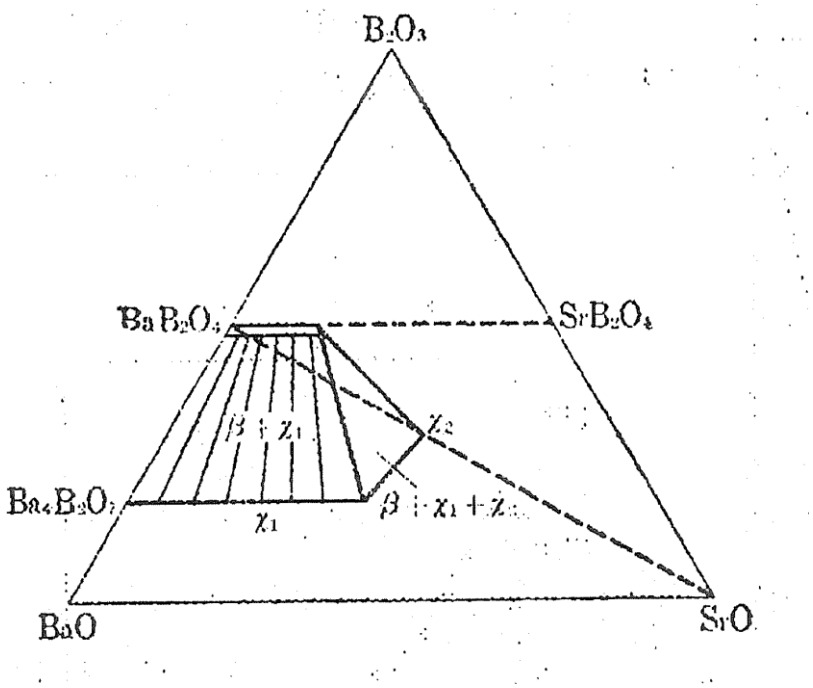

Fig. 3.19.3 Isothermal section at 880 °C as reported by Wang et al.

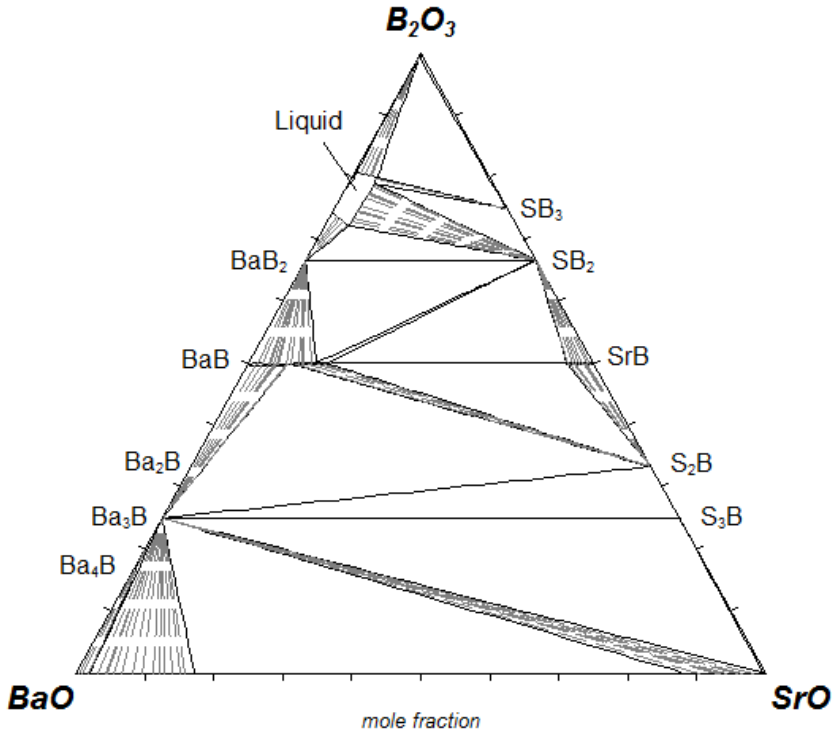

Fig. 3.19.4 Optimized isothermal section at 880 °C in the BaO-SrO-B_2O_3 system.

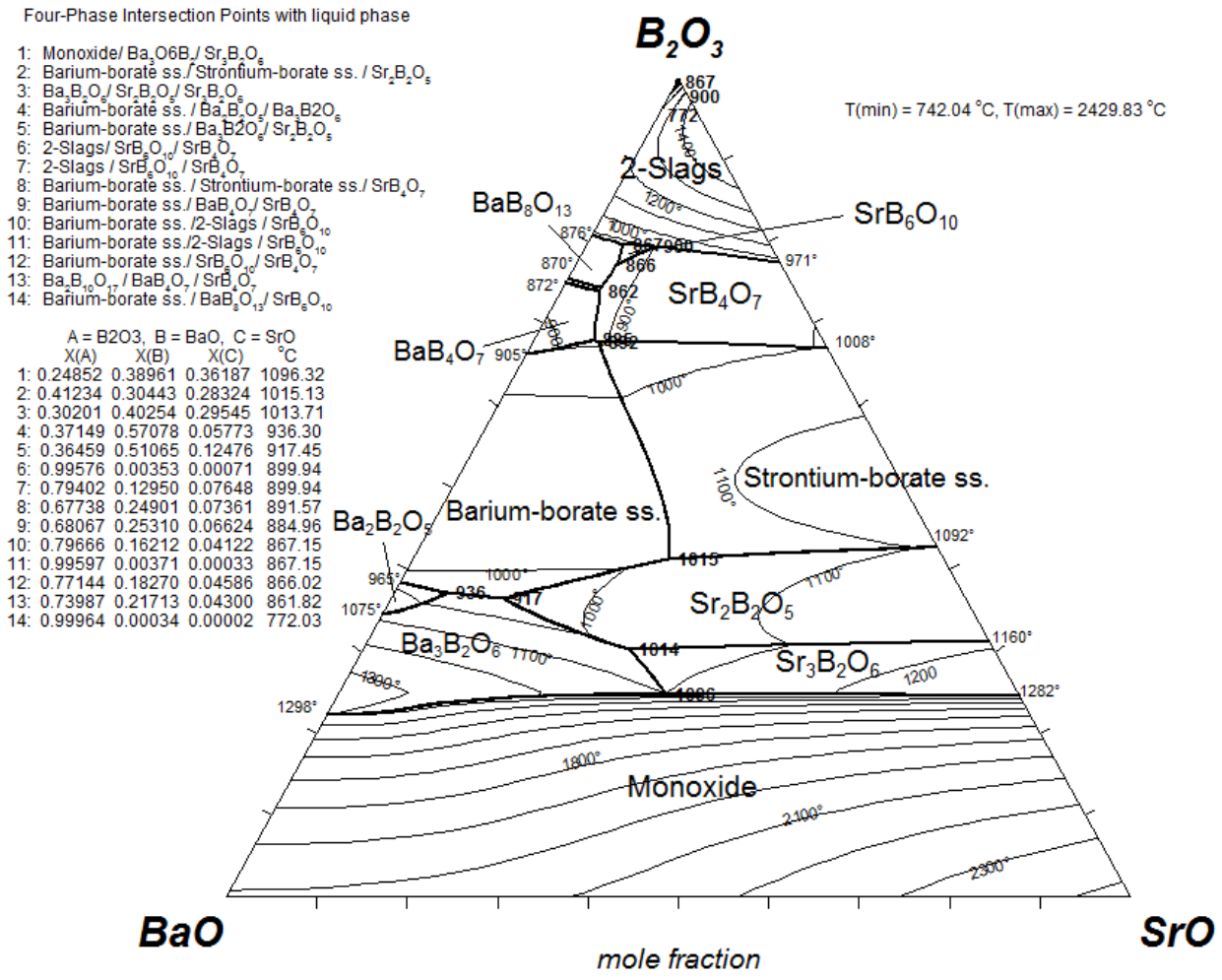

Fig. 3.19.5 Present calculated liquidus (polythermal) projection for the BaO-SrO-B_2O_3 system (isotherms were drawn at the interval of 100 °C).

3.20 The BaO-CaO-B_2O_3 system

Ji, Liang, Xie, and Yu (1995) by quenching and XRD reported sub-solidus phase equilibria in the system as shown in Fig. 3.20.1. They equilibrated the B_2O_3-rich (B_2O_3> 0.5mol) samples at 780 °C and other samples at 1040 °C. The exact compositions of the samples studied were not reported. The final results were reported in the form of Fig. 3.20.1. These data can be compared with the present calculations at 800 °C in Fig. 3.20.2. Ji, et al. (1995) reported three ternary compounds as stable: $CaBa_2B_6O_{12}$ (CBa_2B_3), $CaBa_2B_2O_6$ (CBa_2B), $Ca_5Ba_2B_{10}O_{22}$ ($C_5Ba_2B_5$). They indexed the crystal structure of CBa_2B_3 as $R\bar{3}c$ (isostructural to HT-BaB), of CBa_2B as $P2$ or Pm and of $C_5Ba_2B_5$ as $P2_1$ space group symmetry. No other thermodynamic data for these compounds could be found in the literature. The present optimized thermodynamic parameters for these phases are presented in Table 3.20.1. As the CBa_2B_3 and HT-BaB phases are isostructural some solubility among these phases is expected (HT-BaB is stable above 925 °C). However, no experimental data proving this could be found. In the present calculations this solubility was neglected. The crystal structure of LT-BaB (space group R3*c*) differs from that of CBa_2B_3. Hence, in the present calculations at 800 °C, no mutual solubility was assumed among these phases. Ji, et al. (1995) reported solubility of Ca in the Ba_4B phase at 800 °C as shown in Fig. 3.20.1. This solubility is reproduced in the present calculations in Fig. 3.20.2. The solid solution was treated with a single-sublattice random mixing model (i.e. $[Ba,Ca]_4B_2O_7$]).

The calculated melting temperatures of the ternary compounds in Table 3.20.1 are quite reasonable. Also, for all these compounds the entropies of formation (from the compounds used

to calculate the heat capacities in Table 3.20.1) are equal to zero. The Gibbs energy of the liquid phase in the ternary system was calculated from the corresponding binary systems by treating B_2O_3 as asymmetric component [Pelton and Chartrand (2001)]. The present calculated liquidus (polythermal) projection for the BaO-CaO-B_2O_3 system is presented in Fig. 3.20.3.

There are phases in the BaO-CaO-B_2O_3 system which have the same stoichiometries: C_3B-Ba_3B, CB-BaB,CB_2-BaB_2. Some amount of mutual solubility among these phases can be expected. The crystal structure of the C_3B phase belongs to the R3*c* space group [Vegas, Cano, and Garcia-Blanco (1975)]. No data on the crystal structure for the Ba_3B phase could be found in the literature. The crystal structure of the CB phase belongs to the Pnca space group [Zachariasen and Ziegler (1932)] whereas BaB (the low- and high-temperature polymorphs) belong to R3*c* and $R\bar{3}c$ space groups [Liebertz (1988)]. Thus the CB and BaB phases are not isostructural. However, CB_2 and BaB_2 belong to the same monoclinic P21/c space group [Kindermann (1978); Block and Perloff (1965)]. In the present calculations, in the absence of any experimental evidence, no mutual solubility was calculated among these phases with same stoichiometries. Moreover, a large size difference between the Ba and Ca atom would mitigate against any appreciable mutual solubility among these phases.

Table 3.20.1 Optimized parameters in the BaO-CaO-B_2O_3 system.

$CaBa_2B_6O_{12}$ (CBa_2B_3)		
ΔH^0_{298} = –6104106 J	S^0_{298} = 367.371 J/mol/K	ΔS^0_{298}[(a)] = 0
T_m[(b)] = 1111 °C	ΔS^0_{298}[(d)] = 23.633	
$C_p = C_p (CB_2) + C_p (BaB) + Cp (BaO)$		
(298.15 < *T* <1500 K)		
$CaBa_2B_2O_6$ (CBa_2B)		
ΔH^0_{298} = -3365634 J	S^0_{298} =249.139 J/mol/K	ΔS^0_{298}[(a)] = 0
T_m[(c)] = 1138 °C	ΔS^0_{298}[(d)] = 13.301	
$C_p = C_p (CB) + 2\ C_p (BaO)$		
(298.15 < *T* < 1500 K)		
$Ca_5Ba_2B_{10}O_{22}$ ($C_5Ba_2B_5$)		
ΔH^0_{298} = –11584338	S^0_{298} = 669.142 J/mol/K	ΔS^0_{298}[(a)] = 0
T_m[(c)] = 1086 °C	ΔS^0_{298}[(d)] = 66.504	
$C_p = 5\ C_p (CB) + 2\ C_p (BaO)$		
(298.15 < *T* < 1500 K)		
$[Ca,Ba]B_8O_{13}$ solid solution (ss)		
$G^0(CaB_8O_{13}, ss) = G^0(CaO) + 4G^0(B_2O_3) - 167360$		
q^{11}_{BaCa} = –62760		

(a) compounds used to calculated the heat capacities as reference
(b) congruent melting temperature
(c) incongruent melting temperature
(d) oxides (stable at room-temperature) as reference

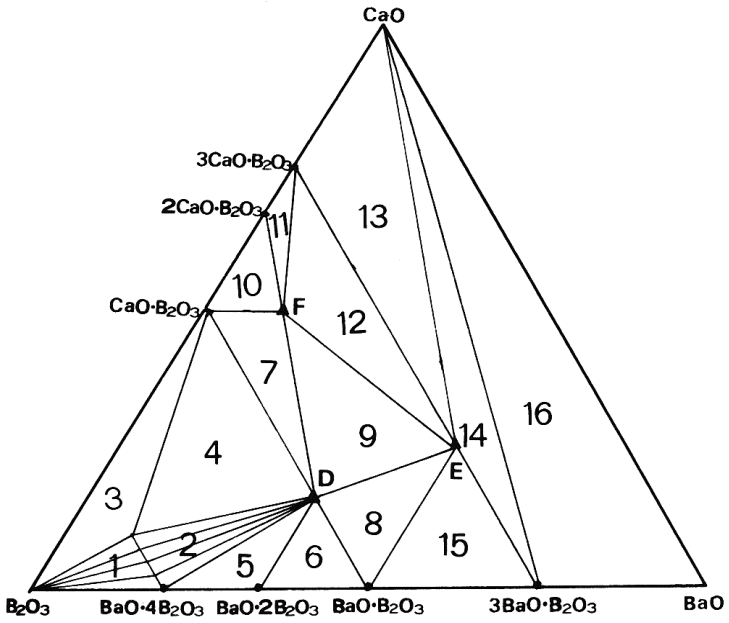

Fig. 3.20.1 Phase equilibria as reported by Ji et al.

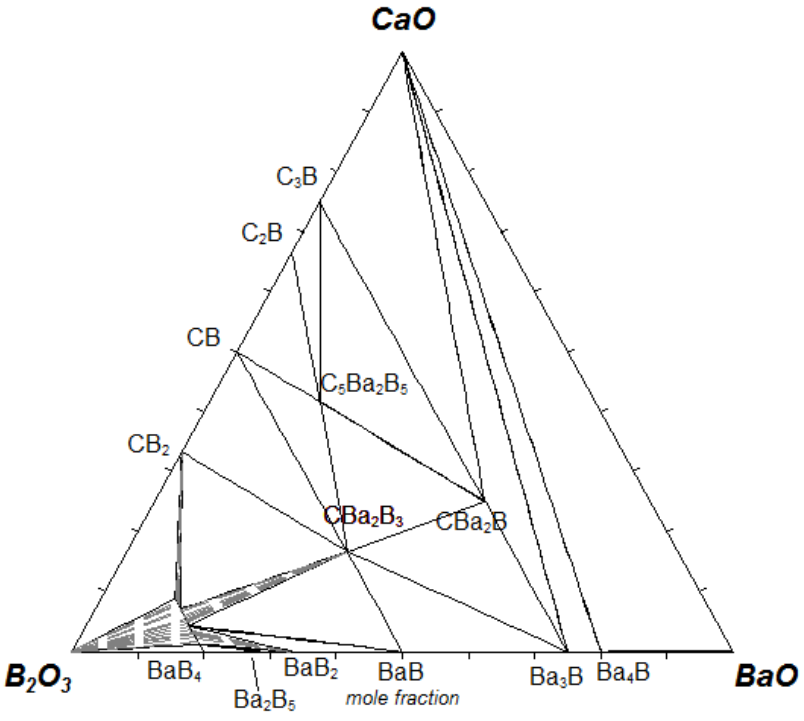

Fig. 3.20.2 Optimized isothermal section at 800 °C in the BaO-CaO-B_2O_3 system.

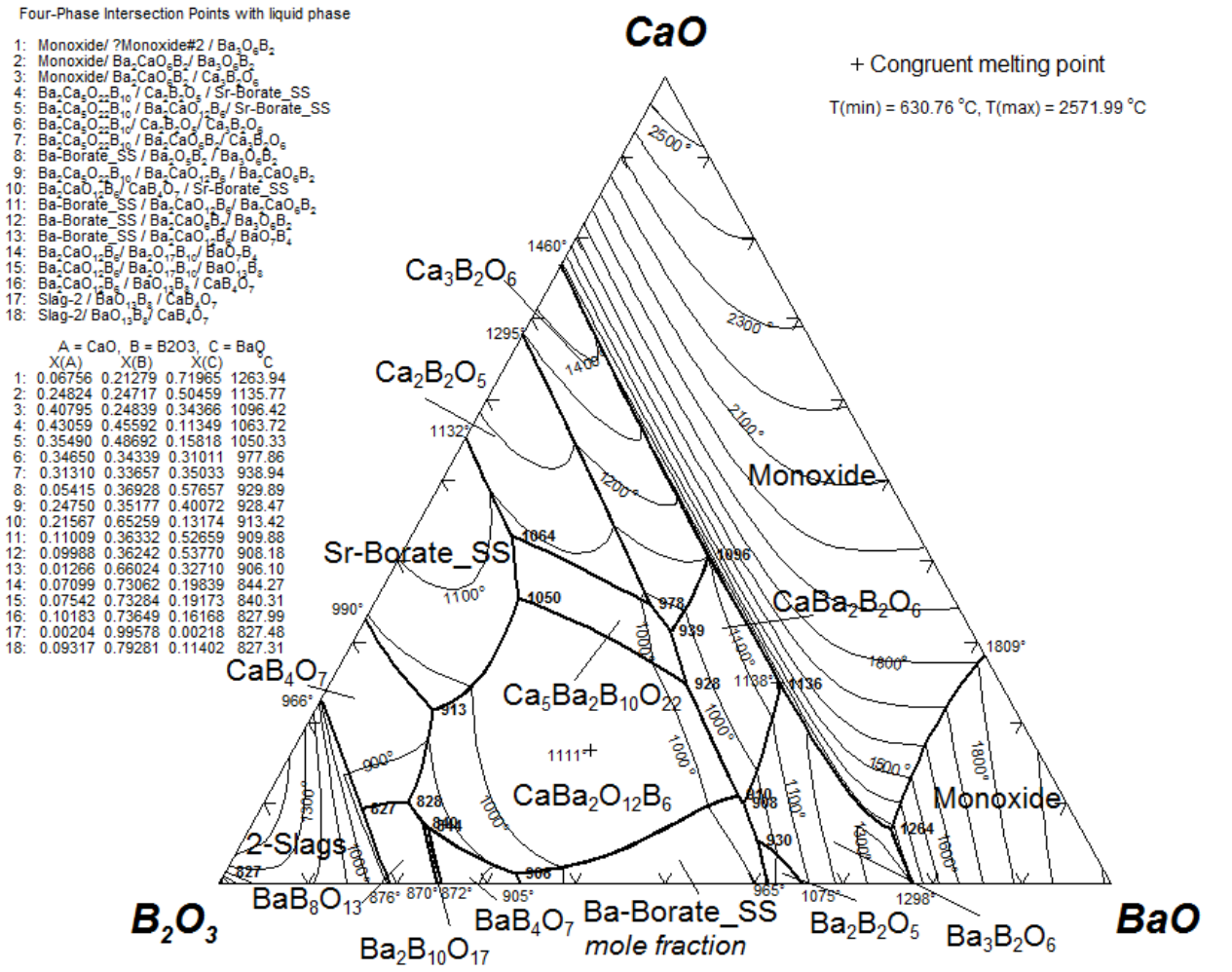

Fig. 3.20.3 Present calculated liquidus (polythermal) projection of the BaO-CaO-B_2O_3 system (isotherms were drawn at the interval of 100 °C).

3.21 The BaO-Al_2O_3-B_2O_3 system

The estimations in this ternary system obtained from the optimized model parameters were far from experimental data. The reason for this could be the complex structure of the alumino-borate liquid phase. A relatively larger number of parameters for the liquid phase (Table 3.21.1) were required to fit the available data. The Gibbs energy of the liquid phase in the BaO-Al_2O_3-B_2O_3 system was calculated from the corresponding binary systems by treating B_2O_3 as an asymmetric component i.e. BaO, Al_2O_3 and $BaAl_2O_4$ were kept in the same group (Chartrand and Pelton,

2001). The $BaO\text{-}Al_2O_3$ binary system contains $BaAl_2$ associates see (Sec.2.7, $BaO\text{-}Al_2O_3$ and Sec. 3.15, $BaO\text{-}Al_2O_3\text{-}SiO_2$) as separate component in the liquid system. The $g^0_{BaAl2O4}$ (see Sec.2.7, $BaO\text{-}Al_2O_3$ and Sec. 3.15, $BaO\text{-}Al_2O_3\text{-}SiO_2$) was fixed from the optimization of the $BaO\text{-}Al_2O_3\text{-}SiO_2$ system. This value made these associates practically unstable in the $BaO\text{-}Al_2O_3\text{-}B_2O_3$ ternary system. Moreover, the presence of these associates is important in those systems where charge compensation effect occur. Such effect is not possible in this system, firstly because there is no imbalance of charge when B^{+3} is substituted by Al^{+3}, and secondly because such substitution is less probable due to larger size difference between the radii of these two ions. The optimized parameters of the system are presented in Table 3.21.1.

Huebner (1970) by quenching and XRD reported an isothermal section at 700 °C, shown in Fig. 3.21.1. He reported six ternary compounds in the system: (BaO = Ba, Al_2O_3 = A, B_2O_3 = B): BaAB, $BaAB_2$, $Ba_3A_2B_2$, Ba_2AB_4, $Ba_5A_2B_6$, $Ba_{10}AB$. As is evident in Fig. 3.21.1, Huebner (1970) reported non-stoichiometry for the phase BaAB (SSII in Fig. 3.21.1) and solid solubility among the binary BaB and Ba_2B phases (SSI in Fig. 3.21.1). In the binary $BaO\text{-}B_2O_3$ system, there are no data for such solubility among these binary phases. Hence, this solubility was neglected in the present calculations. Also, there are no other data for the non-stoichiometric nature of the BaAB phase. In fact, later phase diagram measurements on the section $BaAB\text{-}Al_2O_3$ (Fig. 3.21.4) do not suggest this phase as non-stoichiometric. The phase relationships at 700 °C reported by Huebner (1970) can be compared with present calculations in Figs. 3.21.2 and 3.21.3. Fig. 3.21.2 was calculated by emitting the liquid phase from the calculations. Huebner (1970) did not find the liquid phase stable at 700 °C; however -according to the present optimization based

on other phase diagram data (Fig. 3.21.4)- the liquid phase appears at 700 °C as shown in Fig. 3.21.3. Huebner (1970), Miyazaki, Kimura, Maiwa, Nakamura, and Kannan (2004) and Hovhannisyan (2005), by DTA, determined melting behavior and temperatures for all the ternary compounds (except for $Ba_{10}AB$). All these data can be compared with the present calculated melting temperatures of these compounds in Table 3.21.1. In the present calculations the presence of $Ba_{10}AB$ was neglected, because further evidence is required to prove its stability. The optimized entropies of formation of the ternary compounds presented in Table 3.21.1 are always less than 10 J/(mol of metallic atoms) which is quite reasonable.

The phase diagram measurements on the BaAB-Al_2O_3 section by Kimura, Numazawa, and Sato (1997), Hovhannisyan (2003); Hovhannisyan (2004), and Toroyan, Oganesyan, and Kostanyan (1982), all by DTA, is well reproduced in Fig. 3.21.4. Hovhannisyan (2003) first reported congruent melting behavior for the BaAB phase, but later he reported [Hovhannisyan (2005)] incongruent behavior (into Liquid+Al_2O_3) for the same phase. Ye, Zeng, Wu, Huang, and Chen (1998) determined a trigonal structure in the *R*32 space group for the BaAB phase.

The calculated liquidus (polythermal) projection for the BaO-B_2O_3-Al_2O_3 system is presented in Fig. 3.21.5. As can be seen in this figure, the present calculations show small immiscibility in the liquid phase between the $Ba_3B_2O_6$ and $BaAl_2O_4$ primary phase regions. There are no experimental data to prove this immiscibility. In the present work, it was found very difficult to suppress this immiscibility in this region.

Table 3.21.1 Optimized thermodynamic parameters, in Joules, in the BaO-Al_2O_3-B_2O_3 system (I = incongruent, C = congruent).

$BaAl_2B_2O_7$ (BaAB)		
ΔH^0_{298} = –3655840 J/mol	S^0_{298} = 243.500 J/mol/K	$\Delta S^0_{298}{}^{(a)}$ = 49.180
$\Delta S^0_{298}{}^{(b)}$ = 66.661		
T_m = 985 ºC, I (Liq. + A_9B_2)	Exp. (°C) = 910, C[1]; 910, I[2]; 995, I (Liq.+Al_2O_3)[3]	
$C_p = C_p$ (BaB) + C_p (Al_2O_3)		
$BaAl_2B_4O_{10}$ ($BaAB_2$)		
ΔH^0_{298} = –5005576 J/mol	S^0_{298} = 264.000 J/mol/K	$\Delta S^0_{298}{}^{(a)}$ = –19.820
$\Delta S^0_{298}{}^{(b)}$ = 33.211		
T_m = 815 ºC, I (Liq.+A_9B_2)	Exp. (°C) = 805, C[1]; 785, I[2]; 850, I (Liq.+A_9B_2+BaAB)[3]	
$C_p = C_p$ (BaB_2) + C_p (Al_2O_3)		
$Ba_3Al_4B_4O_{15}$ ($Ba_3A_2B_2$)		
ΔH^0_{298} = –7925984 J/mol	S^0_{298} = 638.000 J/mol/K	$\Delta S^0_{298}{}^{(a)}$ = 92.469
$\Delta S^0_{298}{}^{(b)}$ = 212.253		
T_m = 904 ºC, C	Exp. (°C) = 945, C[1]; 900, I[2]; 930, C[3]	
C_p = 2 C_p (BaA,HT) + C_p (BaB_2)		
$Ba_2Al_2B_8O_{17}$ (Ba_2AB_4)		
ΔH^0_{298} = –8280652 J/mol	S^0_{298} = 514.000 J/mol/K	$\Delta S^0_{298}{}^{(a)}$ = –2.820
$\Delta S^0_{298}{}^{(b)}$ = 103.242		
T_m = 802 ºC, C	Exp. (°C) = 810, C[1]; 810, I[2]; 860, C[3]	
$C_p = C_p(Al_2O_3)$+ 2 C_p(BaB_2)		
$Ba_5Al_4B_{12}O_{29}$ ($Ba_5A_2B_6$)		
ΔH^0_{298} = –14557536 J/mol	S^0_{298} = 1080.000 J/mol/K	$\Delta S^0_{298}{}^{(a)}$ = 68.469
$\Delta S^0_{298}{}^{(b)}$ = 294.315		
T_m = 822 °C, I (Liq.+ BaB)	Exp. (°C) = 855, C[1]; 820, C[2]; 870, C[3]	
C_p = 2 C_p (BaA,HT) + 3 C_p (BaB_2)		
Liquid phase (Ternary interaction parameters) (in Joules)		
$g^{003}_{\text{B-Ba(Al)}}$ = –104600		
$g^{002}_{\text{B-Ba(Al)}}$ = –117152		
$g^{001}_{\text{B-Ba(Al)}}$ = –83680		
$g^{011}_{\text{B-Ba(Al)}}$ = 41840		

(a) From the compounds used to calculated heat capacities

(b) From oxides

[1] Hubner (1970)

[2] Miyazaki et al. (2004)

[3] Hovhannisyan (2005)

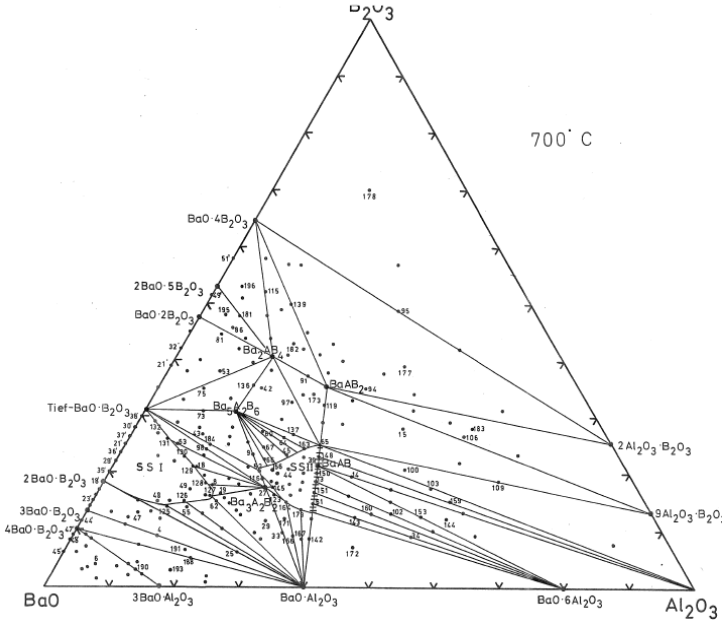

Fig. 3.21.1 Phase equilibria in the BaO-B_2O_3-Al_2O_3 system as reported by Hubner.

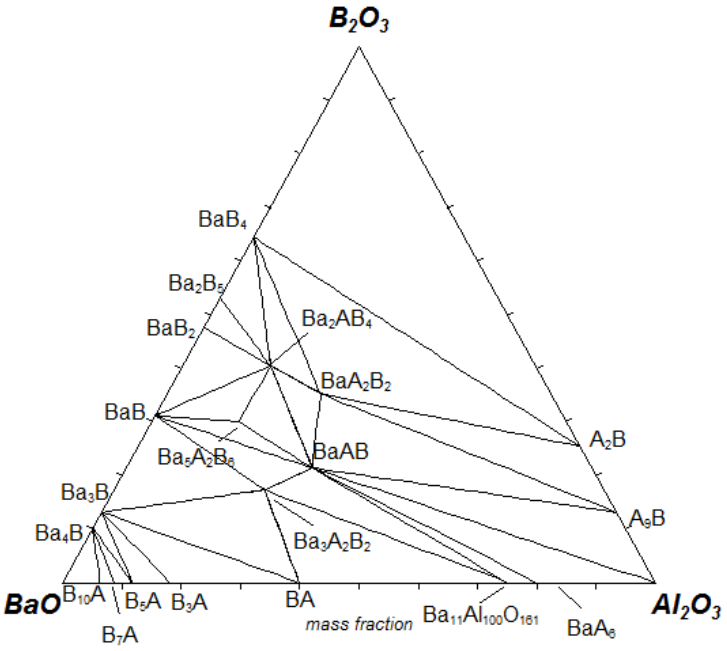

Fig. 3.21.2 Present calculated phase equilibria at 700 °C (by suspending liquid phase from calculations) in the BaO-B_2O_3-Al_2O_3 system.

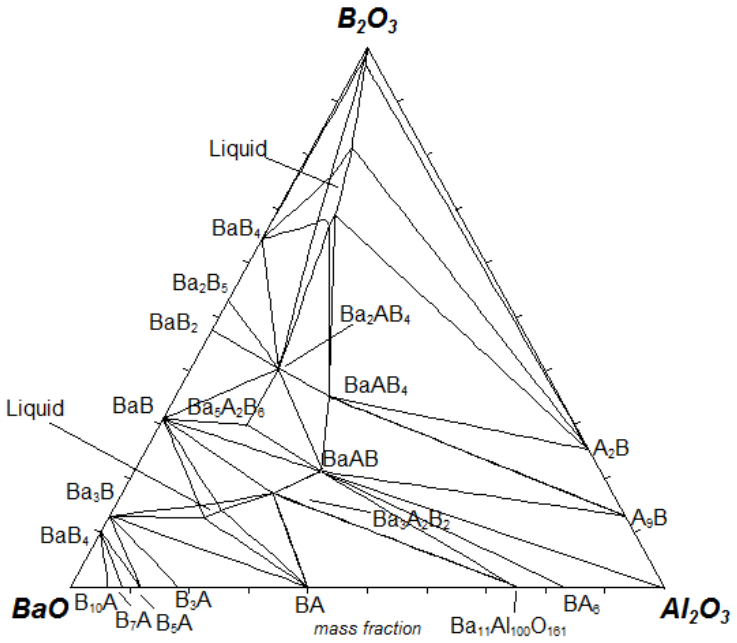

Fig. 3.21.3 Present calculated phase equilibria at 700 °C in the BaO-B_2O_3-Al_2O_3 system.

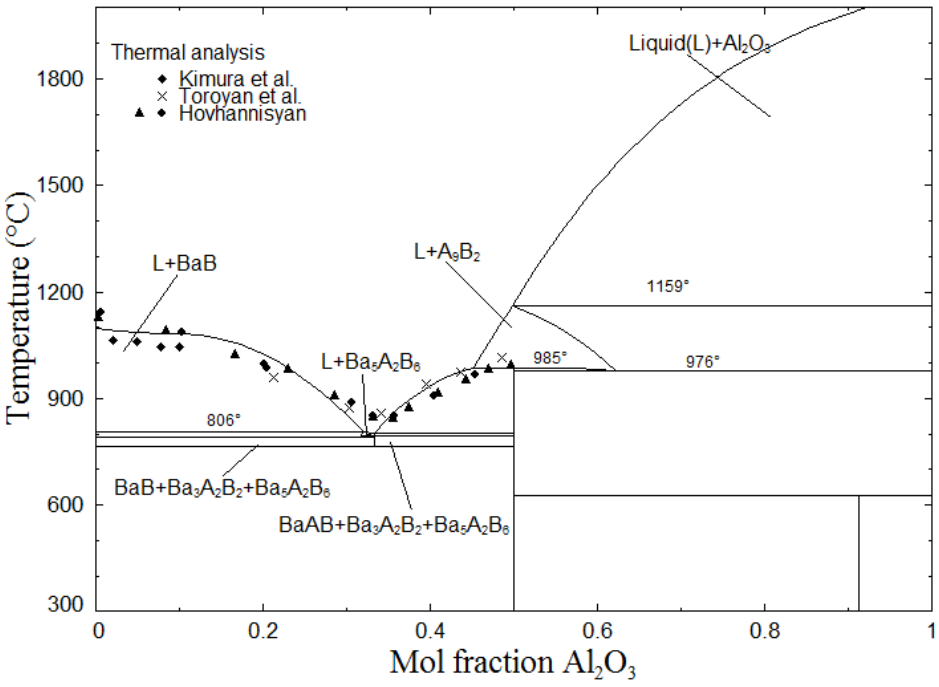

Fig. 3.21.4 Optimized phase diagram of the BaB_2O_4-Al_2O_3 section.

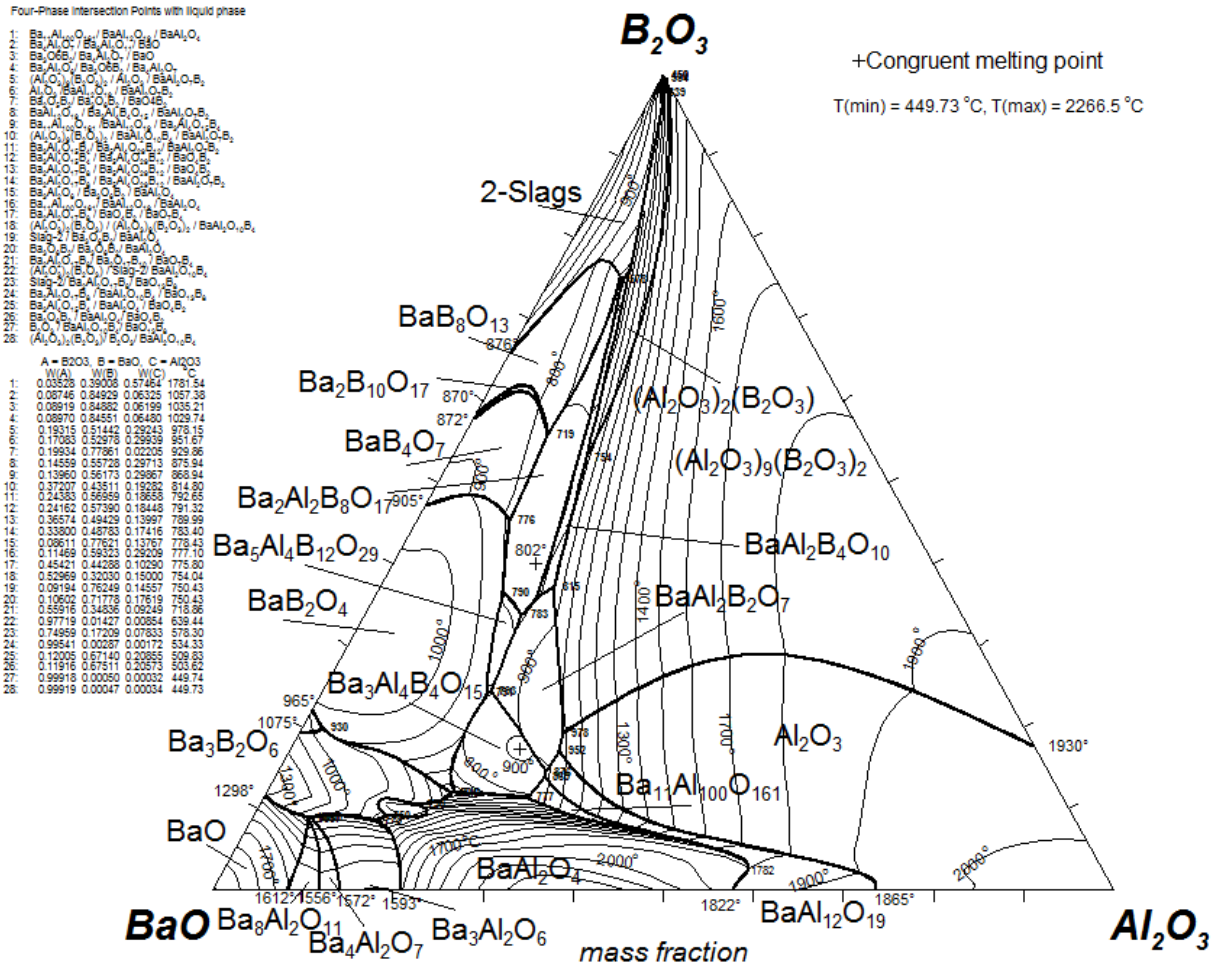

Fig. 3.21.5 Present calculated liquidus (polythermal) projection of the BaO-B_2O_3-Al_2O_3 system (isotherms were drawn at the interval of 100 °C)..

3.22 The SrO-Al_2O_3-B_2O_3 system

The Gibbs energy of the liquid phase in the SrO-Al_2O_3-B_2O_3 system was calculated from the corresponding binary systems by treating B_2O_3 as an asymmetric component i.e. SrO, Al_2O_3 and $SrAl_2O_4$ were kept in the same group (Chartrand and Pelton, 2001). The SrO-Al_2O_3 binary system contains $SrAl_2$ associates see (Sec. 2.6, SrO-Al_2O_3 and Sec. 3.16, SrO-Al_2O_3-SiO_2) as separate component in the liquid system. The $g^0_{SrAl2O4}$ (see Sec. 2.6, SrO-Al_2O_3 and Sec. 3.16,

SrO-Al_2O_3-SiO_2) was fixed from the optimization of the SrO-Al_2O_3-SiO_2 system. This value made these associates practically unstable in the SrO-Al_2O_3-B_2O_3 ternary system. Moreover, the presence of these associates is important in those systems where charge compensation effect occur. Such effect is not possible in this system, firstly because there is no imbalance of charge when B^{+3} is substituted by Al^{+3}, and secondly because such substitution is less probable due to larger size difference between the radii of these two ions. The optimized parameters of the SrO-Al_2O_3-B_2O_3 system are presented in Table 3.22.1. During simultaneous optimization, effort was made to use parameters for the liquid phase which are similar in form as obtained for the liquid phase in the BaO-Al_2O_3-B_2O_3 system. It can be seen that all the parameters obtained for the SrO-Al_2O_3-B_2O_3 system are same in form as obtained for the BaO-Al_2O_3-B_2O_3 system.

Hovhannisyan (2003) reported phase diagram points on the SrB_2O_4-Al_2O_3 section which are reproduced well in Fig. 3.22.1. He reported, by XRD, $SrAl_2B_2O_7$ (SAB) as a stable phase on this section. He also reported incongruent melting of this compound at 1085 °C into Liquid + Al_2O_3. In a different work, Hovhannisyan (2005) by quenching and XRD reported another ternary compound, $Sr_2Al_2B_2O_8$ (S_2AB), melting incongruently at 950 °C into Liquid + $SrAl_2O_4$ (SA). According to the present calculations, this phase melts congruently at 950 °C. In the present calculations, while optimizing the thermodynamic properties for the S_2AB phase, care was taken that this phase must not appear on the SrB_2O_4-Al_2O_3 section. Analogously to the $BaAB_2$, $Ba_3A_2B_2$, Ba_2AB_4, $Ba_5A_2B_6$ compounds in the BaO-Al_2O_3-B_2O_3 system, Hovhannisyan (2005) performed annealing and quenching experiments to check the stability of SAB_2, $S_3A_2B_2$, S_2AB_4, $S_5A_2B_5$ compounds (SrO=S, Al_2O_3=A, B_2O_3=B). He concluded that these phases are not stable in

the SrO-Al_2O_3-B_2O_3 system. The present calculated liquidus (polythermal) projection for the SrO-B_2O_3-Al_2O_3 system is presented in Fig. 3.22.2.

Table 3.22.1 Optimized thermodynamic parameters, in Joules, in the SrO-Al_2O_3-B_2O_3 system (I = incongruent, C = congruent).

$SrAl_2B_2O_7$ (SAB)		
ΔH^0_{298} = –3676740 J/mol	S^0_{298} = 209.500 J/mol/K	ΔS^0_{298} [(a)] = 27.171
ΔS^0_{298} [(b)] = 51.150		
T_m = 1085 ºC, I (Liq. + A_9B)	Exp. (°C) = 1085 ºC, I (Liq.+Al_2O_3) [Hovhannisyan (2003)]	
$C_p = C_p$ (SA,HT) + C_p (B_2O_3)		
$Sr_2Al_2B_2O_8$ (S_2AB)		
ΔH^0_{298} = –4390315 J/mol	S^0_{298} = 263.400 J/mol/K	ΔS^0_{298} [(a)] = 27.991
ΔS^0_{298} [(b)] = 51.470		
T_m = 950 ºC, C	Exp. (°C) = 950 ºC, I (Liq.+SA) [Hovhannisyan (2005)]	
$C_p = C_p$ (SA,HT) + C_p (B_2O_3) + SrO		
Liquid phase (Ternary interaction parameters) (in Joules)		
$g^{003}_{B\text{-}Sr(Al)}$ = – 104600		
$g^{002}_{B\text{-}Sr(Al)}$ = –121336		
$g^{001}_{B\text{-}Sr(Al)}$ = –79496		
$g^{011}_{B\text{-}Sr(Al)}$ = 41840		

(a) compounds used to calculate heat capacities as reference.
(b) Oxides (stable at room-temperature) as reference

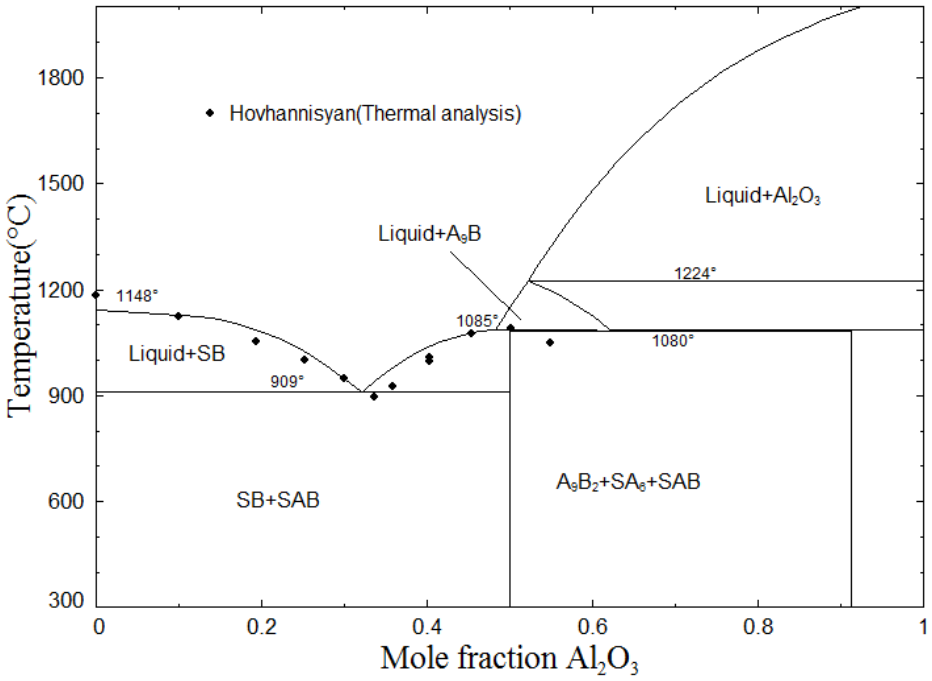

Fig. 3.22.1 Optimized phase diagram of the section SrB_2O_4-Al_2O_3

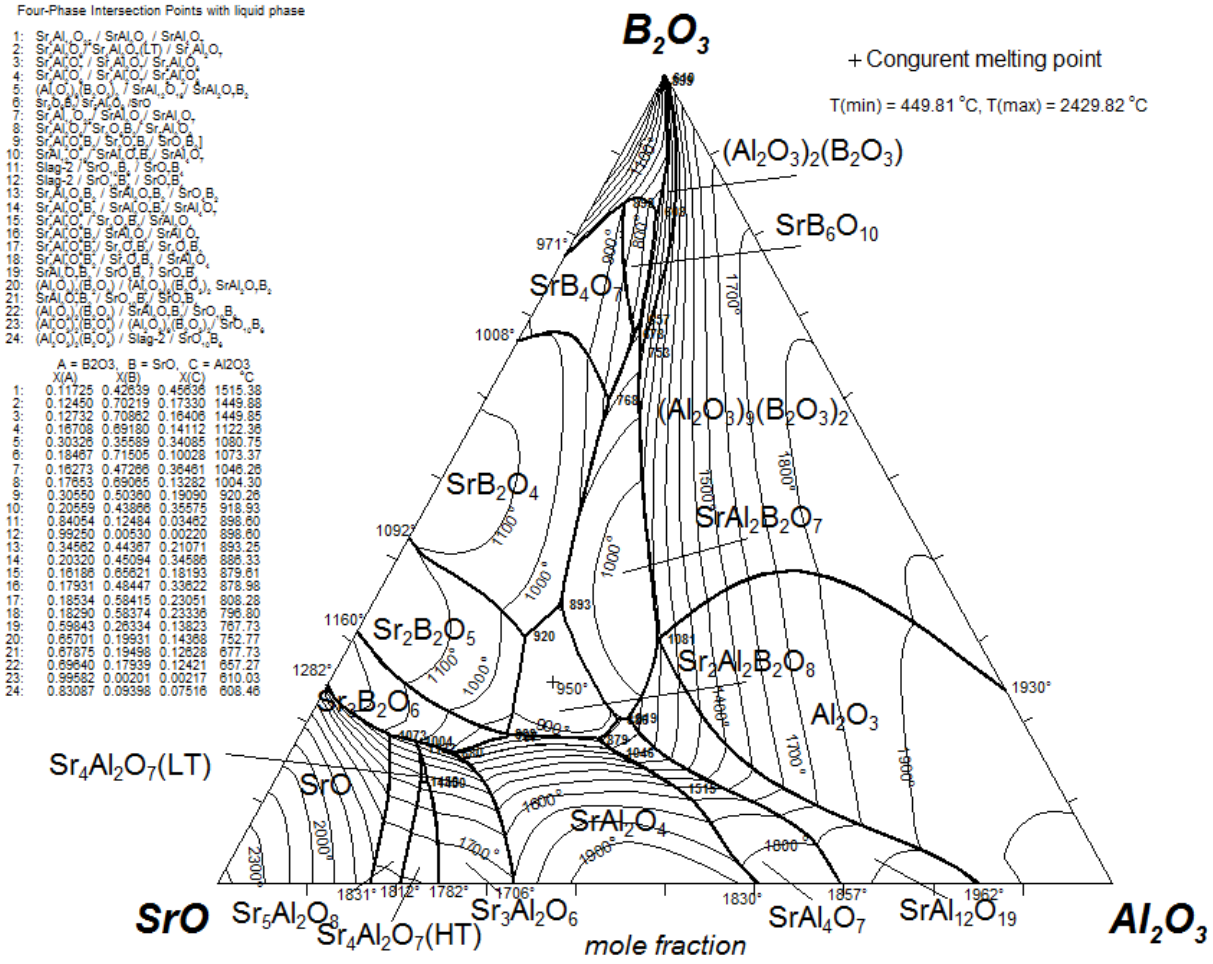

Fig. 3.22.2 Present calculated liquidus (polythermal) projection of the SrO-B_2O_3-Al_2O_3 system (isotherms were drawn at the interval of 100 °C)..

3.23 Liquidus projection for some ternary systems

No phase diagram and thermodynamic data could be found in the literature for these systems:

SrO-BaO-CaO, SrO-BaO-MgO, SrO-CaO-MgO, BaO-CaO-MgO, SrO-MgO-Al_2O_3, SrO-CaO-B_2O_3. SrO-MgO-B_2O_3 , BaO-MgO-B_2O_3

In this section liquidus (polythermal) projections, calculated from the optimized binary model parameters, for these ternary systems are presented.

The systems SrO-BaO-CaO, SrO-BaO-MgO, SrO-CaO-MgO and BaO-CaO-MgO have monoxide solution as the only stable solid phase. The stability of the monoxide phase and the Gibbs energy of the liquid phase in these ternary systems were calculated from the respective optimized binary parameters. The liquidus (polythermal) projections for these systems are presented in Figs. 3.23.1-3.23.4.

In the system SrO-MgO-Al_2O_3, the Gibbs energy of the liquid phase was calculated from the respective binary systems by treating Al_2O_3 as asymmetric component [Pelton and Chartrand (2001)]. The liquidus (polythermal) projections for this system is presented in Figs. 3.235. The mutual solid solubilities between the $MgAl_2O_4$ phase (spinel) and $SrAl_2O_4$ (monoclinic, $P6_322$) were neglected since the different structures of these compounds and the large ionic size difference between the Sr and Mg atoms mitigate against any appreciable solid solubility between them.

In the systems SrO-CaO-B_2O_3, SrO-MgO-B_2O_3 and BaO-MgO-B_2O_3, the Gibbs energy of the liquid phase was calculated from the respective binary systems by treating B_2O_3 as asymmetric component [Pelton and Chartrand (2001)]. The liquidus (polythermal) projections for these systems are presented in Figs. 3.23.6-3.23-8. The various stoichiometric phases appearing in these respective binary systems have different structures. Some amount of solubility between the solid phases with similar stoichiometry cannot be ruled out completely. However, the mutual solid solubilities among the solid phases, in the absence of any experimental data, were neglected.

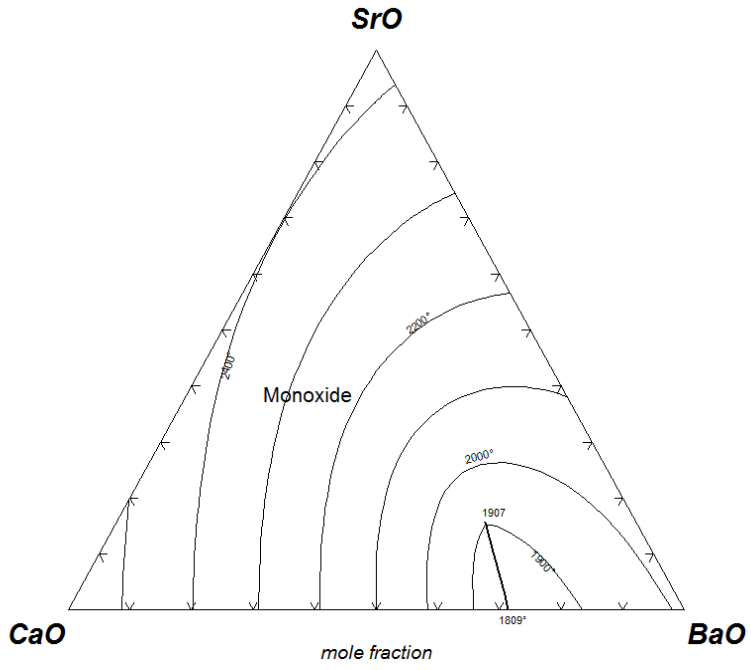

Fig. 3.23.1 Present calculated liquidus (polythermal) projection of the SrO-BaO-CaO system (isotherms were drawn at the interval of 100 °C).

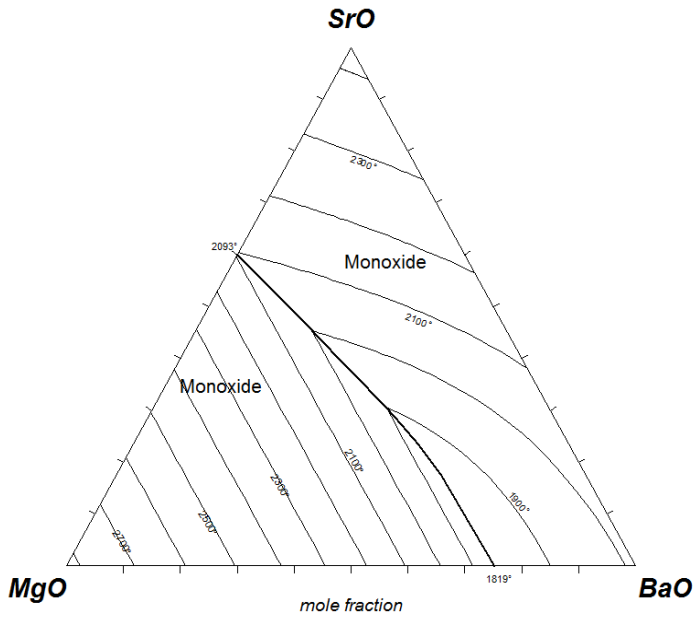

Fig. 3.23.2 Present calculated liquidus (polythermal) projection of the SrO-BaO-MgO system (isotherms were drawn at the interval of 100 °C).

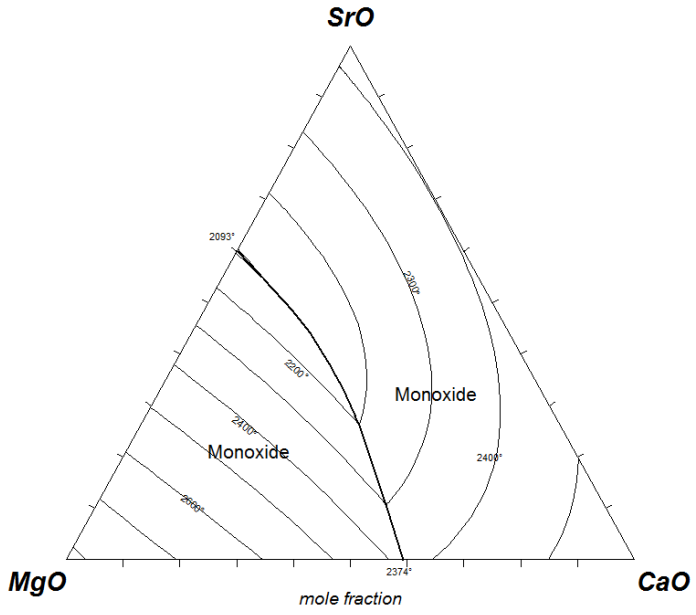

Fig. 3.23.3 Present calculated liquidus (polythermal) projection of the SrO-CaO-MgO system (isotherms were drawn at the interval of 100 °C).

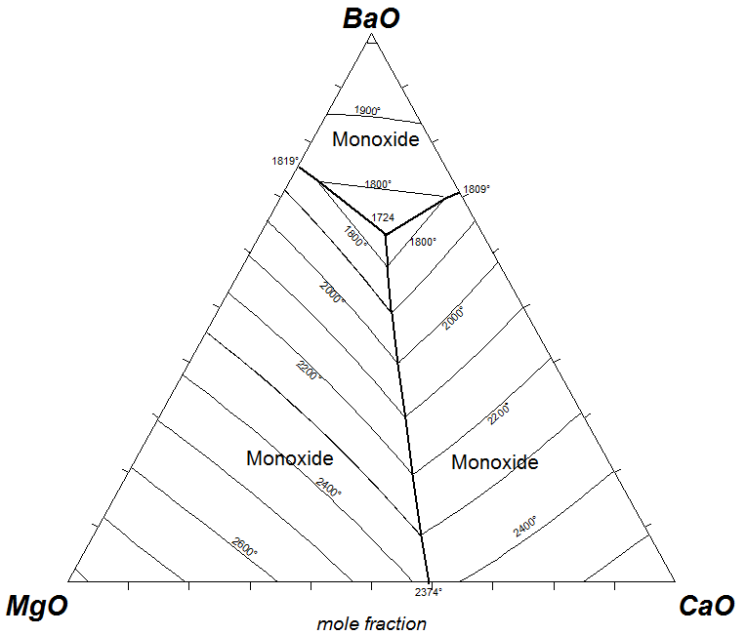

Fig. 3.23.4 Present calculated liquidus (polythermal) projection of the BaO-CaO-MgO system (isotherms were drawn at the interval of 100 °C).

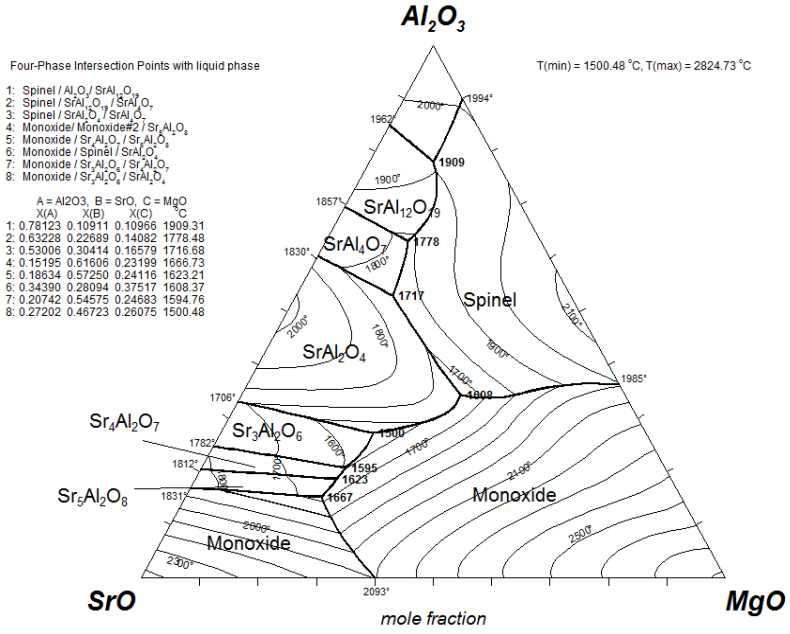

Fig. 3.23.5 Present calculated liquidus (polythermal) projection of the SrO-MgO-Al_2O_3 system (isotherms were drawn at the interval of 100 °C).

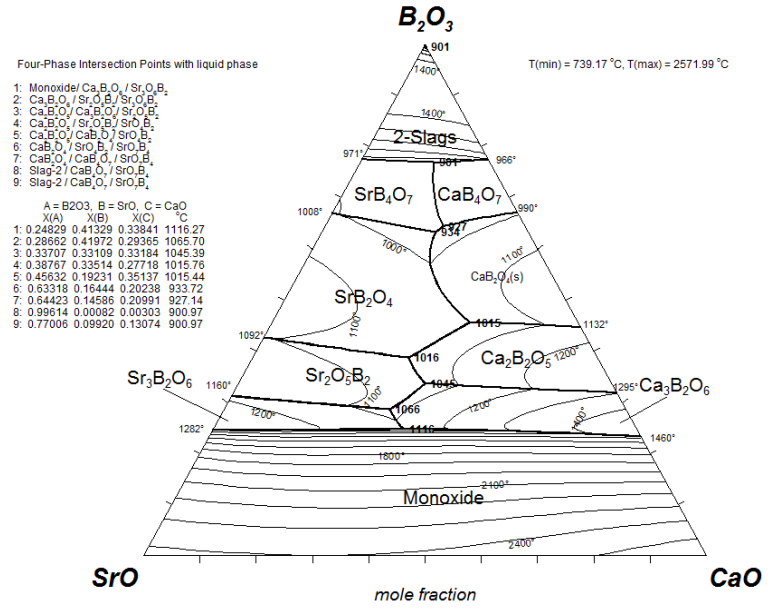

Fig. 3.23.6 Present calculated liquidus (polythermal) projection of the SrO-CaO-B_2O_3 system (isotherms were drawn at the interval of 100 °C).

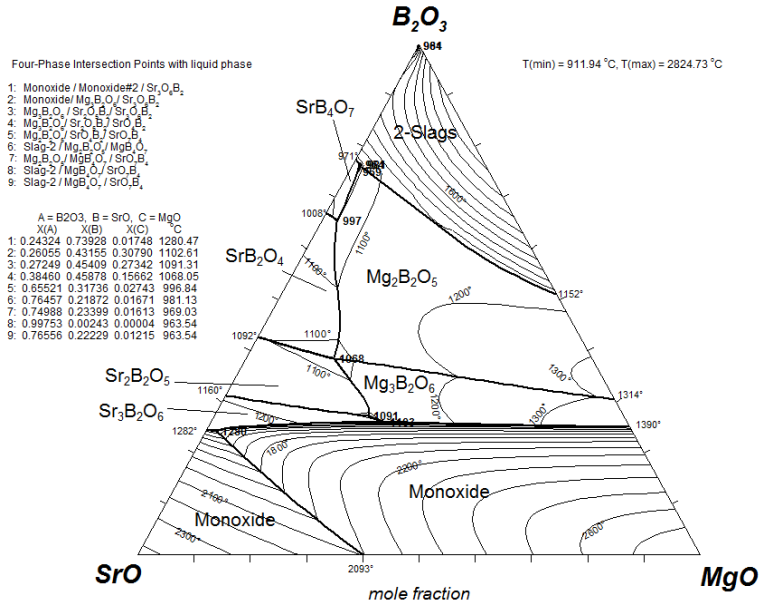

Fig. 3.23.7 Present calculated liquidus (polythermal) projection of the SrO-MgO-B_2O_3 system (isotherms were drawn at the interval of 100 °C).

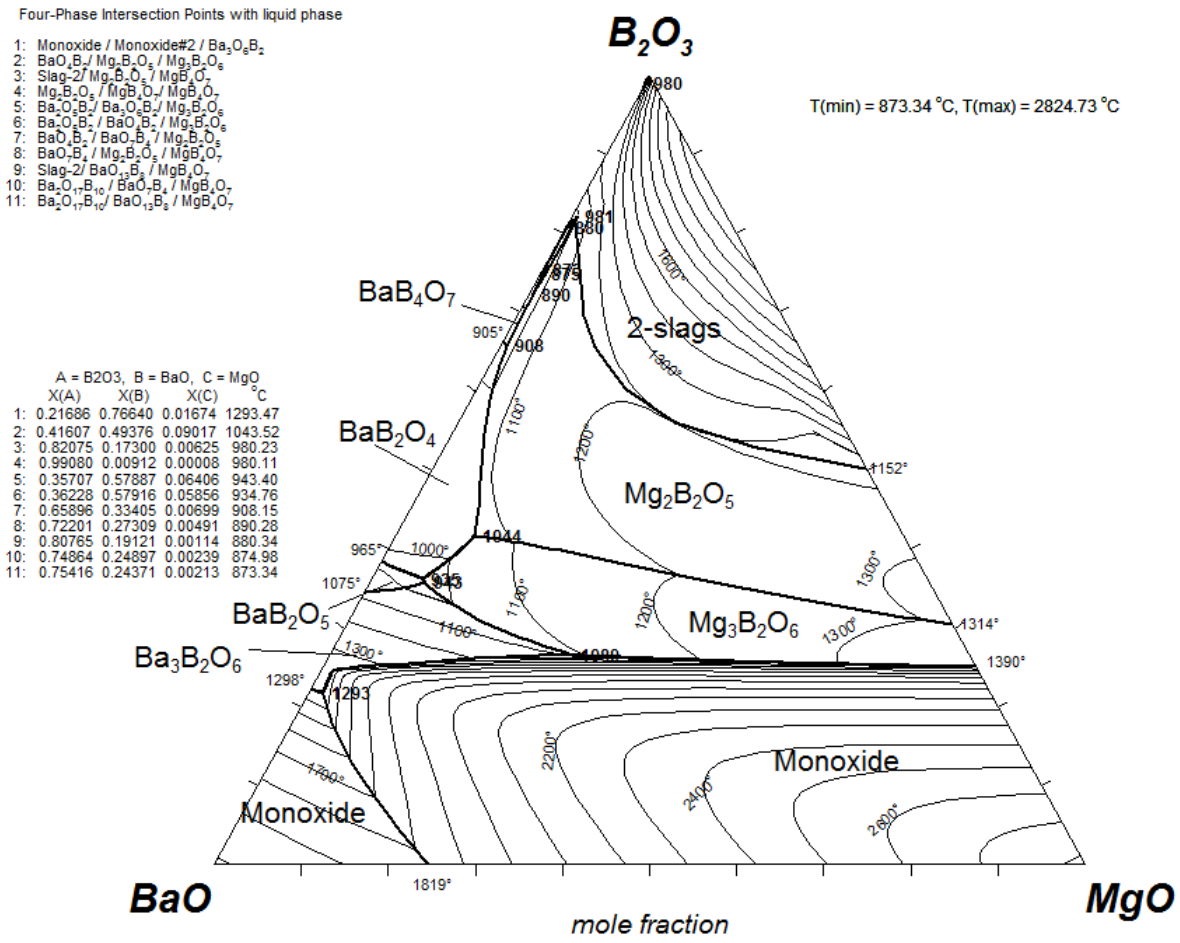

Fig. 3.23.8 Present calculated liquidus (polythermal) projection of the BaO-MgO-B_2O_3 system (isotherms were drawn at the interval of 100 °C).

3.23 Summary of the optimized phases

All the phases (in the binary and ternary systems) optimized in the present work are listed here (the elements listed inside round brackets ( ) are solutes in the matrix formed by the elements in square brackets [ ]):

Liquid phase, MgO-CaO-SrO-BaO-Al_2O_3-SiO_2-B_2O_3

Stoichiometric solid phases

Monoxide phase - [Ca,Mg,Sr,Ba,(Al)] O. The solubility of Al_2O_3 in this phase is very small.

Pseudowollastonite - [Ca,Sr,(Ba)]SiO_3.

Wollastonite - [Ca,(Ba,Sr,Mg)]SiO_3.

$BaSiO_3$ solid solution - [Ba,(Ca,Sr)]SiO_3.

α'-Ca_2SiO_4 - [Ca,Sr,Ba,(Mg)]$_2SiO_4$. The solubility of Mg_2SiO_4 is very small.

α-Ca_2SiO_4 - ([Ca,Sr,Ba,(Mg)]$_2SiO_4$). The solubility of Mg_2SiO_4 is very small.

Ba_3SiO_5 or **Sr_3SiO_5 solid solution -** [Ba,Sr,(Ca)]$_3SiO_5$.

Ca_3SiO_5 solid solution - [Ca,(Sr,Ba)]$_3SiO_5$.

Walstromite (non-stoichiometric $BaCa_2Si_3O_9$) - [Ca,Ba,(Sr)][Ca,Ba,(Sr)]$CaSi_3O_9$. This phase is stable on the $CaSiO_3$-$BaSiO_3$ section and the $SrSiO_3$ phase dissolves in it. But, this phase is not stable on the $CaSiO_3$-$SrSiO_3$ and $BaSiO_3$-$SrSiO_3$ sections.

T-phase - Ba_2Ca[Ba,Ca]Si_2O_8. This phase is stable on the Ca_2SiO_4-Ba_2SiO_4 section. In the absence of any experimental data, the solubility of Mg_2SiO_4 and Sr_2SiO_4 is neglected.

[Ca,Sr,Ba]$_2$$MgSi_2O_7$ (Akermanite)

$[Ca,Sr,Ba]_3MgSi_2O_8$ (Merwinite)

Diopside (Clinopyroxene) - $[Ca,Mg,(Sr)]MgSi_2O_6$. In the absence of any experimental data, the solubility of Ba is neglected.

$BaCa_2MgSi_2O_8$ - $[Ba,Ca][Ca,Ba]_2MgSi_2O_8$. This phase is stable on the $Ba_3MgSi_2O_8$-$Ca_3MgSi_2O_8$ section. In the absence of any experimental data, the solubility of Sr is neglected.

Strontium or **Barium meta-aluminate solid solution, β** - $[Sr,Ba,(Ca)]Al_2O_4$.

Calcium meta-aluminate solid solution, α - $[Ca,(Sr,Ba)]Al_2O_4$.

Low-temperature $BaAl_2O_4$ solution - $[Ba,(Ca,Sr)]Al_2O_4$.

Low-temperature $SrAl_2O_4$ solution - $([Sr,(Ba,Ca)]Al_2O_4$.

Cubic phase - $[Ca,Sr,Ba]_3Al_2O_6$.

Strontium or **Calcium di-aluminate solid solution** - $[Ca,Sr]Al_4O_7$.

Hexa-aluminate solid solution - $[Ca,Sr,Ba]Al_{12}O_{19}$.

Tetra-barium or -strontium aluminate solid solution - $[Ba,Sr,(Ca)]_4Al_2O_7$.

Octa-barium aluminate solid solution - $[Ba,(Ca,Sr)]_8Al_2O_7$.

BaB_2O_4 solid solution - $[Ba,(Sr)]B_2O_4$.

SrB_2O_4 solid solution - $([Sr,(Ba)]B_2O_4)$.

BaB_8O_{13} solid solution - $[Ba,(Sr,Ca)]B_8O_{13}$.

4. EXPERIMENTAL INVESTIGATIONS IN THE SrO-B_2O_3-SiO_2 SYSTEM

In the present work, a few experimental data points in the SrO-B_2O_3-SiO_2 system were generated. The thermodynamic optimization for this system is presented in section 3.18. As can be seen there, very few ternary experimental data are available in the literature for this system. The only reliable data are for the boundaries of the miscibility gap in the ternary system. The fitting of these data depends largely on the Gibbs energy of the liquid phase. During thermodynamic optimization for this ternary system, a need for new experimental data was identified. New data were necessary to reduce the number of degrees of freedom. A few experiments were performed in the present work to fill this gap. These newly obtained data improved the thermodynamic optimization of this ternary system. These data can also be useful to various glass companies as this ternary system is an important component of many commercial glasses.

In the present work, two sets of experiments were performed. In the first set, a glass of composition A (Table 4.1) was used to determine the composition of the liquid phase at 1150 °C in equilibrium with the SiO_2 and $SrSiO_3$ (SrS) phases (Fig. 4.1). In the second set, a glass of composition B (Table 4.1) was used to determine the temperature of the eutectic comprising the SiO_2, SrS and SrB_2O_4 (SrB) phases. Equilibrium samples from composition B were also used to determine the composition of the liquid phase in equilibrium with the SiO_2 and SrS phases at 1050 and 1000 °C. In the present work the preceding optimization, based only on the data available in the literature of this ternary system, was used as a guide to choose compositions A and B. To find the liquid composition in equilibrium at 1150 °C with the SrS and SiO_2 phases, a

composition (composition A in Table 4.1) was chosen which lies inside the triangle formed by the SiO_2, SrS and liquid phases in the isothermal section at 1150 °C (Fig. 4.1). Care was taken that the point lay close to the liquid phase composition, so that a maximum amount of the liquid phase can be formed with a sufficient amount of the other phases (SrS and SiO_2). Similarly, a composition (composition B in Table 4.1) close to the calculated (in the preceding optimization) eutectic point comprising the SiO_2, SrS and SrB phases was chosen to investigate the eutectic temperature. Thus the experiments were designed to generate the maximum amount of information with the minimum number of experiments, using the preceding optimization (based only on the data available in the literature) as a guide.

The source of SrO was reagent grade SrO powder (99.9 wt%) from Sigma Aldrich. The source of B_2O_3 (99.98 wt%) and SiO_2 (99.8 wt%) were reagent grade powders from Alfa Aesar. Compositions A and B were prepared in batches of 3 g by mixing SrO, B_2O_3 and SiO_2 in appropriate proportions in an agate mortar filled with acetone for 60 min. Glasses were made by melting, in a platinum crucible, the sample of composition A, in a preheated box furnace at 1300 °C for 20 min, and the sample of composition B, in a preheated box furnace at 1250 °C for 20 min. It must be noted that 3 wt.% excess B_2O_3 was added to compensate any losses by volatilization during melting. The melt was quenched to room temperature in water in an open atmosphere to produce a clear transparent glass. The glass was then again crushed, ground and stored in a desiccator. To prevent the loss of material during long heat treatments, the glasses were encapsulated in platinum capsules and brought to different equilibration temperatures. The glass samples were heat treated inside a welded platinum capsule. The heat-treatment schedule of

these samples is given in Table 4.1. After the heat treatment, the capsules were quenched to room temperature in water in an open atmosphere.

The quenched capsules were then cast in epoxy and longitudinal polished sections of the charges were made for identification of the products in backscattered electron (BSE) images. Electron probe microanalysis (EPMA) of the quenched liquids was performed on the JEOL 8900 probe at McGill University using wavelength-dispersive spectrometry (WDS). An accelerating voltage of 15 kV was used with 20 nA beam current and counting times of 20 s on peaks and 10 s on backgrounds. The raw data were reduced with the ZAF corrections using strontium titanate ($SrTiO_3$), quartz (SiO_2), and titanium diboride (TiB_2). Many analyses were performed on the liquid phase and the data were converted to mass fractions of oxides and averaged.

The detection of boron by EPMA is not sufficiently good, especially if SiO_2 is present. Boron has small atoms and emits relatively weak X-rays. The situation is made worse by the presence of Si, since it absorbs X-rays emitted by boron. This can be seen in Table 4.2, where the total of the contents of SrO, B_2O_3, and SiO_2 does not add up to 100%. In the present work, the content of B_2O_3 was calculated by subtracting the contents of SrO and SiO_2 from 100%. In Table 4.2, these amounts - the one obtained by EPMA from analysis and the one recalculated by subtraction from difference - are reported.

The BSE images of samples heat-treated at different temperatures are given in Figs. 4.2-4.6. At 1000 °C, Fig. 4.4 shows three phases (Liquid, SrS and SiO_2) in equilibrium. However, at 950 °C (Fig.4.5), and 900 °C (Fig. 4.6) there are four phases visible (the fourth phase is SrB). The WDS spectrum for these four phases is presented in Fig. 4.7 (boron was not scanned here). The temperature 950 °C should lie below the eutectic temperature, since in a ternary system four phases cannot remain in equilibrium. In other words, the liquid in Figs. 4.5 and 4.6 is metastable. Upon further heat treatment for a sufficient length of time, the liquid phase would disappear at this temperature. These results thus bracket the eutectic temperature between 950 and 1000 °C. The compositional analyses of the liquid phase in equilibrium with the SrS and SiO_2 phases at 1150, 1050 and 1000 °C are presented in Table 4.2. The preceding optimization of this ternary system, based only on the data from the literature, was refined to fit the experimental data obtained in the present work. The present final optimized value of the eutectic temperature is 991 °C. The average values of the liquid composition are reasonably well fitted in Fig. 4.1; these are same points which are plotted in Fig. 3.18.7, but in mole fraction.

Table 4.1 Compositions studied and different heat treatment of sample in the SrO-B_2O_3-SiO_2 system.

Composition A (mass %)		Composition B (mass %)
SiO_2 = 46.98 SrO = 47.72 B_2O_3 = 5.39 Melted for 20 min at 1300 °C to form sample 1		SiO_2 = 37.56 SrO = 43.59 B_2O_3 = 18.84 Melted for 20 min at 1250 °C to form samples 2 to 5
	Temperature (°C)	Days
Sample 1	1150	10
Sample 2	1050	15
Sample 3	1000	15
Sample 4	950	20
Sample 5	900	20

Table 4.2 Composition analysis of the liquid phase by EPMA in equilibrium with SiO_2 and $SrSiO_3$ at 1150 °C (Sample 1) 1050 °C (Sample 2) and 1000 °C Sample 3 (Compositions in mass % and B_2O_3(from difference) = 100-SrO-SiO_2).

Name	B_2O_3(from analysis)	SrO	SiO_2	Total	B_2O_3(from difference)
Sample 1	6.0	43.1	44.7	93.8	12.2
Sample 1	8.8	43.9	45.1	97.8	11.0
Sample 1	7.4	43.1	45.0	95.5	11.9
Sample 1	7.3	44.2	44.7	96.2	11.1
Sample 1	7.0	43.9	44.1	95.0	12.0
Sample 1	7.4	43.5	45.0	95.8	11.5
Sample 1	8.5	44.2	44.9	97.7	10.9
Sample 1	7.8	44.7	45.1	97.5	10.2

Sample 1	9.0	42.5	45.4	96.9	12.2
Sample 1	7.9	43.9	45.3	97.1	10.8
Average	7.7	43.7	44.9	96.3	11.4
Std. Deviation	0.91	0.65	0.36	1.30	0.67
Sample 2	9.0	45.2	37.0	91.2	17.7
Sample 2	9.7	44.9	37.0	91.5	18.1
Sample 2	8.9	46.1	37.6	92.5	16.4
Sample 2	11.0	45.6	37.2	93.8	17.2
Sample 2	10.3	45.8	37.3	93.4	16.9
Average	9.8	45.5	37.2	92.5	17.3
Std. Deviation	0.92	0.46	0.23	1.14	0.68
Sample 3	13.8	45.6	33.7	93.1	20.7
Sample 3	11.1	45.4	33.7	90.2	20.9
Sample 3	10.6	45.3	34.2	90.2	20.5
Sample 3	14.0	45.4	33.7	93.0	20.9
Sample 3	11.9	44.5	33.8	90.2	21.7
Average	12.3	45.2	33.8	91.3	20.9
Std. Deviation	1.52	0.45	0.23	1.59	0.48

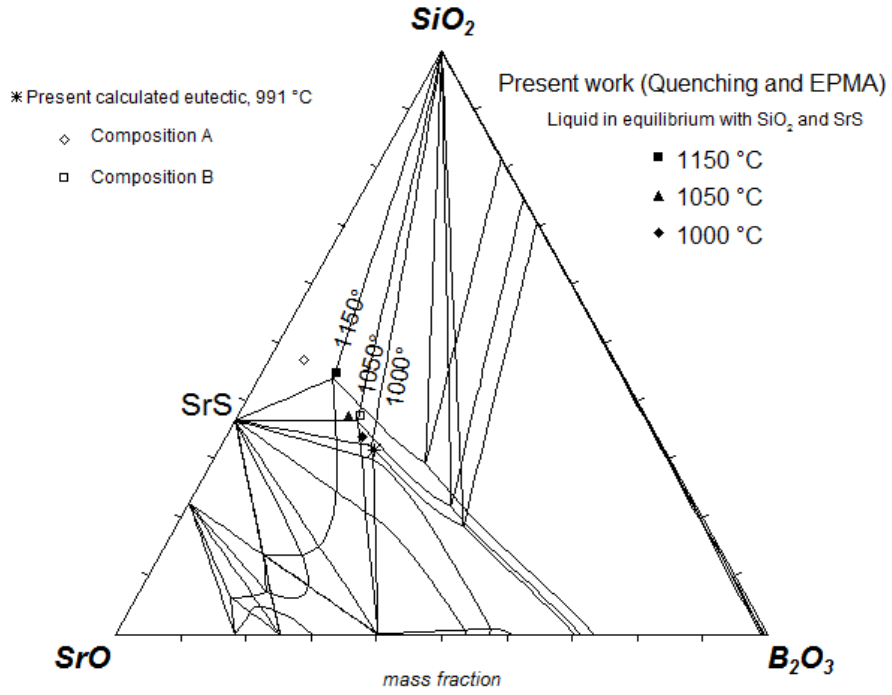

Fig. 4.1 The liquid phase in equilibrium with SiO_2 and $SrSiO_3$ phases.

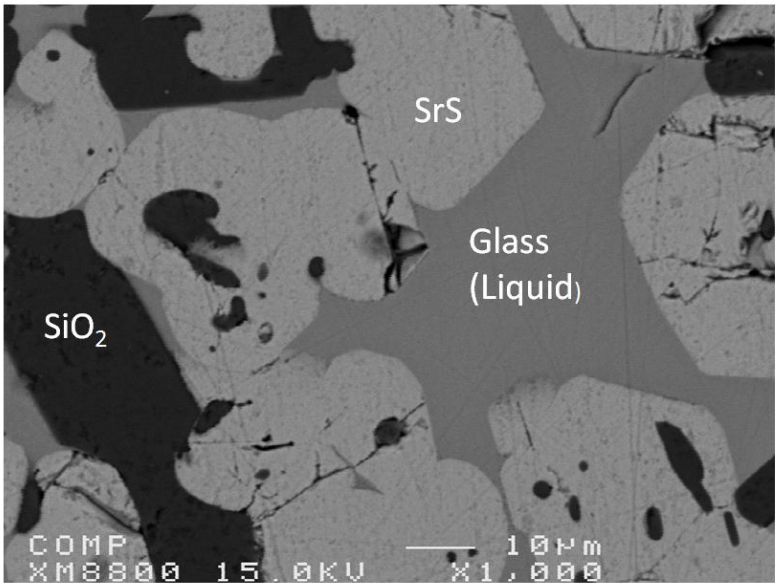

Fig. 4.2 BSE image of sample 1 (1150 °C).

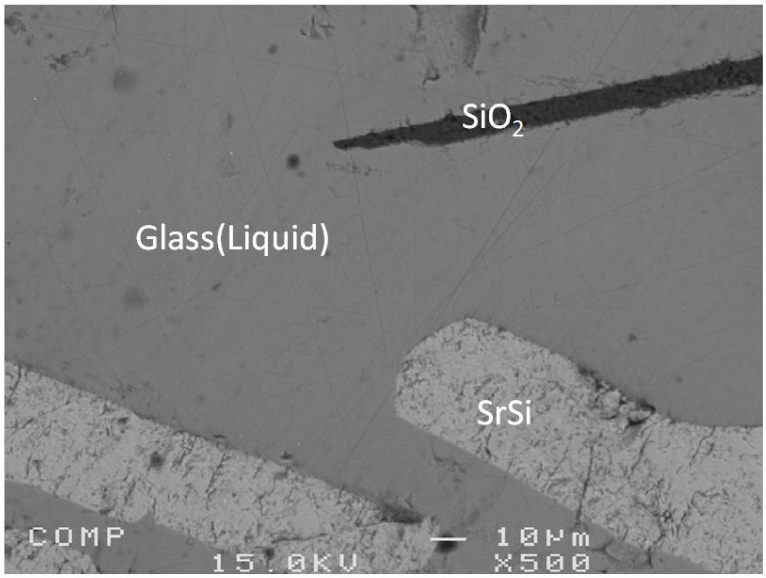

Fig. 4.3 BSE image of sample 2 (1050 °C).

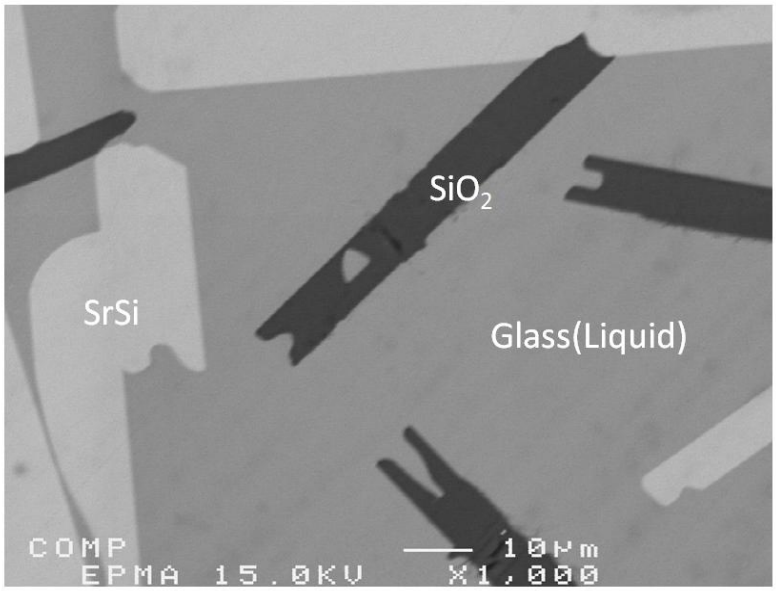

Fig. 4.4 BSE image of sample 3 (1000 °C).

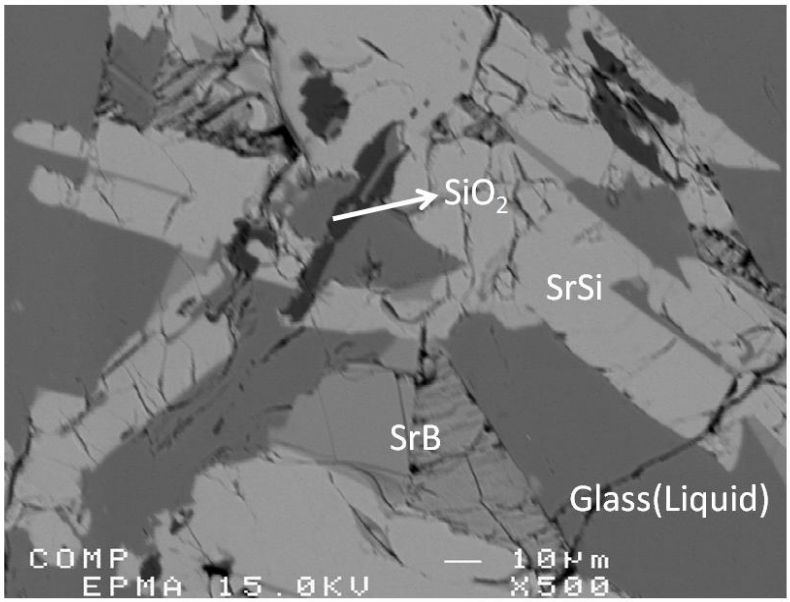

Fig. 4.5 BSE image of sample 4 (950 °C).

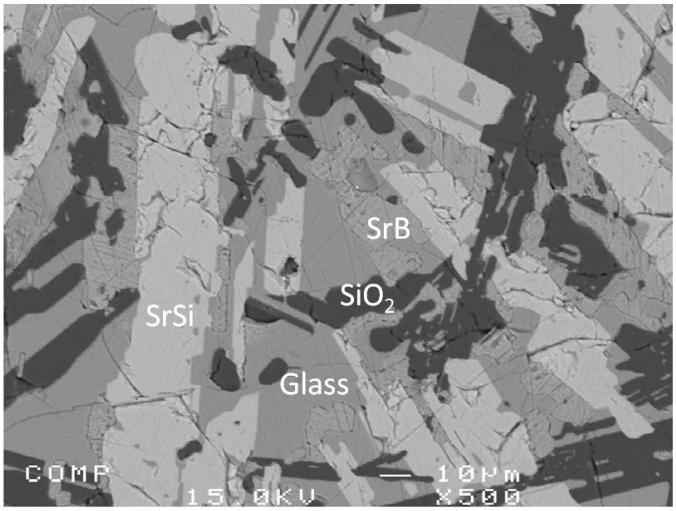

Fig. 4.6 BSE image of sample 5 (900 °C).

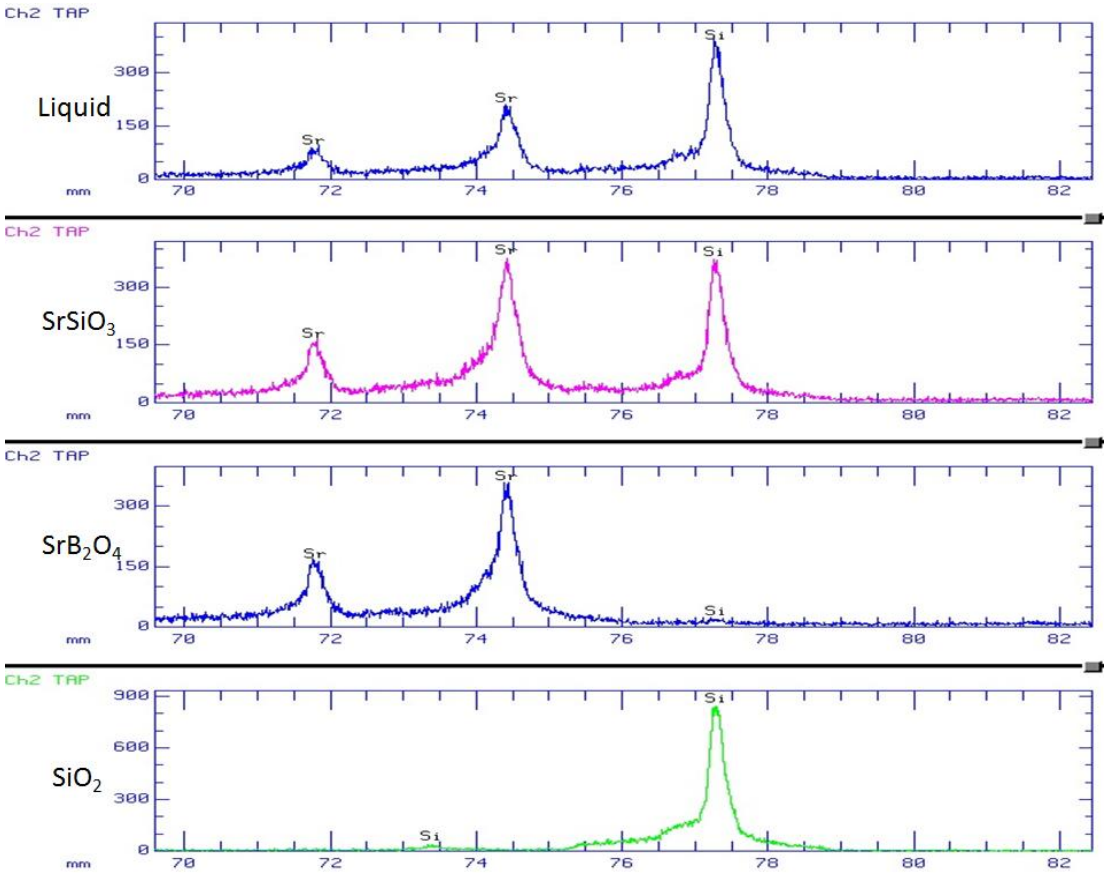

Fig 4.7 WDS spectra of the four phases (boron was not scanned here).

CONCLUSIONS

As the aim of the present work was to prepare a critically evaluated thermodynamic database as part of a broader research project to develop a multicomponent database for the CaO-MgO-BaO-SrO-Al_2O_3-B_2O_3-SiO_2 system, 11 binary, 17 ternary and 5 quaternary were critically evaluated and optimized. All the available thermodynamic and phase equilibria data were critically evaluated in order to obtain one set of optimized model parameters representing the Gibbs energies of all the phases in these systems. The reliable experimental data were reproduced within the experimental error limits. The Modified Quasichemcial Model (MQM), capable of taking into account short-range ordering in the solutions, was used to model the liquid phase. The optimized enthalpies of mixing in the liquid phase in the binary systems containing SiO_2, Al_2O_3 and B_2O_3 are quite negative and of the order of -100 kJ/mol of oxides . This is an indication of strong short-range ordering in the liquid phase.

No reliable experimental data are available for the liquid phase in the BaO-SrO, BaO-CaO, BaO-MgO, SrO-CaO and SrO-MgO systems (Sec. 2.3). The liquid in these systems was assumed to be an ideal solution. Phase diagram data for the miscibility gap in the monoxide phase in the BaO-SrO and SrO-CaO systems were reproduced well. Interaction parameters for the monoxide phase in the BaO-CaO, BaO-MgO and SrO-MgO systems were estimated, in the absence of any experimental data in the literature, by an ionic radii function from the literature (Sec. 2.3).

The thermodynamic properties of the solid phases in the SrO-SiO_2 (Sec. 2.4) and BaO-SiO_2 (Sec. 2.5) systems are better known in the literature than the thermodynamic properties of the liquid

phase in these systems. The ΔH^0_{298} and S^0_{298} of the ortho- and meta-silicates in these systems are well reproduced in the present work. All the phase diagram and thermodynamic data were simultaneously optimized to obtain the thermodynamic properties of the liquid phase. The available phase diagram data in these systems were reproduced quite satisfactorily.

The different phase diagram data available in the literature for the $SrO\text{-}Al_2O_3$ system are not very consistent (Sec. 2.6). The same is true of the $BaO\text{-}Al_2O_3$ system (Sec. 2.7). This caused a difficulty in fitting the available data in these binary systems. The final decision on the optimized thermodynamic parameters for these binary systems was based also upon the optimization of the ternary systems containing these binary systems. In such cases higher-order phase diagram data are helpful in deciding the efficacy and reliability of the binary optimized parameters.

The different phase diagram and thermodynamic data in the $BaO\text{-}B_2O_3$ (Sec. 2.8) and $SrO\text{-}B_2O_3$ (Sec. 2.9) system were well reproduced. The $BaO\text{-}B_2O_3$ system is the only system among those optimized in this work in which there are enthalpy of mixing data in the liquid phase. These data were reasonably well reproduced. In the literature, mass spectrometric measurements of the B_2O_3 gas was used to report the enthalpy of formation for some of the solid phases in these binary systems. In the present work, the original data of B_2O_3 vapor pressure, rather than the derived quantity in terms of enthalpy of formation for the solid phases, were used in the optimization.

All the available data in the $BaO\text{-}SrO\text{-}SiO_2$ (Sec. 3.1) $CaO\text{-}SrO\text{-}SiO_2$ (Sec 3.2), and $BaO\text{-}CaO\text{-}SiO_2$ (Sec 3.3) systems were well reproduced. No ternary interaction parameter was required for

the liquid phase in the BaO-SrO-SiO_2 system and very small interaction parameters were used for the liquid phase in the CaO-SrO-SiO_2, and BaO-CaO-SiO_2 systems. The optimized thermodynamic parameters from these systems reproduced reasonably well the available data in the higher-order $CaSiO_3$-$SrSiO_3$-$BaSiO_3$ system (Sec. 3.4). The solubility limits of the various solid phases such as wollastonite, pseudowollostanite, walstromite, appearing in these systems were well reproduced.

The various phase diagram data in the temperature range 1200-1700 °C for the SrO-MgO-SiO_2 system (Sec. 3.5) are well reproduced. The diopside phase (a stable phase in the CaO-MgO-SiO_2 system) is not stable in the SrO-MgO-SiO_2 system. However, there are reported data for the solubility of strontium in this phase. This solubility limit was well reproduced together with the other phase diagram data in the CaO-SrO-MgO-SiO_2 (Sec. 3.6) system.

No thermodynamic data are available for the five ternary compounds in the BaO-MgO-SiO_2 system (Sec. 3.7). The available phase diagram data in this system are reasonably well reproduced. However, during optimization the need was discovered to restrict the various degrees of freedom for some thermodynamic data for these ternary compounds. No reliable phase diagram data were present for the BaO-SrO-MgO-SiO_2 system (Sec. 3.8). The only available data on the akermanite section in this system were tentatively optimized. The solubility limits in the merwinite section in the BaO-CaO-MgO-SiO_2 (Sec. 3.9) system were well reproduced.

All the available data in the $CaO-SrO-Al_2O_3$ (Sec. 3.10), $BaO-CaO-Al_2O_3$ (Sec 3.11) and $BaO-SrO-Al_2O_3$ (Sec. 3.12) systems were well reproduced. No ternary interaction parameters were required for the liquid phase in the $BaO-SrO-Al_2O_3$ and $BaO-CaO-Al_2O_3$ systems. A very small interaction parameter was used for the liquid phase in the $CaO-SrO-Al_2O_3$ system. The solubility limits in the metaaluminate phases in these systems were well reproduced. The optimized thermodynamic parameters for these metaaluminates well reproduced the available data in the higher-order $CaAl_2O_4$-$SrAl_2O_4$-$BaAl_2O_4$ system (Sec. 3.13). The $BaO-MgO-Al_2O_3$ system (3.14) is relatively less well determined. In fact, only a few data on the solid phase equilibria in the Al_2O_3-rich corner are available in the literature. The Gibbs energy of the liquid phase in this system was estimated solely from the corresponding binary systems.

For the alumino-silicate systems $BaO-Al_2O_3-SiO_2$ (Sec. 3.15) and $SrO-Al_2O_3-SiO_2$ (Sec. 3.16) which have complex liquid structures, $BaAl_2$ and $SrAl_2$ associates were included as a separate component, to take into account the charge compensation effect, of the liquid phase. The thermodynamic modeling of such liquid solutions by double substitution of Si atoms by Al atoms has not been reported before in the literature. This double substitution method has been used first time in the present work. This helped in fitting the available data in these systems. These associates are practically unstable in these binary systems, but are stable in appreciable amounts in the ternary systems in the SiO_2-rich corner. In the alumino-borate systems $BaO-Al_2O_3-B_2O_3$ (Sec. 3.21) and $SrO-Al_2O_3-B_2O_3$ (Sec. 3.22), relatively large numbers of parameters were required to fit the available data. The reason for this could again be the complex structure of the liquid phase in these systems. The MQM is not intended to provide a complete theory for these complex liquid structures. It is rather a mathematical formalism capable of properly reflecting

structural changes in a solution. It has the characteristics required for relatively reliable interpolations and extrapolations. Hence, sometimes these methods, such as introducing a separate component in the liquid phase or using a large number of parameters, might be required to fit the available data.

The available phase diagram data in the BaO-SrO-B_2O_3 system (Sec. 3.19) were reasonably well reproduced. Very small interaction parameters in the liquid phase were used. The solubility limits of the solid metaborate phases were well reproduced. In the literature, no reported phase diagram data are available for the liquid phase in the BaO-CaO-B_2O_3 system (Sec. 3.20). The Gibbs energy of the liquid phase in this system was estimated solely from the corresponding binary systems. The reported subsolidus phase equilibria were well reproduced. The thermodynamic properties of the three ternary components in this system were optimized on the basis of these subsolidus phase equilibria.

The BaO-B_2O_3-SiO_2 system (Sec. 3.17) has been well studied and all the data were reasonably well reproduced. Ternary interaction parameters were also added for optimal fit of the available data. In the present work, a few experiments were performed in the SrO-B_2O_3-SiO_2 system (Chapter 4) to fill the gap caused by missing data in this system. These newly obtained data improved the thermodynamic optimization of this system (Sec. 3.18). The experiments were designed to generate the maximum amount of information with a minimum number of experiments using the preceding optimization (based only on the data available in the literature) as a guide. The reported activities, obtained by high-temperature mass spectrometry, for the

liquid phase in the $BaO-B_2O_3-SiO_2$ and $SrO-B_2O_3-SiO_2$ systems were given less weight during optimization of the available data. More experimental work is required to corroborate these data.

For the eight ternary systems (in the present seven-component system) where no experimental data were available, the Gibbs energy of the liquid phase was estimated from the corresponding binary systems using different "geometric model". The use of future experimental data on these systems will enhance the applicability of the databases prepared in the present work. The present optimized thermodynamic parameters will be incorporated into the FToxide database of the FactSage thermochemical software and be made available to users for various applications.

REFERENCES

Antipov, E. V., Lykova, L. N., Paromova, M. V., Rozanova, O. N., & Kovba, L. M. (1987). Crystal structure of barium aluminate (Ba3Al2O6). *Koord. Khim., 13*(8), 1119-1122.

Appendino, P. (1971). Most Basic Zone of the Barium Oxide-Alumina System. *Ann. Chim., 61*(12), 822-830.

Appendino, P. (1972a). Balances in a Solid Equilibria in the System SrO-BaO-Al2O3. *Rev. Int. Hautes Temp. Refr., 9*, 297-302.

Appendino, P. (1972b). Research on the ternary calcium oxide-barium oxide-alumina system. *Ceramurgia, 2*, 103-106.

Appendino, P., & Appendino Montorsi, M. (1969). Solida State Equilibriums in the Barium Oxide-Strontitum Oxide-Silica System. *Ann. Chim. (Rom, Italy), 59*(8-9), 806-816.

Argyle, J. F., & Hummel, F. A. (1963). Liquid Immiscibility in the System BaO-SiO2. *Phys. Chem. Glasses, 4*(3), 103-105.

Argyle, J. F., & Hummel, F. A. (1965). System PbO-BaO-MgO-SiO2. I. Phase studies in subsidiary ternary systems. *Glass Industry, 46*((10;12)), 583-587; 627-588; 710-518.

Asano, M., & Kou, T. (1988). Thermochemical properties of strontium borates, SrBO2(g) and SrB2O4(s). *J. Chem. Thermodyn., 20*(10), 1149-1156.

Asano, M., & Kou, T. (1989). Thermochemical Properties of Barium borates [BaBO2(g) and Ba3B2O6(s)]. *J. Chem. Thermodyn., 21*(8), 837-845.

Asano, M., & Kou, T. (1990). Vaporization and thermochemical properties in the barium oxide-boron oxide system. *High Temp. Sci., 29*(3), 171-187.

Bambauer, H.U., Schoeps, M., & Pentinghaus, H. (1984). Feldspar phase relations in the system NaAlSi3O8-SrAl2Si2O8. *Bull. Minr*. 107(3-4), 541-51.

Barany, R., King, E. G., & Todd, S. S. (1957). Heats of Formation of Crystalline Silicates of Strontium and Barium. *J. Am. Chem. Soc., 79*(14), 3639-3641.

Barin, I. (1995). *Thermochemical Data of Pure Substances: Third Edition*: Wiley-VCH, Germany.

Barry, T. L. (1968). Equilibriums and europium(II) ion luminescence of subsolidus phases bounded by Ba3MgSi2O8, Sr3MgSi2O8, and Ca3MgSi2O8. *J. Electrochem. Soc., 115*(7), 733-738.

Baylor, R. J., & Brown, J. J. J. (1976a). Phase separation of glasses in the system strontium oxide-boron oxide-silicon dioxide. *J. Am. Ceram. Soc., 59*(3-4), 131-136.

Baylor, R. J., & Brown, J. J. J. (1976b). Subsolidus phase equilibria in the system strontium oxide-boron oxide-silicon dioxide. *J. Am. Ceram. Soc., 59*(1-2), 21-23.

Benna, P. (1982). Calcium-strontium substitution in clinopyroxenes along the join calcium magnesium silicate-strontium magnesium silicate (CaMgSi2O6-SrMgSi2O6). *TMPM, Tschermaks Mineral. Petrogr. Mitt., 30*(1), 37-46.

Benna, P., Chiari, G., & Bruno, E. (1987). Structural modifications in clinopyroxene solid solutions: The calcium-magnesium and calcium-strontium substitutions in the diopside structure. *Mineral. Petrol., 36*(1), 71-84.

Bergeron, C.J., Risbud, S.H. (1984). *Introduction to phase equilibria in ceramics*. Columbus, Ohio: Amer. Ceramic. Soc.

Blander, M. (1962). Thermodynamic properties of molten salt solutions. *U. S. A. E. C., ORNL-3293*, 97.

Block, S., & Perloff, A. (1965). The crystal structure of barium tetraborate, BaO.2B2O3. *Acta Crystallogr., 19*(3), 297-300.

Boikova, A. I., Paramonova, V. A., & Domanskii, A. I. (1972). 3CaOSiO2 solid solutions in tristrontium silicate. *Inorg. Mater., 8*(11), 1748-1751.

Bokeriya, B. N., Tsagareishvili, D. S., & Gvelesiani, G. G. (1970a). Enthalpy and Heat Capacity of Barium Aluminate at High Temperatures. *Soobshch. Akad. nauk Gruz. SSR, 58*(2), 369-372.

Bokeriya, B. N., Tsagareishvili, D. S., & Gvelesiani, G. G. (1970b). Enthalpy and Heat Capacity of Strontium Aluminate at High Temperatures. *Soobshch. Akad. nauk Gruz. SSR, 58*(3), 601-603.

Boyko, E. R., & Wisnyi, L. G. (1957). *Structure and optical properties of CaO2Al2O3 and SrO2Al2O3*. Unclassified and Declassified Reports Published by the Atomic Energy Commission and Its Contractors.

Braniski, A. (1961). Similarities and differences in calcium, strontium and barium cements. *Zem.-Kalk-Gips, 14*, 17-26.

Brisi, C. (1963). Research about the System Lime-Barium Oxide-Silic Acid. *Ind. Ital. Cemento, 33*, 397-402.

Brisi, C., & Abbattista, F. (1960). Heat of Formation of Strontium Aluminates. *Ann. Chim., 50*, 165-169.

Brisi, C., & Appendino, P. (1965). Solid State Equilibriums in the CaO-BaO-SiO2 System. *Ann. Chim. (Rome), 55*(5), 461-468.

Brisi, C., & Montorsi, M. A. (1962). The lime-barium oxide-alumina system. *Ann. Chim. (Rome, Italy), 52*, 785-794.

Buckner, D. A., & Roy, R. (1960). Subsolidus Study of the System CaSiO3-SrSiO3. *J. Am. Ceram. Soc., 43*(1), 52-53.

Butt, Y. M., Timashev, V. V., & Kaushanskii, V. E. (1965). Solid solutions of 3SrOSiO2 in 3CaOSiO2 and their properties. *Inorg. Mater., 1*(5), 715-717.

Capron, M., & Douy, A. (2002). Strontium Dialuminate SrAl4O7: Synthesis and Stability. *J. Am. Ceram. Soc., 85*(12), 3036-3040.

Carli, F. D. (1927). Borati anidri di argento, bario e zinco. *Atti Reale Acad. Naz. Linc., 5*, 41-47.

Catti, M., & Gazzoni, G. (1983). The b = a ' phase transition of strontium silicate (Sr2SiO4). II. X-ray and optical study, and ferroelasticity of the b form. *Acta Crystallogr., Sect. B, B39*(6), 679-684.

Catti, M., Gazzoni, G., & Ivaldi, G. (1983). Structures of Twinned b -Strontium Silicate (Sr2SiO4) and of a '-Strontium Barium Silicate (Sr1.9Ba0.1SiO4). *Acta Crystallogr., Sect. C, C39*(1), 29-34.

Catti, M., Gazzoni, G., & Ivaldi, G. (1984). Order-Disorder in the a '-(Calcium, Strontium) Silicate ((Ca, Sr)2SiO4) Solid Solution: a Structural and Statistical-Thermodynamic Analysis. *Acta Crystallogr., Sect. B, B40*(6), 537-544.

Catti, M., Gazzoni, G., Ivaldi, G., & Zanini, G. (1983). The b .dblarw. a ' phase transition of strontium silicate (Sr2SiO4). I. Order-disorder in the structure of the a ' form at 383 K. *Acta Crystallogr., Sect. B, B39*(6), 674-679.

Cenerino, G., Chevalier, P. Y., & Fischer, E. (1992). *Thermodynamic calculation of phase equilibria in oxide complex systems: Prediction of some selected fission product (BaO, SrO, La2O3) releases*.

Chakoumakos, B. C., Lager, G. A., & Fernandez-Baca, J. A. (1992). Refinement of the structures of strontium aluminate (Sr3Al2O6) and the hydrogarnet Sr3Al2(O4D4)3 by Rietveld analysis of neutron powder diffraction data. *Acta Crystallogr., Sect. C: Cryst. Struct. Commun., C48*(3), 414-419.

Chartrand, P., & Pelton, A. D. (1999). Modeling the charge compensation effect in silica-rich Na2O-K2O-Al2O3-SiO2 melts. *Calphad*, 23(2),219-230.

Chartrand, P., & Pelton, A. D. (2001). The Modified Quasichemical Model. III - Two Sublattices. *Metall. Mater. Trans. A, 32A*(6), 1397-1407.

Chenot, C. F. (1967). Phase boundaries in a portion of the system. *J. Am. Ceram. Soc., 50*(2), 117-118.

Chernyshova, I. V., Semenov, Y. V., Agoshov, V. M., Gambino, M., Gaune, P., & Bros, J. P. (1991). Thermodynamic Properties of Strontium and Barium Feldspars. *Thermochim. Acta, 175*(2), 119-127.

Clemens, K., Yoshiyagawa, M., & Tomozawa, M. (1981). Liquid-Liquid Immiscibility in Barium Oxide-Boron Oxide. *J. Am. Ceram. Soc., 64*(6), C-91-C92.

Cordfunke, E. H. P., Konings, R. J. M., Van der Laan, R. R., & Ouweltjes, W. (1993). The Thermochemical Properties of Barium Borate, Ba3B2O6(s). *J. Chem. Thermodyn., 25*(3), 343-347.

Crichton, S. N., & Tomozawa, M. (1997). Prediction of Phase Separation in Binary Borate Glasses. *J. Non-Cryst. Solids, 215*(2, 3), 244-251.

Dear, P. S. (1957a). Subliquidus equilibriums for the ternary system SrO-Al2O3-SiO2. *Bull. Va. Polytech. Inst., Eng. Exp. Stn. Ser., 50*(No. 11), 12 pp.

Dear, P. S. (1957b). X-ray Diffraction Data for Silicates, Aluminates, and Aluminosilicates of Strontium. *Eng. Expt. Sta. Ser., 117*, 16 pp.

Delacarte, V., Kahn-Harari, A., & Thery, J. (1993). Barium hexaaluminoferrites with new structural features. *Mater. Res. Bull., 28*(5), 435-443.

Doersam, G., Liebscher, A., Wunder, B., Franz, G., & Gottschalk, M. (2009). Crystal structure refinement of synthetic Ca0.43Sr0.57[SiO3]-walstromite and walstromite-fluid Ca-Sr distribution at upper-mantle conditions. *Eur. J. MIneral., 21*(4), 705-714.

Dougill, M. W. (1957). Crystal structure of calcium monoaluminate. *Nature (London, U. K.), 180*, 292-293.

Duran, T., Serena, S., Pena, P., Caballero, A., De Aza, S., & De Aza, A. H. (2008). Experimental establishment of the CaAl2O4-MgO and CaAl4O7-MgO isoplethal sections within the Al2O3-MgO-CaO ternary system. *J. Am. Ceram. Soc., 91*(2), 535-543.

Dumbaugh, W. H. (1992). US Patent No. 5116787.

Emanuelson, A., Solberg, C., Evju, C., & Hansen, S. (2001). Crystal structures of cementitious compounds Part 1: calcium oxide, calcium hydroxide, calcium silicates. *ZKG Int., 54*(12), 702-704, 706-707.

Eriksson, G. (1975). Thermodynamic studies of high-temperature equilibriums. XII. SOLGASMIX, a computer program for calculation of equilibrium compositions in multiphase systems. *Chemica Scripta*, 8(3), 100-103.

Eriksson, G., & Hack, K. (1990). ChemSage - a Computer Program for the Calculation of Complex Chemical Equilibria. *Metall. Trans., 21B*(6), 1013-1023.

Eriksson, G., & Pelton, A. D. (1993). Critical Evaluation and Optimization of the Thermodynamic Properties and Phase Diagrams of the CaO-Al2O3, Al2O3-SiO2, and CaO-Al2O3-SiO2 Systems. *Metall. Trans., 24B*, 807-816.

Eriksson, G., Wu, P., Blander, M., & Pelton, A. D. (1994). Critical Evaluation and Optimisation of the Thermodynamic Properties and Phase Diagrams of the MnO-SiO2 and CaO-SiO2 Systems. *Can. Metall. Q., 33*(1), 13-21.

Eskola, P. (1922). The Silicates of Strontium and Barium. *Am. J. Sci., 5th Ser., 4*, 331-375.

Eysel, W. (1970). Crystal Chemistry of Oxyortho Compounds A3BO5 [Especially Sr3SiO5,Ba3SiO5, Ba3GeO5,K3BeF5, Rb3BeF5, and Cd3SiO5]. *Neues Jahrb. Mineral., Monatsh., 12*, 534-547.

FactSage (2008). *www.factsage.com*, Montreal, Quebec, Canada.

Fields, J. M. J., Dear, P. S., & Brown, J. J. J. (1972). Phase Equilibriums in the System BaO-SrO-SiO2. *J. Am. Ceram. Soc., 55*(12), 585-588.

Fine, A.-H., (1977) National Bureau of Standard, Special Publication 496, *Application of phase diagram in metallurgy and ceramics*, 355-367.

Flidlider, G. V., Kovtunenko, P. V., Kiseleva, E. V., & Bundel, A. A. (1966). Parallelism between the heat of formation of solid solutions of alkaline earth oxides and their ability for thermionic emission. *Russ. J. Phys. Chem., 40*(10), 1329-1331.

Foster, W. R., & Lin, H.-C. (1969). System BaO-Al2O3-SiO2. II. Binary System Celsian (BaAl2Si2O8)-Silica (SiO2). *Am. J. Sci., 267-A*, 134-144.

Fu, C.-B., Dong, H.-J., Liu, C.-Y., & Wang, Y.-P. (2010). Synthesis, structure and luminescence properties of phosphor CaAl2O4 activated by Tb+. *Optoelectron. Adv. Mater., Rapid Commun., 4*(1), 73-76.

Fukuda, K., Maki, I., & Adachi, K. (1992). Structure change of calcium silicate (Ca2SiO4) solid solutions with barium concentration. *J. Am. Ceram. Soc., 75*(4), 884-888.

Gebert, W. (1968). BaAl2SiO6, a new compound in the barium oxide-aluminum oxide-silicon oxide system. *Naturwissenschaften, 55*(8), 387.

Ghanbari-Ahari, K., & Brett, N. H. (1988). Phase equilibria and microstructure in the system zirconia-magnesia-silica-strontia. Part 2: The ternary system magnesia-silica-strontia. *Br. Ceram. Trans. J., 87*(3), 103-106.

Glasser, F. P. (1974). Polymorphism of Ba3Al2O6 and Solid Solution between Ba3Al2O6, Sr3Al2O6 and Ca3Al2O6. *Cem. Concr. Res., 4*, 745-752.

Glasser, L. S. D., & Glasser, F. P. (1968). The crystal structure of walstromite, Ca2BaSi3O9. *Amer. Mineral., 53*(1-2), 9-13.

Glushkova, V. B., & Keler, E. K. (1957). Conditions for the Formation of the Barium Silicates. III. Preparation and Properties of Tribarium Silicate. *Zh. Neorg. Chem., 2*, 1254-1258.

Gobbels, M., Kimura, S., & Woermann, E. (1998). The aluminum-rich part of the system BaO-Al2O3-MgO. I: Phase relationships. *J. Solid State Chem., 136*(2), 253-257.

Grebenshchikov, R. G., & Shitova, V. I. (1970). Solid Solutions of Strontium and Barium Orthosilicates and Orthogermanates. *Izv. Akad. Nauk SSSR, Neorg. Mater., 6*(4), 773-775.

Greig, J. W. (1927). Immiscibility in Silicate Melts. Part I. *Am. J. Sci., 5th Ser., 13*(73), 1-44.

Grosse, H. P., Tillmanns, E., & Mineral, I. (1974). Barium metasilicate, BaSiO3(h). *Cryst. Struct. Commun., 3*(4), 603-605.

Guertler, W. (1904). The Melting-Points of Mixtures of Alkaline Earths with Boric Anhydride. *Z. Anorg. Chem., 40*(Z. Anorg. Chem.), 337-354.

Haberey, F., Oehlschlegel, G., & Sahl, K. (1977). Solid-solution crystals of the composition strontium barium aluminate gallate ferrite ((Sr, Ba)(Al, Ga, Fe)12O19) as possible substrates for hexaferrite films. *Ber. Dtsch. Keram. Ges., 54*(11), 373-378.

Hageman, V. B., & Oonk, H. A. (1986). Liquid Immiscibility in the SiO2+MgO, SiO2+SrO, SiO2+La2O3, and SiO2+Y2O3 Systems. *Phys. Chem. Glasses, 27*(5), 194-198.

Hageman, V. B. M., & Oonk, H. A. J. (1979). The Region of Liquid Immiscibility in the System Boron Oxide-Barium Oxide. *Phys. Chem. Glasses, 20*(6), 126-129.

Hageman, V. B. M., & Oonk, H. A. J. (1987). Liquid Immiscibility in the Boron Oxide-Magnesia, Boron Oxide-Calcia, Boron Oxide-Strontia, and Boron Oxide-Barium Oxide Systems. *Phys. Chem. Glasses, 28*(5), 183-187.

Hageman, V. B. M., Van den Berg, G. J. K., Janssen, H. J., Oonk, H. A. J., (1986). A reinvestigation of liquid immisibility in the SiO_2-CaO System. *Phys. Chem. Glasses*, 27, 100-106.

Hahn, T., & Eysel, W. (1970). Solid Solubility in the System Zn2SiO4-Zn2GeO4-Be2SiO4-Be2GeO4. *Neues Jahrb. Mineral., Monatsh., 6*, 263-276.

Hamilton, E. H., Cleek, G. W., & Grauer, O. H. (1958). Some Properties of Glasses in the System Barium Oxideboric Oxide-Silica. *J. Am. Ceram. Soc., 41*(6), 209-215.

Hanic, F., Chemekova, T. Y., & Udalov, Y. P. (1979). Strontium Oxide-Alumina System. *Zh. Neorg. Khim., 24*(2), 471-475.

Hemminger, H., and Sarge, S. M., (1999), *Handbook of Thermal Analysis and Calorimetry*, D-38116, Braunschweig, Germany.

Henderson, C. M. B., & Taylor, D. (1982). The structural behavior of the nepheline family I Strontium and barium aluminates. *Mineral. Mag., 45*(337), 111-127.

Henning, O., & Paeselt, G. (1965a). Infrared Investigation of Binary Systems of Inorganic Salts. I. Sr2SiO4-Ba2SiO4 System. *Ztschr. Chem., 5*(11), 424-425.

Henning, O., & Paeselt, G. (1965b). Infrared Investigations of Binary Systems of Inorganic Salts. II. The System Ca2SiO4-Sr2SiO4. *Ztschr. Chem., 5*(12), 468.

Hesse, K. F., & Liebau, F. (1980). Crystal chemistry of silica-rich barium silicates. I. Refinement of the crystal structures of Ba4[Si6O16], Ba5[Si8O21] and Ba6[Si10O26], silicates with triple, quadruple and quintuple chains. *Z. Kristallogr., 153*(1-2), 3-17.

Hillert, M. (2000). The compound energy formalism. *J. Alloy. Compounds.* 320(2), 161-176.

Hilpert, K., Beske, H., & Naoumidis, A. (1975). Mass spectrometric study of the vaporization of barium aluminum oxides (Ba3Al2O6 and BaAl12O19). *High Temp. Sci., 7*(3), 159-166.

Hilpert, K., Naoumidis, A., & Wolff, G. (1975). Mass spectrometric study of the evaporation of aluminum barium oxide (BaAl2O4). *High Temp. Sci., 7*(1), 1-10.

Hovhannisyan, R. M. (2003). Rafaelites - New Kinds of Glass Ceramics with Low Thermal Expansion and Low Melting Temperatures on the Basis of Alkaline Earth Aluminium Borates. *Glass. Technol., 44*(2), 96-100.

Hovhannisyan, R. M. (2004). *BaB2O4, BaAl2B2O7, BaTi(BO3)2: glasses and glass ceramics on their basis*.

Hovhannisyan, R. M. (2005). Some Aspects of Glass and Glass Ceramics Formation of Stoichiometric Compositions in the RO-Al2O3-B2O3 Systems. *Ceram. Trans., 170*(Melt Chemistry, Relaxation, and Solidification Kinetics of Glasses), 201-211.

Hovhannisyan, R. M. (2006). Binary alkaline earth borates: phase diagram correction and low thermal expansion of crystallised stoichiometric glass compositions. *Phys. Chem. Glasses, 47*(4), 460-464.

Huebner, K. H. (1969). Borates 2BaO . 5B2O3, low-Ba . B2O3, 2BaO . B2O3 and 4BaO . B2O3. *Neues Jahrb. Mineral. Monatsh., 8*, 335-342.

Huebner, K. H. (1970). Ternary system barium oxide-aluminum oxide-boron oxide. *Neues Jahrb. Mineral. Abh, 112*(2), 150-160.

Huntelaar, M. E., Booij, A. S., Cordfunke, E. H. P., & Van der Laan, R. R. (1998). The thermodynamic properties of Sr3MgSi2O8(s) from T = (0 to 1500) K. *J. Chem. Thermodyn., 30*(4), 497-507.

Huntelaar, M. E., & Cordfunke, E. H. P. (1993). The Ternary System Barium Silicate-Strontium Silicate-Silica BaSiO3-SrSiO3-SiO2. *J. Nucl. Mater., 201*, 250-253.

Huntelaar, M. E., Cordfunke, E. H. P., & Ouweltjes, W. (1992a). The standard molar enthalpies of formation of barium silicate (BaSiO3)(s) and barium silicate (Ba2SiO4)(s). *J. Chem. Thermodyn., 24*(10), 1099-1102.

Huntelaar, M. E., Cordfunke, E. H. P., & Ouweltjes, W. (1992b). The Standard Molar Enthalpies of Formation of Strontium Silicates SrSiO3(s) and Sr2SiO4(s). *J. Chem. Thermodyn., 24*(2), 139-143.

Huntelaar, M. E., Cordfunke, E. H. P., & Scheele, A. (1993). Phase Relations in the Strontium Oxide-Silica-Zirconium Dioxide System I. The System SrO-SiO2. *J. Alloys Compd., 191*(1), 87-90.

Huntelaar, M. E., Cordfunke, E. H. P., & Westrum, E. F. J. (1992). The Heat Capacity and Derived Thermophysical Properties of Some Alkaline Earth Silicates and Zirconates from 5 to 1000 K. I. Crystalline Strontium Silicates (SrSiO3 and Sr2SiO4). *J. Phys. Chem. Solids, 53*(6), 801-806.

Irgashov, K., Tarasov, V. D., & Chekhovskii, V. Y. (1985). Thermodynamic Properties of Strontium Oxide in the Solid and Liquid Phases. *Teplofiz. Vys. Temp., 23*(1), 86-91.

Ito, S., Banno, S., Suzuki, K., & Inagaki, M. (1977). Phase transition in strontium monoaluminate. *Z. Phys. Chem. (Wiesbaden), 105*(3-4), 173-178.

Ito, S., Banno, S., Suzuki, K., & Inagaki, M. (1979). Solid solubilities in the alkaline-earth metal aluminates. *Yogyo Kyokaishi, 87*(7), 344-349.

Iyi, N., Gobbels, M., & Kimura, S. (1998). The aluminum-rich part of the system BaO-Al2O3-MgO. II: crystal structure of the β-alumina-related compound, Ba2Mg6Al28O50. *J. Solid State Chem., 136*(2), 258-262.

Iyi, N., Inoue, Z., Takekawa, S., & Kimura, S. (1984). The crystal structure of barium hexaaluminate phase I (barium beta -alumina). *J. Solid State Chem., 52*(1), 66-72.

Iyi, N., Inoue, Z., Takekawa, S., & Kimura, S. (1985). The crystal structure of barium lead hexaaluminate phase II. *J. Solid State Chem., 60*(1), 41-50.

Iyi, N., Takekawa, S., Bando, Y., & Kimura, S. (1983). Electron microscopic study of barium hexaaluminates. *J. Solid State Chem., 47*(1), 34-40.

Jacob, K. T., & Varghese, V. (1995). Solid-State Miscibility Gap and Thermodynamics of the System BaO-SrO. *J. Mater. Chem., 5*(7), 1059-1062.

Jacob, K. T., & Waseda, Y. (1998). Solid-State Immiscibility and Thermodynamics of the Calcium Oxide-Strontium Oxide System. *J. Am. Ceram. Soc., 81*(4), 1065-1068.

Jaeger, F. M., & Van Klooster, H. S. (1916). Investigations in the field of silicate chemistry. IV. Some data on the meta- and orthosilicates of the bivalent metals: beryllium, magnesium,

calcium, strontium, barium, zinc, cadmium and manganese. *Proc. K. Ned. Akad. Wet., 18*, 896-913.

Jak, E., & Hayes, P. C. (2004). *Phase equilibria determination in complex slag systems*. Johannersburg, Cape Town, South Afica.

JANAF Thermochemical Tables, r. E. (1985). *14*(6), 383.

Ji, Y., Liang, J., Xie, S., & Yu, Y. (1995). Subsolidus phase equilibria of the CaO-B2O3-BaO system. *J. Am. Ceram. Soc., 78*(3), 765-768.

Jiang, H., Zhang, L., Huang, Y., Jia, D., & Guo, Z. (2007). Synthesis and optical properties of ultra-fine Sr5Al2O8:Eu3+ nanorod phosphor from a low-heating-temperature solid-state precursor method. *Mater. Sci. Eng., B, 145*(1-3), 23-27.

Jung, I.-H. (2003). Ph. D. Thesis. *Critical Evaluation and Thermodynamic Modeling of Phase Equilibria in Multicomponent Oxide Systems.* Ecole Polytechnique, Montreal, Quebec, Canada.

Jung, I.-H. (2003). The thermodynamic optimization of the BaO-SiO2 system. Unpublished work. Mcgill university, Montreal, Quebec, Canada.

Kadyrova, Z. R. (1999). The formation of the hexagonal Ca1-xSrxAl12O19 solid solution. *Zh. Neorg. Khim., 44*(12), 2074-2076.

Kadyrova, Z. R., & Daminova, D. A. (1997). Phase relations in the CaAl12O19-BaAl12O19 system. *Uzb. Khim. Zh.*(4), 8-12.

Kadyrova, Z. R., Syrazhiddinov, N. A., & Tuganova, S. K. (1996). SrAl12O19-BaAl12O19 system. *Dokl. Akad. Nauk Resp. Uzb.*(4), 26-27.

Kahlenberg, V. (2001). Crystal structure of Ba8[Al3O10][AlO4], a novel mixed-anion Ba aluminate related to kilchoanite. *Mineral. Mag., 65*(4), 533-541.

Kang, Y.-B. and Lee, H.-G., (2005), Experimental study of phase equilibria in the MnO-SiO_2-"TiO_2"-Ti_2O_3 system. *ISIJ International*, 45(11), 1552-1560.

Kang, H. G., Park, J. K., Kim, C. H., & Choi, S. C. (2009). Luminescence properties of MAl12O19:Mn4+ (M=Ca, Sr, Ba) for UV LEDs. *J. Ceram. Soc. Jpn., 117*(May), 647-649.

Kaplun, A.B., Meshalkin, A.B., (2004), Oscillation method of phase analysis as powerful method of comprehensive study of physical–chemistry properties and phase equilibria for new materials design. *Journal of Crystal Growth*, 275, e1975–e1981.

Kattner, U.R. (1997). The thermodynamic modeling of multicomponent phase equilibria. *J. Metals.* 49(12), 14-19.

Kaufman, L., & Bernstein, H. (1970). *Computer Calculation of Phase Diagrams with Special Reference to Refractory Metals.* New York: Academic Press.

Kikuchi, R. (1951). A theory of cooperative phenomena. *Phys. Rev*. 81, 988-1003.

Kim, J.-B., Lee, K.-S., Suh, I.-H., Lee, J.-H., Park, J.-R., & Shin, Y.-H. (1996). Strontium metaborate, SrB2O4. *Acta Crystallogr., Sect. C: Cryst. Struct. Commun., C52*(3), 498-500.

Kimura, H., Numazawa, T., & Sato, M. (1997). Melt supercooling behavior and crystal growth of Ba(B1-xMx)2O4 (M: Al or Ga). *J. Cryst. Growth, 174*(1-4), 308-312.

Kimura, K., Ohgaki, M., Tanaka, K., Morikawa, H., & Marumo, F. (1990). Study of the bipyramidal site in magnetoplumbite-like compounds, SrM12O19 (M = aluminum, iron, gallium). *J. Solid State Chem., 87*(1), 186-194.

Kimura, S., Bannai, E., & Shindo, I. (1982). Phase Relations Relevant to Hexagonal Barium Aluminates. *Mater. Res. Bull., 17*(2), 209-215.

Kindermann, B. (1978). Synthesis and crystallographic data of calcium borate, CaB4O7. *Z. Kristallogr., Kristallgeom., Kristallphys., Kristallchem., 146*(1), 61-66.

Klasens, H. A., Hoekstra, A. H., & Cox, A. P. M. (1957). Ultraviolet fluorescence of some ternary silicates activated with lead. *J. Electrochem. Soc., 104*, 93-100.

Kockel, A., & Oehlschlegel, G. (1969). The Ternary Compound, BaO.Al2O3.SiO2. *Neues Jahrb. Mineral. Monatsh., 1*, 15-24.

Konishi, T., Asano, T., Ishii, Y., Soga, K., Inoue, H., Makishima, A., et al. (2000). Effects of Eu2O3 on Liquid-Liquid Phase Separation of PbO-B2O3, BaO-B2O3 and SrO-B2O3 Glasses. *J. Non-Cryst. Solids, 265*(1-2), 19-28.

Kouta, H., Kuwano, Y., Suda, K., Ishizawa, N., & Marumo, F. (1994). High-temperature powder x-ray diffraction study of barium metaborate, BaB2O4. *Rep. Res. Lab. Eng. Mater., Tokyo Inst. Technol., 19*, 9-17.

Kovba, L. M., Lykova, L. N., Antipov, E. V., Paromova, M. V., & Rozanova, O. N. (1987). Barium Aluminum Oxides. *Zh. Neorg. Khim., 32*(2), 537-539.

Krzhizhanovskaya, M. G., Bubnova, R. S., Krivovichev, S. V., Belousova, O. L., & Filatov, S. K. (2010). Synthesis, crystal structure and thermal behavior of Sr3B2SiO8 borosilicate. *J. Solid State Chem., 183*(10), 2352-2357.

Kuroki, T., Saito, Y., Matsui, T., & Morita, K. (2009). Evaluation of Phase Diagrams for the Al2O3-CaO-SrO System by In-Situ Observation Using Confocal Laser Microscope. *Mater. Trans.*, 1-7.

Lapina, I. V., Semenov, Y. V., & Khodakovskii, I. L. (1989). Thermodynamic properties of calcium-, strontium-, and barium feldspars based on calorimetric data. *Geokhimiya, 7*, 1033-1037.

Lazic, B., Kahlenberg, V., Kaindl, R., & Kremenovic, A. (2009). On the symmetry of Ba3Al2O6 X-ray diffraction and Raman spectroscopy studies. *Solid State Sci., 11*(1), 77-84.

Levin, E. M., & Cleek, G. W. (1958). Shape of Liquid Immiscibility Volume in the System Barium Oxide-Boric Oxide-Silica. *J. Am. Ceram. Soc., 41*(5), 175-179.

Levin, E. M., & McMurdie, H. F. (1949). The System BaO-B2O. *J. Am. Ceram. Soc., 32*, 99-105.

Levin, E. M., & Ugrinic, G. M. (1953). The System Barium Oxide-Boric Oxide-Silica. *J. Res. Nat. Bur. Stand., 51*(1), 37-56.

Levitskii, V. A., Skolis, Y. Y., Chentsov, V. N., & Golovanova, Y. G. (1972). Thermodynamic Properties of Binary Oxide Systems at High Temperatures. V. Thermodynamic

Parameters of the Interaction of Strontium Oxide with Strontium Aluminate, SrAl2O4. *Zh. Fiz. Khim., 46*(6), 1411-1413.

Liang, J.-K. Z. Y. L., & Huang, Q.-Z. (1982). The Kinetic Study of BaB2O4 Phase Transition. *Huaxue Xuebao, 40*(11), 994-1000.

Liebertz, J. (1988). Space group symmetry of the two forms of barium borate (BaB2O4). *Z. Kristallogr., 182*(1-4), 307-308.

Lin, H.-C., & Foster, W. R. (1968). System Barium Oxide-Aluminum Oxide-Silicon Dioxide. I. Polymorphism of Celsian. *Am. Mineral., 53*(1-2), 134-144.

Lin, H.-C., & Foster, W. R. (1969). System Barium Oxide-Aluminum Oxide-Silicon Dioxide. III. Binary System Sanbornite-Celsian. *Mineral. Mag., 37*(288), 459-465.

Lin, H.-C., & Foster, W. R. (1970). System Baria-Alumina-Silica. V. Ternary System Sanbornite-Celsian-Silica. *J. Am. Ceram. Soc., 53*(10), 549-551.

Liu, B., & Barbier, J. (1993). Structures of the stuffed tridymite derivatives, BaMSiO4 (M = Co, Zn, Mg). *J. Solid State Chem., 102*(1), 115-125.

Liu, H., Guo, C., Fan, S., & Xu, Y. (1997). Study on crystal structure and microstructure of SrB4O7 doped with Li by x-ray powder diffraction. *Wuji Cailiao Xuebao, 12*(1), 17-23.

Liu, J., Duan, C.-g., Mei, W. N., Smith, R. W., & Hardy, J. R. (2002). Polymorphous Transformations in Alkaline-Earth Silicates. *J. Chem. Phys., 116*(9), 3864-3869.

Liu, Z.-H., & Huang, H.-S. (2006). Synthesis and thermochemistry of SrB2O4× 4H2O and SrB2O4. *Thermochim. Acta, 448*(1), 59-62.

Liu, Z.-H., Wang, Y., & Huang, H.-S. (2007). Determination of Standard Molar Enthalpies of Formation for the Two Barium Borates BaB2O4·xH2O (x = 4, 0) by Microcalorimetry. *J. Chem. Eng. Data, 52*(2), 487-490.

Lopatin, S. I., Shugurov, S. M., Stolyarova, V. L., & Tyurnina, N. G. (2006). Thermodynamic properties of silicate glasses and melts: II. System SrO-SiO2. *Russ. J. Gen. Chem., 76*(12), 1878-1884.

Luck, R., Gerling, U., Predel, B. (1989). An entropy paradox of the association model, *Z.Metallkunde*, 80(4),270-275.

Massazza, F. (1955). The Systems SrO-SiO2 and SrO-SiO2-CaO. *Chim. l'Ind. (Milan, Italy), 37*, 939-943.

Massazza, F. (1959). The System SrO-Al2O3. *Chim. l'Ind. (Milan, Italy), 41*, 108-115.

Massazza, F. (1961). Thermochemical Research on the SrO-Al2O3 System. *Ann. Chim. (Rom, Italy), 51*, 898-903.

Massazza, F. (1962). Ricerche nel sistema quaternario CaO-SrO-MgO-SiO2. Il sistema 2CaO.MgO.2SiO2-2SrO.MgO.2SiO2. *Ann. Chim. (Rome), 52*, 611-619.

Massazza, F. (1963). Preparation of calcium and barium aluminates based on hydraulic cements. I. Solid state system CaO-BaO-Al2O3. *Ann. Chim. (Rome, Italy), 53*(7), 1002-1017.

Massazza, F., & Cannas, M. (1959). The system CaO-Al2O3-SrO. *Ann. Chim. (Rome, Italy), 49*, 1342-1351.

Massazza, F., & Cannas, M. (1961). Thermochemical measurements in the system SrO-Al2O3-CaO. I. Heats of formation in the system 3CaO.Al2O3-3SrO.Al2O3. *Ann. Chim. (Rome, Italy), 51*, 904-911.

Massazza, F., & Fadda, R. (1964). The quaternary system CaO-SrO-MgO-SiO2 II The 3CaOMgO2SiO2-3SrOMgO2SiO2 systems. *Ann. Chim. (Rome, Italy), 54*(3-4), 294-302.

Massazza, F., & Fadda, R. (1966). Thermochemical studies of the system 2CaO.Al2O3.SiO22SrO.Al2O3.SiO2. *Annali di chimica, 56*(1-2), 78-86.

Massazza, F., & Sirchia, E. (1959). Equilibriums at the temperature of fusion in the ternary system SrO-Al2O3-CaO. *Ann. Chim. (Rome, Italy), 49*, 1352-1370.

Mateika, D., & Laudan, H. (1979). Czochralski Growth of Barium Hexaaluminate Single Crystals. *J. Cryst. Growth, 46*(1), 85-90.

Matkovic, B., Popovic, S., Grzeta, B., & Halle, R. (1986). Phases in the System Ba2SiO4-Ca2SiO4. *J. Am. Ceram. Soc., 69*(2), 132-134.

Meshalkin, A. B., & Kaplun, A. B. (2005). Study of Phase Equilibria in System BaO-B2O3 from 32 to 67 mol% B2O3. *J. Cryst. Growth, 275*(1-2), e301-e305.

Mirbabaeva, N. N., Sirazhiddinov, N. A., & Grebenshchikov, R. G. (1974). Phase equilibriums in the barium akermanite - strontium akermanite (Ba2MgSi2O7-Sr2MgSi2O7) system. *Inorg. Mater., 10*(5), 758-760.

Miyazaki, A., Kimura, H., Maiwa, K., Nakamura, H., & Kannan, C. V. (2004). Characterization of SHG candidate crystals in barium aluminum (gallium) borates. *Cryst. Res. Technol., 39*(4), 333-336.

Moir, G. K., Gard, J. A., & Glasser, F. P. (1975). Crystal Chemistry and Solid Solutions Amongst the Pseudowollastonite-Like Polytypes of the Calcium, Strontium, and Barium Silicates CaSiO3, SrSiO3, and BaSiO3. *Z. Kristallogr., 141*(5-6), 437-450.

Mondal, P., & Jeffrey, J. W. (1975). Crystal structure of tricalcium aluminate, Ca3Al2O6. *Acta Crystallogr., Sect. B, B31*(3), 689-697.

Muller, F., & Demirok, S. (1989). Thermochemical Study of the Liquid Systems BaO-B2O3 and CaO-B2O3. *Glastech. Ber., 62*(4), 142-149.

Mumme, W., Cranswick, L., & Chakoumakos, B. (1996). Rietveld crystal structure refinements from high temperature neutron powder diffraction data for the polymorphs of dicalcium silicate. *Neues Jahrb. Mineral., Abh., 170*(2), 171-188.

Nacken, R. (1930). Determination of the Heats of Formation of Silicates from their Oxides. *Zement, 19*, 818-825.

Nadachowski, F., & Grylicki, M. (1959). Phase Equilibriums in the System 2BaO.SiO2-2CaO.SiO2. 2MgO.SiO2. *Silikattechnik, 10*(2), 77-80.

Nagel, S. R., Eagan, R. J., & Bergeron, C. G. (1970). Enthalpy of fusion of SrO.2B2O3. *J. Am. Ceram. Soc., 53*(4), 227-228.

Nurse, R. W. (1952). Tristrontium Silicate-a New Compound. *J. Appl. Chem., 2*, 244-246.

O'Daniel, H., & Tscheischwili, L. (1942). The Structures of K2BeF4, Sr2SiO4 and Ba2SiO4. *Z. Kristallogr., 104*, 348-357.

Ohta, Y., Morinaga, K., & Yanagase, T. (1982). Liquid-Liquid Immiscibility in Several Binary Borate Systems. *Yogyo Kyokai Shi, 90*(9), 511-516.

Ol'shansky, Y. I. (1951). Equilibrium of the Two Immiscible Liquids in the Silicate Systems of the Earth Metals. *Dokl. Akad. Nauk SSSR, 76*(1), 93-96.

Paeselt, G., & Henning, O. (1968). Formation of Mixed Crystals in Orthosilicate Systems. *Wissenschaftliche Zeitschrift der Hochschule fuer Architektur und Bauwesen Weimar, 15*(3), 319-323.

Pan, X. M., Wang, C., & Jin, Z. P. (2004). Assessment of the Thermodynamics and Phase Diagram of the SrO-B2O3 System. *Z. Metallkd., 95*(1), 40-44.

Park, C.-H., Hong, S.-T., & Keszler, D. A. (2009). Superstructure of a phosphor material Ba3MgSi2O8 determined by neutron diffraction data. *J. Solid State Chem., 182*(3), 496-501.

Pelton, A.D. (2001). A general "geometric" thermodynamic model for multicomonent solutions. *Calphad.* 25 (2), 319-328.

Pelton, A. D., & Blander, M. (1984). *Computer-Assisted Analysis of the Thermodynamic Properties and Phase Diagrams of Slags*. Proceedings of the Second International Symposium on Metallurgical Slags and Fluxes, TMS-AIME, Warrendale, PA. 281-294.

Pelton, A. D., & Chartrand, P. (2001). The Modified Quasichemical Model. II - Multicomponent Solutions. *Metall. Mater. Trans. A, 32A*(6), 1355-1360.

Pelton, A. D., Chartrand, P., & Eriksson, G. (2001). The modified Quasichemical Model. IV - Two Sublattice Quadruplet Approximation. *Metall. Mater. Trans. A, 32A*(6), 1409-1415.

Pelton, A. D., Decterov, S. A., Eriksson, G., Robelin, C., & Dessureault, Y. (2000). The Modified Quasichemical Model. I - Binary Solutions. *Metall. Mater. Trans. B, 31B*(4), 651-659.

Pelton, A.D., & Kang, Y., -B. (2007). Modeling short-range ordering in solutions. *Int. J. Mat. Res.* 10, 907-917.

Pelton, A. D., & Schmalzried, H. (1973). On the geometrical representation of phase equilibria**.** *Met. Trans.* 4(5), 1395-404.

Peppler, R. B., & Newman, E. S. (1951). Heats of Formation of Some Barium Aluminates. *J. Res. Natl. Bur. Stand., 47 (Reaearch Paper 2269)*, 439-442.

Pieper, G., Eysel, W., & Hahn, T. (1972). Solid Solubility and Polymorphism in the System Sr2SiO4-Sr2GeO4-Ba2GeO4-Ba2SiO4. *J. Am. Ceram. Soc., 55*(12), 619-622.

Ponomarev, V. I., Kheiker, D. M., & Belov, N. V. (1970). Crystal structure of calcium dialuminate. *Kristallografiya, 15*(6), 1140-1143.

Prodjosantoso, A. K., & Kennedy, B. J. (2003). Solubility of SrAl2O4 in CaAl2O4 - a high resolution powder diffraction study. *Mater. Res. Bull., 38*(1), 79-87.

Prodjosantoso, A. K., Kennedy, B. J., & Hunter, B. A. (2000). Synthesis and structural studies of strontium-substituted tricalcium aluminate Ca3-xSrxAl2O6. *Aust. J. Chem., 53*(3), 195-202.

Purt, G. (1960). Binary System BaO-Al2O3. *Radex Rundschau*, 198-202.

Raynor, G.V. (1976) in: Physical Metallurgy, 2nd edn: Cahn, R.W. (Ed.), Amsterdam: North Holland, Chap. 7.

Richet, P., & Bottinga, Y. (1985). Heat capacity of aluminium-free liquid silicates. *Geochim. Cosmochim. Acta, 49*(2), 471-486.

Risold, D., Hallstedt, B., & Gauckler, L. J. (1996). The strontium-oxygen system. *CALPHAD: Comput. Coupling Phase Diagrams Thermochem., 20*(3), 353-361.

Rodehorst, U., Carpenter, M. A., Marion, S., & Henderson, C. M. B. (2003). Structural Phase Transitions and Mixing Behaviour of the Ba-Aluminate (BaAl2O4)-Sr-Aluminate (SrAl2O4) Solid Solution. *Mineral. Mag., 67*(5), 989-1013.

Rog, G. (1980). Determination of the Standard Free Enthalpies of Formation of Barium Silicates. *Polska Akad. Nauk, Ceramika, 30*, 63-67.

Róg, G., Langanke, B., Borchardt, G., & Schmalzried, H. (1974). Determination of the Standard Gibbs Free Energies of Formation of the silicates of cobalt, Magnesium, and Strontium by EMF Measurements. *J. Chem. Thermodyn., 6*, 1113-1119.

Roth, R. S. (1990). *User Aspect of Phase Equilibria in High Tc Ceramic Superconductors*.

Roth, R. S., & Levin, E. M. (1959). Phase Equilibrium in the Subsystem Barium Disilicate-Dibarium Trisilicate. *J. Res. Nat. Bur. Stand, 62*(5), 193-200.

Ruez, P. H. (1971). Strontium and barium substitution in merwinite. *Compass Sigma Gamma Epsilon, 49*(1), 25-26.

Saulov, D. (2007). Shortcomings of the recent modifications of the quasichemical solution model. *Calphad.* 31 (3), 390–395.

Schumacher, E. E. (1926). Melting Points of Barium, Strontium and Calcium Oxides. *J. Am. Chem. Soc., 48*(2), 396-405.

Semler, C. E., & Foster, W. R. (1969). System BaO-Al2O3-SiO2. IV. The System Celsian-Alumina and the Join Celsian-Mullite. *J. Am. Ceram. Soc., 52*(12), 679-680.

Semler, C. E., & Foster, W. R. (1970). Studies in the System BaO-Al2O3-SiO2: VI, The System Celsian-Silica-Alumina. *J. Am. Ceram. Soc., 53*(11), 595-598.

Seo, W.-G., Zhou, D., & Tsukihashi, F. (2005). Calculation of thermodynamic properties and phase diagrams for the CaO-CaF2, BaO-CaO and BaO-CaF2 systems by molecular dynamics simulation. *Mater. Trans., 46*(3), 643-650.

Seward, T. P. I., Uhlmann, D. R., & Turnbull, D. (1968). Phase Separation in the System BaO-SiO2. *J. Am. Ceram. Soc., 51*(5), 278-285.

Shimizu, M., Kimata, M., & Iida, I. (1995). Crystal structure of Ba2MgSi2O7 melilite: the longest tetrahedral Mg-O distance. *Neues Jahrb. Mineral., Monatsh.*(1), 39-47.

Shukla, Adarsh (2008). Masters Thesis. *Development of a critically evaluated thermodynamic database of magnesium alloys*. Ecole Polytechnique, Montreal, Quebec, Canada.

Spencer, P.J. (2008). A breif history of CALPHAD, *Calphad*, 32(1),1-8.

Starczewski, M. (1964). Treatise on Solid State Reactions in the Ternary System SrO-Al2O3-SiO2. *Zeszyty Nauk. Politech. Slask., Chem., 22*, 5-75.

Stevels, A. L. N. (1978). Effect of non-stoichiometry on the luminescence of europium(2+)-doped aluminates with the β-alumina-type crystal structure. *J. Lumin., 17*(1), 121-133.

Stewart, D. R., & Rindone, G. E. (1963). High-Temperature Energy Relations in Borates: Alkaline-Earth and Lead Borate Compounds and Their Glasses. *J. Am. Ceram. Soc., 46*(12), 593-596.

Stolyarova, V. L., Lopatin, S. I., & Shilov, A. L. (2009). Thermodynamic properties of silicate glasses and melts: VI. System SrO-B2O3-SiO2. *Russ. J. Gen. Chem., 79*(9), 1778-1784.

Stull, D. R., & Prophet, H. (1985). *JANAF Thermochemical Tables*: U.S. Department of Commerce, Washington.

Swamy, V., Jung, I.-H., & Decterov, S. A. (2009). Thermodynamic modeling of the Al2O3-B2O3-SiO2 system. *J. Non-Cryst. Solids, 355*(34-36), 1679-1686.

Teoreanu, I., & Ciocea, N. (1978). Compatibility and modular relations in the chemistry of mixed aluminous cements. *Cemento, 75*(2), 71-82.

Thomas, R. H. (1950). Phase Equilibrium in a Portion of the Ternary System BaO-Al2O3-SiO2. *J. Am. Ceram. Soc, 33*(2), 35-44.

Thompson, J. G., Withers, R. L., & Hyde, B. G. (1987). Further Consideration of Phases in the System Barium Silicate (Ba2SiO4)-Calcium Silicate (Ca2SiO4). *J. Am. Ceram. Soc., 70*(12), C-383-C-386.

Tillmanns, E., & Grosse, H. P. (1978). Refinement of tribarium silicate. *Acta Crystallogr., Sect. B, B34*(2), 649-651.

Toropov, N. A., & Fedorov, N. F. (1964). System Ca2SiO4-Ba2SiO4. *Rus. J. Inorg. Chem., 9*(8), 1047-1050.

Toropov, N. A., & Galakhov, F. Y. (1952). State Diagram of the System Barium Oxide-Alumina. *Dokl. Akad. Nauk SSSR, 82*, 69-70.

Toropov, N. A., Galakhov, F. Y., & Bondar, I. A. (1954). Diagram of State for the Ternary System BaO-Al2O3-SiO2. *Bull. Acad. Sci. USSR, Division of Chemical Science (English Translation)*, 647-655.

Toropov, N. A., Galakhov, S. Y., & Bondar, I. A. (1956). Phase Diagram of the Triple System CaO-BaO-SiO2. *Izvestiya Akademii Nauk SSSR, Otdelenie Khim. Nauk, 6*, 641-648.

Toropov, N. A., & Konovalov, P. F. (1943). Solid Solutions of Ca and Sr Orthosilicates. *Dokl. Akad. Nauk SSSR, Ser. A, 40*, 178-180.

Toroyan, V. P., Oganesyan, R. M., & Kostanyan, K. A. (1982). Effect of alumina on the physicochemical properties of alumina-barium borate glasses. *Arm. Khim. Zh., 35*(10), 635-640.

Tyurnina, N. G., Belousova, O. L., Domanskii, A. I., Doronina, L. A., & Ugolkov, V. L. (2010). Glass formation region and order of formation of crystalline phases in the SrO-B2O3-SiO2 system. *Glass Phys. Chem., 36*(3), 294-303.

Tyurnina, Z. G., Lopatin, S. I., Shugurov, S. M., & Stolyarova, V. L. (2006). Thermodynamic Properties of Silicate Glasses and Melts: I. System BaO-SiO2. *Rus. J. Gen. Chem., 76*(10), 1522-1530.

Tyurnina, Z. G., Lopatin, S. I., & Stolyarova, V. L. (2008). Thermodynamic properties of silicate glasses and melts: IV. System BaO-B2O3-SiO2. *Russ. J. Gen. Chem., 78*(1), 14-18.

Utsunomiya, A., Tanaka, K., Morikawa, H., Marumo, F., & Kojima, H. (1988). Structure refinement of calcium aluminate (CaO6Al2O3). *J. Solid State Chem., 75*(1), 197-200.

Van-der Kemp, W. J. M., Blok, J. G., van der Linde, P. R., Oonk, H. A. J., Schuijff, A., & Verdonk, M. L. (1994). Binary Alkaline Earth Oxide Mixtures: Estimation of the Excess Thermodynamic Properties and Calculation of the Phase Diagrams. *Calphad, 18*(3), 255-267.

Van Laar, J.J. (1908). Melting-point and freezing-point curves in binary systems, when the solid phase is a mixture (amorphous solid solution or mixed crystals) of both components. First part. *Z. phys. Chem*. 63, 216-253.

Vegas, A., Cano, F. H., & Garcia-Blanco, S. (1975). Crystal structure of calcium orthoborate. Redetermination. *Acta Crystallogr., Sect. B, B31*(5), 1416-1419.

Von Oehlschlegel, G. (1971). Binary Partial BaO.2SiO2-2BaO.3SiO2 System. *Glastechn. Ber., 44*(5), 194-204.

Von Oehlschlegel, G., & Ohnmacht, W. (1975). Equilibrium Relations in the Partial System SiO2-Ba2Si3O8-BaAl2Si2O8. *Glastechn. Ber., 48*(11), 232-236.

Vulkov, V., Stavrakeva, D., & Ivanova, D. (1981). Phase study in the pseudobinary system barium silicate (Ba2SiO4)-magnesium silicate (Mg2SiO4). *Stroit. Mater. Silik. Prom-st., 22*(3), 5-8.

Walz, L., Heinau, M., Nick, B., & Curda, J. (1994). The crystal structure of alkaline earth aluminates Ba3Al2O6 and Ba2.33Ca0.67Al2O6 (Ba7Ca2Al6O18). *J. Alloys Compd., 216*(1), 105-112.

Wallenberger, F. T., & Smrcek, A. (2010). The liquidus temperature; its critical role in glass manufacturing. *Int. J. Appl. Glass Sci., 1*(2), 151-163.

Wang, G., Huang, Q., & Liang, J. (1984). Phase equilibrium relation in barium borate (BaB2O4)-strontium borate (SrB2O4) and barium borate (BaB2O4)-strontium oxide binary sections. *Huaxue Xuebao, 42*(6), 503-508.

Wartenberg, H., & Prophet, E. (1932). Melting-Point Diagrams of Highly Refractory Oxides. V. Systems with Magnesia. *Z. Anorg. Allgem. Chem., 208*, 369-379.

Wei, Z. F., Chen, X. L., Wang, F. M., Li, W. C., He, M., & Zhang, Y. (2001). Phase relations in the ternary system SrO-TiO2-B2O3. *J. Alloys Compd., 327*(1-2), L10-L13.

Weller, W. W., & Kelley, K. K. (1964). *Low Temperature Heat Capacities and Entropies at 298.15°K. of Crystalline Silicates of Barium and Strontium*. US Department of the Interior.

Winkle, L. W., & Muan, A. (1973). *Phase Relations in the System SrSiO3-CaSiO3-BaSiO3*.

Witzmann, H., & Beulich, W. (1964). Formation of non-aqueous strontium borates. Contribution to the diagram of state of the system SrO-B2O3. *Z. Phys. Chem., 225*(5/6), 336-341.

Witzmann, H., & Herzog, G. (1964). Luminescence-optical behavior of alkaline earth borate luminophors. *Z. Phys. Chem., 225*(3/4), 197-208.

www.webelements.com. (2012). Retrieved 1-3-2012, 2012, from http://www.webelements.com/

Yang, H., & Prewitt, C. T. (1999). On the crystal structure of pseudowollastonite (CaSiO3). *Am. Mineral., 84*(5-6), 929-932.

Ye, N., Zeng, W. R., Wu, B. C., Huang, X. Y., & Chen, C. T. (1998). Crystal structure of barium aluminum borate, BaAl2B2O7. *Z. Kristallogr. - New Cryst. Struct., 213*(3), 452.

Ye, X., Zhuang, W., Deng, C., Yuan, W., & Qiao, Z. (2006). Thermodynamic Investigation on the Al2O3-BaO Binary System. *Calphad, 30*(3), 349-353.

Ye, X., Zhuang, W., Wang, J., Yuan, W., & Qiao, Z. (2007). Thermodynamic Description of SrO-Al2O3 System and Comparison with Similar Systems. *J. Phase Equilib. Diff., 28*(4), 362-368.

Yonesaki, Y., Takei, T., Kumada, N., & Kinomura, N. (2009). Crystal structure of Eu2+-doped M3MgSi2O8 (M: Ba, Sr, Ca) compounds and their emission properties. *J. Solid State Chem., 182*(3), 547-554.

Yu, H., Chen, Q., & Jin, Z. (1999). Thermodynamic Reassessment of the BaO-B2O3 System. *J. Phase Equilib., 20*(5), 479-484.

Zachariasen, W. H., & Ziegler, G. E. (1932). The crystal structure of calcium metaborate, CaB2O4. *Z. Kristallogr., Kristallgeom., Kristallphys., Kristallchem., 83*, 354-361.

Zhou, S., Arroyave, R., Randall, C. A., & Liu, Z.-K. (2005). Thermodynamic Modeling of the Binary Barium-Oxygen System. *J. Am. Ceram. Soc., 88*(7), 1943-1948.

Zimmermann, E., Hack, K., & Neuschutz, D. (1995). Thermochemical assessment of the binary system Ba-O. *CALPHAD: Comput. Coupling Phase Diagrams Thermochem., 19*(1), 119-127.